ACTA UNIVERSITATIS SZEGEDIENSIS

ACTA
MINERALOGICA-PETROGRAPHICA

Tomus XLIII **Szeged, 2002**

Published by the Department of Mineralogy, Geochemistry and Petrology, University of Szeged

ACTA MINERALOGICA-PETROGRAPHICA
established in 1922
HU ISSN 0365-8066

Abbreviated title:

Acta Mineral. Petrogr., Szeged

The Acta Mineralogica-Petrographica is published by the Department of Mineralogy, Geochemistry and Petrology, University of Szeged

---

On the cover: SEM image of zircon crystal from granite, Battonya Unit (Sample 1610, Mezőhegyes-19 borehole)(see Pál-Molnár and Kovács, pp. 65-69)

Designed by: Elemér Pál-Molnár & György Sipos

Acta Mineralogica-Petrographica, Szeged 2002, Vol. 43, pp. 1-18

ACTA
Mineralogica
Petrographica

ROCK-FORMING MINERALS OF ALKALINE VOLCANIC SERIES ASSOCIATED WITH THE CHEB-DOMAŽLICE GRABEN, WEST BOHEMIA

J. ULRYCH[1], J. K. NOVÁK[1], F. E. LLOYD[2], K. BALOGH[3], GY. BUDA[4]

[1] Institute of Geology, Academy of Sciences of the Czech Republic, CZ-165 02 Praha 6, Rozvojová 135, Czech Republic
[2] University of Reading, Reading RG6 6AB, Whiteknights, United Kingdom
[3] Institute of Nuclear Research, Hungarian Academy of Sciences, H-4026 Debrecen, Bem tér 18/C, Hungary
[4] Department of Mineralogy, Eötvös Loránd University, H-1117 Budapest, Pázmány Péter sétány 1/C, Hungary

ABSTRACT

The Middle to Late Miocene intraplate alkaline volcanism of W Bohemia is associated with the uplift of the NE flank of the Cheb-Domažlice Graben. Two coexisting cogenetic volcanic series have been recognised: (i) weakly alkaline series basanite – trachybasalt – (basaltic) trachyandesite – trachyte – rhyolite (15.9-11.4 Ma) and (ii) strongly alkaline series olivine nephelinite – tephrite (16.5-8.3 Ma). The chemistry of the minerals characteristically reflects the differentiation development of the above rock series. Early crystallization in the mafic rocks is manifested by olivine phenocrysts (Fo_{66-76}), melilite, Ti-magnetite and (Ti,Fe^{3+})-diopside to fassaite; in the intermediate rocks by diopside; and in the felsic rocks by (Mn,Ti)-magnetite, diopside, and high-temperature K-oligoclase (phenocryst cores). Continuing to late crystallisation in mafic to intermediate rocks is represented by kaersutite, nepheline (at T <700°C; also occurs with melilite in ijolite pegmatoidal segregations) and labradorite to andesine, with K-andesine to K-oligoclase rims in transitional rocks. In the felsic compositions, ongoing crystallisation is characterised by Mn-magnesioriebeckite, Mn-winchite and Mg-biotite; feldspars are prevalently anorthoclase (perthite), which occasionally mantles K-oligoclase and is succeeded by Na-sanidine (matrix or rare rims to anorthoclase phenocrysts). Feldspars and quartz in the matrix of the felsic rocks terminate crystallization. Late magmatic minerals are analcime, replacing plagioclase and nepheline, carbonates and barite in the mafic rocks. Mn-oxyhydroxide, nontronite, rare sulphur and organic matter reflect crystallization in the postmagmatic stage.

ABBREVIATIONS USED IN THE TEXT:

CDG – Cheb-Domažlice Graben
WAS – weakly alkaline series associated with the Cheb-Domažlice Graben
SAS – strongly alkaline series associated with the Cheb-Domažlice Graben

INTRODUCTION

The Cenozoic alkaline volcanism of the Bohemian Massif is an integral part of the Central European Volcanic Province, which extends from France to Germany, Czech Republic and Poland (Wimmenauer, 1974). It is a surface manifestation of a large, sheet-like region of up welling found in the upper mantle from the eastern Atlantic Ocean to central Europe and the western Mediterranean (sensu Hoernle et al., 1995).

Contrasting associations of weakly alkaline (silica undersaturated to oversaturated) and strongly alkaline (undersaturated) magmatic series are known from many continental intraplate volcanic provinces (Wilson et al., 1995). Alkaline magmas may follow simultaneously either a silica saturated to oversaturated differentiation trend (rhyolites, Q-trachytes), or an undersaturated one (phonolite), reflecting the individual differences in chemistry of the primary magma (Foland et al., 1993). However, assimilation-fractional crystallisation processes, centred in the lower-crust magma chamber, play the decisive role in the development of both series, but especially of WAS (Wilson et al., 1995). Similar alkaline rocks series are known from Siebengebirge (Vieten et al., 1988), Westerwald (Schreiber et al., 1999), Hocheifel (Huckenholz and Büchel, 1988) and in particular from Cantal, Massif Central (Downes, 1989; Wilson et al., 1995) within the Cenozoic European Volcanic Province. The Euganean Magmatic Complex in the hinterland of the Alpine Orogen also reveals geochemical similarities in particular in felsic members of the rock series (Milani et al., 1999).

GEOLOGICAL SETTING

Cenozoic volcanism in W Bohemia is associated with the uplifted northeastern flank of the young CDG (NNW-SSE striking, 150 km long and 5-10 km wide) formed by the Tepelská vrchovina Highland and Slavkovský les Mts. The ENE-WSW trending Ohře Graben occurring to the north is limited by the CDG. By convention (Wohnig, 1904), the Střela river valley defines the boundary between the volcanics of the Tepelská vrchovina Highland and those of the Doupovské hory Mts. in the Ohře Rift.

From the early beginning of the 20th century geologists were intrigued by W Bohemian rocks of exceptional petrographical composition ("andesitic character" of Wohnig ,1904), some of them within the Tertiary Volcanic Subprovince of the Bohemian Massif. Shrbený (1979) noted "silica higher-saturated" types. Subsequently, Ulrych et al. (1999) identified two contrasting rock groups, a weakly alkaline series (WAS) and a strongly alkaline series (SAS).

Tertiary volcanic rocks of both series are concentrated in the Teplá Crystalline Complex; the WAS is associated with the unit exclusively. They occur rarely also in the Mariánské Lázně Metabasite Complex (e.g., Podhorní vrch Hill near Mariánské Lázně) and the Slavkovský les Crystalline Units (e.g., Buková Hill near Horní Slavkov). Geochemical distribution of the young volcanics within the SE flank of the CDG lacks obvious zonation (Fig. 1). The undifferentiated products (e.g., olivine nephelinite to basanite of Podhorní vrch, Polom and Lysina Hills) are above all spatially associated with faults belonging to the Mariánské Lázně Fault Zone (Ulrych et al., 2000a). Nevertheless, the most primitive rocks of melilite-bearing olivine nephelinite composition are present only in the area of Český Chloumek (16.5 Ma - Wilson et al., 1994). These volcanic rocks can be associated with some younger NE-SW trending faults (Litoměřice Deep Fault Zone) that spatially coincide with the Variscan major thrust of the Mariánské Lázně Metabasite Complex over the Saxothuringian para-autochthonous domain (Kachlík, 1993). The melilite-bearing volcanics are commonly characteristic of the main fault zones limiting the Ohře Rift, in W Bohemia region mostly associated with the Krušné hory Fault Zone (Kopecký, 1978; Ulrych et al., 1999; Ulrych et al., in press a). However, rare older volcanic products (29.5 Ma) also occur in the area of the NE flank of the CDG (leucite basanite from Políkno – Ulrych et al. in press b).

The differentiated products of the WAS (concentrated in the Teplá, Toužim and Manětín areas) are generally characteristic of the outer parts of the CDG. The rare trachytic occurrences as Špičák, Stěnský vrch hills and "Mordloch" have been described by Wohnig (1904), Berounský vrch Hill and reclassification of Stěnský vrch Hill trachyte as rhyolite by Pivec et al. (in press), Dobrá Voda and Kojšovice localities (trachyte accompanied by rhyolite) by Vrána (2000).

Špičák Hill is a trachytic extrusive bulbous dome. The nearby Stěnský vrch Hill can be interpreted as a laccolith with a gneissic roof

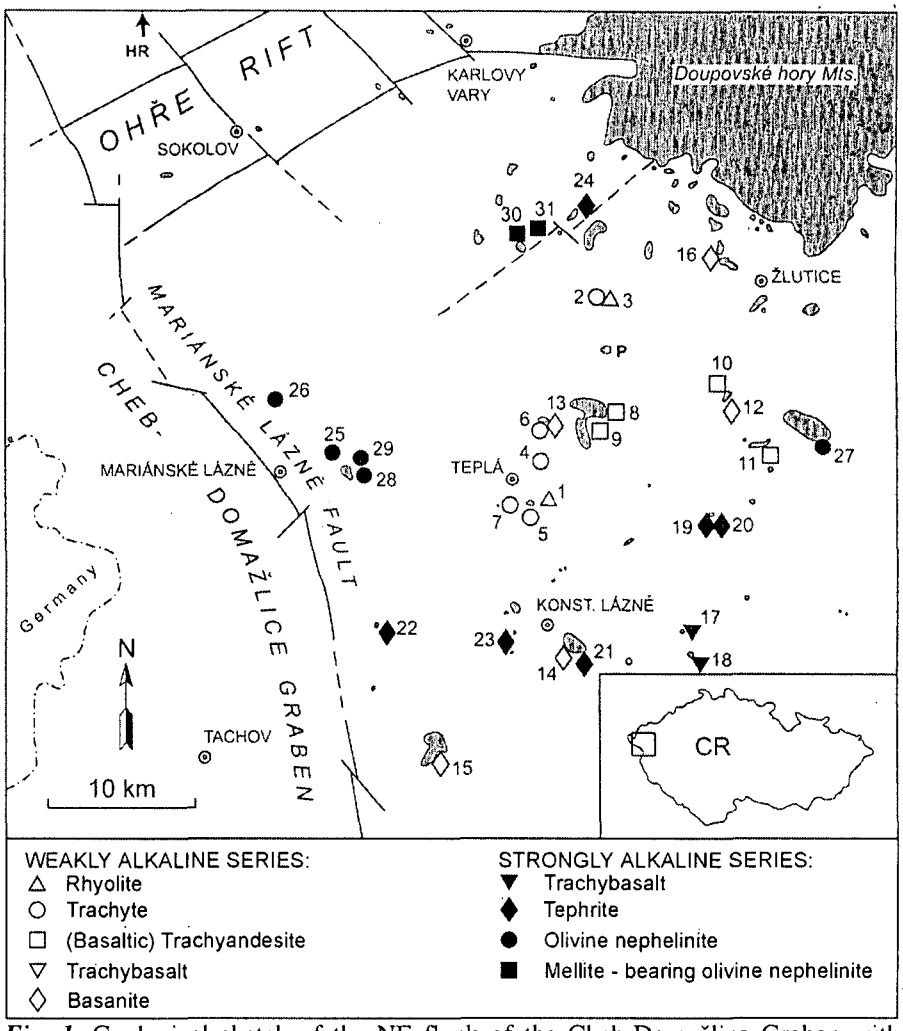

Fig. 1. Geological sketch of the NE flank of the Cheb-Domažlice Graben with marked out occurrences of the Tertiary volcanics and sampling

preserved (Ulrych et al., 1991). Basaltic trachyandesites and trachybasalts form variable groups of flows (typically developed at Doubravický vrch Hill). Zbraslavský vrch Hill consists of two lava flows and a feeding channel filled by agglutinate, giving an asymmetric "flag-form" volcanic structure (Fediuk, 1995). A horseshoe-shaped group of hills is formed by Třebouňský vrch Hill, which represents a relict of feeder channel filling, and the Branišovský vrch Hill lava flow. The Okrouhlé Hradiště Hill is a relict of a large flow(s). Vlčí hora Hill is a large composite volcano (Ulrych, 1986; Ulrych et al., 2000c).

Volcanic rocks of the SAS are more abundant in comparison to the WAS forming mostly smaller intrusions such as stocks and diatremes (for comparative overview see Fig. 1). A major locality is the large polyphase volcano Podhorní vrch (Cajz, 1992; Ulrych et al., 2000c). The melilite-bearing olivine nephelinites from Chloumecký kopec Hill are relicts of a volcanic edifice with preserved rim of Upper Eocene Staré Sedlo Formation. Chlumská hora Hill is the largest relict of an olivine nephelinite flow (4 by 1.2 km) occurring together with other characteristic "table mountains", e.g., Vladař Hill south of the formal boundary (see above) of the Doupovské hory Mts. Pekelský vrch Hill Nečtiny is a relict of a composite volcano with products of trachybasalt-tephrite composition.

Sampling and analytical methods

Thirty one representative rock samples were used for the geochemical (Ulrych et al., in press b) and the present mineralogical study. The sampling covers the elevated block of the CDG (Fig. 1). Sampling sites are presented together with their geological characteristics, petrography and modal mineralogy of the rocks in

Table 1. Rock samples were prepared for the study by use of common methods described, e.g. in Ulrych et al. 2000c and Ulrych et al. in press b).

K-Ar isotope measurements were taken in the Institute of Nuclear Research of the Hungarian AS, Debrecen. An Ar extraction and its measurement were made on the mass spectrometer by the method of isotope dilution ^{38}Ar according to procedure described by Balogh (1985) and Odin et al. (1982).

Rock-forming minerals were analysed in the Institute of Geology, AS CR, Prague with a JXA 50A electron microprobe with spectrometer EDAX PV 9400, using an accelerating voltage of 20 kV, beam current of 1.5 10^{-9} A, beam diameter of 2 μm and counting time of 120 s per analysis (analyst A. Langrová). Standards employed are natural mineral (olivine, kaersutite, jadeite, diopside, leucite, apatite, barite) and synthetic phases (SiO_2, TiO_2, Fe_2O_3, Cr_2O_3, MgO) and the ZAF correction method was used.

AGE RELATIONS OF VOLCANIC SERIES

The new K-Ar data and a review of the published data (Wilson et al., 1994; Ulrych et al., in press a, b and Pivec et al.

Table 1. Geological and petrological characteristic of the representative rocks of the weakly and strongly alkaline series

Locality	Sample No.	Root name in TAS* classific.	Sub-root name	Normative characteristic	Mineral composition	Country rock (xenoliths)	Structure texture	Volcanic form
WEAKLY ALKALINE SERIES								
Stěnský vrch Hill	202	rhyolite		Q-, Ns-normative	anorthoclase quartz magnesioriebeckite	gneiss	holocrystalline porphyritic with trachytic matrix	dome (laccolith?)
Špičák Hill	180	trachyte	high K-type	Q-normative	anorthoclase, sanidine, oligoclase, quartz, winschite, biotite, Ti-magnetite, titanite, apatite, Mn-oxyhydroxide, sulphur	gneiss	holocrystalline porphyritic with trachytic matrix	dome
Prachometský vrch Hill	186	trachyte	high K-type	Q-normative	sanidine, anorthoclase diopside-hedenbergite-augite series, Ti-magnetite, titanite, apatite	amphibolite	holocrystalline fine-porphyritic with trachytic matrix	dome
Třebouňský vrch Hill	251	trachy-andesite	latite	Ne-, Ol-normative	andesine, anorthoclase diopside-augite series kaersutite, nepheline, Ti-magnetite, titanite, apatite	mica schist	holocrystalline porphyritic with trachytic matrix	lava flow
Doubravický vrch Hill	256	basaltic trachy-andesite	sho-shonite	Ne-, Ol-normative	bytownite, anorthoclase diopside-augite series nepheline, Ti-magnetite, titanite, apatite, zeolite, carbonate, barite	PermoCarboniferous sediments	holocrystalline pilotaxitic, vesicular	lava flow
Zbraslavský vrch Hill	255	trachybasalt	hawaiite	Ne-, Ol-normative	andesine, sanidine, kaersutite, diopside, Ti-magnetite, titanite, apatite, carbonate	gneiss and PermoCarboniferous sediments	holocrystalline fine porphyritic with pilotaxitic matrix "sonnenbrand"	lava flow
Prachomety II	Z-13	basanite		Ne-, (Ol-) normative	ferrisalite-ferrifassaite, labradorite, (andesine), K-oligoclase, serp.olivine, Ti-magnetite, apatite, (analcime)	mica schist	porphyritic with holocrystalline matrix	intrusion (partly brecciated)
Vlčí hora Hill,	P-1	basanite - analcimized		Ne-, Ol-normative	ferrisalite-ferrifassaite, kaersutite, Ti-magnetite,apatite	phyllite to mica schist	porphyritic in holocrystalline matrix, magacrysts: kaersutite, diopside, olivine	complex volcano

Table 1. continued

Locality	Sample No.	Root name in TAS* classific.	Sub-root name	Normative characteristic	Mineral composition	Country rock (xenoliths)	Structure texture	Volcanic form
STRONGLY ALKALINE SERIES								
Vinice Hill	Z-22	trachybasalt	hawaiite	Ne-, Ol-normative	kaersutite, ferrisalite, phenocrysts, labradorite-andesine, K-oligoclasse, ferrisalite in matrix	phyllite to mica schist	holocrystalline fine porphyritic	intrusion
Pekelský vrch Hill	Z-24	tephriete		Ne-, (Ol-) normative	ferrisalite-ferrifassaite, phenocrysts, labradorite, K-andesine Ti-magnetite, apatite in matrix	mica schist	fine porphyritic holocrystalline fluidal matrix	small volcano
Okrouhlé Hradiště Hill	Z-19	tephrite		Ne-, Ol-normative	(olivine), ferrifassaite, labradorite, analcime,	phyllite to mica schist, xenolite: pyroxenite and dunite with glassy rims	holocrystalline fine-porphyritic	differentiated lava flow(s)
Polom in Mariánské Lázně	Z-15	olivine (contam.)		Ne-, Ol-normative	olivine, ferrifassaite, labradorite, serp. olivine, Ti-magnetite, apatite	granite xenoliths: granite with glassy rims, pyroxenite	porphyritic with holocrystalline matrix	intrusion (partly brecciated)
Lysina Hill	Z-14	olivine nephelinite(contam.)		Ne-, Ol-normative	olivine, ferrifassaite, nepheline, Ti-magnetite,apatite	granite xenoliths: granite	porphyritic with holocrystalline matrix	intrusion
Český Chloumek	Z-16	melilite-bearing olivine nephelinite		Ne-, Ol-normative (melilite)	olivine, ferrifassaite, nepheline, melilite, Ti-magnetite	Miocene sediments and granite, xenoliths: wehrlite?	holocrystalline microporphyritic	dyke-like intrusion

in press) are presented in Table 2A, B together with chemical analyses of the rocks. Based upon this data and the distribution scheme of Cenozoic volcanism in the Bohemian Massif (Ulrych et al., 1999), two coexisting volcanic series of Middle to Late Miocene age associated with the NE flank of the CDG were recognized (Fig. 2):

(i) Weakly alkaline series - WAS (15.9-11.4 Ma), cf. Pivec et al. (in press);

(ii) Strongly alkaline series - SAS (16.5-8.3 Ma) developed to a limited degree only.

The ultimate development of the volcanism of the NE flank of the CDG was at about 12 Ma. However, the onset of the volcanism (16-17 Ma) is characteristic of the more distal regions of the CDG. This activity of the CDG NE flank provides a link between the Oligocene-Miocene strongly alkaline series of the Western Ohře Rift (24-16 Ma, average 22 Ma) (Ulrych et al., in press a) and the Pliocene to Quaternary (0.43-0.11 Ma) primitive alkaline volcanics occurring at the intersection of the OR and CDG structures in the vicinity of Cheb (Wilson et al., 1994; Wagner et al., 1998). From K-Ar data of Wilson et al. (1994) and Ulrych et al. (in press a) on basanitic rocks (Hory in Karlovy Vary -15.5 Ma and Horní Rotava in the Krušné hory Mts. - 14.8 Ma) it follows that the Middle Miocene volcanism in W Bohemia was not restricted to the CDG area only.

The age-related Group of Late Miocene Intrusives (13-9 Ma; sills and dykes) represents the final volcanic episode of

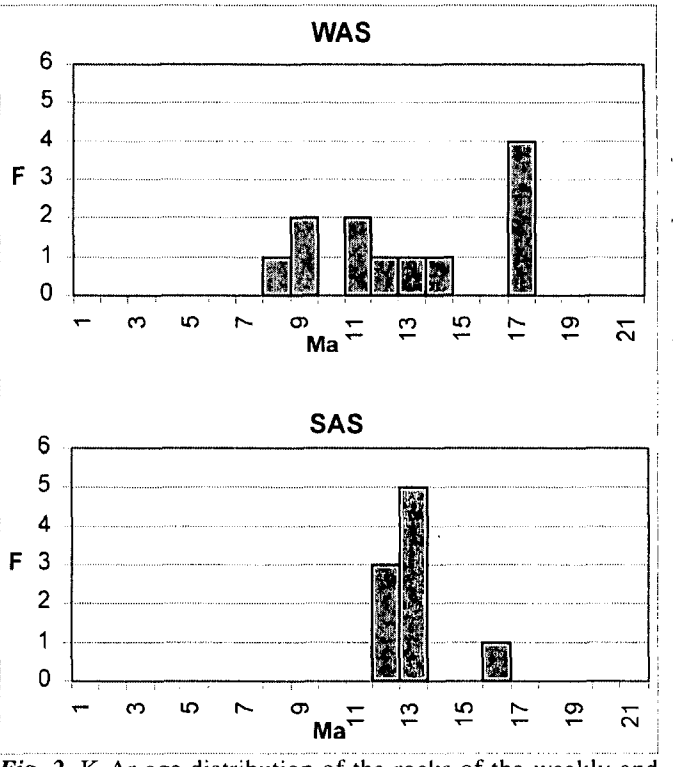

Fig. 2. K-Ar age distribution of the rocks of the weakly and strongly alkaline series associated with the Cheb-Domažlice Graben. For data see Table 2a, b. Vertical axis – frequency of K-Ar experimental data

the České středohoří Mts. Area. It was described from a block of coal-bearing basinal Ohře Rift sediments in the Bílina-Most area (Cajz et al., 1999). Products of a similar final episode (13 Ma) of the volcanic cycle are known from many areas of the CEVP such as Heldburger Gangschar, Rhön, Hessian Basin, Vogelsberg and Westerwald (11-6 Ma, Lippolt 1983).

The recurrence of volcanism and changes in its chemical characteristics coincide with tectonism (Downes, 1996), causing principal changes in tectonic settings and character of magmas from calc-alkaline to alkaline in the Carpathians. This change reflects Late Miocene E-W compression in the Alpine Orogeny linked to entry of continental crust into the subduction zone. Volcanism of the CDG NE flank thus parallels the development of the graben structure, as revealed by the minimal Middle Miocene (?) relict of a sedimentary fill in the Lažany-Vlčí hora Hill area (Zartner, 1939) preserved below the underlying basanite flow (11.7 Ma – Wilson et al., 1994).

Table 2A. Chemical analyses of rocks of the weakly alkaline series

Sample No	1	2	3	4	5	6	7	8	9	10	11	12	13	14	15	16
	202	ZC-30B	ZC-30A	ZC-20A	180	186	203	251	251a	255a	256	255	Z-13	P-3	P-1	P-19
Rock type	RY	RY	TR	TR	TR	TR	TR	TA	TA	TA	BTA	TB	BA	BA	BA	BA
SiO_2(wt.%)	70,18	74,45	65,66	65,39	65,77	62,91	62,90	53,46	55,17	55,57	51,83	45,24	42,24	42,91	43,81	41,43
TiO_2	0,03	0,08	0,24	0,40	0,31	0,55	0,30	1,67	1,41	1,76	1,68	2,68	2,46	3,37	3,11	3,90
Al_2O_3	15,12	13,76	17,98	17,82	17,57	18,20	19,14	18,22	17,70	17,75	18,83	16,33	12,64	11,99	12,49	11,27
Fe_2O_3	1,23	1,29	1,51	1,43	1,93	1,08	2,99	4,64	3,28	5,10	5,29	6,21	5,14	5,12	4,59	5,02
FeO	0,08	0,05	0,07	0,13	0,08	0,14	0,10	1,92	3,00	1,56	2,18	4,50	5,99	5,88	6,56	7,21
MnO	0,04	0,02	0,05	0,06	0,24	0,12	0,10	0,18	0,19	0,17	0,22	0,21	0,22	0,18	0,20	0,22
MgO	0,05	0,16	0,06	0,10	0,14	0,06	0,12	2,36	1,82	1,63	2,02	4,22	11,19	11,11	9,60	9,25
CaO	0,41	0,20	0,80	1,25	0,76	2,13	1,03	5,63	5,60	6,09	6,81	9,73	11,54	13,97	13,30	14,61
Na_2O	6,60	3,06	7,39	6,79	6,27	7,40	6,49	5,15	5,02	4,98	4,85	3,79	3,85	2,39	3,16	2,98
K_2O	4,48	4,91	5,92	6,00	5,56	4,91	5,55	3,74	4,09	3,50	3,02	1,47	1,41	1,70	1,77	1,74
P_2O_5	0,03	0,09	0,03	0,06	0,07	0,10	0,04	0,55	0,43	0,50	0,62	0,79	0,82	0,57	0,69	0,75
H_2O^+	1,17	1,20	0,44	0,30	0,42	1,24	0,67	1,28	1,26	0,86	1,11	2,01	2,02	0,59	0,29	1,32
H_2O^-	0,04	0,22	0,12	0,09	0,32	0,34	0,63	0,82	0,40	0,28	0,96	1,43	0,52	0,21	0,27	0,22
F	0,03	0,06	0,04	0,06	0,06	0,03	0,04	0,11	0,07	0,02	0,09	0,12				
Cl	0,01				0,02	0,02		0,11			0,13	0,01				
CO_2	0,19	0,03	<0.01	0,05	0,40	0,44	<0.10	0,05	0,01	0,02	0,04	0,91	0,03	0,13	0,07	0,20
	99,69	99,58	100,31	99,93	99,92	99,67	100,10	99,89	99,45	99,79	99,68	99,65	100,07	100,12	99,91	100,12
O=2F	-0,01	-0,03	-0,02	-0,03	-0,03	-0,01	-0,02	-0,05	-0,03	-0,01	-0,04	-0,05				
O=2Cl								-0,02			-0,03	-0,05				
Total	99,67	99,55	100,29	99,90	99,89	99,66	100,08	99,82	99,42	99,78	99,61	99,55	100,07	100,12	99,91	100,12
Rb (ppm)	436	282	153	213	191	133	162	110	90	102	83	61	49	39	40	39
Cs	6,5	6,2	2,8	2,6	2,2	1,5	1,40	1,9	1,3	0,9	0,87	0,78	0,94	0,57		
Sr	126				128	1270	480	1338	1189	1040	1287	1069	1002	728	877	941
Ba	420	215	143	564	434	1546	1242	1455	1290	1451	1258	906	828	487	580	788
Ga	34				35	28	25	18	17	14	16	14				
As	6				6	11		4	5	4	3	2	3,1			
Sc	0,3	5,6	1,6	1,2	1,4	6,7	0,9	6,3	6,9	7,9	6,2	16	23	34	17	33
Y	35				35	36	25	40	34	34	39	31	21	22	26	21
La	84	10	156	101	132	171	131	144	160	140	121	95	114	121	137	113
Ce	115	21	216	155	220	152	186	251	241	218	228	176	177	180	211	171
Nd	16,0	10,0	40,0	37,0	71,0	14,0	54,0	102,0	99,0	100,8	106,0	87,0	78,3	79,0	84,0	75,1
Sm	2,8	2,2	2,9	4,3	9,2	4,4	5,9	14,3	14,7	15,3	15,6	13,7	11,4	13,3	16,9	13,9
Eu	0,3	0,2	1,0	1,2	1,9	1,5	1,6	4,2	3,8	3,6	4,6	4,2	3,4	3,4	4,4	3,7
Gd	2,7				6,2	4,1	5,0	12,3	10,2	9,4	12,5	12,1	13,8	10,9	12,1	11,6
Tb	0,47	0,40	0,50	0,50	0,95	0,71	0,59	0,85	1,43	1,36	1,60	1,40	1,06	1,44	1,58	1,22
Yb	3,7	3,6	3,3	2,8	3,7	3,1	2,8	2,9	3,9	3,9	3,4	2,6	2,19	3,01	4,50	3,00
Lu	0,51	0,43	0,48	0,41	0,58	0,45	0,47	0,51	0,38	0,44	0,58	0,45	0,33	0,33	0,41	0,38
Th	72,3	9,0	33,0	33,0	26,3	21,4	27,6	15,6	14,1	15,9	14,0	10,2	13,2	10,0	12,0	13,0
U	5,4	7,0	7,1	6,3	7,8	5,1	3,4	4,0	4,5	6,6	3,2	2,7	3,2	2,1	1,9	1,0
Zr	380				517	661	626	460	505	363	512	322	252	243	288	299
Hf	14,5	2,9	11,7	13,2	12,8	14,6	14,9	12,4	11,8	10,5	11,5	9,2	6,8	9,9	9,4	8,9
V							15						198	301	310	330
Nb	139				160	133	126	122	154	123	149	116	89	70	85	117
Ta	8,7				10,2	9,1	8,8	10,5	10,1	7,7	9,2	6,8	5,4	6,1	7,1	7,6
Cr	7				12	10	4	11	26	21	16	15	219	175	230	258
Co	0,5	3,7	0,5	1,1	0,6	1,2	1,0	5,7	11	14	3,6	5,0	51	54	45	41
Ni	5				5	5	5	6	10	17	7	13	237	157	120	99
Cu	5				5	5	0,2	37	17	29	11	21		155	87	150
Zn	115	56	72	46	63	200	98	137	95	143	195	129	128	70	90	95

Table 2A. continued

Sample No	1	2	3	4	5	6	7	8	9	10	11	12	13	14	15	16
	202	ZC-30B	ZC-30A	ZC-20A	180	186	203	251	251a	255a	256	255	Z-13	P-3	P-1	P-19
Rock type	RY	RY	TR	TR	TR	TR	TR	TA	TA	TA	BTA	TB	BA	BA	BA	BA
K/Rb	85,28	144,51	321,15	233,80	241,61	306,41	284,35	282,20	377,19	284,80	302,00	200,02	238,84	361,79	367,28	370,31
Rb/Sr	3,46				1,49	0,10	0,34	0,08	0,08	0,10	0,06	0,06	0,05	0,05	0,05	0,04
Sr/Ba	0,30				0,29	0,82	0,39	0,92	0,92	0,72	1,02	1,18	1,21	1,49	1,51	1,19
Zr/Nb	2,73				3,23	4,97	4,97	3,77	3,28	2,95	3,44	2,78	2,83	3,47	3,39	2,56
Y/Nb	0,25				0,22	0,27	0,20	0,33	0,22	0,28	0,26	0,27	0,24	0,31	0,31	0,18
La/Nb	0,60				0,83	1,29	1,04	1,18	1,04	1,14	0,81	0,82	1,29	1,73	1,62	0,96
Th/U	13,40	1,29	4,65	5,24	3,37	4,20	8,12	3,90	3,13	2,41	4,38	3,78	4,13	4,76	6,32	13,00
Zr/Hf	26,20				40,39	45,27	42,01	37,10	42,80	34,57	44,52	35,00	37,06	24,55	30,64	33,60
Nb/Ta	15,98				15,69	14,62	14,32	11,62	15,25	15,97	16,20	17,06	16,48	11,48	11,97	15,39
SREE	225,48	47,80	420,21	302,16	445,53	351,26	587,36	532,06	534,51	492,71	493,28	392,45	402,27	412,49	472,36	392,65
$(La/Yb)_N$	16,28	1,99	33,91	25,87	25,59	39,57	33,56	35,62	29,45	25,67	25,53	26,21	37,47	28,86	21,89	26,97
Eu/Eu*	0,33	0,41	1,87	1,41	0,73	1,06	0,88	0,94	0,90	0,85	0,97	0,98	0,83	0,84	0,89	0,85
#Mg	8,12	21,70	8,09	12,89	13,91	10,17	8,27	44,81	39,07	35,73	37,90	46,73	68,85	68,96	65,32	62,32
Gd/Gd*	0,13	0,00	0,00	0,00	0,16	0,15	0,15	0,28	0,24	0,24	0,31	0,39	0,44	0,34	0,32	0,38
Age (Ma)	12,4				12,5	11,9		12,1		11,4	12,9		12,8		11.7*	15.9*

1-202 rhyolite, Stěnský vrch Hill near Teplá, AQ
2-ZC30B rhyolite, Kojšovice (Vrána 2000), B
3-ZC30A trachyte, Kojšovice (Vrána 2000), B
4-ZC20A trachyte, Dobrá Voda (Vrána 2000), B
5-180 trachyte, Špičák Hill near Teplá, Q
6-186 trachyte, Prachometský v. Hill near Teplá, AQ
7-203 trachyte, Berounský v. Hill near Heřmanov, B
8-251 trachyandesite, Třebouňský v. Hill near Teplá, AQ
9-251a trachyandesite, Branišovský v. Hill near Teplá Shrbený 1979), AQ
10-255a trachyandesite, Zbraslavský v. Hill near Manětín (Shrbený 1979), AQ
11-256 basaltic trachyandesite, Doubravický v. Hill near Manětín, AQ
12-255 trachybasalt?, Zbraslavský vrch Hill near Manětín, AQ
13-Z13 basanite, Prachomety II near Teplá, AQ
14-P3 basanite, Okrouhlé Hradiště Hill near Konstantinovy Lázně, AQ
15-P1 basanite, Vlčí hora Hill near Černošín, AQ
16-P19 basanite, Holý v. Hill near Ratiboř, Q

Explanations: Q - active quarry, AQ - abandoned quarry, NO - natural outcrop, B - boulders

Table 2B. Chemical analyses of rocks of the strongly alkaline series

Sample No.	17	18	19	20	21	22	23	24	25	26	27	28	29	30	31
	Z-20	Z-22	Z-23	Z-24	Z-19	P-2	P-4	Z-26	Z-15	Z-14	226	M-1	M-2	P-16	Z-16
Rock type	TB	TB	TB	TE	TE	TE	TE	TE	ON	ON	ON	ON	ON	MON	MON
SiO_2 (wt.%)	47,32	45,66	45,89	44,91	45,55	40,27	41,59	44,98	43,67	43,98	40,99	39,58	40,60	40,90	39,19
TiO_2	2,55	2,89	2,86	2,85	3,07	3,91	3,66	1,99	3,51	2,10	4,18	1,98	1,95	2,20	2,70
Al_2O_3	16,14	15,80	15,28	15,83	15,20	13,65	14,79	12,04	13,87	12,21	13,76	10,20	10,87	11,60	11,39
Fe_2O_3	4,80	6,12	4,77	4,99	4,93	4,80	5,17	2,48	5,62	4,18	7,51	6,39	4,34	4,08	3,99
FeO	5,65	5,25	6,45	6,45	6,14	8,12	8,93	8,05	5,40	6,33	7,56	5,85	6,83	7,10	7,99
MnO	0,22	0,23	0,23	0,23	0,21	0,24	0,25	0,17	0,18	0,17	0,23	0,22	0,21	0,19	0,20
MgO	4,00	4,34	5,41	5,41	6,11	7,90	6,25	12,46	6,98	13,02	6,42	15,02	14,52	12,50	12,49
CaO	9,81	9,93	10,73	10,73	11,05	12,39	12,02	11,22	11,80	11,33	11,24	12,45	12,13	13,59	15,81
Na_2O	4,24	4,23	3,59	3,59	3,65	3,49	3,97	2,62	3,69	3,33	3,75	3,93	3,64	2,74	3,00
K_2O	1,90	1,13	2,21	2,21	2,19	2,22	0,87	1,31	0,72	0,94	1,89	1,33	0,97	1,10	1,11
P_2O_5	1,00	1,08	0,94	0,94	0,74	0,92	0,90	0,60	0,51	0,52	0,94	0,97	0,88	0,82	0,88
H_2O^+	2,06	1,73	1,01	1,01	0,95	0,50	1,09	1,69	2,23	1,69	0,80	1,23	1,78	2,64	1,12
H_2O^-	0,21	0,61	0,34	0,34	0,35	0,02	0,20	0,14	0,79	0,26	0,20	0,82	0,51	0,33	0,31
CO_2	0,07	0,02	0,04	0,04	0,07	0,49	0,37	0,07	0,02	0,13	0,03	0,08	0,28	0,07	0,03
Total	99,97	99,02	99,75	99,53	100,21	98,92	100,06	99,82	98,99	100,19	99,50	100,05	99,51	99,86	100,21
Rb	52	53	50	46	51	55	65	32	70	52	47	31	27	52	37
Cs	0,79	0,86	0,73	1,10	0,71	0,80	0,41	0,5	1,70	1,90	0,57	0,42	0,44	3,30	3,30
Sr	1046	979	858	967	829	1088	1190	594	895	600	1254	988	836	816	1151
Ba	814	787	718	644	642	691	731	501	616	611	985	849	627	964	1005
Ga												11	11		
As	1,9	1,7	2	1,6	1,4			1,8	2,3	1,5					
Sc	14	16	19,7	20	25	22	16	26,4		28	25	24	24	28	27
Y	31	29	22	20	21	31	30	17	21	16	32	23	20	17	25
La	106,7	106,1	84,5	83,3	81,9	99,2	118,9	43,6	70,4	52,9	110,0	99,4	83,1	76,9	89,7
Ce	185	182	144,0	146,0	142,9	138,9	166,2	71,8	122,4	85,6	181,1	142,0	126,0	122,4	137,1
Nd	92,0	89,1	70,3	72,1	70,0	66,0	73,2	37,1	64,7	43,7	73,2	55,7	53,1	61,9	66,0
Sm	14,5	14,7	11,9	11,7	11,5	12,5	14,1	6,94	10,4	7,48	16	9,1	9,1	10,3	12,8
Eu	4,1	4,2	3,46	3,52	3,33	3,31	3,57	2,26	3,08	2,35	3,62	2,73	2,52	3,18	2,64
Gd	13,1	13,3	11,8	11,8	11,6	10,7	11,0	7,8	9,6	8,9	8,7	8,7	6,7	11,2	10,1
Tb	1,45	1,45	1,17	1,16	1,11	1,19	1,19	0,89	1,03	0,88	1,52	1,03	0,92	1,07	1,09
Yb	3,3	3,5	2,49	2,49	2,42	2,66	2,91	1,50	1,87	1,68	2,48	1,66	1,66	1,71	1,79
Lu	0,49	0,49	0,36	0,34	0,34	0,28	0,33	0,25	0,32	0,24	0,31	0,25	0,27	0,22	0,18

Table 2B. continued

Sample No.	17	18	19	20	21	22	23	24	25	26	27	28	29	30	31
	Z-20	Z-22	Z-23	Z-24	Z-19	P-2	P-4	Z-26	Z-15	Z-14	226	M-1	M-2	P-16	Z-16
Rock type	TB	TB	TB	TE	TE	TE	TE	TE	ON	ON	ON	ON	ON	MON	MON
Th	9,7	9,5	9,4	8,4	8,6	16,0	9,0	5,0	6,5	6,4	8,1	10,5	9,3	9,3	14,0
U	3,1	2,7	2,5	2,4	2,4	1,0	1,0	0,9	1,7	1,6	1,9	5,2	4,8	1,9	1,9
Zr	426	403	285	280	279	361	366	138	230	135	243	177	159	283	231
Hf	10,9	10,8	8,2	8,2	8	8,1	8,5	4,1	7,1	4,1	8,9	3,9	3,8	5,4	7,0
V	166	202	212	210	240	321	389	158	278	179	288	133	150	192	233
Nb	89	88	74	73	71	122	112	43	55	48	104	85	76	102	144
Ta	6,0	6,0	5,6	5,7	5,4	7,0	6,4	2,8	4,1	3,5	6,1	5,2	4,6	6,5	6,1
Cr	22	27	45	48	62	44	33	422	67	370	354	410	445	324	271
Co	16	21	24	25	30	41	40	56,0	38	55	42	52	55	49	56
Ni	11	13	17	17	30	57	37	162	45	249	207	236	271	173	222
Cu						81	66				73	83	67		77
Zn	143	150	139	160	115	117	112	103	94	101	116	69	93	108	115
K/Rb	303,27	176,96	366,86	398,76	356,41	335,02	111,09	339,78	85,37	150,04	333,77	356,10	298,19	175,58	249,00
Rb/Sr	0,05	0,05	0,06	0,05	0,06	0,05	0,05	0,05	0,08	0,09	0,04	0,03	0,03	0,06	0,03
Sr/Ba	1,29	1,24	1,19	1,50	1,29	1,57	1,63	1,19	1,45	0,98	1,27	1,16	1,33	0,85	1,15
Zr/Nb	4,79	4,58	3,85	3,84	3,93	2,96	3,27	3,21	4,18	2,81	2,34	2,08	2,09	2,77	1,60
Y/Nb	0,35	0,33	0,30	0,27	0,30	0,25	0,27	0,28	0,38	0,33	0,31	0,27	0,26	0,17	0,17
La/Nb	1,20	1,21	366,86	1,14	1,15	0,81	1,06	1,01	1,28	1,10	1,06	1,17	1,09	0,75	0,62
Th/U	3,13	3,52	0,06	3,50	3,58	16,00	9,00	5,56	3,82	4,00	4,26	2,02	1,94	4,89	7,37
Zr/Hf	39,08	37,31	34,76	34,15	34,88	44,57	43,06	33,66	32,39	32,93	27,30	45,38	41,84	52,41	33,00
Nb/Ta	29,67	29,33	19,47	26,07	26,30	17,43	17,50	30,71	26,19	28,24	17,05	16,35	16,52	31,88	23,61
SREE	420,62	414,38	329,98	332,41	325,10	334,74	391,40	172,13	283,79	203,68	396,95	320,56	283,39	288,88	321,40
$(La/Yb)_N$	22,98	22,06	24,34	24,00	24,28	26,75	29,31	20,85	27,00	22,59	31,82	42,95	35,91	32,26	35,95
Eu/Eu*	0,88	0,90	0,88	0,91	0,87	0,85	0,84	0,94	0,93	0,88	0,85	0,93	0,94	0,90	0,69
#Mg	45,69	45,83	34,76	50,91	54,78	57,11	49,11	71,76	58,33	73,01	48,46	73,08	73,93	70,88	69,34
Gd/Gd*	0,40	0,41	0,46	0,45	0,46	0,43	0,37	0,60	0,44	0,58	0,27	0,35	0,30	0,52	0,42
Age (Ma)	10,4	13,5	13,0	10,5	9.0* 6,5	11.8*	8.3*	16.5*		16,2			12.4* 17,0	16.5*	

17-Z20 trachybasalt, Skupečský v. Hill near Konstantinovy Lázně, AQ
18-Z22 trachybasalt, Vinice Hill near Konstantinovy Lázně, AQ
19-Z23 trachybasalt, Pekelský v. Hill near Nečtiny, Q
20-Z24 tephrite, Pekelský v. Hill near Nečtiny, Q
21-Z19 tephrite, Okrouhlé Hradiště Hill near Konstantinovy Lázně, AQ
22-P2 tephrite, Homole Hill near Planá, AQ
23-P4 tephrite, Krasíkov Hill near Konstantinovy Lázně, NO
24-Z26 olivine nephelinite (crystalline rocks and magnetite xenoliths), Číhaná AQ
25-Z15 olivine nephelinite (granite xenoliths), Polom in Mariánské Lázně, AQ
26-Z14 olivine nephelinite (granite xenoliths), Lysina Hill near Kynžvart, NO
27-226 olivine nephelinite, Chlumská hora Hill near Manětín (Shrbený 1979), AQ
28-M1 olivine nephelinite (massive), Podhorní v. Hill near Mariánské Lázně, NO
29-M2 olivine nephelinite (brecciated), Podhorní vrch Hill near Mariánské Lázně, AQ
30-P16 melilite-bearing olivine nephelinite, Chloumecký kopec Hill near Č. Chloumek, NO
31-Z16 melilite-bearing olivine nephelinite, Český Chloumek q, AQ

Ages designated by asterisk (Wilson et al. 1994) other (K. Balogh and E. Árva-Sós, Debrecen).

PETROGRAPHY

A survey of the principal rock types, localities, their geological and petrographical characteristics, main modal mineralogy and geochemistry are shown in Table 1. For more detailed petrographic and geochemical characteristic of the rocks see Shrbený (1979), Ulrych et al. (2000c, in press b) and Pivec et al. (in press).

Rock-forming minerals

Quartz occurs as interstitial grains in the matrix (<0.4 mm in size) and as prismatic euhedral crystals (up to 5 mm in size) in fissures in rhyolite and trachyte from Špičák Hill. In trachyte it occurs in paragenesis with Mn-oxyhydroxide coatings and with an organic matter of white colour. Wohnig (1904) also described quartz in vesicles of trachyte from Prachometský vrch Hill.

Feldspars are broadly distributed in the felsic rocks as phenocrysts and matrix minerals. They commonly reveal characteristic ternary composition due to a higher content (>5 mol.%) of the third component (sensu Barth, 1969; Table 3; Fig. 3).

Alkali feldspars dominate in rhyolite and trachytes, reaching 80-90 vol.%. Where anorthoclase is the sole feldspar, as in the rhyolite of the Stěnský vrch Hill, it forms phenocrysts (up to 8 mm). Zoned hypautomorphic phenocrysts (up to 12 mm) of alkali feldspar occur in trachyte from Špičák and Prachometský vrch hills. The phenocrysts of trachyte from Špičák Hill (antiperthites or perthites) are – in optimum examples – formed by (i) a high-temperature K-oligoclase core ($Ab_{70-75}An_{16-21}Or_{09-11}$) or its diffuse relicts of Ca-anorthoclase composition ($Ab_{60}An_{16}Or_{24}$), (ii) ubiquitously mantled by anorthoclase with perthitic texture ($Or_{31-43}Ab_{47-63}An_{05-11}$), and with (iii) rare Na-sanidine rims similar in composition to the matrix (K>Na)-phase. The disordered sanidine structure was checked using optical method. Matrix feldspar is Na-sanidine

($Or_{59}Ab_{40}An_{01}$) and K-oligoclase ($Or_{07}Ab_{80}An_{13}$) compositions. The sanidine is in composition identical with the feldspar of trachyte from Drachenfels ($Or_{62}Ab_{36}An_{02}$), cf. Vieten et al. (1988).

Anorthoclase (Table 3, No. Z-13) in basanite, (No. 256/28) in basaltic trachyandesite, (No. 251/20) in trachyandesite, or sanidine (255/40) in trachybasalt are probably of xenocrystic origin and may indicate some magma mixing between mafic and felsic compositions. Sanidine in trachybasalt has appreciable BaO contents (max. 3.75 wt.%). Wilson et al. (1995) reported higher BaO contents (about 1 wt.%) in K-feldspar of the trachytes in Cantal. Rare anorthoclase laths (Or_{20-22}) occur in the matrix of intermediate and basic rocks.

The presence of ternary feldspars with anhydrous ferromagnesian minerals in rhyolites and Q-normative trachytes indicate high temperatures of origin (Nekvasil, 1992). As recognised by Carmichael (1963) and Nekvasil (1990) the most common reaction in these rock types would be the crystallisation of alkali feldspars through the reaction of older plagioclases with melt. This explains the presence of partially resorbed cores of high-temperature ternary plagioclases and/or ternary alkali feldspars (generally

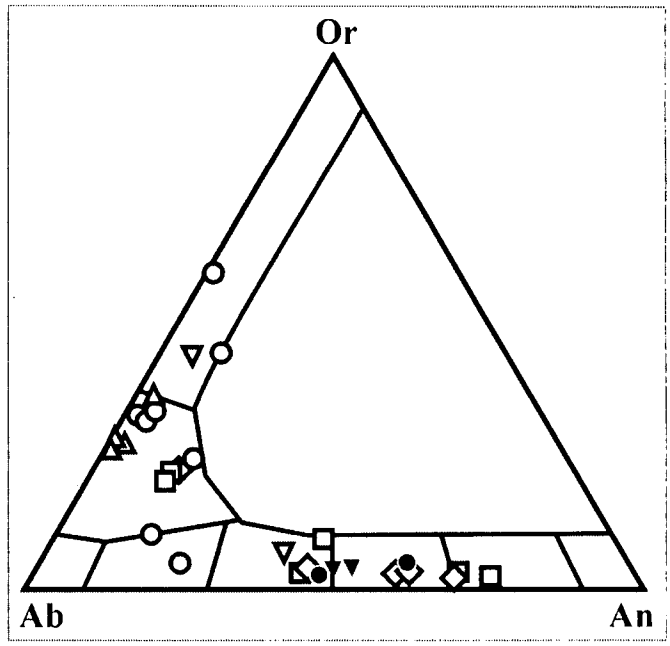

Fig. 3. Feldspars in An-Ab-Or diagram (mol.%). Symbols as in Fig. 1.

Table 3. Representative chemical analyses of feldspars

Sample	202/	202/	202/	180/	180/	180/	180/	180/	180/	186/	186/	251/	251/	256/	256/	256/	256/
No.	9C	10R	18M	23C	24R	25C	26R	27M	28M	12C	13R	23C	20	30C	29C	27R	28
Rock type		RY					TR			TR		TA				BTA	
SiO_2	67,52	67,36	68,33	65,21	66,59	66,61	65,75	64,21	67,22	63,78	68,59	57,31	64,79	50,31	51,15	59,30	62,37
TiO_2								0,08		0,01	0,04	0,07	0,03	0,01	0,11	0,08	0,03
Al_2O_3	18,57	17,95	16,78	20,04	18,54	19,58	18,93	22,53	17,05	22,65	17,91	26,35	21,50	31,65	31,08	23,86	22,68
FeO	0,36	0,16	0,47	0,20	0,20	0,25	0,47	0,33	0,38	0,09	0,06	0,03	0,07	0,08	0,05	0,06	0,01
MnO	0,11	0,03		0,14	0,07	0,13	0,01	0,03	0,01			0,04	0,01	0,00	0,05		
MgO								0,02				0,03		0,02	0,04		
BaO			0,09		0,23	0,01	0,26			0,23	0,18			0,05	0,19	0,41	0,23
CaO	0,57	0,67	0,19	3,34	1,09	3,25	2,16	2,62	0,17	4,72	0,44	8,84	2,82	14,62	13,65	8,55	2,95
Na_2O	8,24	7,16	8,52	7,00	7,01	8,27	5,60	9,01	4,51	8,18	7,39	6,06	7,78	2,61	3,07	5,06	7,83
K_2O	4,91	6,61	4,68	4,25	5,86	1,70	7,17	1,15	10,14	0,78	5,58	0,49	3,58	0,32	0,45	1,93	4,05
P_2O_5	0,06			0,06	0,06	0,06	0,06		0,11								
Total	100,3	99,94	99,06	100,2	99,65	99,86	100,4	99,98	99,59	100,4	100,1	99,22	100,5	99,67	99,84	99,25	100,1
								Number of ions per 32(O)									
Si	11,99	12,07	12,27	11,63	11,96	11,78	11,82	11,35	12,21	11,25	12,17	10,35	11,48	9,19	11,58	10,75	11,19
Al	3,888	3,790	3,551	4,214	3,926	4,083	4,013	4,695	3,650	4,709	3,745	5,608	4,487	6,811	4,314	5,097	4,793
Ti								0,011		0,001	0,005	0,010	0,004	0,001		0,011	4,000
P	0,009			0,009	0,009	0,009	0,008		0,170						0,042		
Fe^{2+}	0,053	0,024	0,071	0,030	0,030	0,037	0,071	0,049	0,058	0,013	0,008	0,005	0,010	0,012		0,009	2,000
Mn	0,017	0,005		0,021	0,011	0,019	0,002	0,004	0,002	0,000	0,000	0,006	0,002	0,000			
Mg								0,005		0,000	0,000	0,008	0,000	0,005			
Ba			0,006		0,016	0,001	0,018			0,016	0,013			0,004	0,270	0,029	0,016
Ca	0,108	0,129	0,037	0,638	0,210	0,616	0,416	0,496	0,033	0,893	0,084	1,712	0,535	2,862	0,199	1,662	0,567
Na	2,838	2,489	2,966	2,421	2,442	2,837	1,953	3,089	1,588	2,800	2,544	2,123	2,674	0,925	1,901	1,780	2,724
K	1,113	1,512	1,072	0,967	1,343	0,384	1,645	0,259	2,350	0,176	1,264	0,113	0,809	0,075	1,664	0,447	0,927
Z	15,89	15,86	15,82	15,85	15,89	15,87	15,84	16,06	16,03	15,96	15,92	15,96	15,97	16,00	15,90	15,85	15,98
X	4,129	4,159	4,152	4,077	4,052	3,894	4,105	3,902	4,031	3,899	3,918	3,977	4,034	3,884	4,105	3,938	10,23
Ab	69,9	60,3	72,7	60,1	60,9	73,9	48,4	80,3	40,0	72,1	65,1	53,8	66,6	23,9	47,1	45,4	64,3
An	2,7	3,1	0,9	15,9	5,2	16,1	10,3	12,9	0,8	23,0	2,2	43,4	13,3	74,0	4,9	42,4	13,4
Or	27,4	36,6	26,3	24,0	33,5	10,0	40,8	6,8	59,2	4,5	32,4	2,9	20,1	1,9	41,2	11,4	21,9
Cn			0,1		0,4	0,0	0,5	0,2		0,4	0,3	0,0	0,0	0,1	6,7	0,7	0,4

Table 3. continued

Sample No.	Z22/1	Z22/2	Z22/3M	255/32	255/40	P1/1C	P1/1R	P1/2M	Z-13C	Z-13R	Z-13	Z14/1	Z14/2
Rock type		TB		TB			BA			BA		ON	
SiO_2	55,69	55,78	56,08	58,96	62,98	52,87	52,39	52,70	53,04	55,47	63,07	52,98	54,85
TiO_2	0,31	0,38	0,34	0,08			0,15	0,26	0,23	0,33	0,22	0,31	0,35
Al_2O_3	27,50	27,01	27,03	25,22	19,91	29,79	29,38	29,22	29,62	28,00	22,05	28,81	27,81
FeO	0,94	0,79	0,65	0,09	0,27	0,56	0,84	1,27	0,64	0,70	0,70	0,66	0,78
MnO		0,08		0,03		0,09	0,14	0,28	0,05	0,08	0,25		0,22
MgO	0,03	0,04	0,03	0,00		0,06	0,05	0,04	0,06	0,05	0,06	0,08	0,10
BaO	0,26	0,25		0,95	3,75	0,25	0,39	0,23	0,33	0,26	0,37		
CaO	10,19	9,14	9,95	8,03	1,01	12,57	11,89	11,63	10,94	9,06	2,85	12,18	9,97
Na_2O	4,97	5,47	5,48	6,07	5,33	4,12	4,00	4,14	4,64	5,98	7,07	4,10	4,98
K_2O	0,62	0,55	0,51	1,13	7,09	0,29	0,56	0,37	0,41	0,66	3,81	0,81	0,43
P_2O_5		0,25	0,12				0,46	0,48	0,45	0,28	0,52	0,31	0,34
Total	100,51	99,74	100,19	100,56	100,34	100,60	100,25	100,62	100,41	100,87	100,97	100,24	99,83
Number of ions per 32 (O)													
Si	10,038	10,099	10,105	10,581	11,587	9,570	9,529	9,548	9,588	9,956	11,217	9,620	9,923
Al	5,842	5,764	5,740	5,330	4,314	6,355	6,298	6,239	6,311	5,923	4,622	6,166	5,930
Ti	0,042	0,052	0,046	0,011			0,021	0,035	0,031	0,045	0,029	0,042	0,048
P		0,038	0,018		0,042		0,071	0,074	0,069	0,043	0,078	0,048	0,052
Fe^{2+}	0,142	0,120	0,098	0,014		0,085	0,128	0,192	0,097	0,105	0,104	0,100	0,118
Mn		0,012		0,005		0,014	0,022	0,043	0,008	0,012	0,038		0,034
Mg	0,008	0,011	0,008			0,016	0,014	0,011	0,016	0,013	0,016	0,022	0,027
Ba	0,018	0,018		0,067	0,270	0,018	0,028	0,016	0,023	0,018	0,026		
Ca	1,968	1,773	1,921	1,544	0,199	2,438	2,317	2,258	2,119	1,742	0,543	2,370	1,932
Na	1,737	1,920	1,914	2,112	1,901	1,446	1,411	1,454	1,626	2,081	2,438	1,443	1,747
K	0,143	1,127	0,117	0,259	1,664	0,067	0,130	0,086	0,095	0,151	0,864	0,188	0,099
Z	15,923	15,953	15,909	15,911	15,901	15,925	15,918	15,896	15,999	15,966	15,947	15,876	15,952
X	4,016	3,981	4,059	4,012	4,105	4,083	4,048	4,060	3,984	4,123	4,029	4,123	3,957
Ab	44,9	50,0	48,4	53,0	47,1	36,4	36,3	38,1	42,1	52,1	63,0	36,1	46,2
An	50,9	46,2	48,6	38,8	4,9	61,4	59,6	59,2	54,9	43,6	14,0	59,2	51,1
Or	3,7	3,3	3,0	6,5	41,2	1,7	3,3	2,2	2,5	3,8	22,3	4,7	2,6
Cn	0,5	0,5		1,7	6,7	0,5	0,7	0,4	0,6	0,5	0,7		

C - core, R - rim (of phenocrysts), P - phenocryst, M - matrix

anorthoclase rimmed by sanidine) in K-feldspars phenocrysts in the trachytes (Table 3). Trachyte crystallisation need not lead to complete resorption of plagioclase Nekvasil (1992). The extent of resorption of plagioclase will depend upon pressure, bulk H_2O and the bulk chemistry of the melt. Partial to complete resorption of plagioclase can occur in Q-normative trachytes under H_2O buffered conditions, particularly if silica saturation is not attained until the later stages of crystallisation.

Plagioclases predominate in the more basic members of the WAS (trachyandesite and basaltic trachyandesite). They prevail in the matrix (up to 50 vol.%), as phenocrysts they are more rare. Partially resorbed oligoclase cores (to anorthoclase) in trachyte have been discussed above. Plagioclase composition in the intermediate rocks (trachyandesite, basaltic trachyandesite) is andesine (An_{43-42}). and in basanite, tephrite and trachybasalt is labradorite (An_{64-51}) with low contents of Or- and Cn-components (Table 3). Plagioclases in trachybasalts show a minimum variability in An-content within the range of andesine. Rare plagioclase is K-andesines (Table 3, No. 255/32R) in trachybasalt. This, together with the zero "ordering index" (Oi), indicates their high-temperature origin. They are characterised by high BaO content (up to 1 wt.%).

Nepheline was only detected in WAS rocks in the matrix of trachyandesite from Třebouňský vrch and basaltic trachyandesite from Doubravický vrch Hills. The nepheline compositions (Table 4) plotted in the ternary diagram Ne-Ks-Qz-H_2O system at 700 °C and 1 kbar p_{H2O} (Fig. 4) are not so far from the "Barth join", which denotes the compositional trend for natural nephelines (Dollase and Thomas, 1978). In accordance with the criteria of Wilkinson and Hensel (1994) the studied nephelines crystallised at temperatures lower than 700°C. In contrast to the WAS, nepheline is common in the matrix of olivine nephelinite, basanite and tephrite. Both sparse homogeneous microphenocrysts ($Ne_{70-72}Ks_{24}Q_{03-05}$) and interstitial patches of nepheline are characteristic for melilite-bearing olivine nephelinite from Chloumecký vrch Hill. Large crystals (up to 12 mm in size) enriched in Ne-component ($Ne_{76-79}Ks_{19-20}Q_{02-04}$) occur in the ijolite pegmatoidal segregations in the melilite-free olivine nephelinite of Podhorní vrch Hill (Ulrych et al., 2000c). The nephelines reflect host rock chemistry. The proximity to the Ne – Ks join, higher Ks and lower Qz of nephelines from the ijolite is consistent with the segregation bulk chemistry compared with parent rocks (cf. Fig. 4). SAS nepheline is relatively richer in Ks-component and distinctly lower in Q-component (<5) (Fig. 4). Analcimization is confined to crystal rims and cleavage, only.

Table 4. Representative chemical analyses of nephelines and analcimes

Sample No.	251/1	251/2	256/1	29/C	29/R	29/C	29/R	Z14/1	Z14/2	Z16/1V	Z16/2M	Z19/1
Rock type	TA		BTA	ON		Ijolite in ON		BA		MON		TE
SiO_2	44,48	44,26	45,09	42,30	42,21	41,89	41,13	42,66	42,95	42,11	42,09	56,24
TiO_2	0,00	0,00	0,06	0,05	0,08	0,05	0,03	0,18	0,25	0,19	0,11	
Al_2O_3	33,01	33,01	32,61	33,69	33,12	33,42	33,98	32,52	32,96	33,47	32,31	22,26
Fe_2O_3	0,78	0,95	0,92	1,62	1,09	1,17	1,11	0,93	0,88	0,82	1,29	0,40
MnO						0,02	0,03					0,01
MgO						0,05	0,04	0,57	0,54	0,76	0,71	0,07
CaO	1,15	1,28	1,07	0,51	0,52	0,15	0,14	2,18	1,86	1,60	3,23	5,34
Na_2O	16,87	16,45	16,65	16,11	16,18	16,38	16,56	15,78	15,76	14,42	14,45	7,38
K_2O	3,56	3,70	3,52	5,80	5,89	6,29	6,36	4,47	4,10	7,37	6,06	1,20
Total	99,85	99,65	99,92	100,08	99,09	99,42	99,38	99,29	99,30	100,74	100,25	92,90
Number of ions per 4 (O)												48 (O)
Si	2,117	2,112	2,141	2,020	2,056	2,039	2,014	2,063	2,067	2,028	2,037	32,518
Al	1,852	1,857	1,825	1,878	1,901	1,918	1,943	1,853	1,870	1,900	1,843	15,169
Ti			0,002	0,002	0,003	0,002	0,001	0,007	0,009	0,007	0,004	
Fe^{3+}	0,028	0,034	0,033	0,059	0,040	0,043	0,041	0,034	0,032	0,030	0,047	0,174
Mn						0,001	0,001					0,005
Mg						0,004	0,003	0,041	0,039	0,055	0,051	0,060
Ca	0,059	0,065	0,054	0,027	0,027	0,008	0,007	0,113	0,096	0,083	0,167	3,308
Na	1,557	1,522	1,533	1,522	1,528	1,546	1,572	1,479	1,471	1,346	1,356	8,273
K	0,216	0,225	0,213	0,361	0,366	0,391	0,397	0,276	0,252	0,453	0,374	0,885
Z	3,997	4,003	4,001	3,959	4,000	4,002	3,999	3,956	3,977	3,964	3,931	47,861
X	1,832	1,813	1,800	1,910	1,921	1,950	1,980	1,909	1,857	1,936	1,949	12,526
Ne (mol.%)	77,85	76,82	75,43	75,80	76,30	76,42	78,60	80,54	78,42	72,28	70,39	
Ks	10,81	11,37	10,49	18,00	18,30	19,33	19,85	15,01	13,42	24,31	24,44	
Qz	11,34	11,81	14,08	6,20	5,40	4,25	1,55	4,45	8,15	3,41	5,17	

Analcime patches mainly result from a low-temperature transformation of nepheline or plagioclase in the matrix of basanites (Okrouhlé Hradiště, Polom, Vlčí hora and Lysina hills) and basanite of Prachomety II (for analyses see Table 4). Analcime occurs rarely in vesicles.

Melilite is present in matrix of melilite-bearing olivine nephelinite at Český Chloumek (Table 5). Anomalous, large rusty crystals (up to 18 mm in length) occur in the ijolite pegmatoidal segregations in the melilite-free olivine nephelinite of Podhorní vrch Hill (Ulrych et al., 2000c). Melilite of the ijolite is characterized by appreciable amount of soda-melilite and ferroåkermanite end-members, accompanied by åkermanite molecule (Table 5) in comparison to usual chemical composition of melilite in the matrix (cf. Pivec et al., 1998). Such replacement of Ca (Mg,Al) by Na (Fe^{2+},Fe^{3+}) in melilite structure causes a marked lowering of the melting point of the magma (Yoder, 1973).

Olivine occurs in olivine nephelinite and basanite as (i) xenocrysts from disaggregated mantle xenoliths (>2-3 mm, Fo_{88-90}), (ii) euhedral phenocrysts (about 10 vol.%, 0.5-1 mm, Fo_{66-76}) and (iii) rare irregular matrix grains. Olivine of all types is mostly substantially altered (iddingsitisation and serpentinization). Phenocryst olivine in olivine nephelinite has a restricted compositional range (Fo_{81-84}, CaO = 0.3-0.7 wt.%), in contrast with the groundmass (Fo_{59-68}), which is often serpentinised (Table 6). The exceptional accessory olivine of tephrite from Okrouhlé Hradiště Hill is Fo-rich poor (Fo_{49-52}, CaO = 0.8-0.9 wt.%).

Clinopyroxene occurs in minor to substantial amounts in major rocks of the WAS. It occurs as phenocryst and in groundmass of in trachyte occurring in Prachometský vrch Hill.

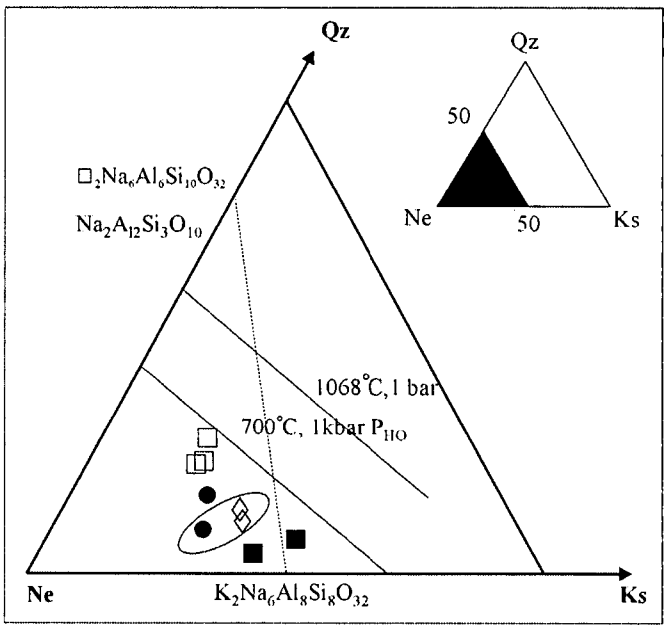

Fig. 4. Nephelines in Ne-Ks-Qz diagram. The dashed line ("Barth join") denotes the composition of natural nephelines (Dollase and Thomas 1978); the full line solution of feldspar in nepheline at 1068 °C, 1 bar (Donnay et al. 1959, Wilkinson and Hensel 1994); the dashed-dot line marks the limit of solid solutions at 700 °C (Hamilton 1961). Shaded area corresponds to nepheline composition of coarse-grained nepheline-clinopyroxene-melilite/leucite + K-feldspar exsolution in olivine nephelinite of Podhorní vrch Hill (Ulrych et al. 2000c). Symbols as in Fig. 1.

Phenocryst in all the rocks occurs as hypautomorphic, columnar crystal (0.2 to 2 mm in size) showing weak concentric and/or sectoral zoning (e.g., in the trachybasalt of Zbraslavský vrch Hill). Their compositions (Table 7) are diopside (Morimoto, 1988; Fig. 5), they often plot above the (Wo>50) boundary of the "fassaite" field, reflecting high Ti, Al, and Fe^{3+} contents. Clinopyroxene megacrysts (up to 50 mm in size) from basanite and tuffs from Vlčí hora Hill reveal the same composition (Ulrych and Kašpar, 1977). Clinopyroxenes in trachyte from Prachometský vrch Hill and in most trachyandesitic rocks are relatively enriched in Fs-component, more so than clinopyroxenes from trachytic rocks of Siebengebirge (Vieten, 1979, 1980). Both WAS and SAS clinopyroxenes contain minor Na_2O and MnO, which are highest in trachyte (maximum = 1.75 and 2.56 wt.%, respectively).

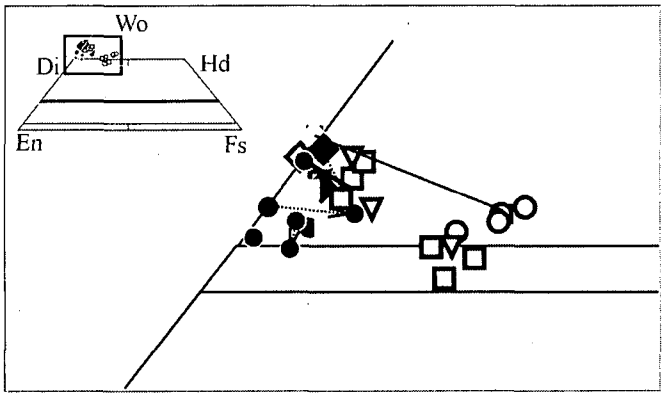

Fig. 5. Clinopyroxenes in Morimoto's ed. (1988) classification diagram. Dashed lines join core and rim, arrows point to the rim. Symbols as in Fig. 1.

Table 5. Representative chemical analyses of melilite

Sample No.	Z16/1C	Z16/2R	M2/C	M2/R
Rock type	MON		Ijolite segr. in ON	
SiO_2	42,86	43,75	42,89	40,77
TiO_2	0,26	0,21	0,16	0,16
Al_2O_3	7,07	7,97	6,36	7,37
FeO	4,23	4,06	5,79	7,16
MnO	0,23	0,18	0,10	0,22
MgO	7,58	6,81	7,07	4,74
BaO			0,02	0,05
CaO	34,38	33,04	32,13	33,90
Na_2O	3,02	3,25	5,61	5,10
K_2O	0,27	0,30	0,09	0,10
Total	99,90	99,57	100,22	99,57
Number of ions per 14 (O)				
Si	3,907	3,968	3,939	3,821
Al	0,760	0,852	0,688	0,814
Ti	0,018	0,014	0,011	0,011
Fe	0,322	0,308	0,445	0,561
Mn	0,018	0,014	0,008	0,017
Mg	1,030	0,921	0,968	0,662
Ca	3,358	3,211	3,162	3,404
Ba			0,001	0,002
Na	0,534	0,572	0,999	0,927
K	0,031	0,035	0,011	0,012
Na mel	26,88	29,03	32,75	39,96
Geh	5,69	7,12	14,8	8,54
Aker	62,54	46,55	46,07	32,5
Di mel	5,17	13,25	6,38	19
Wo	0,28	4,06		

Table 6. Representative chemical analyses of olivine

Sample No.	Z13/1	Z13/2	P1/1	P1/2	Z15/1	Z15/2	Z14/P	Z14/2M	Z14/3M	Z16/1	Z19/1C	Z19/1R	Z19/2
Rock type	BA		BA		ON		ON			MON	TE		
SiO_2	38,18	38,70	39,63	39,30	38,20	39,54	39,49	39,08	39,36	39,91	39,13	39,13	38,85
TiO_2	0,25	0,26	0,37	0,24	0,26	0,21	0,29	0,31	0,24	0,12	0,23	0,38	0,23
Al_2O_3	0,48	0,40	1,07	1,23	0,53	0,61	0,37	0,56	0,62	0,44	1,59	2,09	2,24
FeO	22,58	20,73	26,63	25,22	21,80	22,41	22,08	22,69	22,42	14,67	35,33	34,90	35,95
MnO	1,05	0,79	0,78	0,88	0,49	0,73	0,64	0,77	0,75	0,34	0,90	0,97	1,01
NiO	n.d.	n.d.	n.d.	n.d.	n.d.	n.d.	n.d.	0,30	0,19	n.d.	n.d.	n.d.	n.d.
MgO	37,05	38,44	30,53	31,74	37,73	37,32	36,57	35,96	36,10	41,41	22,03	21,74	20,84
CaO	0,47	0,31	0,71	0,61	0,56	0,53	0,43	0,33	0,30	0,53	0,80	0,80	0,88
Total	100,06	99,63	99,72	99,22	99,57	101,35	99,87	100,00	99,98	97,42	100,01	100,01	100,00
Number of ions per 4(O)													
Si	1,995	2,009	2,101	2,083	1,995	2,027	2,051	2,037	2,047	2,051	2,153	2,147	2,144
Al^{IV}	0,005				0,005								
Al^{VI}	0,025	0,024	0,067	0,077	0,027	0,037	0,023	0,034	0,038	0,027	0,103	0,135	0,146
Ti	0,010	0,010	0,015	0,010	0,010	0,008	0,011	0,012	0,009	0,005	0,010	0,016	0,010
Fe	0,987	0,900	1,181	1,118	0,952	0,961	0,959	0,989	0,975	0,631	1,625	1,601	1,659
Mn	0,046	0,035	0,035	0,040	0,022	0,032	0,028	0,034	0,033	0,015	0,042	0,045	0,047
Ni								0,010	0,008				
Mg	2,886	2,974	2,413	2,508	2,937	2,852	2,831	2,795	2,798	3,173	1,807	1,778	1,715
Ca	0,026	0,017	0,040	0,035	0,031	0,029	0,024	0,018	0,017	0,029	0,047	0,047	0,052
Fo	73,2	76,3	65,8	67,8	74,5	73,6	73,7	72,6	73,0	82,5	51,5	51,2	49,4
Fa	25,0	22,6	32,2	30,2	24,2	24,8	25,0	25,7	25,5	16,4	46,2	46,1	47,8
Te	1,2	0,6	1,0	1,1	0,6	0,8	0,7	0,9	0,9	0,4	1,2	1,3	1,4

Table 7. Representative chemical analyses of clinopyroxenes

Sample No.	186/ 7C	186/ 9R	186/ 8M	186/ 1M	251/ 3C	251/ 4R	251/ 2C	251/ 1R	256/ 1C	256/ 2R	256/ 7M	256/ 5M	255/ 1C	255/ 2R	255/ 3R	255/ 7M
Rock type	TR				TA				BTA				TB			
SiO_2	49,81	49,36	49,97	49,36	48,59	47,77	49,88	45,87	50,53	45,92	49,51	45,07	51,01	44,37	47,50	41,71
TiO_2	0,54	0,91	0,84	1,06	1,57	1,92	1,75	2,49	0,42	3,12	1,93	3,34	0,39	3,47	1,95	5,29
Al_2O_3	2,70	1,48	1,70	2,49	4,77	4,50	5,18	8,12	2,47	5,78	3,54	6,94	2,22	6,80	5,68	9,41
FeO	12,81	15,10	15,13	14,80	8,42	8,63	9,99	10,54	13,17	9,17	7,96	9,32	12,45	8,66	8,73	8,52
MnO	1,31	2,51	2,56	2,22	0,21	0,23	0,35	0,34	0,35	0,26		0,21	0,69	0,11	0,17	0,22
MgO	10,55	8,50	8,15	8,76	12,25	12,61	12,07	11,06	10,69	11,30	13,29	10,43	10,68	11,11	11,95	10,92
CaO	21,43	20,24	20,70	20,20	22,78	22,97	20,68	20,49	20,54	22,79	21,91	22,43	20,39	23,71	22,76	21,88
Na_2O	1,00	1,75	1,73	1,68	1,20	1,08	0,78	0,80	1,16	1,11	1,26	1,47	1,74	0,81	0,79	1,36
K_2O						0,09			0,12	0,16	0,11	0,15	0,13	0,15	0,20	0,19
Total	100,15	99,85	100,78	100,57	99,79	99,80	100,68	99,71	99,45	99,54	99,51	99,46	99,70	99,19	99,73	99,50
Number of ions per 4 cations and 6 (O)																
Si	1,882	1,893	1,902	1,875	1,806	1,777	1,854	1,724	1,917	1,723	1,839	1,695	1,921	1,673	1,774	1,564
Al^{IV}	0,118	0,067	0,076	0,111	0,194	0,197	0,146	0,276	0,083	0,256	0,155	0,305	0,079	0,302	0,226	0,416
Fe^{3+}		0,040	0,022	0,014	0,000	0,026	0,000	0,000	0,000	0,021	0,006	0,000	0,000	0,024	0,000	0,021
Al^{VI}	0,003				0,015		0,081	0,084	0,028			0,003	0,019		0,024	0,000
Ti	0,015	0,026	0,024	0,030	0,044	0,054	0,049	0,070	0,012	0,880	0,054	0,094	0,011	0,098	0,055	0,149
Cr															0,000	0,000
Fe^{3+}	0,157	0,184	0,178	0,188	0,177	0,198	0,024	0,109	0,122	0,189	0,149	0,227	0,171	0,196	0,159	0,246
Fe^{2+}	0,247	0,260	0,282	0,268	0,085	0,044	0,287	0,222	0,296	0,077	0,093	0,065	0,221	0,052	0,114	0,001
Mg	0,594	0,486	0,462	0,496	0,679	0,699	0,669	0,620	0,605	0,632	0,736	0,585	0,600	0,625	0,665	0,610
Mn	0,042	0,082	0,083	0,071	0,007	0,007	0,011	0,011	0,011	0,008		0,007	0,022	0,004	0,005	0,007
Ca	0,868	0,832	0,844	0,822	0,907	0,915	0,824	0,825	0,835	0,916	0,872	0,904	0,823	0,958	0,911	0,879
Na	0,073	0,130	0,128	0,124	0,086	0,078	0,056	0,058	0,085	0,081	0,091	0,107	0,127	0,059	0,057	0,099
K						0,004			0,006	0,008	0,005	0,007	0,006	0,007	0,010	0,009
Wo	50,7	52,7	53,2	51,8	53,6	55,2	44,9	47,8	47,4	56,4	51,3	58,1	49,5	58,6	53,1	59,0
En	34,7	30,8	29,1	31,3	40,3	42,1	36,4	35,9	34,3	38,9	43,3	37,6	36,1	38,2	38,8	41,0
Fs	14,4	16,5	17,7	16,9	5,0	2,7	15,6	12,9	16,8	4,8	5,5	4,2	13,3	3,2	6,6	0,0
Jd	0,2	0,0	0,0	0,0	0,9	0,0	3,1	3,4	1,6	0,0	0,0	0,2	1,2	0,0	1,4	0,0

Table 7. continued

Sample No.	Z13/1 C	Z13/1 R	Z13/2 M	Z19/1	Z19/2 M	P1/ 1C	P1/ 2C	Z15/1	Z15/2	Z24/1 C	Z24/1 R	Z24/2 M	Z14/1 C	Z14/1 R	Z14/2 M	Z16/1 C	Z16/1 R	Z16/C
Rock type	BA			BA		BA		ON		ON			ON			MON		
SiO_2	45,13	46,24	43,57	45,30	46,47	44,03	42,12	44,90	45,13	47,48	44,98	42,43	50,81	48,98	49,63	45,36	49,37	45,18
TiO_2	3,92	2,80	3,23	2,63	2,54	3,73	4,42	3,33	3,92	2,16	3,24	4,14	0,97	1,13	1,53	2,92	1,32	2,68
Al_2O_3	6,75	5,69	7,68	7,66	7,42	6,84	8,77	7,46	6,75	4,77	6,49	9,66	5,53	6,91	4,68	7,02	2,17	7,30
Cr_2O_3	0,15	0,25	0,23	0,36	0,42	0,23	0,27	0,10	0,15	0,35	0,37	0,24	1,17	1,56	0,79	0,34	0,30	0,27
FeO	7,13	9,03	8,87	6,70	6,31	7,62	7,99	7,46	7,13	8,55	8,00	8,90	4,60	4,87	5,29	7,89	12,98	7,22
MnO	0,32	0,41	0,27	0,31	0,23	0,17	0,16	0,34	0,32	0,45	0,34	0,37	0,37	0,35	0,44	0,29	0,39	0,43
MgO	11,90	12,10	11,45	12,15	12,45	11,89	11,17	11,90	11,90	12,56	11,59	10,67	14,55	13,18	13,70	11,62	9,76	11,26
CaO	23,30	23,45	23,10	24,27	23,75	23,93	24,13	23,68	23,30	23,41	23,93	22,27	21,11	21,16	22,09	23,82	23,07	24,50
Na_2O	1,18	0,60	1,04	0,69	0,70	0,88	0,84	0,92	1,18	0,60	1,01	1,20	1,14	1,41	1,07	0,96	0,61	0,85
K_2O	0,17	0,03	0,17	0,11	0,05	0,12	0,11	0,01	0,17	0,00	0,15	0,13	0,25	0,18	0,08	0,18	0,21	0,12
Total	99,95	100,60	99,61	100,18	100,34	99,44	99,98	100,10	99,95	100,33	100,10	99,94	100,40	99,73	100,00	100,40	100,18	99,81
Number of ions per 4 cations and 6 (O)																		
Si	1,678	1,720	1,629	1,677	1,715	1,649	1,573	1,667	1,678	1,767	1,675	1,584	1,848	1,800	1,838	1,682	1,880	1,685
Al^{IV}	0,296	0,249	0,339	0,323	0,285	0,302	0,386	0,326	0,296	0,209	0,285	0,416	0,152	0,200	0,162	0,307	0,097	0,315
Fe^{3+}	0,026	0,030	0,032	0,000	0,000	0,000	0,000	0,006	0,026	0,024	0,040	0,000	0,000	0,000	0,000	0,011	0,023	0,000
Al^{VI}	0,000	0,000	0,000	0,011	0,038	0,000	0,000	0,000	0,000	0,000	0,000	0,009	0,085	0,099	0,043	0,000	0,000	0,006
Ti	0,110	0,078	0,091	0,073	0,070	0,105	0,124	0,093	0,110	0,060	0,091	0,116	0,026	0,031	0,043	0,081	0,038	0,075
Cr	0,004	0,007	0,007	0,010	0,012	0,007	0,008	0,003	0,004	0,010	0,011	0,007	0,034	0,045	0,023	0,010	0,009	0,008
Fe^{3+}	0,192	0,160	0,246	0,207	0,145	0,239	0,250	0,210	0,192	0,145	0,209	0,260	0,072	0,102	0,091	0,223	0,091	0,218
Fe^{2+}	0,004	0,090	0,000	0,000	0,049	0,000	0,000	0,015	0,004	0,096	0,000	0,018	0,068	0,047	0,073	0,011	0,299	0,007
Mn	0,010	0,013	0,008	0,010	0,007	0,005	0,005	0,011	0,010	0,014	0,011	0,012	0,011	0,011	0,014	0,009	0,012	0,013
Mg	0,659	0,671	0,638	0,670	0,685	0,664	0,622	0,659	0,659	0,697	0,643	0,594	0,789	0,722	0,756	0,642	0,554	0,626
Ca	0,928	0,935	0,926	0,963	0,939	0,960	0,967	0,942	0,928	0,933	0,955	0,891	0,823	0,833	0,877	0,946	0,941	0,979
Na	0,086	0,043	0,075	0,050	0,050	0,064	0,061	0,066	0,085	0,043	0,073	0,087	0,080	0,100	0,077	0,069	0,045	0,061
K	0,008	0,001	0,008	0,005	0,002	0,006	0,005	0,000	0,008	0,000	0,007	0,006	0,011	0,008	0,004	0,008	0,010	0,005
Wo	58,3	55,1	59,2	58,6	54,9	59,1	60,8	58,3	58,3	54,1	59,7	58,9	46,8	49,0	50,1	59,2	52,4	60,5
En	41,4	39,6	40,8	40,8	40,0	40,9	39,2	40,8	41,4	40,4	40,3	39,3	44,8	42,4	43,3	40,2	30,9	38,7
Fs	0,2	5,3	0,0	0,0	2,9	0,0	0,0	1,0	0,2	5,6	0,0	1,2	3,9	2,8	4,2	0,7	16,7	0,5
Jd	0,0	0,0	0,0	0,7	2,2	0,0	0,0	0,0	0,0	0,0	0,0	0,6	4,6	5,8	2,4	0,0	0,0	0,4

The compositional variation of clinopyroxene in basanites and tephrites is largely a function of ferrian diopside and ferrian fassaite variants. High fO_2 during crystallization is reflected in high Fe^{3+} in both octahedral and (tetrahedral) positions (calculated on the base of stoichiometry). This translates to a lower Fs-component and almost all clinopyroxenes are characterised by low Si-contents compensated by substitution of Al^{IV} and Fe^{IV}.

Amphibole is a minor phase in rhyolite and trachyte of Špičák Hill. Microphenocrysts are columnar, with strong pleochroism and typically rimmed by biotite. The alkali amphiboles are Mn-varieties (up to 6.1 wt.% MnO), manganoan magnesioriebeckite in rhyolite and manganoan winchite in trachyte using Leake's (1978) classification (Table 8). Magnesioarfvedsonite of similar composition is known from alkali trachyte in Siebengebirge (Vieten, 1965; Vieten et al., 1988) and fenites in the Čistá Massif (Ulrych, 1978).

Strongly corroded, originally euhedral phenocrysts (up to 12 cm) of kaersutite rimmed by clinopyroxene

Table 8. Representative chemical analyses of amphiboles

	magnesio riebeckite	winchite	kaersutite		kaersutite megacryst	kaersutite veinlet
Sample No.	202/1	180/1	251/11	251/10	P1/1R	P1/2M
Rock type	RY	TR	TA		BA	
SiO_2	54,07	53,72	39,34	39,09	39,00	39,15
TiO_2	0,27	0,52	5,09	5,44	5,03	5,10
Al_2O_3	0,77	1,45	12,38	12,64	13,56	13,55
$Fe_2O_{3\,tot}$	17,66	12,11				
Cr_2O_3						
FeO			11,18	12,06	8,54	9,52
MnO	6,06	4,43	0,14	0,13	0,32	0,34
MgO	8,43	15,05	13,01	11,83	13,85	13,09
CaO	2,98	7,26	12,09	12,12	12,69	12,57
Na_2O	7,39	3,63	2,67	2,81	2,50	1,95
K_2O	0,84	0,71	1,61	1,37	2,14	1,96
H_2O^+	2,07	2,12	2,00	2,00	1,98	1,98
Total	100,54	101,00	99,51	99,49	99,61	99,21
Number of ions per 23 (O)						
Si^{IV}	7,849	7,608	5,889	5,872	5,788	5,836
Al^{IV}	0,132	0,242	2,111	2,128	2,212	2,164
Ti						
Fe^{IV}	0,019	0,150				
Al^{VI}			0,073	0,109	0,159	0,216
Ti	0,029	0,055	0,573	0,614	0,561	0,572
Cr						
Fe^{3+}	1,385	1,141				
Fe^{2+}	0,525	0,000	1,400	1,515	1,06	1,187
Mg	1,824	3,178	2,903	2,649	3,064	2,908
Mn	0,745	0,531	0,018	0,017	0,04	0,043
Ca	0,464	1,101	1,939	1,951	2,018	2,007
Na					0,097	0,066
Na	2,080	0,997	0,775	0,818	0,622	0,498
K	0,156	0,128	0,307	0,263	0,405	0,373

Table 9. Representative chemical analyses of biotite

Sample No.	180/ 1C	180/ 1R	180/ 2C	180/ 2R
Rock type	TR			
SiO_2	36,02	35,46	38,01	37,49
TiO_2	4,07	5,90	4,93	5,50
Al_2O_3	14,25	14,91	13,72	15,80
FeO	15,33	16,73	14,17	13,33
MnO	1,41	1,31	1,77	1,46
MgO	14,82	13,02	14,82	13,69
CaO				0,01
Na_2O	0,57	0,69	0,81	0,56
K_2O	9,35	8,46	9,31	9,33
Total	95,82	96,48	97,54	97,17
Number of ions per 22 (O)				
Si	5,675	5,558	5,833	5,730
Al^{IV}	2,325	2,442	2,167	2,270
Al^{VI}	0,319	0,310	0,313	0,574
Ti	0,482	0,696	0,569	0,632
Fe^{2+}	2,020	2,193	1,819	1,704
Mn	0,188	0,174	0,230	0,189
Mg	3,481	3,042	3,391	3,119
Ca				0,002
Na	0,174	0,210	0,241	0,166
K	1,879	1,692	1,823	1,819
Z	8,000	8,000	8,000	8,000
Y	6,490	6,415	6,322	6,218
X	2,053	1,902	2,064	1,987

and titanian magnetite occur in trachyandesite. Their chemical composition is close to that of amphibole megacrysts worldwide. They are also similar to polycrystalline aggregates (15 by 10 cm) of oxykaersutite in basanite and its tuff from the nearby Vlčí hora Hill at Černošín (Ulrych, 1986). The basanite includes also infrequent oxykaersutite veinlets as a result of re-equilibration (?) between melt and megacrysts (phenocrysts or cumulates)?

Biotite is found only in trachyte from Špičák Hill. It occurs in the form of (i) rare euhedral phenocrysts (up to 4 mm) and smaller inclusions in the alkali feldspar phenocrysts (Mg# = 0.61-0.62) and (ii) rims of amphibole microphenocrysts composed of subhedral dark brown flakes (Mg# = 0.58), locally opaque due to tiny inclusions of titanian magnetite. Micas are typically Fe-Mg biotite, exceptionally phlogopite (Table 9). A low content of micas and amphiboles in rocks of both series gives evidence of a relatively dry parental magma.

Titanomagnetite in trachytes (manganoan titanian magnetite) is characterised by a high amount of Mn (up to 6.6 wt.% MnO, cf. Table 10). The higher contents of Ti (up to 19.9 wt.%), Al, Cr, Mg, and V are characteristic, especially for titanomagnetites from trachybasalts, basanites and olivine nephelinites. Concentric zoning is manifested mostly in an increase of Ti towards rims, accompanied by a decrease of Mn, Al and Mg.

Accessory minerals

Accessory minerals occur sporadically in the rocks. Euhedral, partly corroded *titanite* occurs in the entire range of rocks except for rhyolite. For its chemical composition see Table 11. Needle-like *apatite* is a rare accessory and is mainly concentrated in the more mafic and intermediate rocks of the WAS.

Table 10. Representative chemical analyses of titanian magnetites

Sample No.	180/1C	180/2R	186/3	186/4	251/8	251/9	256/12	256/13	255/17	255/18
Rock type	TR	TR	TR	TR	TA	TA	BTA	BTA	TB	TB
SiO_2	0,13	0,06	0,23	0,16	0,38	0,24			0,08	0,12
TiO_2	9,05	10,98	10,27	9,06	13,93	15,88	13,41	15,44	16,11	13,81
Al_2O_3	0,41	0,46	0,50	0,63	1,37	1,26	1,30	1,28	2,83	3,52
Cr_2O_3									0,12	0,13
Fe_2O_3	50,76	47,02	47,55	50,64	39,99	37,01	41,11	37,54	36,44	40,28
FeO	33,33	38,22	35,87	32,56	40,44	40,76	40,83	41,40	39,71	37,46
MnO	5,63	2,65	4,53	6,64	2,57	2,73	1,73	2,73	1,34	1,12
MgO	0,23	0,12	0,20	0,33	0,96	1,25	0,45	0,71	3,62	3,98
CaO	0,04	0,20	0,07	0,02	0,13	0,72	0,11	0,10	0,07	0,08
V_2O_5										
Total	99,10	99,71	99,28	100,04	99,77	99,85	99,94	99,20	100,32	100,50
Number of ions per 3 cation and 4 (O) positions										
Si	0,005	0,002	0,009	0,006	0,014	0,009			0,003	0,004
Ti	0,258	0,309	0,297	0,258	0,399	0,446	0,376	0,431	0,434	0,371
Al	0,018	0,020	0,022	0,027	0,059	0,054	0,057	0,056	0,119	0,147
Cr									0,003	0,004
Fe^{3+}	1,494	1,383	1,404	1,481	1,162	1,071	1,211	1,101	1,026	1,125
Fe^{2+}	1,038	1,189	1,120	1,007	1,242	1,248	1,272	1,284	1,183	1,107
Mn	0,178	0,084	0,143	0,208	0,080	0,085	0,055	0,086	0,040	0,034
Mg	0,014	0,015	0,014	0,019	0,058	0,096	0,029	0,043	0,195	0,213
Ca	0,002	0,008	0,003	0,001	0,005	0,028	0,004	0,004	0,003	0,003
cation	3,000	3,000	3,000	3,000	3,000	3,000	3,000	3,000	3,000	3,000
$MgAl_2O_4$	1,8	1,9	2,1	2,7	4,8	4,2	4,8	4,4	9,0	11,7
$MgMgTiO_4$	0,5	0,4	0,3	0,5	2,3	5,4	0,1	1,2	10,3	11,2
$MnMnTiO_4$	17,7	7,7	13,5	20,5	6,5	6,6	4,6	6,8	3,1	2,7
$FeFeTiO_4$	33,2	49,2	42,1	29,9	56,3	57,4	58,4	60,0	52,6	45,6
$MnCr2O_4$	0,0	0,0	0,0	0,0	0,0	0,0	0,0	0,0	0,0	0,0
$MgCr_2O_3$	0,0	0,0	0,0	0,0	0,0	0,0	0,0	0,0	0,0	0,0
$FeCrO_4$	0,0	0,0	0,0	0,0	0,0	0,0	0,0	0,0	0,3	0,3
Fe_3O_4	46,8	40,7	42,1	46,4	30,1	26,4	32,2	27,6	24,7	28,6

Table 10. continued

Sample No.	Z13/1c	Z13/2	P-1/1	P-1/2	Z15/1	Z15/2	Z14/1	Z14/2	Z17/1	Z17/2
Rock type	BA	BA	BA	BA	ON	ON	ON	ON	MON	MON
SiO_2	0,06	0,08	0,04	0,04	0,06	0,04	0,12	0,07	0,19	0,12
TiO_2	20,05	19,90	6,37	14,52	12,30	15,47	19,08	20,79	23,72	22,21
Al_2O_3	2,31	2,27	4,09	8,37	2,18	2,80	2,54	3,04	2,34	2,45
Cr_2O_3	0,15	0,17	0,23	0,15	0,74	0,70	0,71	0,32	0,44	0,37
Fe_2O_3	29,71	29,24	53,23	34,01	43,56	36,44	30,11	27,41	21,65	25,26
FeO	43,27	43,20	30,16	34,66	38,32	40,50	42,36	42,30	45,62	43,64
MnO	1,42	1,55	1,64	1,37	0,79	1,25	0,91	0,99	1,49	1,34
MgO	3,68	3,39	3,21	5,71	2,21	2,32	3,48	4,53	3,70	4,51
CaO			0,21	0,43	0,22	0,14	0,25	0,40	0,77	0,36
V_2O_5			0,77	0,79	0,46	0,60	0,53	0,33		
Total	100,65	99,80	99,95	100,06	100,84	100,26	100,10	100,18	99,92	100,26
Number of ions per 3 cation and 4 (O) positions										
Si	0,002	0,003	0,001	0,001	0,002	0,001	0,004	0,002	0,007	0,004
Ti	0,538	0,541	0,173	0,378	0,336	0,423	0,520	0,557	0,644	0,596
Al	0,097	0,096	0,173	0,340	0,093	0,119	0,108	0,127	0,098	0,102
Cr	0,004	0,005	0,007	0,004	0,021	0,020	0,020	0,009	0,012	0,010
Fe^{3+}	0,836	0,831	1,511	0,928	1,243	1,043	0,856	0,768	0,611	0,707
Fe^{2+}	1,287	1,299	0,906	1,000	1,156	1,226	1,273	1,254	1,362	1,292
Mn	0,043	0,047	0,050	0,040	0,024	0,038	0,028	0,030	0,045	0,040
Mg	0,195	0,182	0,180	0,310	0,127	0,131	0,196	0,255	0,226	0,252
Ca	0,000	0,000	0,008	0,016	0,009	0,005	0,010	0,015	0,029	0,014
cation	3,000	3,000	3,000	3,000	3,000	3,000	3,000	3,000	3,000	3,000
$MgAl_2O_4$	6,7	6,6	17,4	24,6	7,9	9,2	7,5	8,5	6,2	6,7
$MgMgTiO_4$	10,2	9,2	9,4	10,1	6,9	5,4	9,9	12,8	11,1	13,1
$MnMnTiO_4$	3,0	3,3	5,0	2,9	2,1	2,9	1,9	2,0	2,8	2,6
$FeFeTiO_4$	61,5	62,3	20,5	41,8	48,4	56,4	60,8	60,0	66,9	62,2
$MnCr2O_4$	0,0	0,0	0,0	0,0	0,0	0,0	0,0	0,0	0,0	0,0
$MgCr_2O_3$	0,0	0,0	0,0	0,0	0,0	0,0	0,0	0,0	0,0	0,0
$FeCrO_4$	0,3	0,3	0,7	0,3	1,8	1,5	1,4	0,6	0,8	0,7
Fe_3O_4	18,4	18,2	46,9	20,3	32,9	24,5	18,3	16,0	12,2	14,7

Subhedral isometric grains of *zircon* are a typical accessory of trachytes and rhyolite. Submicroscopic crystals (20-30 μm in size) of rare oxide *fersmanite* (Ca,TR) $(Nb,Ti)_2$ $(O,OH)_6$ occur in matrix of trachyte from Špičák. The tentative chemical analysis (in wt.%) of fersmanite is as follows: Nb_2O_5 (50.0), Ta_2O_5 (4.2), TiO_2 (13.0), ThO_2 (2.8), UO_2 (2.7), Ce_2O_3 (4.5), Fe_2O_3 (2.4), MnO (1.7), CaO (18.6).

Late magmatic and postmagmatic minerals

Carbonates and sulphates are commonly present in the rocks. The younger hydrothermal calcites occur both in basaltic trachyandesite and in trachybasalt, where also complex carbonate of the intermediate composition between *rhodochrosite* and *calcite* was found (Table 11). *Barite* grains were identified in the matrix of basaltic trachyandesite (Table 11).

Mn-oxyhydroxide is very characteristic mineral of the Špičák trachyte. It occurs as an irregular network of subvertical veins and small veinlets (from 1 mm to 10 cm wide), vugs fillings, pseudomorphs after feldspars and in irregular impregnations copying the fluidal structure of the rock. In the apparently (by the naked eye) homogeneous monomineral veins the Mn-mineral forms only up to 10 vol.%. It cements very fine crushed material (feldspars, quartz, clay mineral) of the host rocks. The Mn-mineral is probably a product of a younger hydrothermal precipitation in fissures. It represents a poorly crystalline, originally colloidal phase, most probably a mixture of Mn-oxyhydroxides. A chemical study (Table 11) of the oxidation state (Ulrych et al., 1997) shows that Mn is mainly present in tetravalent form (8.55 wt.% from the total content of manganese expressed as 12.35 wt.% of MnO); the minor part (3.79 wt.%) corresponds to the trivalent form of Mn.

Sulphur and organic matter were rarely found in the altered and cavernous part of the Špičák trachyte as a yellow powder coating vugs (Ulrych et al., 1997). The sulphur crystallised most probably as a result of decomposition of gaseous volcanic emanations (oxidation of H_2S or reduction of SO_2).

Table 11. Representative chemical analyses of accessory and secondary minerals

Sample No.	180	186	180	256	256	255	255
Rock type		TR		BTA		TB	
Mineral	titanite		Mn-oxy hydroxide	barite	calcite	Mn-carbonate	calcite
SiO_2	29,63	31,82					
TiO_2	36,87	36,07	0,75				
Al_2O_3	1,44	1,56	2,61	0,01			
Fe_2O_3			15,00	0,46			
FeO	1,44	2,02			0,77	0,24	0,49
MnO	0,38	0,38	71.87*	0,22	0,16	31,87	0,04
MgO	0,33	0,02	0,37	0,78	0,03	0,32	0,18
CaO	26,92	26,93	1,68		55,48	25,04	55,20
BaO		0,12		63,22	0,21		0,02
Na_2O	0,07	0,25	0,56				
K_2O	0,08	0,03	2,24				
H_2O			4,92				
Total	97,16	99,18	100,00	64,69	56,65	57,47	55,93

Nontronite occurs in numerous veinlets, vugs and concentrations around the feldspar glomerophyres (Melka et al., 2001) in the trachyte of Špičák Hill. It forms 50-100 μm sized flakes, yellow-green in colour, occurring mixed with finely fragmented feldspars and goethite, sometimes in association with Mn-oxyhydroxide.

GEOCHEMISTRY

Chemical analyses of the basanites and their proposed differentiates (see below) are presented in Table 2A, while olivine nephelinites, tephrites and trachyandesites are given in Table 2B. Position of the rocks of both series is presented in the TAS diagram (Fig. 6) of Le Maitre ed. (1989).

In the TAS diagram (Le Maitre, 1989) the majority of the W Bohemian rocks plot in the basanite, tephrite, trachybasalt, basaltic trachyandesite, trachyandesite, trachyte, and rhyolite fields (Fig. 6). Three samples (Lysina, Polom, Číhaná) plot as alkali-basalts because they contain numerous microxenoliths of the surrounding granitic rocks. Their mineral composition indicates that their original bulk chemistry was more

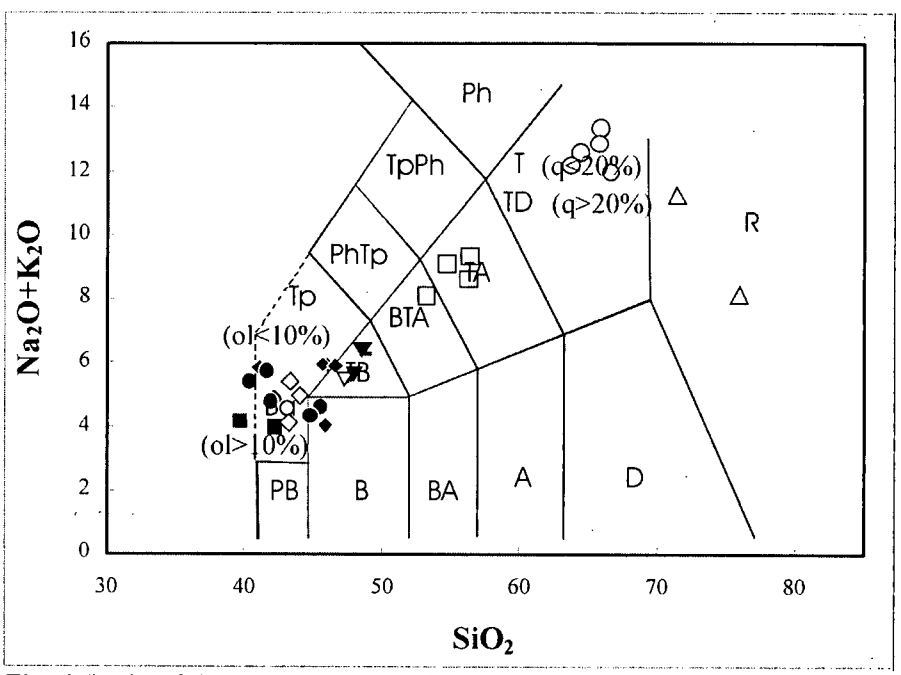

Fig. 6. Rocks of the weakly and strongly alkaline series associated with the Cheb-Domažlice Graben plotted in TAS diagram (Le Maitre ed. 1989). Symbols as in Fig. 1.

undersaturated in silica. Although most of the mafic rocks plot in the basanite field, they vary significantly in modal composition (see mineralogy section), which was used to distinguish olivine nephelinites and basanites.

In terms of Na_2O and K_2O most of the rocks belong to the potassic series: potassic trachybasalt - shoshonite - latite - trachyte - rhyolite (classification of Le Maitre, 1989); see Fig. 6. The rare rock samples represented only by hawaiite (flow at Zbraslavský vrch Hill) and latite (agglutinate in a feeding channel of Třebouňský vrch Hill) are members of sodic series in the same classification.

In comparison to Siebengebirge (Vieten et al., 1988) and Cantal, Massif Central (Wilson et al., 1995), the volcanic rocks of W Bohemia reveal a similar extent of fractionation, but at a lower level of alkalinity (cf. Fig. 2 in Pivec et al., in press). The rhyolite from the laccolith of Stěnský vrch Hill with a gneissic roof reveals some stoping features, suggesting contamination of the magma by the host rock (cf. Ulrych et al., 2000b).

According to TAS and Harker's diagrams, trachybasalts, trachyandesite and trachytes can be considered as representatives of the Weakly Alkaline Series (WAS) series. This series corresponds to that from the Cantal, Massif Central (Wilson et al., 1995). In Cantal, a Strongly Alkaline Series (SAS) has also been recognised. Initially, a similar series, composed of olivine nephelinite-tephrite-phonolite was thought to exist in W Bohemia, but the two large phonolite bodies considered to represent the felsic end of this series proved to belong to an older series (26-31 Ma) characteristic of Doupovske hory Mts. (Ulrych et al., in press a). However, strongly alkaline volcanism is definitely represented in W Bohemia by the (olivine) nephelinites. Thus, analogous to Cantal, both weakly and strongly alkaline rocks are present.

The WAS shows no evidence of commonly recognized crustal assimilation in trachytic and rhyolitic rocks (cf. Wilson et al., 1995). They have relatively stable ratios of incompatible elements (Ulrych et al., in press b) that have not been significantly affected by crustal assimilation.

Discussion and Conclusions

The volcanism in W Bohemia is genetically associated with the uplift of NE-flank of the CDG. Two contemporaneous series were recognised there:
WAS: basanite – trachybasalt – (basaltic) trachyandesite – trachyte – rhyolite,
SAS: (melilite-bearing) olivine nephelinite – tephrite.

The contemporaneous rock series represents products of the Middle to Late Miocene episode, which is part of the continuous Cenozoic volcanic activity in the Bohemian Massif (Ulrych et al., 1999). Despite the similar age of both series, their initial magmas differ in degree of partial melting of the mantle source. Initial nephelinitic magma was formed by a lower degree of partial melting than the basanitic magma.

The age of the volcanism associated with the CDG coincides with the Late Miocene intrusions in the České středohoří Mts. (13-9 Ma; Cajz et al., 1999), young volcanism in Germany (11-6 Ma; Lippolt, 1983) and with the time of the tectonic event (Downes, 1996) causing principal changes in chemical composition of volcanism in Carpathians.

Initial parent magmas (nephelinitic and basanitic) probably formed by different degrees of partial melting of metasomatised mantle lithosphere, with amphibole, olivine, garnet and clinopyroxene in residuum. Metasomatised mantle lithosphere has also been reported as a likely source of primitive alkaline magma from other parts of the Bohemian Cenozoic Volcanic Province (Svobodová and Ulrych, in press). The mantle source was enriched in incompatible elements compared to PM. Geochemical similarity of the rocks to OIB points to mantle metasomatism associated with plume-material.

The chemistry of the minerals characteristically reflects the differentiation development of the above rock series. Minerals of the differentiation series can be classified to:

1. The early magmatic crystallization

- Olivine phenocrysts (Fo_{66-76}), melilite, Ti-magnetite and (Ti,Fe^{3+})-diopside to fassaite in the mafic rocks,
- (Mn,Ti)-magnetite, diopside and high-temperature K-oligoclase (cores to anorthoclase phenocrysts) characterise the felsic rocks.

2. The continuous to late magmatic crystallization

- Kaersutite phenocrysts, nepheline at temperatures < 700°C (together with melilite in ijolite pegmatoidal segregations) and crystallization of labradorite-andesite series are characteristic of the mafic rocks,
- Andesine, sometimes with K-andesine to K-oligoclase rims and problematic olivine in tephritic rock (Fo_{49-52}) are typical of transitional types;
- Mn-magnesioriebeckite, Mn-winchite, Mg-biotites and anorthoclase perthite (occasionally with K-oligoclase cores and/or Na-sanidine rims) represent the felsic rocks; Na-sanidine and quartz in the matrix of the felsic rocks terminate the crystallization.

3. Late magmatic to postmagmatic crystallization

- Analcimes replacing plagioclases and nepheline, carbonates of calcite-rhodochrosite series and barite are products of the late magmatic stage in the mafic rocks,
- The presence of Mn-oxyhydroxide, nontronite, rare sulphur and organic matter in the felsic rocks reflects the postmagmatic stage.

Acknowledgements

This research was supported by the Grant Agency of the Czech Republic No. 205/99/0907 and the Research Program of the Institute of Geology AS CEZ: Z3010912. The K-Ar dating was sponsored by the Hungarian Academy of Sciences Foundation T 014961 performed in the scope of Hungarian-Czech Project: Comparative volcanostratigraphy of Neoidic volcanism of the Bohemian Massif and Pannonian Basin. The authors thank A. Langrová, Geological Institute AS CR for providing the microprobe analyses. For review of an early version of the manuscript and helpful and perceptive suggestions leading to a considerable improving of the manuscript we are indebted to F. Fediuk, Geohelp and E. Pivec, Geological Institute AS CR both from Praha.

References

Balogh, K. (1985): K/Ar dating of Neogene volcanic activity in Hungary. Experimental technique, experiences and methods of chronologic studies, 277-278. ATOMKI Rep. D/1, Debrecen.

Barth, T. F.W. (1969): Feldspars. Wiley Interscience, New York.

Behr, H. (1992): Lineare Krustenstrukturen im Umfeld der KTB lokation. In: KTB Report, 92-3, 3-82. Hannover.

CAJZ, V. (1992): Volcanic history of Podhorní vrch Hill (Western Bohemia). Čas. Mineral. Geol., **37**, 63-64 (in Czech).

CAJZ, V., VOKURKA, K., BALOGH, K., LANG M., ULRYCH, J. (1999): The České středohoří Mts.: Volcanostratigraphy and geochemistry. Geolines, **9**, 21-28.

CARMICHAEL, I. S. E. (1963): The crystallization of feldspar in volcanic acid liquids. Quat. J. Royal Soc., **119**, 95-131.

DOLLASE, W. A., THOMAS, W. M. (1978): The crystal chemistry of silica rich alkali-deficient nepheline. Contrib. Mineral. Petrol., **66**, 311-318.

DONNAY, G., SCHAIRER, J.F., DONNAY, J. D. H. (1959): Nepheline solid solutions. Mineral. Mag., **32**, 93-109.

DOWNES, H. (1989): Magma mixing in undersaturated alkaline volcanics, Cantal, Massif Central, France. Mineral. Mag., **53**, 43-53.

DOWNES, H. (1996): Neogene magmatism and tectonics in the Carpatho-Pannonian region. Mitt. Gesell. Geol.-Bergbaustud. Österr., **41**, 104. In: Decker L. (ed.): Pancardi Workshop 1996, Wien.

FEDIUK, F. (1995): Volcanics of Zbraslavský vrch Hill between the towns Manětín and Toužim (W Bohemia). Zpr. geol. Výzk. 1994, 48-50 (in Czech).

FOLAND, K. A., LANDOLL, J. D., HENDERSON, C. M. B., JIANFENG, C. (1993): Formation of cogenetic quartz and nepheline syenites. Geochim. Cosmochim. Acta, **57**, 697-704.

HAMILTON, D. L. (1961): Nephelines as crystallization temperatures indicators. J. Geol., **69**, 321-329.

HOERNLE, K., ZHANG, Y., GRAHAM, D. (1995): Seismic and geochemical evidence for large-scale mantle upwelling beneath the Eastern Atlantic and Western and Central Europe. Nature, **374**, 34-39.

HUCKENHOLZ, H. G., BÜCHEL, G. (1988): Tertiärer Vulkanismus der Hocheifel. - Exkursionsführer 66 Jahrestagung der DMN in Bonn. Fortschr. Mineral, **66**, 43-82.

KACHLÍK, V., 1993: The evidence for Late Variscan nappe thrusting of the Mariánské Lázně Complex on the Saxothuringian terrane (W Bohemia). Čas. Mineral. Geol., **38**, 43-58.

KOPECKÝ, L. (1978): Neoidic taphrogenic evolution of young alkaline volcanism of the Bohemian Massif. Sbor. Geol. Věd., Ř. Geol., **30**, 91-107.

LE MAITRE, R.W. (ed.) (1989): A Classification of Igneous Rocks and Glossary of Terms. Blackwell Sci. Publ., Oxford.

LEAKE, B. E. (ed.) (1978): Nomenclature of amphiboles. Mineral. Mag., **42**, 533-565.

LIPPOLT, H. (1983): Distribution of volcanic activity in space and time. In Fuchs, K. (ed.): Plateau Uplift, 112-120. Springer, Berlin.

MELKA, K., ULRYCH, J., NOVÁK, J. K., LANGROVÁ, A. (2001): Nontronite from Špičák Hill near Teplá: product of the late magmatic alteration of trachyte. Abstract. Mid-European Clay Conference, Sept. 9-14, 2001, Stará Lesná, Slovakia.

MILANI, L., BECCALUVA, L., COLTORTI, M. (1999): Petrogenesis and evolution of the Euganean Magmatic Complex, Veneto Region, North-East Italy. Eur. J. Mineral., **11**, 379-399.

MORIMOTO, M. (ed.) (1988): Nomenclature of pyroxenes. Mineral Mag., **52**, 535-550.

NEKVASIL, H. (1990): Reaction relations in the granite system: implications for trachytic and syenitic magmas. Amer. Mineralogist, **75**, 560-571.

NEKVASIL, H. (1992): Ternary feldspar crystallization in high temperature felsic magmas. Amer. Mineralogist, **77**, 592-604.

ODIN, G. S. et 35 collaborators (1982): Interlaboratory standards for dating purposes. In: Odin G. S. (ed.): Numerical Dating in Stratigraphy, 123-150. Wiley and Sons, Chichester.

PECERILLO, A., TAYLOR, S. R. (1976): Geochemistry of Eocene calc-alkaline volcanic rocks from the Kastomonu area, northern Turkey. Contrib. Mineral. Petrol., **58**, 68-81.

PIVEC, E., ULRYCH, J., HÖHNDORF, A., RUTŠEK, J. (1998): Melilitic rocks from northern Bohemia: Geochemistry and mineralogy. N. Jb. Mineral., Abh., 312-339.

PIVEC, E., ULRYCH, J., ÁRVA-SÓS, E., NEKOVAŘÍK, Č. (in press): Weakly alkaline trachybasalt-rhyolite series from the Teplá Highland, Western Bohemia: geochemical constraints. Geologica Bavarica, 25 pp.

SCHREIBER, U., ANDERS, D., KOPPEN, J. (1999): Mixing and chemical interdiffusion of trachytic and latitic magma in a subvolcanic complex of the Tertiary Westerwald (Germany). Lithos, **46**, 695-714.

SHRBENÝ, O. (1979): Geochemistry of the West Bohemian neovolcanites. Čas. Mineral. Geol., **24**, 9-21.

SVOBODOVÁ, J., ULRYCH, J. (in press): Alkaline rocks with carbonatite affinity in the Bohemian Massif, Czech Republic. – Proc. Symp. Carbonatite Assoc. Rocks, 12-18 February 2001, Chennai, India, 25 pp.

ULRYCH, J., KAŠPAR, P. (1977): Relation of microhardness to the structure of monoclinic pyroxenes and amphiboles. Acta Univ Carol., Geol., Kratochvíl Vol., 13-19.

ULRYCH, J. (1978): Magnesioarfvedsonite from fenites near Hůrky in the Čistá Massif (West Bohemia). Čas. Mineral. Geol., **23**, 67-70.

ULRYCH, J. (1986): Oxykaersutite from Vlčí hora Hill in western Bohemia in comparison with kaersutites of the Bohemian Massif. Sbor. Západočes. Muz., Odd. Přír., 1-46 (in Czech).

ULRYCH, J., KOPECKÝ, L., KROPÁČEK, V. (eds.) (1991): Guide to post-symposium excursion: Neoidic volcanism of the Bohemian Massif. SCEAVR Meeting 1991, Prague.

ULRYCH, J., PIVEC, E., POVONDRA, P. (1997): Sulphur and Mn-oxyhydroxides from trachyte of Špičák Hill near Teplá. Bull. min. petr. odd. Nár. Mus. v Praze, **4-5**, 210-212 (in Czech).

ULRYCH, J., PIVEC, E., LANG, M., BALOGH, K., KROPÁČEK, V. (1999): Cenozoic intraplate volcanic rock series of the Bohemian Massif: a review. Geolines, **9**, 123-129.

ULRYCH, J., CAJZ, V., PIVEC, E., NOVÁK, J. K. ULRYCH J., NEKOVAŘÍK, Č. (2000a): Cenozoic intraplate alkaline volcanism of western Bohemia. Stud. geoph. geod., **44**, 346-351.

ULRYCH, J., PIVEC, E., HÖHNDORF, A., BALOGH, K., BENDL, J., RUTŠEK, J. (2000b): Rhyolites from the Roztoky Intrusive Centre, České středohoří Mts.: xenoliths or dyke differentiates? Chem. Erde, **60**, 327-352.

ULRYCH, J., PIVEC, E., LANG, M., LLOYD, F. E. (2000c): Ijolitic segregations in melilite nephelinite of Podhorní vrch volcano, Western Bohemia. N. Jb. Mineral., Abh., **175**, 317-348.

ULRYCH, J., BALOGH, K., CAJZ, V., NOVÁK, J. K., FRÁNA, J. (in press a): Cenozoic alkaline volcanic series in W Bohemia: age relations and geochemical constraints. Acta Montana, Ser. A Geodynamics, 20 pp.

ULRYCH, J., ŠTĚPÁNKOVÁ, J., LLOYD, F. E., BALOGH, K. (in press b): Coexisting Miocene alkaline volcanic series associated with the Cheb-Domažlice Graben, W Bohemia: geochemical characteristics. Geologica Carpathica, 25 pp.

VIETEN, K. (1965): Mangan-reicher Fluortaramit aus dem Alkalitrachyt der Hohenburg bei Berkum (Siebengebirge). N. Jb. Mineral., Mh., 166-171.

VIETEN, K. (1979): The minerals of the volcanic rocks association of the Siebengebirge I. Clinopropyroxenes. 1. Variation of chemical composition of Ca-rich clinopyroxenes (salites) in dependence of the degree of magma differentiation. N. Jb. Miner., Abh., **135**, 270-286.

VIETEN, K. (1980): The minerals of volcanic rocks association of the Siebengebirge. I. Clinopyroxenes. 2. Variation of chemical compositions of Ca-rich clinopyroxenes (salites) in the course of crystallization. N. Jb. Miner., Abh., **140**, 54-88.

VIETEN, K., HAMM, M., GRIMMEISEN, W. (1988): Tertiärer Vulkanismus des Siebengebirges Exkursionsführer 66. Jahrestagung der DMN in Bonn. Fortschr. Mineral., **66**, 1-42.

VRÁNA, S. (2000): New occurrences of trachyte near Teplá in western Bohemia. Zpr. geol. Výzk. v roce 1999, 84-85 (in Czech).

WAGNER, G. A., GÖGEN, K., JONCKHEERE, R., KÄMPF, H., WAGNER, I., WODA, C. (1998): The age of Quaternatry volcanoes Železná hůrka and Komorní hůrka (Western Eger Rift), Czech Republic: alpha-recoil track, TL, ESR and fission track chronometry. In: Magma and Rift Basin Evolution Excursion Guide, Abstracts, Czech Rep., Liblice, Sept. 7-11, 1998, 95-96, Czech Geol. Survey, Prague.

WILKINSON, J. F. G., HENSEL, H. D. (1994): Nephelines and analcimes in some alkaline igneous rocks. Contrib. Mineral. Petrol., **118**, 79-91.

WILSON, M., DOWNES, H., CEBRIA, J. M. (1995): Contrasting fractionation trends in coexisting continental alkaline magma series, Cantal, Massif Central, France. J. Petrology, **36**, 1729-1750.

WILSON, M., ROSENBAUM, J. M., ULRYCH, J. (1994): Cenozoic magmatism of the Ohře Rift, Czech Republic: geochemical signatures and mantle dynamics. Abstracts IAVCEI, Ankara.

WIMMENAUER, W. (1974): The alkaline province of Central Europe and France. In: Sørensen H. (ed.): The Alkaline Rocks, 286-291. Wiley and Sons, London.

WOHNIG, K. (1904): Trachytische und andesitische Ergussgesteine vom Tepler Hochland. Arch. naturwiss. Landesdurchforsch. Böhmen, **13**, 1, 1-43.

YODER, H. S. JR., 1973: Melilite stability and paragenesis. – Fortschr. Mineral., **50**, 140-173.

ZARTNER, W. R. (1939): Tonvorkommen am Fuße des Wolfsberges westlich von Tschernoschin (Sudetengau). Firgenwald, **12**, 20-23.

Received: February 10, 2001; accepted: April 21, 2002

Acta Mineralogica-Petrographica, Szeged 2002, Vol. 43, pp. 19-25

ACTA
Mineralogica
Petrographica

ORGANIC FACIES DISTRIBUTION AT THE PLATFORMWARD MARGIN OF THE KÖSSEN BASIN

MAGDOLNA HETÉNYI

Department of Mineralogy, Geochemistry and Petrology, University of Szeged
H-6701 Szeged, P. O. Box 651, Hungary
e-mail: hetenyi@geo.u-szeged.hu

ABSTRACT

Assessment of the organic facies and that of organic precursors were performed on an 83 m thick core section of the Upper Norian Kössen Formation (Hungary), exposed in Sümeg by Süt-17 borehole. Carbon-dioxide, mineral carbon and organic carbon contents, determined on a large number (70) of samples, exhibit a carbonate-rich, organic-poor sequence. Cyclic variations observed in both forms of carbon, throughout the sequence, reveal cyclic alternations of the platform-derived input and the terrestrial-derived one. Owing to the especially low organic carbon content (C_{org} <0.2 %), half of the investigated rocks, composed mainly of carbonate particles, can not be considered as source rocks either for oil and gas. Most of them were formed under shallow subtidal conditions in a highly oxic environment. Rock Eval pyrolyses performed on selected argillaceous samples (C_{org} >0.2 %) together with organic petrographical data from a small sample set, show that the immature organic matter is of predominantly terrestrial origin and composed of mainly inertinite and vitrinite deposited in oxic environment. The predominance of the highly degraded land plant remnants resulted in organic facies D and CD with very low source potential in rocks containing less than 6 % of C_{carb}. Organic facies CD is also common in rocks containing more than 6 % of C_{carb}. Owing to the negligible amount of oil and minor amount of gas generated by all of these samples, they are rated as non-source rocks in any commercial sense. Gas-prone C facies and B facies with marginal potential for oil generation, observed in some carbonate-rich samples, formed from a mixture of different types of precursors and accumulated also in an oxic environment. The very minor amount of algal-derived liptinite was probably preserved by inclusion in carbonate skeleton.

Key words: carbonate platform, petroleum source potential, organic facies, organic precursors, depositional environment

INTRODUCTION

The Upper Norian–Lower Rhaetian Kössen Formation is regarded as the source rock of heavy sulfur-rich oil of the adjacent oil field in the Transdanubian Range Unit (Hungary) (Clayton and Koncz, 1994). It was deposited in a backplatform basin in the background of the Dachstein platform. Organic petrographical and geochemical data (Brukner-Wein and Vető, 1986; Hetényi, 1989; Hetényi et al., 2002; Vető et al, 2000), as well as geochemical assessment of production and preservation of organic matter (OM) (Vető et al, 2000) have recently been reported. These examinations were performed on thermally immature OM accumulated on the gentle slope located between the basin and a late Triassic carbonate platform of the South-Alpine domain. Parallel variations were observed in the mineral composition and in the organic geochemical features of the Kössen Formation for the two studied boreholes as a function of their paleo-position on the slope. The immature OM is of predominantly marine origin and composed of mainly liptinites in both boreholes. Precursor biomass accumulated at the toe of the slope is mainly of algal origin with a minor bacterial and terrestrial contribution. A significantly higher proportion of bacterial biomass and a very small amount of higher plant remnants were found in the OM of the borehole located on the slope. The source potential of the Kössen Formation is nearly three times higher for the rocks deposited at the toe of the slope than for rocks deposited on the slope. This ratio fairly correlates with the average C_{org} content of the two sequences. Furthermore, rocks accumulated at the toe of the slope contain lower amount of carbonate minerals than those accumulated on the relatively upper part of the slope.

This paper presents the bulk organic geochemical data measured on core samples taken from an immature section of the Kössen Formation deposited on the belt of the slope. Core samples were collected from Süt-17 well (Sümeg). On the basis of these data the petroleum source potential of the rocks were evaluated. Assessment of the organic facies and organic precursors for samples with different carbonate content, as well as that of the geochemical characteristics for depositional environment were attempted.

GEOLOGICAL SETTING

Upper Triassic of the Transdanubian Range (Hungary) is made up from platform carbonates and intraplatform basin deposits (Haas, 2002). This segment of the large (200 km wide) Late Triassic carbonate platform belonging to the passive margin of the Tethys ocean, may have been situated between the North and South Alpine realms in the Triassic (Klimetz, 1983; Ziegler et al., 1983; Parrish, 1993). In the Paleogene the TR block moved eastward reaching its present position in the Early Miocene (Kázmér and Kovács, 1985; Balla, 1988; Haas et al., 1990). The lower unit of the platform, the Upper Carnian-Middle Norian Main Dolomite (Hauptdolomite) Fm. of about 1,000 m thickness is overlain by the Upper Norian-Rhaetian Dachstein Limestone of about 800 m thickness. Development and subsequent dolomitization of the platform was strongly affected by the climate (Balog et al, 1999). Formation of the Kössen Basin started at the very end of the Middle Norian as a result of the

extensional tectonics, which led to the disintegration of the previously existing carbonate platform and to a sea-level rise resulting in drowning of the platform. The basin was filled in by fine terrigenous siliciclastics and platform-derived carbonate particles during the Late Norian-Rhaetian (Haas and Budai, 1995; Haas, 2002). Cyclic alternation of carbonate sedimentation and argillaceous one, reflecting short-term (100-400 ka) sea-level fluctuations, is characteristic of the inner marginal belt of the platform. The carbonate-poor rocks deposited in relatively deeper water when the input of carbonate particles from the back stepping platform decreased (Haas, 1993),

Based on foraminifera and ostracodes the studied sequence, penetrated by Süt-17 well, represents the latest Norian interval (Oravecz-Scheffer, 1987). The carbonate-rich layers are composed mainly of limestone, argillaceous limestone and dolomitic limestone. The marly layers contain calcite, ankerite, and clay minerals (Haas, 1993).

Methods

70 samples were collected from the 83 m thick section of the Süt-17 well. Inorganic carbon (C_{carb}) was determined by measuring the CO_2 released by HCl-acid treatment. C_{org} content, source potential (S1 + S2), hydrogen index (HI) and T_{max} considered as a maturity parameter were measured by standard Rock Eval method using an Oil Show Analyzer. Measurement of oxygen index (OI) was carried out in a Rock Eval II Pyrolyzer. Both types of the Rock Eval pyrolysis were performed on 100 mg powdered samples at 300°C for 4 min, followed by programmed pyrolysis at 25°C/min to 550°C in a helium atmosphere. The organic carbon remaining after pyrolysis was measured by oxidation under air atmosphere at 600°C. (Espitalié et al., 1977; Bordenave et al., 1993).

Organic petrographic observations were performed on a six sample set of different carbonate content with reflected light microscopy in oil immersion.

Results and discussion

Organic and mineral carbon

Carbon-dioxide (CO_2), C_{carb} and C_{org} contents of the studied samples are listed in Table 1. CO_2 and C_{org} contents are plotted along the depth in Fig. 1.

The studied succession is rich in carbonate minerals; CO_2

Table 1: Carbon-dioxide content (CO_2), mineral carbon content (C_{carb}) and organic carbon content (C_{org}) of the samples taken from Süt-17 well

Depth	CO_2	C_{carb}	C_{org}	Depth	CO_2	C_{carb}	C_{org}
434.0	41.5	11.32	0.10	474.8	30.3	8.27	0.17
435.0	32.6	8.89	0.39	475.9	27.3	7.45	0.21
435.8	1.6	0.43	0.80	477.0	16.9	4.61	0.34
437.0	38.8	10.59	0.40	478.0	16.2	4.42	0.14
437.5	29.6	8.08	0.38	479.3	32.0	8.73	0.10
437.9	42.1	11.49	0.09	481.6	40.2	10.97	0.14
439.3	17.6	4.80	0.53	482.5	31.1	8.49	0.67
439.8	15.1	4.12	0.55	483.5	19.3	5.26	0.51
440.0	41.7	11.38	0.05	484.7	40.7	11.11	0.08
444.1	43.3	11.82	0.12	485.9	25.5	6.96	0.50
448.0	43.0	11.73	0.04	486.2	35.0	9.55	0.26
453.2	43.3	11.82	0.04	487.5	41.0	11.19	0.18
453.5	12.6	3.43	0.85	489.4	28.3	7.72	0.64
454.0	7.6	2.07	0.51	490.8	13.3	3.63	1.25
455.0	37.9	10.34	0.12	491.1	38.7	10.56	0.25
455.5	31.2	8.51	0.35	492.0	16.7	4.55	0.77
457.7	42.5	11.60	0.11	493.0	30.2	8.24	0.31
458.4	41.2	11.24	0.12	493.7	36.5	9.96	0.21
460.3	43.7	11.93	0.01	495.0	41.5	11.32	0.02
462.8	42.6	11.62	0.09	501.2	34.7	9.47	0.21
463.7	29.5	8.05	0.35	503.9	42.0	11.46	0.05
464.0	30.0	8.19	0.24	504.5	17.0	4.64	0.47
464.8	41.7	11.38	0.13	506.6	31.6	8.62	0.63
466.0	41.1	11.22	0.05	506.7	40.0	10.92	0.11
467.5	40.7	11.11	0.10	507.2	40.7	11.11	0.03
468.2	38.6	10.53	0.09	508.4	29.5	8.05	0.38
468.6	41.3	11.27	0.12	509.5	35.7	9.74	0.81
469.0	41.3	11.27	0.02	510.8	41.1	11.22	0.22
469.8	36.6	10.00	0.14	511.8	29.6	8.08	0.76
471.0	41.0	11.19	0.06	512.0	39.2	10.70	0.20
471.5	34.2	9.33	0.34	513.0	38.5	10.51	0.16
471.8	19.2	5.24	0.55	515.0	43.4	11.84	0.05
472.2	39.8	10.86	0.14	516.0	39.3	10.72	0.15
473.3	35.4	9.66	0.26	516.7	28.1	7.67	0.49
474.1	38.1	10.40	0.10				

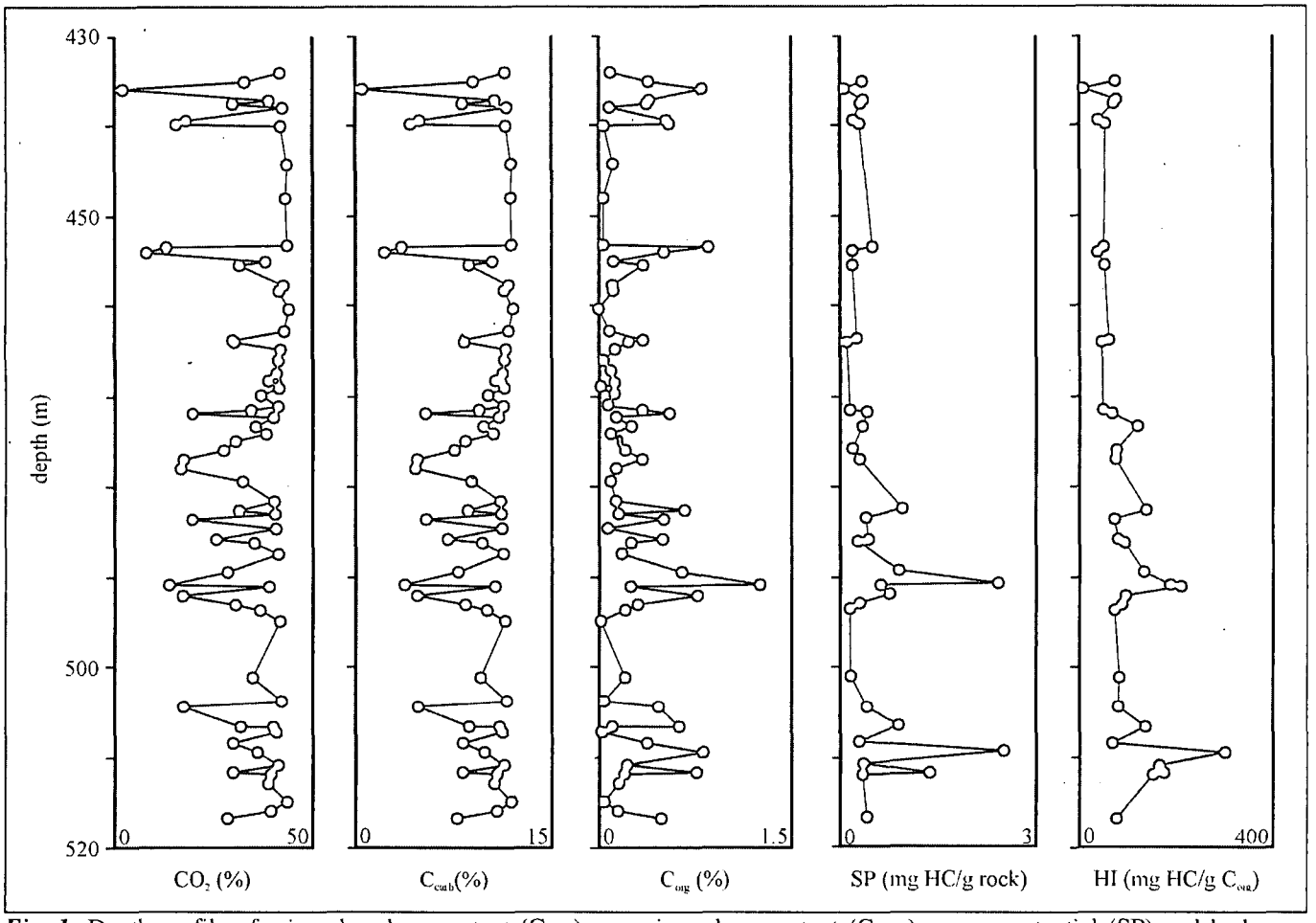

Fig. 1: Depth profile of mineral carbon content (C_{carb}), organic carbon content (Corg), source potential (SP) and hydrogen index (HI) in Süt-17 well

content exceeds 10 % for all but two samples and ranges between 27.3 and 43.3 % for most of the samples. 84% of the rocks contain more than 6% of C_{carb}, which value corresponds to 50 % of $CaCO_3$. (In this paper carbonate rocks refer to those of the studied rocks which contain 50 % or more carbonate minerals. Those rocks containing less than 50 % of carbonate are referred to as carbonate-poor ones.) The organic carbon content is low throughout the entire borehole, less than 1.0 % for all but one (490.8 m) sample.

Both the C_{org} and C_{carb} contents exhibit cyclic variations throughout the succession. The depth profile of CO_2 content and that of C_{org} content appear to be inverse of each other (Fig. 1). A fair, but not close, correlation existing between the two carbon forms is shown in Fig. 2. The very high C_{carb} values (> 10 %) determined for half of the samples suggest strong predominance of platform-derived input. Most of these carbonate-rich ($CaCO_3$ >83 %) samples are especially lean in OM (C_{org} <0.2 %) (Table 1).

On the basis of the results of several previous studies, 0.2 % is considered as the lowest limit of C_{org} content for bulk organic geochemical characterization of rocks. Comprehensive studies of numerous samples of different ages and environment, from all over the world, have led to the conclusion that the minimum values of C_{org} content are 0.5 % for immature detrital source rocks and 0.3 % for carbonate-type source rocks (Hunt, 1972; Tissot and Welte, 1984). The standard pyrolysis method (Rock Eval), developed by Espitalié et al. (1977), is a good tool also for source rock characterization and evaluation of samples containing more than 0.3 % of C_{org}. However, our experiences based on thousands of Rock Eval pyrolyses, show that this method gives fair information about the organic features of the rocks containing at least 0.2 % of C_{org}. Considering this observation, half of the samples (C_{org} >0.2 %) could be selected for more detailed organic geochemical characterization (Table 2).

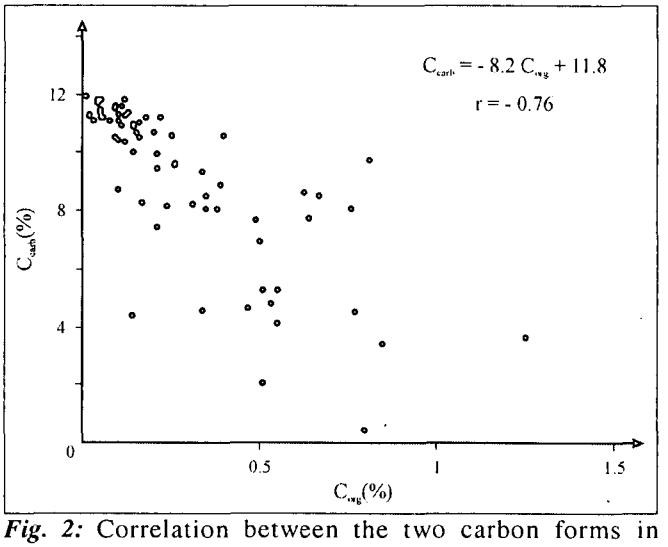

Fig. 2: Correlation between the two carbon forms in Süt-17 well

On the basis of carbonate contents, two groups of the selected samples can be differentiated. More than two thirds of these samples are also relatively rich in carbonate minerals (C_{carb} >6 %). The average value of the C_{org} content is 1.6 times lower for these rocks than for those containing less than 6 % of C_{carb} (Table 3). Cyclic variations of C_{carb} and C_{org} content can be interpreted to mean that water depth repeatedly changed during the deposition of the studied successsion. According to Haas (1993) the shallow subtidal carbonate beds (e.g. 456-462.5, 500-504.5 m depth) in the cyclic Kössen Formation are similar to those of the subtidal C members of the Lofer cycles in the Dachstein Formation suggesting similar depositional conditions. With the sea-level rise the carbonate sedimentation was gradually replaced by deposition of argillaceous sediments (e.g. 462.5-475, 490-500, 504,5-512 m depth). The increasing terrestrial contribution can be recognized not only in the decreasing carbonate content but in the increasing organic carbon content of the samples, too. This observation indicates that OM probably originated mainly from terrestrial-derived precursors.

Petroleum source potential

Petroleum source potential (referred as SP in this paper) represents the amount of hydrocarbon compounds (oil and gas) which can be generated by a rock during thermal evolution.

In contrast with the previously studied sequences of the Upper Norian Kössen Formation, which were classified as good oil-source rocks (Zl-1 well) and as excellent ones (Rzt-1 well), Süt-17 well penetrated a non oil-source succession of the Kössen Formation. SP of the selected samples ranges from 0.08 to 2.41 mg HC/g rock (Table 2), with an average of 0.53 mg HC/g rock (Table 3). According to classification suggested by Tissot and Welte (1984), rocks having SP of less than 2 mg HC/g rock correspond to gas-prone rocks or non-generative ones. Owing to the negligible amount of oil and minor amount of gas generated by these rocks, they are rated as non-source ones in any commercial sense (Espitalié and Bordenave, 1993).

Independently both of their C_{carb} and C_{org} content, selected samples have similar source potential. The average SP values are 0.55 mg HC/g rock for the samples with C_{carb} <6% and average C_{org} 0.65 % and 0.52 mg HC/g rock for samples with C_{carb} >6 % and average C_{org}: 0.39 %. These observations together with the average HI and OI values exhibit that not only the abundance but the quality of the OM is also different in the two groups (Table 3).

Organic facies

Nowdays it is widely accepted that the source potential of any sedimentary rock depends primarily on its organic

Table 2: Rock Eval data, type of kerogen and organic facies for selected samples

Depth (m)	S1	S2	SP	T_{max}	HI	OI	Type of kerogen	Organic facies	C_{org}
435.0	0.06	0.29	0.35	406	74	87	III	CD	0.39
435.8	0.02	0.06	0.08	367	7	51	IV	D	0.80
437.0	0.07	0.30	0.37	376	75	57	III	CD	0.40
437.5	0.06	0.27	0.33	396	69	71	III	CD	0.38
439.3	0.02	0.20	0.22	411	37	43	IV	D	0.53
439.8	0.02	0.29	0.31	413	52	49	III	CD	0.55
453.5	0.09	0.41	0.50	396	48	27	IV	D	0.85
454.0	0.02	0.18	0.20	406	35	33	IV	D	0.51
455.5	0.03	0.18	0.21	399	51	60	III	CD	0.35
463.7	0.06	0.21	0.27	394	60	80	III	CD	0.35
464.0	0.01	0.11	0.12	398	45	125	IV	D	0.24
471.5	0.01	0.16	0.17	401	47	45	IV	D	0.34
471.8	0.06	0.36	0.42	401	65	40	III	CD	0.55
473.3	0.05	0.31	0.36	402	119	100	III	CD	0.26
475.9	0.04	0.16	0.20	390	76	119	III	CD	0.21
477.0	0.06	0.25	0.31	396	73	44	III	CD	0.34
482.5	0.04	0.92	0.96	421	137	47	II	C	0.67
483.5	0.04	0.37	0.41	405	72	54	III	CD	0.51
485.9	0.06	0.39	0.45	407	78	66	III	CD	0.50
486.2	0.05	0.24	0.29	400	92	103	III	CD	0.26
489.4	0.07	0.84	0.91	409	131	50	III	C	0.64
490.8	0.10	2.31	2.41	416	185	44	II-III	C	1.25
491.1	0.11	0.52	0.63	399	208	80	II	C	0.25
492.0	0.05	0.72	0.77	409	93	32	III	CD	0.77
493.0	0.05	0.27	0.32	408	87	67	III	CD	0.31
493.7	0.02	0.15	0.17	408	71	114	III	CD	0.21
501.2	0.01	0.17	0.18	408	80	100	III	CD	0.21
504.5	0.06	0.37	0.43	406	78	61	III	CD	0.47
506.7	0.02	0.89	0.91	416	136	49	III	C	0.63
508.4	0.05	0.25	0.30	402	65	44	III	CD	0.38
509.5	0.07	2.42	2.49	411	298	54	II	BC	0.81
510.8	0.01	0.36	0.37	412	163	86	II-III	C	0.22
511.8	0.05	1.32	1.37	406	173	36	II-III	C	0.76
512.0	0.06	0.30	0.36	396	150	95	III	C	0.20
516.7	0.05	0.37	0.42	402	75	100	III	CD	0.49

S1 (free hydrocarbons), S2 (pyrolysable hydrocarbons) and SP (source potential=S1+S2) given in mg hydrocarbons/g rock; HI (hydrogen index) given in mg hydrocarbons/g C_{org}; OI (oxygen index) given in mg CO_2/g C_{org}, T_{max} (maximum temperature of S2) given in °C, Corg (organic carbon) given in %.

Table 3: Average values of Rock Eval data calculated for selected samples o different carbonate content

C_{carb} %	No. of samples	C_{org} %	S1	S2	SP	T_{max}	HI	OI
<6	11	0.65	0.05	0.50	0.55	402	68	43
>6	24	0.39	0.05	0.48	0.52	403	107	76
0.4-11.2	35	0.47	0.05	0.49	0.53	403	94	66

S1 (free hydrocarbons), S2 (pyrolysable hydrocarbons) and SP (source potential=S1+S2) given in mg hydrocarbons/g rock; HI (hydrogen index) given in mg hydrocarbons/g C_{org}; OI (oxygen index) given in mg CO_2/g C_{org}, T_{max} (maximum temperature of S2) given in °C.

facies (Jones and Demaison, 1982). Organic facies is defined similarly to other facies, such as biofacies. As proposed by Rogers (1980) it refers to a rock body characterized by a specific amount, type and source of OM and type of depositional environment. Organic facies is primarily determined by the amount and the type of the original OM, by the time the OM spends in an oxygenated water column and by the oxygen content of the water near the sediment-water interface during and shortly after deposition (Jones, 1984).

Hydrogen index (HI) and oxygen index (OI) derived from Rock Eval pyrolysis are used as a primary technique for evaluating the source potential of rocks and for identifying the organic facies. In terms of Rock Eval data measured on immature (vitrinite reflectance is 0.5 % R_o or less) OM, four types of kerogens (Tissot et al., 1974; Espitalié et al, 1986) and seven different organic facies (Jones, 1987) are classified. The same organic facies can contain a variety of kerogen types in different mixtures. For example, the gas-prone organic facies C could be composed of dominantly vitrinite or a mixture of algal debris and inertinite deposited under anoxic water or algal debris that was partially oxidized (Jones, 1984).

According to maturity parameter from Rock Eval yrolysis (T_{max} <418°C), all of the selected samples contain immature OM, hence they are suitable for evaluating the organic facies. The low maturity of the OM is also supported by vitrinite reflectance (Ro: 0.35 %) measured on six samples of different carbonate contents.

HI values ranging between 7 and 93 mgHC/g TOC for all but one sample and OI values lower than 62 mg CO_2/g TOC ndicate type III and type IV kerogen in carbonate-lean samples. HI and OI values, varying between wider intervals, (between 45 and 298 mg HC/g TOC and between 36 and 125 mg CO_2/g TOC, respectively) reveal that not only type III and IV kerogens but type II kerogens also occur in carbonates.

Four types of the organic facies (BC, C, CD and D), defined in terms of HI and OI (Jones, 1987), were observed n the series of the selected samples.

More than half of the selected samples (57 %) contain rganic facies CD. The proportion of organic facies C and D is 23 % and 17 %, respectively. Only one sample represents he BC facies.

The practically non-generative organic facies D (HI <50 g HC/g TOC, OI: 20-200 mg CO_2/g TOC) is strongly redominated by OM of the inertinite maceral group. evertheless, half of the samples containing organic facies D re located at the boundary of organic facies D and CD in ig. 3. With regard to the continous transition which can be upposed between the two adjacent organic facies, the amples having HI values above 45 mg HC/g C_{org} can also be ssigned to facies CD. Thus, only three samples from the ppermost part of the succession (435.8, 439.3 and 454.0 m) epresent typical organic facies D. All of them occur in the arbonate-poor layers containing C_{carb} <6 %. Their very low P (from 0.08 to 0.22 mg HC/g rock) in spite of relatively igh C_{org} content (between 0.51 and 0.80 %) suggests a ighly oxic depositional environment and highly reworked errestrial precursor material.

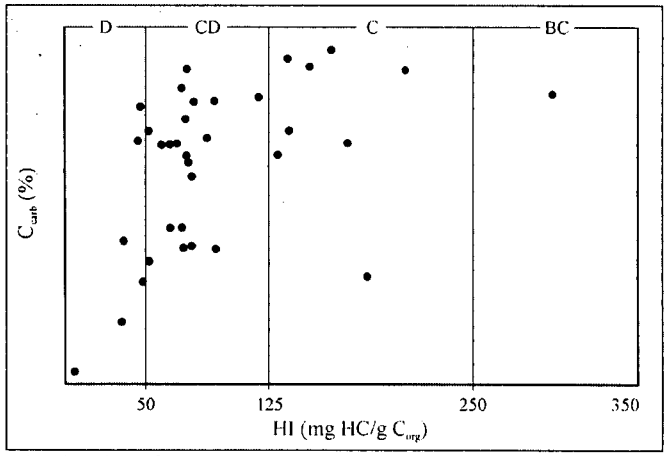

Fig. 3: Plot of carbonate-richness of samples versus hydrogen index for different organic facies determined in Süt-17 well

The carbonate-poor rocks (C_{carb} <6 %), deposited in relatively deeper water when the input of carbonate particles from the back stepping platform decreased (Haas, 1993), preferentially have organic facies CD (Fig. 3). Both HI and OI values of these samples vary in a relatively narrow range, from 48 to 93 mg HC/g TOC and from 32 to 61 mg CO_2/g TOC, respectively. More than half of the carbonate rocks also contain organic facies CD covering the same narrow range of HI values for all but one sample (Table 2 and Fig. 3). OI values ranging between 44 and 125 mg CO_2/g TOC, can show variable oxygenation of the depositional environment. However, it is more likely that the high OI values are due to the inaccurracy of OI determination, which is common for organically lean carbonates. A great variation of organic input can lead to organic facies CD. Terrestrial plant remnants in various stages of degradation and reworked OM are considered the main precursors of this facies. In carbonate sequences highly oxidized algal material can also contribute to the OM (Jones, 1987). Organic petrographical analysis performed on three samples indicates the predominance of degraded inertinite. However, a relatively significant amount of vitrinite and some trace of algal-derived liptinite were also observed in both of the two carbonate-poor samples (492.0, 504.5 m) and in the sample representing the carbonate rocks (485.9 m). The higher SP determined for carbonate-poor rocks are consistent with their higher organic contents (Table 2, 4). This observation together with the same narrow range of HI values and maceral composition of the OM reveal very similar quality of the OM for samples containing organic facies CD.

Organic facies C (HI: 125-250 mg HC/g TOC, OI: 50-150 mg CO_2/g TOC) is considered to be the typical gas-prone facies. It is composed mainly of partially oxidized terrestrial OM and generally occurs in carbonate rocks only in limited amount. Nevertheless, several processes can be

Table 4: Average values of source potential (mg HC/g rock) calculated for samples containing different organic facies

C_{carb} %	Organic facies D	CD	C	BC
<6	0.25	0.44	2.41	–
>6	0.15	0.30	0.79	2.49
average	0.22	0.34	0.99	2.49

involved in the formation of organic facies C in carbonate rocks. A limited amount of higher plant debris is common source of OM composed of mainly vitrinite. However, degradation of algal debris, which is the main precursor of the oil-prone organic facies AB or B, can also lead to the formation of gas-prone C facies. The variation in the oxygen content at the water sediment interface can stabilize the degrading algal-derived OM in the geochemical characteristics of organic facies C (Dean et al., 1981). In anoxic environment this facies can also be formed from a mixture of algal debris and inertinite. On the basis of our results the probable scenario for development of organic facies C in carbonate rocks, studied here, is the existence of a mixture of different organic precursors deposited in an oxic environment. Results of organic petrographical analysis performed on two samples (490.8 and 511.8 m) with different carbonate content (C_{carb} are 3.63 and 8.08 %, respectively) exhibit a small amount of algal-derived OM beside a significant amount of highly degraded inertinite and vitrinite. The algal-derived OM was probably protected from degradation by inclusion in carbonate skeleton. A similar protection effect of carbonate skeleton could play an important role in the preservation of marine OM in the Triassic-Jurassic boundary section of the Csővár Limestone Fm., too. These sediments contain an extremely low amount of hydrogen-rich oil prone kerogen (Pálfy et al., 2001). The remarkably higher SP of samples, having organic facies C compared with samples having organic facies CD (Table 4), can be attributed to the minor input of the oil-prone algal-derived OM. This assumption is confirmed by the different ratios of the average values of C_{org} content (1.5) and that of SP (2.9) calculated for samples containing C and CD facies. Despite the minor well preserved oil-prone algal-derived input, the OM has gas-prone character. No matter what type of kerogen they have, gas-prone rocks produce only a negligible amount of oil. It can be due to the adsorption of hydrocarbons generated by liptinite macerals on inertinite and vitrinite. The adsorbed hydrocarbons are gradually cracked within these macerals and not released until the dry gas stage of maturation is reached. (Albrecht et al., 1976; Behar and Vandenbroucke, 1988). Probably a slightly higher proportion of the relatively well-preserved liptinite resulted in organic facies BC at the top (509.5 m depth) of the lower section containing organic facies C.

Results presented here indicate interlayerings of organic facies C, CD and D. An upward decreasing trend in the H-richness and in the SP of the studied sequence is manifested well by variations of different organic facies. Alternations of C-CD and those of CD-D facies are characteristic below and above 471.5 m, respectively.

Conclusions

The studied succession is rich in carbonates and contains a low amount of organic matter, C_{org} content is less than 1 % for all but one sample. Cyclic variations observed in both of the C_{carb} and C_{org} content can be interpreted by cyclic alternation of carbonate sedimentation and argillaceous one controlled by short-term (100-400 ka) sea-level fluctuation.

The OM is of predominantly terrestrial origin and probably accumulated in an oxic environment.

On the basis of the C_{carb} and C_{org} content three groups of the samples can be differentiated.

1) Half of the samples is composed of mainly carbonate minerals (C_{carb} >10 %) with very low C_{org} content (<0.2 %). These rocks can not be considered as source rocks, either for oil or gas and they are not available for assessment of organic facies. Most of them were formed during shallow subtidal carbonate sedimentation. Due to the highly oxic environment only a negligible part of the OM was preserved.

2) During sea-level rise due to backstepping of the carbonate producing platform the predominantly carbonate sedimentation was progressively replaced by an argillaceous one (Haas, 1993). Decreasing carbonate content is associated with slightly increasing abundance of organic carbon. About 35 % of the samples (average C_{carb} content is 9 %) deposited in relatively deeper water during sea-level rise, when a slightly higher proportion of the OM was preserved resulting in a continous suite of organic facies D-CD-C-BC in the rocks with 0.39 % of average C_{org} content. More than half of these samples contains organic facies CD with low SP (0.34 mg HC/g rock). OM is predominated by degraded inertinite and vitrinite. The significantly higher SP (0.99 mg HC/g rock) of C facies, and that of the only sample containing BC facies (2.49 mg HC/g rock), can be attributed to a minor amount of algal-derived liptinite which was probably preserved by inclusion in carbonate skeleton.

3) The further sea-level rise associated with increasing land-derived contribution resulted in lower abundance of carbonate minerals (C_{carb} <6 %) and higher amount of OM (average C_{org} is 0.65 %) for the 15 % of the samples. The OM originated practically only from terrestrial-derived precursors. These rocks contain organic facies D (SP: 0.25 mg HC/g rock), composed of inertinite, and preferentially organic facies CD (SP: 0.44 mg HC/g rock), composed of inertinite and vitrinite.

The different SP of the rocks, containing the same organic facies and different carbonate content, is consistent with their C_{org} content.

SP displays much scatter and upward decreasing trend. Cyclic alternations of CD facies and the gas-prone C facies are characteristic of the lower section of the studied succession. Variations of CD facies and non-generative D facies were observed for the upper section.

Acknowledgements

The author thanks the Hungarian Scientific Research Fund (OTKA) (grant T- 34168) for financial support. Dr. M. Hámor-Vidó is acknowledged for results of petrographical analysis. Helpful comments of the referees (Dr. J. Haas and Dr. I. Vető) are gratefully appreciated.

References

Albrecht, P., Vandenbroucke, M., Mandenqué, M. (1976): Geochemical studies on the organic matter the Doula Basin (Cameroon). I. Evolution of the extractable organic matter and the formation of petroleum. Geochimica et Cosmochimica Acta, **40**, 791-799.

Balla, Z. (1988): Clockwise paleomagnetic rotations in the Alps in the light of the structural pattern of the Transdanubian Range (Hungary). Tectonophysics, **145**, 277-292.

BALOG, A., READ, J.F., HAAS, J. (1999): Climate-controlled early dolomite, late Triassic cyclic platform carbonates, Hungary. Journal of Sedimentary Research, **69**, 267-289.

BEHAR, F., VANDENBROUCKE, M. (1988): Characterization and quantification of saturates trapped inside kerogen: implications for pyrolysate composition. In Mattiavelli, L. and Novelli, L. (eds.) Advances in Organic Geochemistry 1987. Organic Geochemistry, **13**; 927-938.

BORDENAVE, M. L., ESPITALIÉ, J., LEPLAT, P., OUDIN, J. L., VANDENBROUCKE, M. (1993): Screening techniques for source rock evaluation. In Bordenave, M. L. (ed.): Applied Petroleum Geochemistry. Éditions Technip, Paris, 217-276.

BRUKNER-WEIN, A., VETŐ, I. (1986): Preliminary organic geochemical study of an anoxic Upper Triassic sequence from W. Hungary. Organic Geochemistry, **10**, 113-118.

Clayton, J. L., Koncz, I. (1994): Petroleum geochemistry of the Zala Basin, Hungary. American Association of Petroleum Geologists Bulletin **78**, 1-22.

ESPITALIÉ, J., LAPORTE, J.L., MADEC, M., MARQUIS, F., LEPLAT, P., PAULET, J., BOUTEFEU, A. (1977): Méthode rapide de charactérisation de roches méres, de leur potentiel pétrolier et de leur degré d'evolution. Revue de L'Institute Francais du Petrole, **32**, 23-45. Éditions Technip, Paris.

ESPITALIÉ, J., DEROO, G., MARQUIS, F. (1986): La pyrolyse Rock-Eval et ses applications. Revue de L'Institute Francais du Petrole, **40/5**, 563-784. Éditions Technip, Paris.

ESPITALIÉ, J., BORDENAVE, M.L. (1993): Tools for source rock routine analysis: Rock Eval pyrolysis. In Bordenave, M.L. (ed.): Applied Petroleum Geochemistry, 217-276. Éditions Technip, Paris.

HAAS, J. (1993): Formation and evolution of the „Kössen Basin" in the Transdanubian Range. Földtani Közlöny, **123/1**, 9-54 (in Hungarian).

HAAS, J. (2002): Origin and evolution of Late Triassic backplatform and intraplatform basins in the Transdanubian Range. Geologica Carpathica **53/3**, 159-178.

HAAS, J., BUDAI, T. (1995): Upper Permian-Triassic facies zones in the Transdanubian Range. Rivista Italiana di Paleontologi e Stratigrafia, **101**, 249-266.

HAAS, J., CSÁSZÁR, G., KOVÁCS, S., VÖRÖS, A. (1990): Evolution of the western part of the Tethys as reflected by the geological formations of Hungary. Acta Geodetica Geophysica et Montanistica Hungarica, **25**, 325-344.

HETÉNYI, M. (1989): Hydrocarbon generative features of the upper Triassic Kössen Marl from W. Hungary. Acta Mineralogica-Petrographica, **30**, 137-147.

HETÉNYI, M., BRUKNER-WEIN, A., SAJGÓ, CS., HAAS, J., HÁMOR-VIDÓ, M., SZÁNTÓ, ZS., TÓTH, M. (2002): Variations in organic geochemistry and lithology of a carbonate sequence deposited in a backplatform basin (Triassic, Hungary). Organic Geochemistry (in press)

HUNT, J. M. (1972): Distribution of carbon in crust of Earth. American Association of Petroleum Geologists Bulletin **56**, 2273-2277.

JONES, R. W. (1984): Comparison of carbonate and shale source rocks. In Palacas, J.G. (ed.) Petroleum geochemistry and source rock potential of carbonate rocks, AAPG Studies in Geology **18**, 163-180.

JONES, R. W. (1987): Organic facies. In J. Brooks and D. Welte (eds.) Advances in Petroleum Geochemistry, **2**, 1-90.

JONES, R. W., DEMAISON, G.W. (1982): Organic facies-stratigraphic concept and exploration tool. In R. Saldivar-Sali (ed.): Proceedings of the Second ASCOPE Conference and Exhibition, Manila, 51-68.

KÁZMÉR, M., KOVÁCS, S. (1985): Triassic and Jurassic oceanic/paraoceanic belts in the Carphatian-Pannonian region and its surroundings. In Sengor, A. M. C. (ed.) Tectonic Evolution of the Tethyan Region. Kluwer, Dordrecht, 128-139.

KLIMETZ, M. P. (1983): Speculations on the Mesosoic plate tectonic evolution of eastern China. Tectonics, **2**, 139-166.

ORAVECZ-SCHEFFER, A. (1987): Triassic Foraminifers of the Transdanubian Central Range. Geologica Hungarica, Series Paleontologica, **50**, 1-331.

PÁLFY J., DEMÉNY A., HAAS, J., HETÉNYI M., ORCHARD M.J., VETŐ I. (2001): Carbon isotope anomaly and other geochemical changes at the Triassic-Jurassic boundary from a marine section in Hungary. Geology, **29**, 1047-1050.

PARRISH, J. T. (1993): Climate and supercontinent Pangea. Journal of Geology, **101**, 215-233.

ROGERS, M. A. (1980): Application of organic facies concepts to hydrocarbon source rock evaluation. Proceedings of the 10th World Petroleum Congress, 1979, 23-30.

TISSOT, B. P., DURAND, B., ESPITALIÉ, J., COMBAZ, D. (1974): Influence of nature and diagenesis of organic matter in formation of petroleum. American Association of Petroleum Geologists Bulletin **58**, 499-506.

TISSOT, B. P., WELTE, D. H. (1984): Petroleum Formation and Occurrence, 2nd Edition. Springer, Berlin, pp. 699.

VETŐ, I., HETÉNYI, M., HÁMOR-VIDÓ, M., HUFNAGEL, H., HAAS, J. (2000): Anaerobic degradation of organic matter controlled by productivity variation in a restricted late Triassic basin. Organic Geochemistry, **31**, 439-452.

ZIEGLER, A. M., SCOTESE, C. R., BARETT, S. F. (1983): Mesosoic and Cenozoic paleogeographic maps. In P. Borsche, J. Sundermann (eds.): Tidal Friction and the Earth's Rotation, II. Springer Verlag, New York, 240-252.

Received: October 28, 2002; accepted:November 30, 2002

Acta Mineralogica-Petrographica, Szeged 2002, Vol. 43, pp. 27-38

ACTA
Mineralogica
Petrographica

ORIGIN AND TECTONIC HISTORY OF SOME METAMORPHIC ROCKS FROM SOUTHERN SINAI, EGYPT

ABDEL-AAL ABDEL-KARIM [1], ZUARD PUSKÁS [2], MELINDA JÁNOSI [2]

[1] Geology Department, Faculty of Science, Zagazig University, Egypt.
[2] Department of Petrology and Geochemistry, Eötvös Loránd University, Hungary
e-mail: abdelaalabdelkarim@hotmail.com

ABSTRACT

The Baba schists and gneisses, in the extremely northwestern part of the metamorphic belt of Sinai, have been discussed in terms of the mode of occurrence, evolution of mineral chemistry, major, trace and rare earth elements (REE) and age dating. They exhibit a trondhjemitic composition and comprise four metamorphic zones, namely the chlorite, biotite, almandine and cordierite zone. They are derived from pelitic + semi-pelitic rocks affected by three episodes of metamorphism. The first episode is a low-grade regional metamorphism of greenschist facies, the second episode is lower amphibolite facies metamorphism with higher temperature and similar pressure followed by the third episode of a retrograde metamorphism with decreasing temperature and pressure.

Chemically, the schists and gneisses are similar to crustal sediments and evolved intermediate igneous rocks, which are the source of these sediments. We assume that, they represent metamorphosed pelitic and intermediate volcanoclastic sediments that underwent hydrothermal alteration and were affected by metamorphic differentiation and partial melting. The schists and gneisses have REE patterns analogous to the intermediate igneous rocks of island arc. There are minor but interesting differences between schists and gneisses. The gneisses are characterized by higher contents of TiO_2, Hf, Ta, U, Zr, Nb and REE and lower contents Sc, Cr and Co relative to the schists, probably due to the influence of the accessory zircon, apatite and monazite and/or the more pronounced effects of the metamorphic differentiation on the gneisses.

K-Ar age dating of gneisses gives ages of 620 ± 24 Ma and 602 ± 23 Ma. The former age may represent the nearest estimated age for the formation of the protolith of the gneisses, meanwhile, the second one probably records the age of metamorphism. The schists yield an age of 549 ± 22 Ma, which may be represent the late retrograde metamorphism effected the schists.

Key words: gneisses, schists, Southern Sinai, mode of occurrence, geochemistry, K-Ar age dating, origin, and metamorphic evolution

INTRODUCTION

Metamorphic rocks are of limited distributed in Sinai massif and represent, together with some sediments, the oldest rocks in the Precambrian area of the district. They are believed to have formed through regional metamorphism took place about 1100-1300Ma (El-Shazly et al., 1973; Siedner et al., 1974). These rocks occur in a few exposures in Sinai. The larger exposure is the Wadi Feiran-Solaf belt (Akaad et al., 1967 a, b, 1988; El-Gaby, Ahmed, 1980) which locates only about 30 km south of the studied area.Some of the metamorphic rocks of the Wadi Baba area under study have been examined and mapped by El-Aref et al. (1988, 1989). They studied the geology geochemistry and fabric evolution of the migmatitic rocks. According to them these migmatitic rocks are formed by migmatization processes including metamorphic differentiation, limited and higher degrees of partial melting and were metamorphosed up to amphibolite facies. Only a few age dating of some schists and gneisses from the metamorphic belt of Sinai have been discussed. Elat schists yielded 807 ± 35 Ma with Sr87/ Sr86 initial ratio of 0.7030 for the biotite-muscovite chlorite-garnet schist (Halpern, Tristan, 1981) and 791 ± 48 Ma with 0.7030 initial ratio for age of sedimentation of the biotite-muscovite-amphibole schist (Bielski, 1982). The latter author reported that the Feiran and Fjord gneisses have age of 641-656 Ma with initial Strontium ratio of 0.7073-0.7043. Stern and Manton (1987) reported that the Wadi Feiran paragneisses gave 632 ± 3 Ma for the U-Pb zircon age and 610 Ma ago for Rb-Sr whole rock dating. This paper discusses the petrology, mineral chemistry, geochemistry and age dating aspects to through light on the origin, the tectonic environment and the conditions that prevailed during the metamorphism of these rocks.

METHODS

Thirty nine chemical analyses of chlorite (9), muscovite (6), biotite (11), garnet (10) and cordierite (3) from the schists and gneisses of Wadi Baba area, southwest Sinai have been carried out using a computerized AMRAY-1830 IT6 electron microprobe analyzer operated at 20 KV accelerating voltage, with 1-2 nA specimen current. Ten rock samples from schists and gneisses were analyzed for major elements by standard wet chemical technique. Also, six of these samples were analyzed for the trace elements Sc, Cr, Co, Zn, Rb, Ba, Cs, Hf, Ta, Th, U, Sr, Nb, Y, Zr and rare earth elements (REE). Trace elements were determined by standard instrumental neutron activation analysis (INAA) except for Nb, Y and Zr which were measured by the optical atomic spectro-photometry method (PGS-2C Zeiss Jena) and REE in the Atomic Reactor of Technical University and Sr by atomic absorption technique (AA 474). The analyses of microprobe and major elements together with Sr, Nb, Y and Zr were carried out in the Department of Petrology and Geochemistry of Eotvos University and trace elements University, Budapest. Selected three analyses for biotite fractions separated from the studied schist and gneiss were

measured by K-Ar age dating method. The analyses were carried out in the Institute of Nuclear Research (ATOMKI) of Hungarian Academy of Science in Debrecen, Hungary.

Geological Setting

Schists and gneisses of Wadi Baba constitute an important part in the metamorphic belt of the extreme northwestern Sinai massif (Fig. 1). This belt forms isolated small bodies (up to 2 km^2) exposing in Wadis Baba, Hamata, el-Sih, Nukhul and Khaboba. Many more occurrences of the belt are certainly hidden under widely distributed thick beds of the Cambrian Ordovician sandstone (Weissbrod, 1969) and Carboniferous carbonates (EL-Aref et al., 1988). Schists and gneisses under study constitute the main rock types of Baba metamorphic belt. They form low to moderate hilly rocks, tectonically controlled, trend NNW-SSE and NW-SE direction and exhibit a pronounced banded structure. The general dip of foliation is NW-SE direction with angle dip of 120° / 30°. The studied schists and gneisses are dissected by number of pegmatite and quartz veins, which are often intercalated with the general trend of foliation. The schists and gneisses are deep green to dark grey in colour. The grain size, type of mineral assemblage and grade of metamorphism appear to be graded from schists to gneisses. These rocks are enclosed in the older granites, intruded by younger granites and cut by mafic and felsic dykes and are regionally overprinted by greenschist to lower amphibolite facies. The older granites are massive to gneissose, coarse-grained, dark grey colour and range in composition from quartz diorite to granodiorite. The younger granites are medium to coarse-grained and occasionally porphyritic, pinkish in colour and range from monzogranite to syenogranite and even alkali feldspar granite. They show irregular contact with metasedimentary country rocks. Due to the intrusion of granitic rocks, the original low-grade metasediments (chlorite schists) are subjected to contact metamorphism and subsequently transformed into medium-grade pelitic to semi-pelitic schists and gneisses.

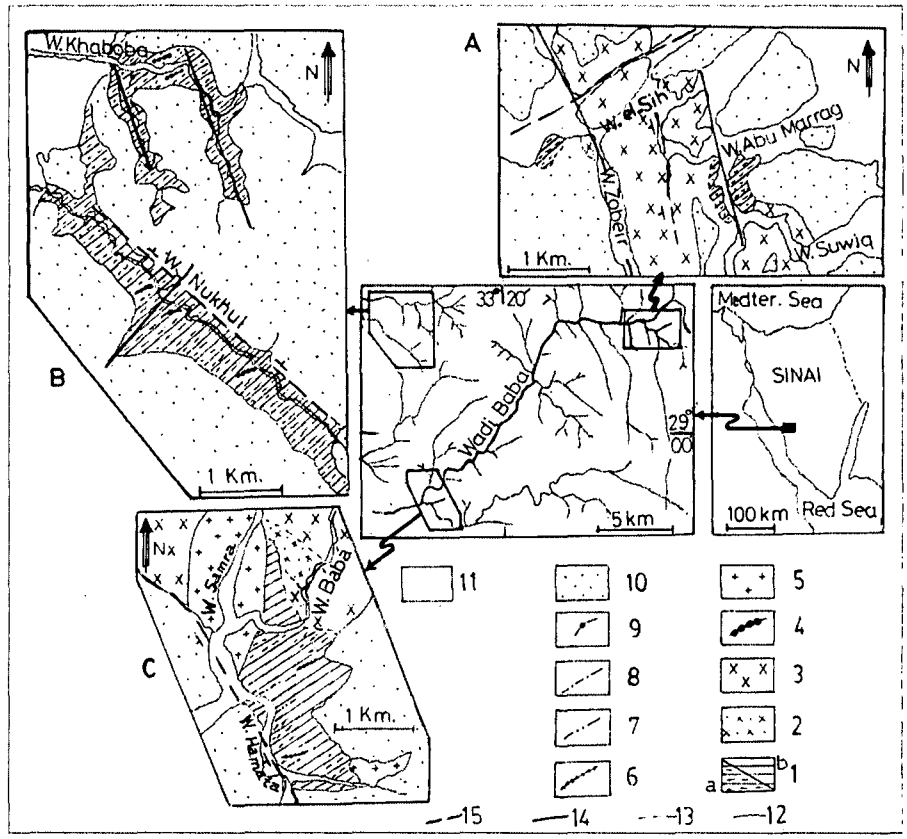

Fig. 1. Location map of the studied schists and gneisses of Wadi Baba area, SW-Sinai. A, B and C) geological maps for Wadis el-Sih, Khaboba and Nukhul and Hamata areas. Designation: 1=Metamorphic rocks, a) schists, b) gneisses; 2=Metagabbro-diorite complex; 3=Older granites; 4=mafic dykes; 5=Younger granites; 6=felsic dykes; 7=pegmatitic veins; 8=quartz veins; 9=basaltic dykes; 10=Phanerozoic sediments; 11= Wadi deposits:12= sharp contacts; 13=gradational contacts; 14=minor tectonic lines; 15=major normal faults

Table 1. The main petrographic features of the Baba schists and gneisses.

Rock name	Metamorphic texture	Mineral assemblage Essential	Accessory	Seconary
Mus-chl-gar-bio schist	porbl, lepbl.	alb, bio, qz, gt, mus.	zir, ap, tou.	chl.
Bio schist	lepbl, poikbl.	olig, bio, qz.	zir, ap.	ser, kao.
Gar-bio schist	porbl, lepbl.	olig, bio, qz, gar.	zir, ap.	chl.
Sil-gar-bio schist	poikbl, lepbl.	ab, bio, qz, gar, sil.	zir, ap, tou.	chl, ser.
Sil-cord-bio schist	lepbl, hel.	ab, bio, qz, crd, sil.	zir, ap, tou.	chl, ser.
Bio gneiss	–	olig, bio, qz, kf.	zir, ap.	ser, kao.
Cord-bio gneiss	lepbl, poikbl.	olig, bio, qz, crd, kf.	mon, ap.	ser.
Gar-cord-bio gneiss	porbl, lepbl.	olig, bio, qz, cord, gar.	zir, mon.	ser, kao.
Sil-cord-bio gneiss	lepbl, hel.	olig, bio, qz, crd, sil.	mus, zir, mon, ap.	ser.

Abbreviations – Minerals: alb=albite, and=andesine, ap=apatite, bio=biotite, chl= chlorite, cord=cordierite, gt=garnet, kao=kaolinite, kf=k-feldspar, mon=monazite, mus=muscovite, olig=oligoclase, qz=quartz, ser=sericite, sil=sillimanite, tou=tourmaline, zir=zircon. Textures: grabl=granoblastic, hel=helicitic, lepbl=lepidoblastic, poikbl=poikiloblastic, porbl=porphyroblastic

PETROGRAPHY

Microscopically, these rocks made up of plagioclase, biotite, quartz, garnet, chlorite, muscovite and cordierite ± sillimanite. The accessory phases include zircon, apatite, tourmaline and monazite. The main secondary phases comprise chlorite, sericite and kaolinite. The main petrographic features including the petrographic varieties, textures and mineral assemblages are summarized in Table 1. Moreover, the modal composition of the studied rocks is listed in Table 2. The present schists and gneisses have been affected by three main phases of deformations. D_1 is represented by the main foliation of the rocks (S_1), mineral lineation and segregation of quartz streaks parallel to the foliation. D_2 resulted in deformation of S_2 and the formation of

Table 2. Results of modal composition of Baba schists and gneisses

Rock name, no.		pla	bi	q	mu	ga	cr	si	k	ch	Acc	Su
Schists.	257	52	10	2	6	5	-	2	-	3	-	100
	210	53	15	2	-	3	-	-	-	3	1	100
	183	50	9	2	2	4	-	5	-	4	-	100
	197	54	15	2	-	-	-	1	-	3	1	100
	280	49	4	2	-	4	5	2	-	8	1	100
Gneisses:	36	49	23	2	2	-	-	-	1	1	1	100
	11	29	35	1	-	-	20	-	1	-	1	100
	265	49	15	1	-	4	12	-	1	-	1	100
	13	48	12	1	-	-	17	4	-	2	1	100

discordant with Se (Fig. 2B). The foliation of the matrix often warps around the garnet porphyroblast. Also, there is a marked cracking or straining in the porphyroblast which is angularly discordant with S_e.c) Syn-tectonic porphyroblast growth in which a classic "snowball garnet" with about 360° rotation during growth (Fig. 2C).This consists of a spiral pattern inclusions within the porphyroblast being rolled by shear along the schistosity plane as it grew.

MINERAL CHEMISTRY

Microprobe data of chlorite, muscovite, biotite, garnet and cordierite occurring in schists and gneisses together with their structural formulae are given in Table 3. The

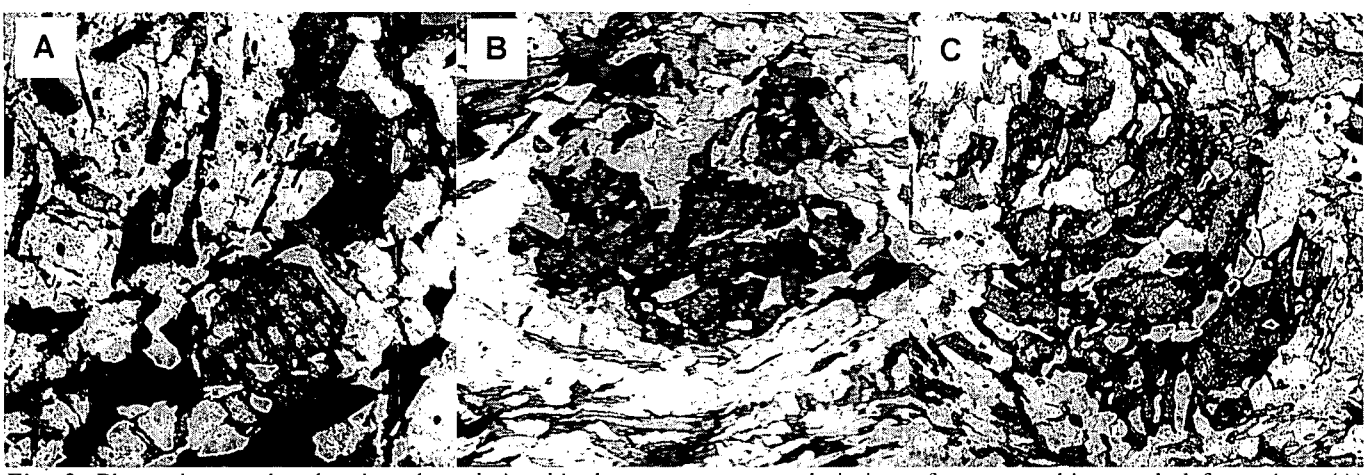

Fig. 2. Photomicrographs showing the relationship between garnet and timing of metamorphism and deformation: *(A)* nucleation and development of idiomorphic garnet in a fine-grained schist, *(B)* pre-tectonic porphyroblast growth in which the Si and cracking of garnet are discordant with Se, *(C)* syn-tectonic porphyroblast growth in which classic "snowball garnet" is rotated more than 180° during growth

second mineral lineation. D_3 is represented by the formation of S_3 and development of minor folds, kinks and granodioritic veins. The relationships between metamorphic textures and the timing of metamorphism and deformation reveal three stages of evolution relative to the pattern of inclusions in garnet porphyroblasts (S_i) and the dominant foliation in the rest rocks (S_e). These features appear in Fig. 2 and comprise the following: a) Nucleation of garnet in fine-grained schist (Fig. 2A) by diffusion of material towards a newly formed nucleus until the rock has begun to equilibrate with it.b) Pre-tectonic porphyroblast growth in which the the internal fabric (S_i) is likely to be

Table 3. Results of microprobe analysis of selected minerals, Baba schists and gneisses

Chlorites									
	Schist						Gneiss		
	257	257	257	183	183	183	36	36	36
	F11	F12	F13	H11	H12	H13	M11	M12	M13
	core		rim	core		rim	core		rim
SiO_2	26.09	26.08	26.16	22.55	25.92	25.6	27.89	27.47	26.90
Al_2O	22.36	22.49	22.85	22.8	23.12	22.73	19.52	19.41	19.94
FeO_t	22.5	22.5	23.02	23.70	23.64	23.7	26.74	26.93	28.26
MgO	17.25	17.23	17.18	15.85	15.72	15.66	14.23	14.32	13.66
Sum	88.20	88.3	89.21	87.90	88.4	87.69	88.38	88.13	88.76
Cation numbers based on 28 Oxygenes									
Si	5.364	5.355	5.326	2.307	5.342	5.329	5.836	5.780	5.664
Al	5.419	5.444	5.484	5.583	5.617	5.578	4.815	4.815	4.394
Fe	3.860	3.855	3.911	4.107	4.065	4.117	4.669	4.728	4.965
Mg	5.283	5.270	5.211	4.904	4.826	4.857	4.436	4.489	4.284
Xmg	0.58	0.58	0.57	0.54	0.54	0.54	0.49	0.49	0.4

analyses minerals exhibit major compositional variations. Graphical representation of these minerals on the AFM diagram (based on Winkler, 1976) is shown in Fig. 3. In this figure, the data points of the studied minerals plot in or near fields of the same mineral assemblage which characterize the pelitic rocks. Chlorites: 3 chlorite grains, 2 from schist and 1 from gneiss were analysed (Table 3).The analysed chlorites were plotted on the $Fe_t/(Fe_t+Mg)$ ratio versus Si classification diagram of Hey (1954) (Fig. 4). In this figure the chlorites of the schist fall in the ripidolite field while that from gneiss fall in the pycnochlorite field. The analysed chlorites from gneiss are enriched in Si compared with that from schist. Nevertheless, the Mg decreases and the Si increases from schist to gneiss with progressive

Table 3 continued

Muscovites							Cordierrites			
	Schist			Gneiss				Schist		Gneiss
	257 G11 core	257 G12	257 G13 rim	36 L11 core	36 L12	36 L13 rim		280 M11 core	280 M12 rim	13 N11
SiO_2	46.37	45.66	46.92	46.23	46.70	45.82	SiO_2	47.50	47.20	46.85
Al_2O_3	33.66	34.49	34.14	34.47	.4.23	34.94	Al_2O_3	61.60	32.38	30.81
TiO_2	0.78	0.50	0.35	0.67	0.63	0.58	FeO_t	8.65	8.73	9.62
FeO_t	0.79	1.81	0.85	0.93	1.21	1.14	MnO	0.05	0.04	0.05
MgO	1.33	1.51	1.32	1.28	1.16	1.18	MgO	8.52	7.55	733
Na_2O	1.67	1.86	1.77	1.71	1.78	1.72	CaO	0.54	0.52	0.53
K_2O	9.77	9.34	0.11	9.22	9.27	9.55	Na_2O	0.05	0.55	0.59
Sum	94.30	98.17	95.46	94.51	94.98	94.64	K_2O	0.45	0.48	0.49
Cation numbers based on 22 Oxygenes							Sum	97.82	97.45	96.27
Si	6.240	6.104	6.241	6.178	6.218	6.120	Cation numbers based on 18 Oxygenes			
Al_{IV}	1.760	1.896	1.759	1.822	1.782	1.880	Si	4.930	4.680	4.520
Z	8.000	8.000	8.000	8.000	8.000	8.000	Al	3.681	3.794	3.580
Al_{VI}	3.578	3.538	3.593	3.607	3.589	3.620	Fe_t	0.847	0.872	0.993
Ti	0.079	0.050	0.035	0.067	0.063	0.058	Mn	0.004	0.003	0.004
Fe	0.092	0.202	0.094	0.104	0.135	0.127	Mg	1.550	1.580	1.482
Mg	0.236	0.301	0.252	0.225	0.230	0.232	Ca	0.103	0.102	0.182
X	3.985	4.091	3.974	4.003	4.017	4.017	Na	0.050	0.060	0.065
Na	0.436	0.482	0.456	0.443	0.459	0.455	K	0.060	0.067	0.092
K	1.577	1.593	1.615	1.572	1.574	1.608	Xmg	0.66	0.61	0.60
Y	2.013	2.075	2.061	2.015	2.021	2.063				
Xmg	0.75	0.68	0.73	0.68	0.63	0.65				

Biotites											
	Schist						Gneiss				
	257 D11 core	257 D12	257 D13 rim	257 E11 core	257 E12	257 E13 rim	36 C11 core	36 C12	36 C13	36 C14	36 C15 rim
SiO_2	34.81	35.28	35.36	36.03	36.05	35.80	35.79	35.45	35.23	34.47	34.94
Al_2O_3	18.89	18.87	19.09	18.70	18.39	18.56	18.26	18.99	18.66	18.76	18.34
TiO_2	2.26	2.28	2.27	3.04	3.03	3.00	2.59	3.09	2.90	2.38	3.20
FeO_t	20.02	20.32	20.81	18.45	18.56	19.14	20.29	20.89	20.80	20.54	20.66
MgO	9.42	9.64	9.93	10.72	10.47	10.74	8.74	8.35	9.09	10.55	8.98
K_2O	9.15	9.08	9.19	8.82	9.03	8.54	8.83	8.77	8.70	8.26	8.95
Sum	94.55	95.47	93.65	95.76	95.53	95.78	94.51	95.54	94.38	94.96	95.07
Cation numbers based on 22 Oxygenes											
Si	5.319	5.336	5.297	5.372	5.399	5.348	5.454	5.354	5.366	5.318	5.322
Al_{IV}	2.681	2.664	2.703	2.628	2.601	2.652	2.546	2.646	2.634	2.682	2.678
Z	8.000	8.000	8.000	8.000	8.000	8.000	8.000	8.000	8.000	8.000	8.000
Al_{VI}	0.721	0.700	0.669	0.658	0.645	0.616	0.734	0.734	0.716	0.712	0.614
Ti	0.260	0.259	0.256	0.341	0.341	0.337	0.397	0.351	0.332	0.285	0.366
Fe	2.134	2.150	2.167	1.920	1.942	1.999	2.167	2.198	2.102	2.3034	2.191
Mg	2.145	2.173	2.217	2.382	2.337	2.392	1.985	1.880	2.064	2.314	2.039
Y	5.260	5.282	5.309	5.301	5.365	5.344	5.293	5.153	5.204	5.335	5.210
K	1.783	1.752	1.756	1.677	1.725	1.628	1.717	1.690	1.690	1.646	1.739
X	1.783	1.752	1.756	1.677	1.725	1.628	1.717	1.690	1.690	1.646	1.739
Xmg	0.50	0.50	0.51	0.55	0.55	0.55	0.48	0.42	0.50	0.50	0.48

Table 3 continued

Garnets										
	Schist					Gneiss				
	257 B11 core	257 B12	257 B13	257 B14	257 B15 rim	265 A11 core	265 A12	265 A13	265 A14	265 A15 rim
SiO_2	36.17	36.29	36.06	35.63	36.11	36.00	36.00	36.12	36.27	36.30
Al_2O_3	19.86	20.04	19.89	20.08	20.11	19.87	19.82	20.04	20.35	20.11
CaO	2.38	2.34	2.84	2.66	2.74	2.79	2.72	2.79	2.29	2.89
MnO	2.85	2.67	1.81	1.60	1.90	3.88	3.72	3.89	3.91	3.88
MgO	3.39	3.25	2.88	2.91	2.91	3.04	2.98	2.71	3.29	3.13
FeO_t	34.94	35.19	36.36	36.69	36.75	33.44	33.76	33.58	34.33	33.77
Sum	99.59	99.75	99.89	99.57	99.99	99.02	99.00	99.13	99.99	99.99
Cation numbers based on 22 Oxygenes										
Si	2.959	2.962	2.953	2.929	2.940	2.961	2.963	2.967	2.943	2.954
Al_{IV}	0.041	0.038	0.047	0.071	0.060	0.039	0.037	0.033	0.057	0.046
Z	3.000	3.000	3.000	3.000	3.000	3.000	3.000	3.000	3.000	3.000
Al_{VI}	1.864	1.880	1.862	1.864	1.860	1.877	1.886	1.897	1.879	1.873
Fe^{3+}	0.136	0.120	0.138	0.136	0.140	0.123	0.114	0.103	0.121	0.127
Y	2.000	2.000	2.000	2.000	2.000	2.000	2.000	2.000	2.000	2.000
Fe^{2+}	2.243	2.280	2.330	2.321	2.322	2.175	2.202	2.222	2.181	2.158
Mn	0.197	0.184	0.125	0.111	0.131	0.270	0.259	0.271	0.269	0.267
Mg	0.413	0.395	0.351	0.357	0.353	0.373	0.366	0.332	0.398	0.380
Ca	0.209	0.205	0.249	0.234	0.239	0.246	0.240	0.245	0.199	0.252
X	3.062	3.064	3.055	3.023	3.045	3.064	3.067	3.070	3.056	3.057
Xmg	0.15	0.14	0.12	0.13	0.12	0.14	0.14	0.13	0.15	0.14
End members										
Alm.	73.2	73.1	76.1	74.4	75.9	71.0	71.0	72.0	71.4	70.5
Pyr.	13.3	13.1	11.4	10.0	11.5	12.1	12.0	11.1	13.0	12.3
Ynd.	6.7	7.0	6.9	6.5	7.0	6.2	6.3	5.1	6.0	6.2
Spess.	6.5	6.0	4.0	3.1	4.1	8.7	8.6	9.0	8.6	8.7
Gros.	0.2	0.8	1.6	2.0	1.4	2.0	2.0	2.8	1.0	2.2

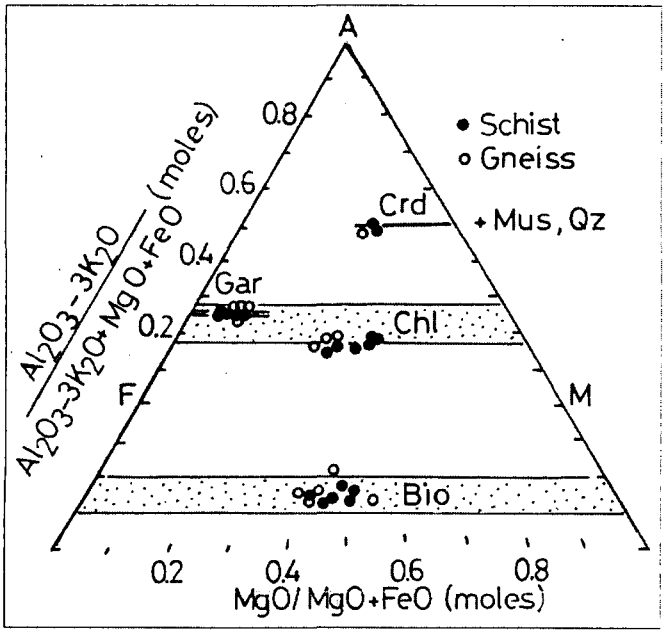

Fig. 3. Graphical representation of the analysed chlorites, biotites, garnets and cordierites into the AFM diagram (Based on Winkler, 1976). A= Al2O3-3K2O/(Al2O3-3K2O+FeO+MgO) (moles), M= MgO/(MgO+FeO) (Moles)

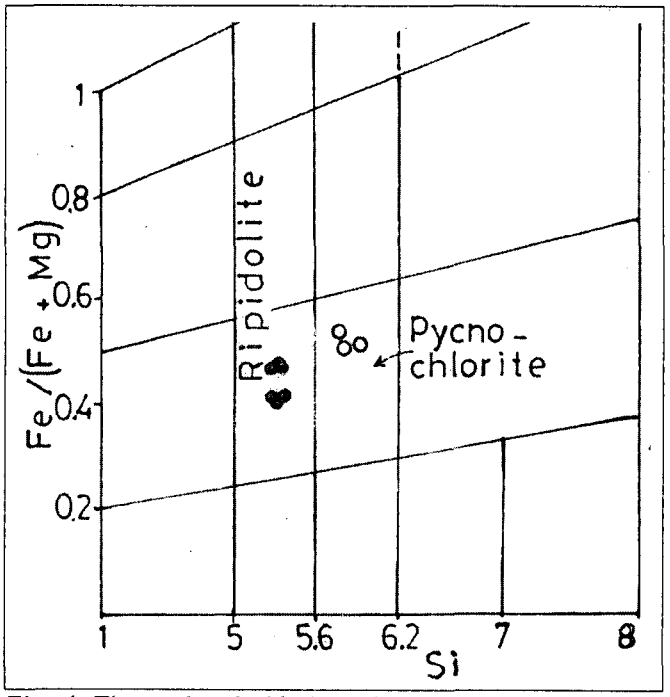

Fig. 4. The analysed chlorites plotted into Fe/(Fe+Mg)-Si classification diagram (after Hey, 1954)

metamorphism. Fet increases and Mg decreases from core to rim of the grain. Moreover, the rim of chlorite grain in gneiss is richer in Fet and poorer in Mg compared with that of schist showing evolutionary trend with the prograde metamorphism. Hyndman (1985) suggested that the composition of chlorites range from Fe-rich in chlorite zone to Mg-rich in garnet&staurolite zone [i.e. Fe_t /(Fe_t +Mg) ratio=0.5-0.8]. The analysed chlorites are Mg-Fe chlorite series and range from 0.55-0.67 with an average of 0.6, indicating their similarity with that formed in the chlorite zone. Muscovites are plotted on classification diagram of Harrison (1990), (Fig. 5A). In this figure the analysed samples from both schist and gneiss fall near the muscovite end member. Miyashiro (1973) classified the zones of muscovites into chlorite, biotite and almandine and stuarolite and sillimanite zones based on Al_2O_3 and FeO_t contents. The present muscovite plots in the field of the muscovite co-existing with the chlorite, biotite and almandine zone (Fig. 5B).

The studied muscovites have higher Si and lower Al and Na suggesting their occurrence in the chlorite zone. Lambert (1959) mentioned that the muscovite of the chlorite zone have higher Si and Fet and lower Al and Na contents than those of the biotite or garnet zone. Biotites: the investigated biotite include 2 grains from schists and 1 from gneiss (Table 3). The composition of biotites from the studied schists and gneisses are shown in Fig. 6 in terms of Al, Mg and Fe (after Nemec, 1972). This figure indicates that the analysed biotites fall on siderophyllite-eastonite line showing an equal values of these terms. Several studies have concluded that the Ti and Mg contents of biotite increase with increasing grade of metamorphism (Guidotti, 1984). The analysed biotitea are characterized by increase of Mg (from 2.15 and 2.38 in core to 2.22 and 2.4 in rim of the schists and from 1.99 in core to 2.04 in rim of the gneisses) with increasing grade, suggesting an increase in metamorphic grade from cor to rim of biotite flakes in both schists and gneisses. This increase of Mg in biotite is equilibrated partially with the decrease of Mg in the chlorite. Garnets were represented by 1 grain from each of schist and gneiss. (Table 3). The composition of garnets are shown in Fig. 7, in terms of pyrope, andradite+ grossular and almandine end-members. In this figure the analysed garnets are almandine showing their pronounced Fe_2+ contents (Alm=70-76 %). The analysed garnets are normally zoned particularly in the schists: the MnO contents decrease from 2.85 in the core to 1.90 in the rim while FeOt increase from 34.94 to 36.75 in the same direction. The contents of FeO_t , CaO and Al_2O_3 increase while MnO and MgO decrease from core to rim of the present almandine crystals from schists and gneisses. This variation in Fe, Ca, Mn, Mg and Al could be interpreted in terms of initial bedding modified by subsequent rotation during deformation (Thompson et al., 1977) or due to the equilibrium of reactions between the garnets and the matrix. Moreover, the analysed almandines are analogous to that from metapelites of the high temperature part of the almandine zone of the Barrovian region which commonly contain about 0.6% MnO, 28% FeO_t, 3-4% MgO and several percent CaO (Atherton, 1968). The isograde of this almandine probably closes to the epidote-amphibolite facies.Cordierites are mostly classified into magnesian- or iron cordierite. The analysed cordierites consist mainly of SiO_2 and Al_2O_3 and equal amounts of FeO

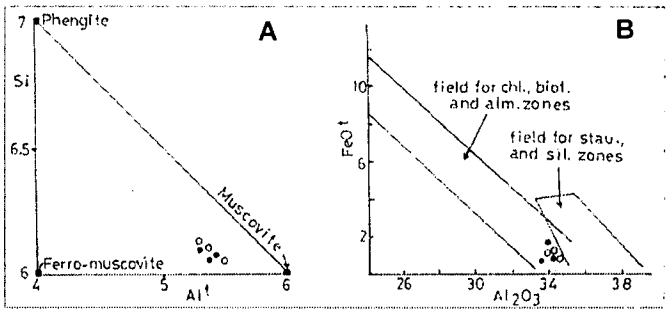

Fig. 5. The analysed muscovites plotted into: *(A)* Si-Alt classification diagram (after Harrison, 1990) and *(B)* FeOt-Al_2O_3 diagram (after Miyashiro, 1973)

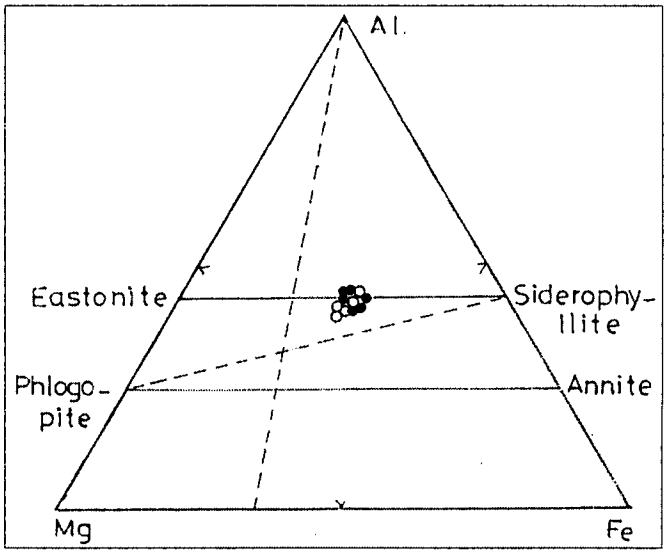

Fig. 6. The analysed biotites plotted into Al-Mg-Fe classification diagram (after Nemec, 1972)

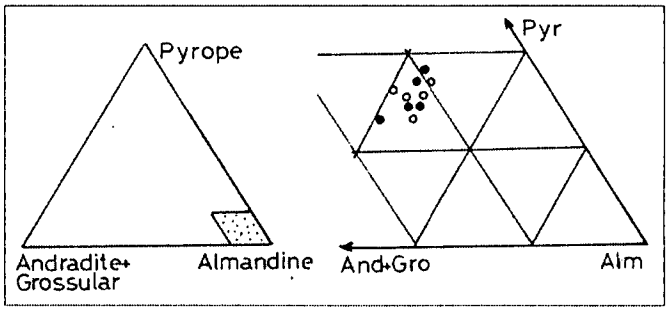

Fig. 7. The analysed garnets plotted into pyrope-andradite +Grossular-almandine diagram

and MgO contents. Consequently, they are analogous to the Fe-Mg cordierite.

The analysed minerals are characterized by XMg cord (0.66-0.60, with average of 0.63) > chl (0.49-0.58, average 0.53) > biot (0.42-0.55, average 0.50) > gar (0.12-0.15, average 0.14). This results are consistent the data given by Yardley (1989) who reported that the XMg cord > XMg chl > XMg biot > XMg gar in the pelitic rocks.

THERMOBAROMETRY

The following series of metamorphic zones have been delineated on the basis of mineral changes in response to P-T conditions. The pelitic chlorite in low grade metamorphic assemblage has crystallized at T=400 °C and PH_2O+2 kb. (Winkler, 1976). Chlorite become unstable at T=505-555 °C

and P=0.5-4 kb (Velde, 1964). Biotite breaks down at temperatures between 400 °C and 800 °C at 2 kb depending on the oxygen fugacity. The studied biotite has Mg/(Mg+Fe) ratio of about 0.5. This ratio is similar to that given by Wones, Eugster (1965) (i.e. 0.45) for the biotite stable up to 800 °C. This indicates that the stability of present biotite is less than 800 °C. The stability of almandine under low oxygen fugacity is expanded greatly with increasing pressure: at 2 kb in the presence of H_2O it is stable up to 350 °C and this range increases to nearly 850 °C at 20 kb in the absence of H_2O (Hsu, 1968). Nevertheless, the stability of the analysed almandine is less than 850 °C. Pure Mg-cordierite has its lower stability limit around 500 °C at 2 kb. The upper stability limit of this cordierite is about 7 kb. In dry systems. Fe-cordierite is similar to its Mg-member in respect to the lower temperature limit. The upper stability limit of Fe-cordierite is about 3.5 kb at 700 °C (Richardson, 1968). Accordingly the stability of present Mg-Fe cordierite is more than 500 °C.

GEOCHEMISTRY

The applicability of the chemical data (Table 4, 5), in illustration of metamorphic evolution, depends to a large extent on the amount of chemical alteration, mobility and

Table 4. Results of the chemical composition of Baba schists and gneisses

	Schists						Gneisses					
	257	280	183	210	142	Av.5	13	36	15	11	266	Av.5
SiO_2	69.23	65.96	64.05	63.12	61.85	64.8	65.70	65.68	63.20	62.11	62.02	63.7
TiO_2	1.06	0.89	1.35	0.71	1.13	1.0	1.05	0.60	1.44	1.65	1.03	1.2
Al_2O_3	13.53	14.63	14.40	14.66	15.24	14.5	14.76	14.54	15.80	15.59	15.71	15.3
Fe_2O_3	0.18	0.28	<0.10	3.26	0.84	0.9	0.85	2.16	0.15	<0.10	0.37	0.7
FeO	4.36	4.55	6.48	2.95	6.05	4.9	5.20	3.75	6.70	6.80	5.73	5.6
MnO	0.06	0.08	0.07	0.07	0.08	0.7	0.07	0.07	0.06	0.06	0.05	0.6
CaO	1.45	1.12	1.30	2.53	1.94	1.7	1.73	2.44	1.52	1.88	1.78	13.9
MgO	2.87	3.62	3.53	3.42	2.98	3.3	2.84	2.99	3.60	3.65	3.45	3.3
Na_2O	2.82	3.03	3.37	3.77	2373	3.1	3.05	3.30	2.99	2.79	2.87	3.0
K_2O	1.97	2.07	1.82	2.23	1.87	2.0	1.93	1.30	2.11	2.60	2.55	2.1
H_2O^-	0.45	0.50	0.42	0.68	0.55	0.5	0.48	0.43	0.40	0.34	0.41	0.4
P_2O_5	0.10	0.12	0.13	0.20	0.09	0.1	0.17	0.18	0.21	0.05	0.07	0.1
LOI	1.82	2.72	2.50	2.30	2.84	2.7	1.64	2.53	1.70	1.96	2.64	2.7
Sum	99.90	99.43	99.52	99.99	98.19	99.2	99.47	99.97	99.88	99.58	98.68	99.6
Sc	17.5	16.3	18.2	-	-	17.3	-	15.0	18.8	19.7	-	17.8
Cr	155.0	210.0	133.0	-	-	166.0	-	183.0	122.0	125.0	-	143.0
Co	18.3	16.5	18.7	-	-	17.8	-	19.2	19.8	19.5	-	19.5
Zn	205.0	101.0	235.0	-	-	180.0	-	208.0	243.0	230.0	-	2270
Rb	102.0	n.d.	134.0	-	-	118.0	-	115.0	153.0	140.0	-	136.0
Ba	570.0	800.30	433.0	-	-	681.0	-	595.0	390.0	380.0	-	455.0
Cs	3.2	n.d.	3.3	-	-	3.2	-	3.4	3.8	3.5	-	3.6
Hf	5.4	4.9	6.4	-	-	5.6	-	8.8	8.2	7.3	-	8.1
Ta	0.8	0.9	0.8	-	-	0.8	-	0.9	1.1	0.9	-	1.0
Th	8.3	5.2	9.3	-	-	7.3	-	7.3	9.8	9.7	-	8.9
U	2.4	1.9	2.5	-	-	2.3	-	2.1	2.9	2.8	-	2.6
Sr	210.0	232.0	202.0	-	-	215.0		203.0	161.0	166.0	-	177.0
Nb	10.0	13.0	11.0	-	-	11.0		12.6	17.0	15.0	-	14.9
Y	22.0	21.0	24.0	-	-	2.2	-	30.0	29.0	27.0	-	28.7
Zr	134.0	131.0	138.0	-	-	134.0	-	155.0	153.0	149.0	-	152.0

257: Mus-chl-gar-bio schist. 13: Sil-cord-bio gneiss. 280: bio schist. 36: Bio gneiss. 183: Sil-gar-bio schist. 15 and 11: Cord-bio gneiss. 210:Gar-bio schist. 266: Gar-cord-bio gneiss. 142: Sil-cord-bio schist. n.d.: not detected. -: not analyzed.

Table 5. Rare earth elements (REE) concentations of Baba schistsand gneisses compared with that of the crust and North American Shales Composite (NASC)

	Schists				Gneisses				I.	II.	III.
	257	280	183	Av.3	36	15	11	Av.3			
La	27.6	22.5	29.3	26.4	39.0	33.1	32.5	34.9	31.6	30.0	32.0
Ce	55.0	47.0	53.7	53.7	70.0	66.0	64.0	66.7	60.2	60.0	73.0
Nd	23.0	22.0	22.3	22.3	22.0	22.5	22.0	22.2	22.3	28.0	33.0
Sm	5.7	5.3	5.6	5.6	6.8	6.4	6.1	6.4	6.0	6.0	5.7
Eu	1.3	1.2	1.2	1.2	1.4	1..8	1.5	1.6	1.4	1.2	1.2
Tb	<1.0	<1.0	1.1	1.1	1.5	1.4	1.2	1.4	1.3	0.9	0.9
Yb	4.4	4.3	4.5	4.5	4.9	5.4	5.1	5.1	4.8	3:0	3.1
Lu	0.7	0.7	0.7	0.7	0.9	1.6	1.4	1.3	1.0	0.5	0.5

I: Average of Baba schists and gneisses. II: Average of continental crust (Taylor, 1964) III: Average of NASC (Haskin et al., 1968).

migration of the elements that occurred during metamorphism. However, the literature shows conflicting opinions regarding direction and magnitude of alteration (Humphris, 1984). The major elements chemistry are considered to suffer more changes during metamorphism. However, the studied rocks are of relatively homogeneous in their chemical composition probably due to the interlayering habit of the schists and gneisses in the field.. This is reflected for example in the narrow range of their content of SiO_2 (61.8 69.2 wt %), Al_2O_3 (13.5-15.8 wt %), FeO (4.5-6.9 wt %) and MgO (2.8-3.6 wt %) as well as the cluster of the data points on the diagrams. On the AFM projection (Fig. 8A) which shows the relationships between the mineral compositions and assemblages, all the analyses cluster on the field of chlorite-cordierite-biotite-garnet. Also on the A*KF diagram (Fig. 8B) the analyses plot on the field of muscovite-cordierite-garnet-biotite. Consequently, they exhibit a greenschist to lower amphibolite facies. TiO_2 contents are moderate (0.6-1.7 wt %). Values of LOI (loss on ignition) are above 2.5 wt % which is due to several modal percent retrograde chlorite. Also, these rocks are characterized by dominance of soda over potash, high aluminum to alkali ratios and high calcium and magnesium contents (Table 4) suggesting that they were probably derived from pelitic sediments. All these chemical feature similarities indicate that the schists and gneisses are comparable and genetically related and their metamorphic evolution is intrinsic to individual samples since they occur as interlayering beds in the field. However, there are minor differences between them. The schists have mildly higher SiO_2 and lower TiO_2 and CaO contents compared with the gneisses. The Niggli al-alk versus c diagram is used to distinguish between igneous and sedimentary rocks. On this diagram (Fig. 9A) the present analyses plot in the field of sedimentary rocks (shale). Moreover, on the (al+fm) (c+alk) versus si diagram (Fig. 9B), these rocks fall in the field of the argillaceous sediments. The HFS (high-field strength) elements (particularly the REE) are mostly considered to behave relatively immobile during metamorphic

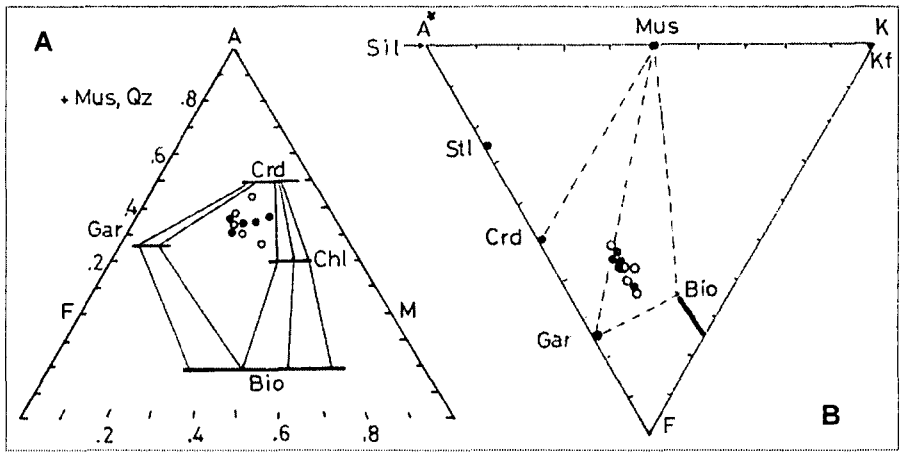

Fig. 8. The Baba schists and gneisses plotted into the combined *(A)* AFM and *(B)* A*KF projections. A*=Al2O3-CaO-Na2O+3.33P2O5, F=FeO+MgO+TiO2, K=KAlO2

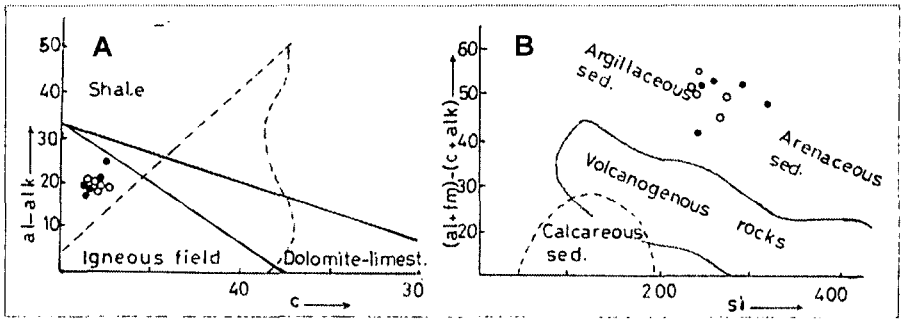

Fig. 8. The Baba schists and gneisses plotted into: *(A)* Niggli al-alk versus c diagram (after Evans and Leake, 1960) and *(B)* Niggli (al+fm)- (c+alk) versus si diagram (after Holdhus, 1971)

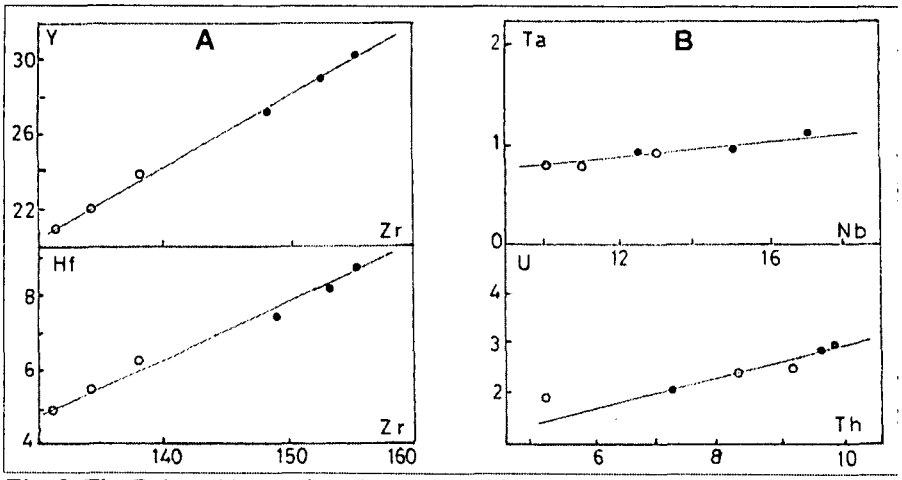

Fig. 9. The Baba schists and gneisses plotted into: *(A)* Zr vs Y and Hf and *(B)* Th vs Na and U vs Th

processes. The concentration of the trace elements in the studied schists and gneisses are mostly similar indicating their genetic relation (Tables 4, 5). However, there are minor but interesting dissimilarities between them. Yttrium concentration ranges from 21 to 30 ppm, and correlates well with the heavy REE (Tb, Yb and Lu, Table 5). Concentrations of Zr have a clear positive correlation with Y (Fig. 10A). Also, Zr correlates well with Hf and has mean Zr/Hf ratio (about 20) which is lower than the the average crustal value of about 33. Nb and Ta exhibit a good positive correlation. The mean Nb/Ta ratio in the schists and gneisses (about 15, Fig. 10B) is higher than the crustal average of about 11 (Taylor, Mclennan, 1985). Higher contents of Cr and lower Co are recorded in the schists compared with

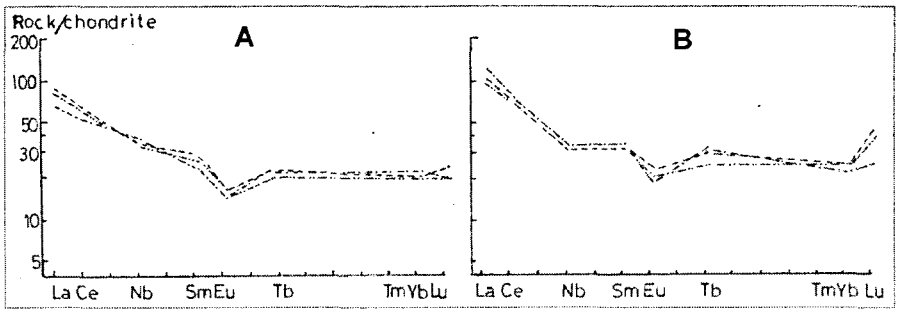

Fig. 11. Chondrite-normalized REE patterns of the studied: *(A)* schists *(B)* gneisses. The normalizing values after Wakita et al. (1971)

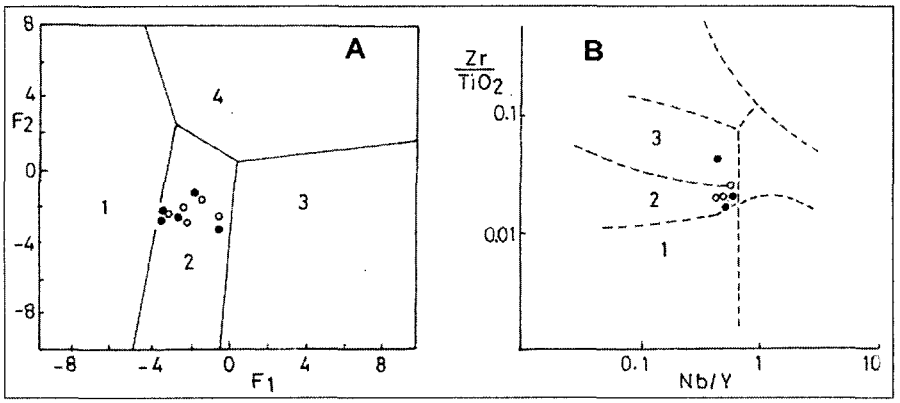

Fig. 12. The studied schists and gneisses plotted into: *(A)* F1-F2 diagram (after Roser and Korsch, 1988). Fields show provenances of 1=mafic igneous, 2=intermediate igneous, 3=felsic igneous rocks and 4=quartoze sedimentary rocks and *(B)* Zr/TiO2 vs Nb/Y diagram (after Winchester and Floyed (1977). Fields: 1=basalt, 2=andesite, 3=dacite-rhyodacite

Table 6. K-Ar age dating of the biotite fraction from Baba schists and gneisses

Sample name	locality	No.	K(%)	^{40}Ar rad. (ccSTP/g)	40AR rad. (%)	Age (Ma)
Cord-bio gneiss	W.Hamata	11	1.034	2.9688-5	75.8	620±24
Bio gneiss	W.el-Sih	36	5.416	1.5024-4	84.0	602±23
Gar-bio schist	W. Baba	60	5.147	1.2827-4	94.7	549±21

gneisses. Moreover, there are no significant correlations among these elements (Sc, Cr and Co), nor do they correlate well with FeOt. Concentrations of Rb is high, whereas Rb and Cs are relatively low in both schists and gneisses. Rb correlates positively with K and has an average K/Rb ratio (130) which is signficantly lower than the crustal average of about 250 (Taylor, Mclennan, 1985). Concentrations of Th (5.2-9.8 ppm) and U (1.9-2.9 ppm) show a significant positive correlation (Fig. 10B). The average Th/U ratio (3.5 ± 1.2) in the schists and gneisses is indistinguishable from the average of crustal value of about 3.8 (Taylor, Mclennan, 1985). Moreover, the concentrations of Hf, Ta, U, Nb and Zr are high in the gneisses compared with schists.The REE data is grouped according to assemblage (Table 5) and the Chondrite- normalized REE patterns are shown in Fig. 11. Overall, the schists and gneisses have similar REE patterns with characteristic negative Eu- anomalies. However, the gneisses are characterized by higher REE abundance (21-103 times chondrites) than the schists (19-90 times), a variety of metamorphic differentiation. REE patterns (Fig. 11) show slightly anomalous kinks for heavy REE (i.e. gneisses) consistent with the fact that Tbn<Lun in several cases may be a manifestation of a zircon effect (Dymek, Smith, 1990). The influence of zircon is emphasized again by the slight enrichment of Th and U and deletion of Nd contents which reflect the lack of apatite and monazite in the studied rocks.REE patterns are characterized by fractionated light REE compared with heavy REE (Lan>Lun). The negative Eu anomalies (as well as low Ca and Sr) probably correspond to the properties inherited from the precursor. The high abundance of REE in gneisses compared with that in schists is attributed to the relative concentrations of light REE in apatite and monazite and heavy REE in zircon and garnet during metamorphism (Nesbitt, 1979). This feature can be ascribed to the changes of fluid chemistry. Therefore, compared to schists, the gneisses have more enriched and fractionated REE patterns. Intermediate igneous rocks probably represent a more appealing precursor for the studied rocks. They contain intermediate primary SiO_2 contents, intermediate values of Sc, Cr, Co; and Zr, Hf, Ta, Th, U contents and slightly enriched and fractionated REE patterns (possibly even with negative Eu anomalies). They underwent hydrothermal alteration. Fig. 12A, a discriminant plot using function 1 (F1) versus function 2 (F2), shows that the data points of the studied rocks fall within the field if intermediate igneous provenance (Roser, Korsch, 1988). Moreover, they fall within the fields of andesite and dacite on the Zr/TiO_2 versus Nb/Y diagram (Fig. 12B).

Dating

The results of K-Ar ages are given in Table 6. While only few age dating are available for the metamorphic rocks of Sinai (Bielski, 1982; Stern, Manton, 1987), there is no age dating have been carried out on the Baba schists and gneisses. The measured K-Ar ages of the separated biotites from cord-bio gneiss of Wadi Hamata (at the entrance of Wadi Baba) and bio gneiss of Wadi el-Sih, gave 620 ± 23.9 Ma and 602 ± 22.9 Ma respectively (Table 6) with average of about 611 Ma. This average is similar to the Rb-Sr whole rock age of the Feiran paragneiss (Stern, Manton, 1987). The former age (620 ± 24 Ma) probably represents the nearest estimation to the age of formation of gneisses. The second age of gneiss (602 ± 23 Ma) can be interpreted as the higher loss of argon of the biotite probably due to the more deformed state of Wadi el-Sih gneiss, the dynamothermal as well as the effect of the metamorphic processes. Alternatively, the two ages of 620 ± 24 and 602 ± 23 Ma of the gneisses are

indistinguishable within the wide error limits. The gar-bio schist of Wadi Baba yields a 549 ± 20.6 Ma age for the separated biotite. It can be argued that this lower age may result from the strong effect of the late regression on the schists.

Discussion and Conclusion

From the former field observations, petrography and mineral chemistry of this study, it likely that most of the metamorphic mineral assemblages in the rocks crystallized under the higher temperatures reached during the P-T-t cycles. Therefore it can be assumed that there are three successive episodes of metamorphism (the early two occurred during prograde while the later during the retrograde phase) as follow:

1) The first episode of metamorphism was low-grade regional metamorphism transforming the original sediments to schists with mineral assemblage (chlorite, albite, muscovite, quartz and biotite) belongs to greenschist facies.

2) The second episode is thermal metamorphism induced by granitic intrusions on the original rocks resulting into contact schists and gneisses. The mineral assemblages of this phase (plagioclase, quartz, muscovite, biotite, garnet and cordierite + sillimanite) belong to lower amphibolite facies.

3) The third episode of metamorphism is the retrograde metamorphism due to decrease in temperature and pressure. This condition is indicated by the formation of chlorite after biotite, garnet or cordierite; muscovite and sericite after sillimanite together with secondary sericite and kaolinite after plagioclase. The metamorphic evolution of the present rocks ranges from greenshist to amphibolite facies which is intrinsic to individual samples ascribed to the interlayering of the schists and gneisses in the field. During these successive episodes the rocks have been affected by three main phases of deformation and garnet evolution. In the Baba area, the source of the heat for contact metamorphism is probably due to the intrusions of granites in the middle part of the area. The temperature of the granitic magma intrusions is generally 700-800 °C (Winkler, 1976). Near the intrusions and the metamorphic rocks there is often masses of granitic gneisses which exhibited a sign of migmatization. To get an idea on the geotectonic position in which the sediments were deposited, log (K_2O/Na_2O) versus SiO_2 diagram after Roser and Korsch (1986) was used. On this diagram the studied schists and gneisses exhibit the island arc setting (Fig. 13A). A systematic relationships involving La-Sc-Th-Co-Hf have proposed by Mclennan and Taylor (1984) and Taylor and Mclennan (1985) to indicate crustal sources of Archean sediments. Fig. (13B) shows data for Baba schists and gneisses plotted on TH-Hf-Co and La-Th-Sc diagrams. On the diagrams, the data fall in the field of NASC (North American Shale Composite) of Gromet et al. (1984), even nearby the TT (Tonalite-Trondhjemite components) of the Talyor, Mclennan (1985) of the mixture band consistent with derivation from these kinds of rocks. These rocks have high contents of La, Sc and Co and low Th and Hf contents. However, the gneisses are characterized by higher contents of La and Hf and lower Th, Sc and Co compared with the schists probably due to either the influence of minor zircon and monazite or the depletion of Th during low grade metamorphism. The studied rocks have high contents of incompatible trace elements (Zr, Nb, Y, Hf, Ta, Th, U, REE). Some or all these elements can be harbored predominantly in minor mineral phases, which could be controlled either by small quantities of detrital minerals (i.e. zircon, monazite) or reflect selective cavenging by these phases during metamorphism (Dymekm, Smith, 1990). The high and variable La contents, as well as variable chondrite normalized

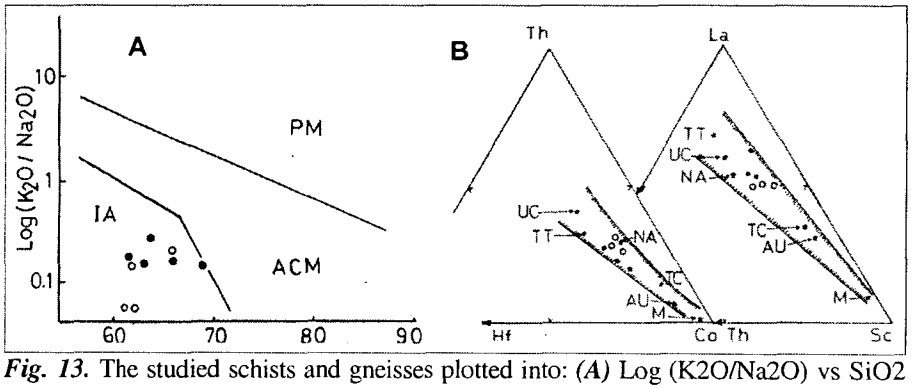

Fig. 13. The studied schists and gneisses plotted into: *(A)* Log (K2O/Na2O) vs SiO2 diagram (after Roser and Korsch, 1986). IA=island arc, ACM=active continental margin, PM=plate margin and *(B)* Th-Hf-Co and La-Th-Sc diagrams. Values of M=mafic component, TT=tonalite-trondhjemite component, AUC=Archaean upper crust, UC=upper crust and TC=total crust are from Taylor and Mclennan (1985); value of NASC=North American Shale Composite taken from Gromet et al. (1984). Stippled regions correspond to a mixing band of the composition of Archaean sediments and metasediments (after Mclennan and Taylor, 1984)

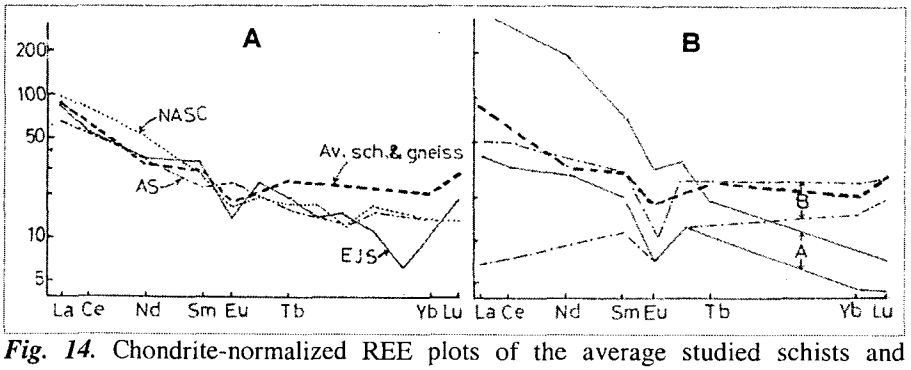

Fig. 14. Chondrite-normalized REE plots of the average studied schists and gneisses compared to: *(A)* NASC of Haskin et al. (1968), European and Japanese Shale (EJS) of Minami (1935) and Archaean Sediments (AS) of Jenner et al. (1981) and *(B)* range of intermediate igneous rocks from continental (A) and island arc (B) setting (Cullers and Graf, 1984)

(Lan/Smn) ratios, could due to either effect. Zircon, apatite and monazite have been observed in thin sections of the schists and gneisses. REE abundance and fractionations have been comparable with references REE of the crust (Taylor, 1964) and North American Shale Composite (NASC) (Haskin et al., 1968, Table 5). However, they are slightly enriched in the heavy REE abundance with respect to the references. Fig. 14A compares the average REE pattern for schists and gneisses to those of Archean sediments (Jenner et al., 1981), NASC (Haskin et al., 1968) and European and Japanese shale (EJS) (Minami, 1935). It appears that the studied rocks have a light REE and negative Eu anomaly quite similar to that from Archean sediments, NASC and EJS, but with a higher heavy REE pattern probably due to the effect of metamorphism or correspond to the properties inherited from the precursor. The high concentration of heavy REE in the examined rocks which particularly susceptible to complexion, are associated with high concentration of alkalis and volatiles (Mineyev, 1963). Furthermore, the average REE of the schists and gneisses is also partially comparable with the range of REE found in continental intermediate rocks (field A) and with the same former rocks formed in island arc (field B) after Cullers and Graf (1984) (Fig. 14B). In this figure, the average REE of the schists and gneisses mostly close to the range of island arc intermediate igneous rocks (field B). According to Cullers and Graf (op. cit.) the island arc rocks have less than 14.5-15 wt % Al2O3, nearly flat REE pattern and negative Eu anomalies, which quite similar to the studied rocks. The trace and REE of the studied schists and gneisses should be used for modeling partial melting, metamorphic differentiation and crystal fractionation processes. From the former petrological and geochemical features, it can be reasonably assumed for the formation of the schists and gneisses: formation of intermediate igneous rocks Ąć weathering, transport and deposition Ąć metamorphism (regional and contact) leading to metamorphic differentiation and possibly partial melting. In the present rocks the metamorphic differentiation can be evident by the occurrence of bands. The bands probably represent synmetamorphic dykes or veins, in some cases formed by anatexis, or developed due to preferential nucleation of phases in pre-existing structural zones (Raymond, 1995). The studied gneisses gave 620 ± 23.9-602 ± 22.9 Ma K-Ar ages with an average of 611 Ma which consistent with the result reported by Stern, Hedge (1985) and Stern, Mantin (1987). They concluded that the tectonomagmatic episode responsible for the formation of these metasedimentary rocks may have been related to the 610-630 Ma compressional events important in the evolution of the Central and Northeastern Desert of Egypt (Stern, Hedge, 1985; Stern, Mantin, 1987).

ACKNOWLEDGEMENTS

The authors are grateful to Prof. M. Okrusch, Mineralogical Institute, Wurzburg University, Germany, for the valuable discussions and critical comments of the manuscript.

REFERENCES

AKAAD, M. K., EL-GABY, S., ABBAS, A. A. (1967a): Geology and petrography of the migmatites around Feiran Oasis, Sinai. Assuit Sci. Techn. Bull., **10**, 67-87.

AKAAD, M. K., EL-GABY, S., ABBAS, A. A. (1967b): On the evolution of Feiran migmatites. J. Geol. Egypt, **11**, pp. 4958.

AKAAD, M. K., EL-GABY, S., AHMED, A. A. (1988): Feiran - Solaf district, Southwestern Sinai, Egypt. Annals Geol. Surv. Egypt, 112-132.

ATHERTON, M. P. (1968): The variation in garnet, biotite and chlorite composition in medium grade pelitic rocks from the Dalradian, Scotland, with particular reference to the zonation of garnet. Contrib. Mineral. Petrol., **18**, 347-371.

BIELSKI, M. (1982): Stages in the evolution of the Arabian-Nubian Massif in Sinai. Ph. D. Thesis, Hebrew Univ., pp. 155.

CULLER, R. L., GRAF, J. L. (1984): Rare earth elements in igneous rocks of the continental crust: Intermediate and silicic rocks-ore petrogenesis. In Henderson, P. (ed.): Rare earth element geochemistry. 275-316.

DYMEK, R. F., SMITH M. S. (1990): Geochemistry and origin of Archaean quartz-cordierite gneisses from the Godthabsfjord region, west Greenland. Contrib. Mineral. Petrol., **105**, 715-730.

EL-AREF, M. M., ABD EL WAHID, M., KABESH, M. (1988): On the geology of the basement rocks, east of Abu Zenima, West Central Sinai, Egypt. Egypt. J. Geol., **32**, 1-2, 1-25.

EL-AREF, M. M., ABD EL WAHID, M., KABESH, M. (1989):Fabric evolution and geochemical characters of the migmatites and associated gneisses of Wadi Baba and Wadi Dafari, West Central Sinai, Egypt. Egyptian Mineralogist, **1**, 27-53.

EL-GABY, S., AHMED, A. A. (1980): The Feiran-Solaf gneiss belt, SW of Sinai, Egypt. In Al-Shanti, A. M. S.(ed.): Evolution and mineralization of the Arabian-Nubian Shield. Inst. App. Geol. (Jeddah), Bull., **3**, 95-105.

EL-SHAZLY, E. M., HASHAD, A.H., SAYYAH, T. A., BASSYUNI, A. (1973): Geochronology of Abu Swayel area, South Eastern esert, Egypt. Egypt. J. Geol., **17**, 1-18.

EVANS, B. W., LEAKE, B. E. (1960): The composition and origin of the stripped amphibolites of Connemers Ireland. J. Petrology, **1**, 337-363.

GIUDOTTI, C. V. (1984): Micas in metamorphic rocks. Reviews in Min., **13**, 357-367.

GROMET, L. P., DYMEK, R. F., HASKIN, L. A., KOROTEV, R. L. (1984): The "North American shale composite". Its compilation, major and trace element characteristics. Geochim. Cosmochim. acta, **48**, 2469-24.

HALPERN, M., TRISTAN, N. (1981): Geochronology of the Arabian-Nubian Shield in southern Israel and eastern Sinai. J. Geol., **89**, 639-648.

HARRISON, T. N. (1990): Chemical variation in micas from the Cairngorm pluton, Scotland. Min. Mag., **54**, 355-366.

HASKIN, L. A., HASKIN, M. A., FREY, F. A., WILDEMAN, T. R. (1968): Relative and absolute terrestrial abundances of the rare earths. In Ahrens L. H. (ed.): Origin and distribution of the elements 1. Pergoman, Oxford. 889-911.

HENDERSON, P. (1984): Rare earth element geochemistry. Elsevier, Amsterdam, Oxford. pp. 510.

HEY, M. H. (1954): A new review of the chlorite. Min. Mag., **30**, 227.

HOLDHUS, S. (1971): Para-amphibolites from Gurskoy and Sandsoy, Sunnmor, West Norway. Norsk, Geol. Tidsskr. **51**, 231-246.

HSU, L.C. (1968): Selected phase relationship in the system Al-Mg-Fe-Si-O-H: a model for garnet equilibria. J. Petr., **9**, 40-83.

HUMPHRIS, S. E. (1984): The mobility of rare earth elements in the crust. In Henderson, P. (ed.): Rare earth element geochemistry. Elsevier-Amsterdam, Oxford. 317-342.

HYNDMAN, D. W. (1985): Petrology of igneous and metamorphic rocks, 2nd ed., McGraw-Hill, New York.

JENNER, G. A., FRYER, B. J., MCLENNAN, S. M. (1981): Geochemistry of the Archaean Yellows Knife Supergroup. Geochim. Cosmochim. Acta, **45**, 1111-1129.

LAMBERT, R. J. (1959): The mineralogy metamorphism of the Moine schists of the Morar and Knoydrat districts of Inverness-shire. Tras. Roy. Soc. Edin., **63**, 553-588.

MCLENNAN, S. M., TAYLOR, S. R. (1984): Archaean sedimentary rocks and their relation to the composition of the Archaean continental crust. In Kroner, A. et al. (eds.): Archaean geochemistry. Springer -Verlag, Berlin. 47-72.

MINAMI, E. (1935): Gehalte Seltener Erden in Europaischen and Japanischen Tonschiefern. Nachr. Ges. Wiss. Geottingen, Math.-Phys. Kl., Fachgruppe, 4, 1, 155-170.

MINEYEV, D. A. (1963): Geochemical differentiation of the rare-earths. Geochemistry (U.S.S.R.), **12**, 1129-1149.

MIYASHIRO, A. (1973): Metamorphism and metamorphic belts. John Willey & Sons, New York.

NEMEC, D. (1972): Paragenetische analyze der regional metamorphen Skarne Westmahrens. Chem. Erde, **34**, 62-84.

NESBITT, H. W. (1979): Mobility and fractionation of rare earth elements during weathering of granodiorite. Nature, **279**, 206-210.

RAYMOND, L. A. (1995): Metamorphic Petrology. Wm. C. Brown Publ., London.

RICHARDSON, S. W. (1968): Staurolite stability in a part of the system Fe-Al-Si-O-H. J. Petrol., **9**, 467-488.

ROSER, B. P, KORSCH, R. J. (1986): Determination of tectonic setting of sandstone-mudstone using SiO_2 content and K_2O/Na_2O ratio. J. Geol., **94**, 635-650.

ROSER, B. P, KORSCH, R. J. (1988): Provenance signature of sandstone-mudstone suite determined using discriminant function analysis of major-element data. Chem. Geol., **67**, 119-139.

SIEDNER, G., SHIMRON, A., PRINGLE, I. (1974): Age relations in basement rocks of the Sinai Peninsula. Int. Meet. Geochronology, Paris. 116-125.

STERN, R. J., HEDGE, C. R. (1985): Geochronological and isotopic constrains on late Precambrian crustal evolution in the Eastern Desert of Egypt. Amer. J. Sci., **285**, 97-127.

STERN, R. J., MANTON, W. I. (1987): Age of Feiran basement rocks, Sinai: Implications for late Precambrian crustal evolution in northern Afro-arabia. J. Geol. Soc. Lond., **144**, 569- 575.

TAYLOR, S. R. (1964): The abundance of chemical elements in the continental crust- a new table. Geochim. Cosmochim. Acta, **28**, 1273-1285.

TAYLOR, S. R., MCLENNAN, S. M. (1985): The continental crust, its composition and evolution. Blackwell Scientific Publications, Oxford.

THOMPSON, A. B., TRACY, R. J., LYTTLE, P. T., THOMPSON, J. B. (1977): Prograde reaction histories deduced from compositional zonation and mineral inclusions in garnet from the Gassetts schist, Vermont. Amer. J. Sci., **277**, 1152-1167.

VELDE, B. (1964): Low-grade metamorphism of micas in pelitic rocks. Carnegie Inst. Wash. Yearbook, **63**, 142-147.

WAKITA, H., REY, P., SCHMITT, R. A. (1971): Abundances of the 14 rare-earth elements and 12 other trace elements in Apollo 12 samples.: five igneous and one breccia rocks and four soils. Proc. 2nd Luner Sci. Conf., 1319-1329.

WEISSBROD, T. (1969): The Paleozoic of Israel and adjacent countries. The Paleozoic outcrops of South western Sinai and their correlations with those of Southern Israel. Geol. Surv. Israel, **48**, pp. 32.

WINCHESTER, J. A,. FLOYED, P. A. (1977): Geochemical discrimination of different magma series and their differentiation products using immobile elements. Chem Geol., **20**, 325-343.

WINKLER, H. (1976): Petrogenesis of metamorphic rocks. Springer-Verlag, New York.

WONES, D. R,. EUGSTER, H. P. (1965): Stability of biotite: experiment, theory and application. Am. Mineral., **50**, 1228-1272.

YARDLEY, B. W. D. (1989): An introduction to metamorphic petrology. Longman, London.

Received: July 11, 2002; accepted: November 23, 2002

Acta Mineralogica-Petrographica, Szeged 2002, Vol. 43, pp. 39-53

ACTA
Mineralogica
Petrographica

MINERALOGY OF PLIOCENE TO PLEISTOCENE PELITIC SEDIMENTS OF THE GREAT HUNGARIAN PLAIN

ISTVÁN VICZIÁN

Geological Institute of Hungary
H-1143 Budapest, Stefánia út 14.
e-mail: viczian@mafi.hu

ABSTRACT

Mineralogical composition of pelitic sediments of the Great Hungarian Plain is reviewed in this paper. Published data and unpublished analyses made in the laboratories of the Geological Institute of Hungary a total of about 150 samples were collected. Determinations were made mainly by X-ray diffraction, the data were systematically corrected by comparison with the results of thermal analysis and partly chemical analysis. All data were revised and recalculated in a uniform system in order to obtain comparable results. In the bulk composition dominant clay minerals are smectite, illite/smectite, illite and chlorite. In the <2 μm fraction the same minerals occur, however, expanded phases are more dominant. Triple mixed-layer illite/smectite/chlorite and kaolinite of various degree of disorder may appear. Clay minerals are essentially detrital, derived from various areas of the surrounding Carpathians and Alps. Sub-basins may differ in degree of disorder and quantitative proportions of clay minerals and quantitative relations of other phases like calcite, dolomite, quartz and feldspars depending on relatively permanent source areas and transport directions. Smaller variations in the transport directions as shown by the micromineralogical composition are normally not reflected in the clay mineral record, neither climatic variations during the Pleistocene seem to have significant effect. In the South Tisza Basin and Maros Alluvial Fan well crystallised detrital phases prevail while in the Körös Basin more mature sedimentary material of lesser crystallinity, higher kaolinite and very low carbonate contents can be found. The clay, carbonate, feldspar and iron minerals deposited may have been modified by flow systems of ground water. In the upper flow regime comprising Pleistocene and Pliocene horizons of the South Tisza Basin and Maros Alluvial Fan dissolution of carbonate minerals and albite and ion exchange on clay minerals may proceed. In the stagnant ground waters filling the Pleistocene and Pliocene beds of the Körös Basin neoformation of pure smectite and kaolinite from dissolution of albite and dissolution of carbonates may be inferred from hydrogeochemical and mineralogical data. Amorphous iron hydroxides underwent crystallisation and reduction producing, in a downward sequence, amorphous "limonite", goethite and siderite. No diagenetic K-fixation and illitisation occurs in this level, however, some kind of palaeo-pedological illitisation may have occurred in those continental sediments. The first main step of burial diagenetic illitisation as well as of kerogen diagenesis starts in the lower groundwater regime which corresponds to the Upper Pannonian stratigraphic horizon, i. e. below the formations discussed in the present paper.

Key words: alluvial deposits, variegated clay, Great Hungarian Plain, Pliocene, Quaternary, clay minerals, rock-water interaction.

INTRODUCTION

The rocks filling the basin of the Great Hungarian Plain and other major sub-basins of the Pannonian Basin, the Dráva Basin and the Little Hungarian Plain, are mainly clastic detrital sediments, the composition of which is primarily determined by source rocks, conditions of transport and sedimentation (Rónai 1985, Jámbor 2001). The unusual thickness of the sedimentary column, deposited even in the youngest geological periods, in the Upper Pliocene and Quaternary, gives way to the secondary processes such as incipient burial diagenesis and interaction with the flowing groundwater.

In the classical works of the research team of Rónai (1972, 1985) and in subsequent studies, petrography was mainly restricted to the micromineralogical analysis (see e. g. Molnár, 1965, Thamó-Bozsó, 1997). Less attention was given to the rock-forming components, such as clay, carbonate and iron minerals. A brief summary of clay mineralogy of Quaternary sediments was made by the present author as part of a broader review of all Hungarian lithostratigraphic formations (Viczián, 1987).

In the present review the stratigraphical and regional geological summaries of Jámbor (1998, 2001) were chosen as geological background. Jámbor (1998) considered that the type of Hungarian Quaternary sediments is defined primarily by the geomorphological conditions of sedimentation and classified sediments as deposited in (I) flatland, (II) hilly and (III) mountainous areas (Fig. 1). Sediments of mountainous and hilly areas were reviewed recently by Viczián (2002). In the following we shall deal with the flatland areas trying to summarise our present knowledge on mineralogical composition of fine-grained sediments of basin areas.

Lithostratigraphic formations defined by the Stratigraphic Commission of Hungary (Császár, ed., 1997), will be grouped according to this major subdivision. In spite of the uncertainties inherent of the use of lithostratigraphic names in the Quaternary, such units were referred to in the present review in order to find a systematic frame for the discussion. Many Quaternary sequences are closely related to the underlying Pliocene formations, it is difficult to draw a sharp boundary between them. This is the reason why in most cases the discussion has been extended to the period preceding the Quaternary.

METHODS

Data on the composition of Quaternary clays are based mainly on results of X-ray diffraction analysis. In cases of old X-ray data made in the laboratory of the Hungarian Geological Institute the original evaluations of the X-ray records were revised by the present author during the preparation of the manuscript in 2001-2002. Such data are indicated in the text as "revised". When possible, only these revised data were used in the discussion in order to avoid sources of error due to variable authors and changing methods during the last decades. In addition to X-ray diffraction, the results of other analytical methods, especially those of thermal analysis will be considered.

RESULTS: MINERALOGY OF QUATERNARY SEDIMENTS OF SUB-BASINS OF THE PANNONIAN BASIN

Geological subdivision, basic data

Out of the three main flatland areas in Hungary the most mineralogical data are available from the Quaternary sediments of the *Great Hungarian Plain (Alföld).* The surface of Alföld is covered primarily by alluvial deposits, wind-blown sand and loess. The thickness of the Quaternary varies in wide ranges (see the map of Franyó, 1992 *in* Nádor et al., 2000) and may exceed 400-600 m in the deepest sub-basins. There are three major sub-basins in the Great Plain area (see Fig. 1): *Jászság Basin* in the north, *South Tisza Basin* along the Tisza river in the south and *Körös Basin* along the Körös river in the east (Rónai, 1985, pp. 69-71). The *Maros river alluvial fan* borders with the *Körös Basin* in the north and with the *South Tisza Basin* in the west. The sediments filling these sub-basins are developed mostly in a cyclic fluvial facies. These sequences were mostly revealed by the key bore holes of the Alföld Programme of the Hungarian Institute of Geology in the 1960-1970 years (Rónai, 1985). Important data were obtained also from other investigations, mostly from water and CH exploration drill holes. Cross sections of the sub-basins along the major bore holes are shown in Figs. 2, 3 and 4, including the basic mineralogy of the lithostratigraphic units.

There is a single bore hole in the *Dráva Basin, Görgeteg-1*, the thick

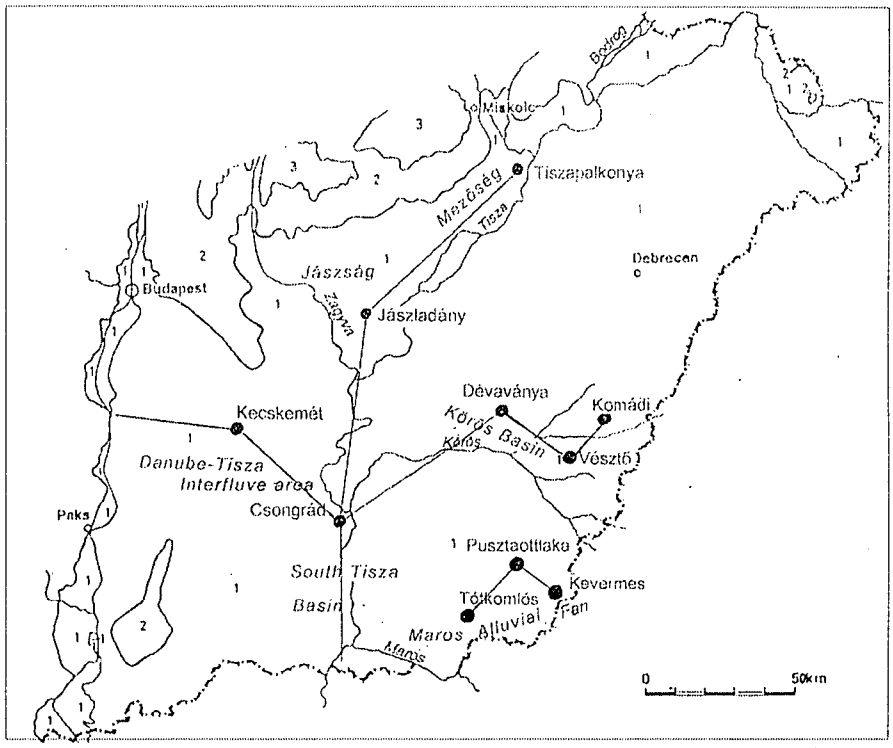

Fig. 1. Index map of the Great Hungarian Plain showing geographical local names mentioned in the paper. The lines of the geological cross sections shown in *Figs. 2-4* are indicated. The map shows the subdivision of the territory according to geomorphologic types of accumulation of Quaternary sediments (Jámbor, 1998, Fig. 4). Legend: 1. basin, 2. hilly, 3. mountainous areas

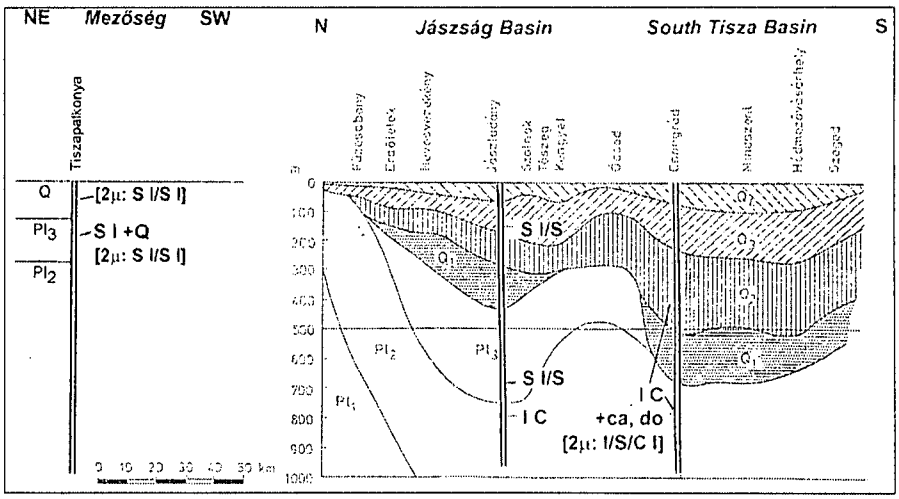

Fig. 2. Characteristic bulk mineral and clay mineral assemblages of Pliocene and Quaternary stratigraphic units of the Great Hungarian Plain along cross sections in north-east – south-west, and north – south direction. Geological cross section across the Jászság and South Tisza Basins according to Rónai (1986, Fig. 4). Geological data for the borehole Tiszapalkonya were taken from Tanács (1986). Abbreviations of the stratigraphic units: Q_1: Lowermost Pleistocene, Q_2: Lower Pleistocene, Q_3: Middle Pleistocene, Q_4: Upper Pleistocene, Q: Pleistocene (undivided), Pl_1: Lower Pannonian, Pl_2: Upper Pannonian, Pl_3: Uppermost Pliocene. Legend: Quantity of minerals in the cross sections: *capital letters:* frequent phases, >50 % of total clay minerals, *lower case letters:* less frequent phases. Minerals: S, s: smectite, I/S, i/s: mixed-layer illite/smectite, i/c: mixed-layer illite/chlorite, I/S/C: mixed-layer illite/smectite/chlorite, I, i: illite, K, k: kaolinite, k/s: mixed-layer kaolinite/smectite, C, c: chlorite, Q, q: quartz, kf: K-feldspar, pl: plagioclase, ca: calcite, do: dolomite, sid: siderite, goe: goethite. In brackets: [2µ: ...]: characteristic minerals in the <2 µm fraction.

Quaternary sequence of which has been studied for clay minerals in the 1990's. Unfortunately, the mineral composition is not yet published, only the values of the *Kübler index* are briefly mentioned by Koloszár et al. (2001). We have no clay mineral data so far from young deposits of the *Little Hungarian Plain*. Therefore the mineralogy of these sub-basins is not discussed in the present review.

Results of the X-ray analysis of bulk rock samples are included in Table 1, those of the clay fraction in Table 2. The compositional ranges given in Table 1 were established in the following manner: Quantitative data given in percent were rounded up to the nearest 5 percent. In the compilation of the tables a few extreme values were not considered.

Quaternary alluvial deposits of the Jászság Basin (Jászladány Clay, Nagyalföld Variegated Clay and Kerecsend Red Clay? Formations) and Mezőség (Jászladány Clay? and Nyékládháza Gravel Formations)

The thick Quaternary sequence of the *Jászság Basin* was recovered by the key borehole *Jászladány-1* of the Alföld Research Programme which crossed 430 m of a fluvial and flood plain sequence consisting of alternating clay and silt beds (Rónai, 1972, see Fig. 2). Today, in the stratigraphic system, this is called Jászladány Clay Formation. Quaternary is underlain by Upper Pliocene carbonate-poor variegated clays between 432 and 730 m (Nagyalföld Variegated Clay and Kerecsend Red Clay? Formations), which are sediments of shallow lakes and flood plains multiply redeposited in a dry and warm period. Below 730 m alternating sand, silt and clay layers represent the Upper Pannonian (Újfalu Sandstone Formation).

A great number of DTA analyses of this sequence were made by Székely in 1965. She has found only *illite* as clay mineral throughout the Quaternary and *illite+kaolinite* in the Pliocene. The first 4 X-ray analyses published from the Alföld area were made on samples from this bore hole by Rischák (1965, see Rónai, 1972, revised). *Smectite+illite/smectite* and less illite were found in a black peaty clay sample of Middle Pleistocene age at 155 m (Jászladány Clay Formation). Much *smectite+illite/smectite*, less illite and chlorite are in two Upper Pliocene samples, in a reddish brown clay sample at 684 m (Kerecsend Red Clay? Formation, see the X-ray pattern in Fig. 5) and in a grey silt sample at 688 m (Nagyalföld Variegated Clay? Formation). It was possible to estimate the proportion of smectite (S%) in the mixed-layer phase on the ethylene glycol treated patterns in all three samples: in falls into the interval 60-100 S% and there is a lesser amount between 0-40 S%. Rónai (1972, p. 54) considered reddish brown clays of Upper Pliocene age in the depth interval 670-685 m as "particularly important" being analogous with the red clays occurring under the loess beds in SE-Transdanubia and in the foothill area of Mátra and Bükk Mts. Indeed, high smectite contents are typical properties of the red clays both at *Jászladány* and in the localities on the northern margins of the Great Hungarian Plain (Kerecsend Red Clay Formation? see the review of Viczián, 2002). High smectite contents in Quaternary clays indicate probably the importance of the volcanic source rocks in the *Jászság Basin* and in the case of the red clays also the climatic conditions. Low carbonate contents are typical in Transdanubian red clays of the upper Tengelic Formation

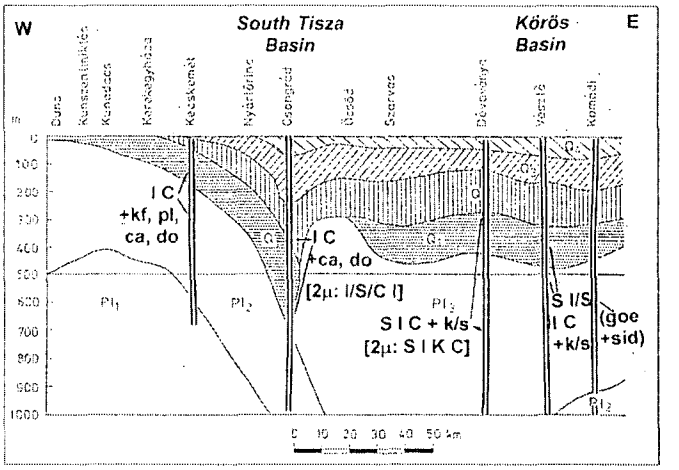

Fig. 3. Characteristic bulk mineral and clay mineral assemblages of Pliocene and Quaternary stratigraphic units of the Great Hungarian Plain along a cross sections in west - east direction. Geological data on the South Tisza and Körös Basins according to Rónai (1986, Fig. 5). For abbreviations of the stratigraphic units and legend of minerals see Fig. 2.

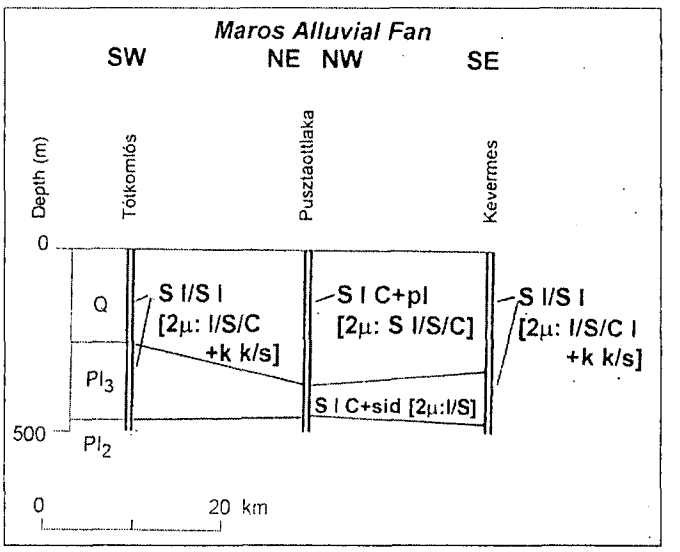

Fig. 4. Characteristic bulk mineral and clay mineral assemblages of Pliocene and Quaternary stratigraphic units across the Maros Alluvial Fan. The section was compiled using the geological data of Franyó (1983). For abbreviations of the stratigraphic units and legend of minerals see Fig. 2.

whereas at Visonta variable calcite contents in the red clay beds are the result of subsequent pedogenic processes (Horváth et al., 2001). In the Upper Pannonian (Újfalu Sandstone Formation) there is more carbonate, and clay minerals are represented by the detrital assemblage of *illite* and *chlorite*.

The borehole *Tiszapalkonya-1* is located in the *Mezőség* area, in NE continuation of the *Jászság Basin* (Fig. 2). The whole Quaternary sequence is here only 128,2 m thick (unpublished report by Tanács, 1986). Only the composition of the <2μ m fraction of 5 Quaternary clay samples was determined. Clays are thin intercalations in a generally coarse-grained sequence. Lithostratigraphic units were not identified, most probably they represent the Jászladány Clay and the Nyékládháza Gravel Formations.

Table 1. Mineral composition of bulk samples of Quaternary and Upper Pannonian formations of various sub-basins of the Great Hungarian Plain

Basin	Borehole	Formation	Age	No.of samples	smec. (* + Na-s)	i/s	illite	kaolinite (*k/s)	chlorite	quartz	K-feldspar	plagioclase	calc.(* +Mg-c)	dol. (* + Fe-d)	siderite	goethite	pyrite	q/fp ratio
JÁSZSÁG, MEZŐSÉG	*Jászladány-1*	Jászladány Clay	Q_1	1	35		15-20	0-5		35		10						3.5
		Kerecsend Red Clay(?)	Q_1	1	45		20		5-10	15-20			0-5	0-5	5			"? "
		Nagyalföld Variegated Clay(?)	Pa_2(Pl)	1	30		20		5-10	35		5						5.8
		Újfalu Sandstone	Pa_2(M)	1	5-10		25		15	15-20		5	15	10-15				3.6
	Tiszapalkonya-1	Nagyalföld Variegated Clay	Pa_2(Pl)	2	10	0-5	10-15	0-5	0-5	55-60		5						5.5-6.1
SOUTH-TISZA, DANUBE-TISZA INTER.	*Kecskemét-1*	Kecskemét Gravel	Q_1	5	0-5	0-5	10-30		5-20	20-50	5-15	5-20	5-15	5-15			tr.	1.1-3.6
		Újfalu Sandstone	Pa_2(M)	16														0.8-3.6
	Csongrád-1	Csongrád Sand	Q_1	9	5-15	0-5	20-30	0-5	10-20	20-25	0-5	5-10	5-15	5-15	tr.		tr.	1.2-4.5
		Újfalu Sandstone	Pa_2(M)	6														2.3-11.5
KÖRÖS	*Dévaványa-1*	Vésztõ Variegated Clay	Q_1	6	10-20	0-10	20-40	0-10*	10-15	25-30	0-5	10	0-5		tr.	tr.		1.1-4.0
		Nagyalföld Variegated Clay	Pa_2(Pl)	13														1.2-4.6
	Vésztõ-1	Vésztõ Variegated Clay	Q_1	4	10	10	15-25	0-5*	5-10	30-50	0-5	5-10	0-5*	tr.		0-5	tr.	2.6-11.3
		Nagyalföld Variegated Clay	Pa_2(Pl)	11														5.3-8.3
MAROS ALLUVIAL FAN	*Pusztaottlaka-I/P*	Vésztõ Variegated Clay	Q_1	14	5-15	0-10	15-30	0-5	5-15	20-40	0-5	10-25	0-5*	0-5			tr.	0.6-2.7
		Nagyalföld Variegated Clay	Pa_2(Pl)	12	5-15	0-10	15-30		5-15	20-40		5-10	0-15	0-5	0-10		tr.	2.3-4.8
	Kevermes-II/P	Vésztõ Variegated Clay	Q1	18	5-30*	5-15	15-30	0-5	5-10	15-40	0-5	5-15	0-10*	0-10*	tr.			0.7-4.3
		Nagyalföld Variegated Clay	Pa2(Pl)	13	20-40*	5-15	20-35	0-5	5-10	10-20	0-5	0-15	0-5			0-5		1.1-7.5
	Tótkomlós-III/P	Vésztõ Variegated Clay	Q1	15	20-35	5-10	15-20	0-5	5-10	20-35	0-5	5-10	0-15	0-5		tr.		1.6-7.0
		Nagyalföld Variegated Clay	Pa2(Pl)	28	15-35	5-20	15-20	0-5	5-10	20-35	0-5	5-10	0-10	0-5	0-5		0-5	3.1-7.3

Q1: Pleistocene, Pa2 (Pl): Upper Pannonian (Pliocene), Pa2 (M): Upper Pannonian (Miocene)
smec.: smectite, + Na-s: (Ca,Mg)- and Na-smectite, i/s: illite/smectite mixed-layer mineral, k/s: kaolinite/smectite mixed-layer mineral, calc.: calcite, + Mg-c: in some samples magnesian calcite, dol.: dolomite, + Fe-d: in some samples Fe-dolomite
tr.: traces
q/fp ratio: quartz/feldspar ratio

Table 2. Mineral composition of the <2 μm fraction of Quaternary and Upper Pannonian formations of various sub- basins of the Great Hungarian Plain

Basin	Borehole	Formation	Age	No.of samples	smectite+i/s (*:i/s/chl)	illite	kaolinite (*: k/s)	kaolinite/ chlorite relation	chlorite	S in i/s (%)
JÁSZSÁG, MEZŐSÉG	*Tiszapalkonya-I*	Pleistocene	Q_1	5	55-75	20-40	0-5*	>	0-5	20-100
		Nagyalföld Variegated Clay	Pa_2(Pl)	3	50-65	30-45	5-10		0-5	60-100
SOUTH-TISZA, DANUBE-TISZA INTERFLUVE	*Kecskemét-1°*	Kecskemét Gravel	Q_1	1	45	50	0-5	<	0-5	
		Újfalu Sandstone	Pa_2(M)	10	0-20	65-90	0-5		5-15	
	Csongrád-1(>5μm)	Csongrád Sand	Q_1	9	35-60*	20-50	5-10	<	5-10	20-40; 60-100
		Újfalu Sandstone	Pa_2(M)	6						0-20; 60-100
	Csongrád-1(>2μm)	Csongrád Sand	Q_1	9	55-70*	20-35	5-10	~	5-10	10-20; 40-100
		Újfalu Sandstone	Pa_2(M)	6						0-20; 40-100
KÖRÖS	*Dévaványa-1*	Vésztõ Variegated Clay	Q_1	6	30-50	30-40	10-20*	~	10-20	20-40; 100
		Nagyalföld Variegated Clay	Pa_2(Pl)	13						0-40; 60-100
MAROS ALLUVIAL FAN	*Pusztaottlaka-I/P*	Vésztõ Variegated Clay	Q_1	14	65-85*	10-25	5-10	~	5-10	70-90
		Nagyalföld Variegated Clay	Pa_2(Pl)	12	65-85					
	Kevermes-II/P	Vésztõ Variegated Clay	Q_1	6	60-75	20-35	5-10*		0-5	0-10; 40-100
		Nagyalföld Variegated Clay	Pa_2(Pl)	6	60-80*	15-30				
	Tótkomlós-III/P	Vésztõ Variegated Clay	Q_1	15	55-80*	10-30	5-10		0-10	60-100
		Nagyalföld Variegated Clay	Pa_2(Pl)	28	60-85*	5-30	5-15*		0-10	80-100

° Data not revised.

Q_1: Pleistocene, Pa_2 (Pl): Upper Pannonian (Pliocene), Pa_2 (M): Upper Pannonian (Miocene)

i/s: illite/smectite, i/s/chl: illite/smectite/chlorite, k/s: kaolinite/smectite mixed-layer minerals

S in i/s: proportion of smectite in illite/smectite (%, approximate estimates)

In cases when kaolinite and chlorite contents fall in the same range, the actual quantitative relations are shown by the signs <, > and ~

The Upper Pliocene Nagyalföld Formation underlies unconformably the Quaternary deposits (128,2-266,2 m), which is, in turn, underlain by the very thick Upper Pannonian Bükkalja Lignite Formation. This latter one is not discussed in the present paper. From the Nagyalföld Formation 2 bulk samples and 3 samples of the <2μ m fraction of clay beds were analysed. X-ray diffraction analysis was made by Viczián in 1986. In the bulk samples there are low carbonate contents. The dominant clay minerals are *smectite* and *illite* while kaolinite and chlorite are low. All clay minerals are opressed by the unusually high amounts of *quartz* which is probably due to the generally coarse-grained nature of the enclosing clastic sequence (Table 1). In the <2μ m fraction of both Quaternary and Nagyalföld Formations, *smectite, illite/smectite* and *illite* are the main components, only little kaolinite and chlorite are left in the fine fraction. There is more kaolinite than chlorite. Kaolinite is disordered in Lower Pleistocene (Table 2). Smectite proportions in the mixed-layers are very variable in the Nagyalföld Fm. (60-100 %) and even more in the Pleistocene (20-100%). The sudden drop in S % values corresponds to the erosional unconformity between Upper Pliocene Nagyalföld Fm. and Pleistocene.

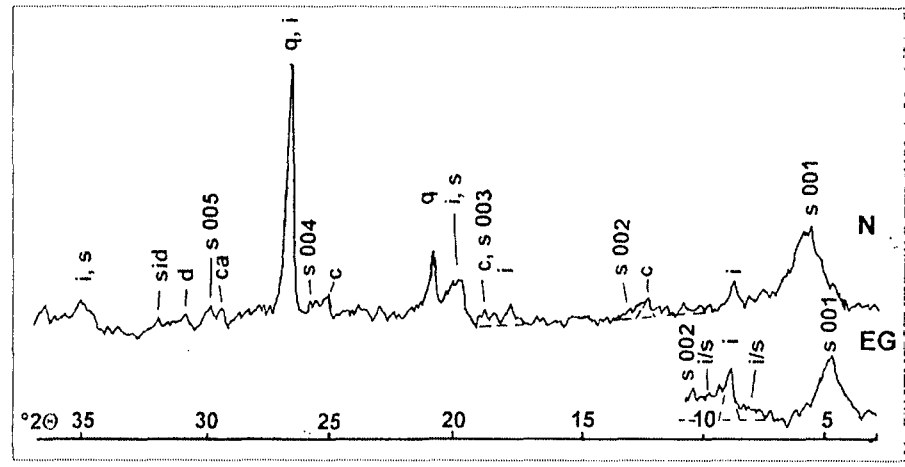

Fig. 5. X-ray diffraction patterns. Borehole Jászladány-1, 683.99-684.24 m, reddish brown clay, bulk sample, Kerecsend Red Clay (?) Formation, Upper Pliocene. Original analysis by Rischák (1965, revised), one of the first X-ray patterns made of the Quaternary deposits of Great Hungarian Plain. Conditions of the measurement: CuK_{α} radiation, N: untreated, EG: ethylene glycol treated sample, random powder specimens. Abbreviations of minerals: see Fig. 2.

Alluvial deposits of the South Tisza Basin (Csongrád Sand Formation) and of the Danube-Tisza Interfluve area (Kecskemét Gravel Formation)

The *South Tisza Basin* is a N-S stretching graben-like structure in which the deepest Quaternary basin of the Alföld area has developed. The thickness of Quaternary exceeds 600 m around the mouth of Körös river into Tisza (see Figs. 2 and 3). The basin is bordered from the west by an eastward dipping flank in the interfluve area of the present-day Danube and Tisza rivers. The thickness of Quaternary decreases westward from 650 m at the Tisza to less than 50 m at the Danube.

Lower and Middle Pleistocene sediments of the *Danube-Tisza Interfluve area* are mostly represented by sand-size (and sometimes gravel-size) fluvial deposits of the ancient Danube river called in the lithostratigraphic system Kecskemét Gravel Formation. There are a few XRD analyses showing the mineral composition of the intercalated clay and silt sediments from the key borehole *Kecskemét-1* (Rónai, 1985, see Fig. 3). The Quaternary sequence is 200 m thick. Quaternary is unconformably underlain by a thick sequence of mostly fine-grained Upper Pannonian fluvio-lacustrine sediments carried into the basin from NW direction (Újfalu, formerly Törtel Formation, see Juhász, 1992). Variegated clays of Pliocene age are missing here, pelitic sediments are of grey colour both in Quaternary and Upper Pannonian.

X-ray data of the bulk rock and <2μ m fraction composition of the whole sequence were determined by Viczián (1980, revised), published and interpreted in the C. Sc. Thesis of Gheith (1981b). The bulk samples in the entire sequence have a very uniform composition: major clay minerals are *illite* and *chlorite*, there are less smectite and illite/smectite, relatively much feldspar minerals: *K-feldspar* and *plagioclase* and carbonates: *calcite* and *dolomite* in nearly equal amounts. Kaolinite is practically absent. There is relatively much feldspar, the quartz/feldspar ratio varies typically between 1-2 in the sandstone and 2-3 in the clay (Table 1). This indicates immature sediments, the sandstone contains much lithic grains. The quantity of quartz – and correspondingly the amount of the rest of minerals – clearly varies with the dominant grain size, there is about 50 % quartz in sand and 20-30 % in silt and clay. Most carbonate minerals are detrital grains. According to Gheith (1981b) the <2μ m fraction is dominated by illite, while other clay minerals, smectite+illite/smectite, kaolinite and chlorite are little. Chlorite is normally more than kaolinite. This composition strikingly contrasts with that of any other Quaternary alluvial sediment from the Alföld. It was, however, not possible to revise these data during the writing this report because the original X-ray patterns are lost.

The overall mineral composition can be considered as typical of the sediment load of the Palaeo-Danube. Very similar compositions were reported from recent bottom sediments of the Danube in Austria (Kralik and Augustin-Gyurits, 1994) and at Bratislava (Konta, 1993). According to Konta, detrital *dolomite* is typical in the sediment load of Danube but absent in other rivers coming from the Bohemian Massif and from the Western Carpathians. In conclusion, Gheith (1981b, p. 179) stated that "the composition of sediments from *Kecskemét* can be directly related to the local erosion of sedimentary and metamorphic rocks and represent more reworked sediments".

The borehole *Csongrád-1* explored a similar coarse-grained fluvial sequence, but with a considerably

thicker Quaternary (650 m), than in the well *Kecskemét-1* (see Figs. 2 and 3). Here the predominantly sandy succession (Csongrád Sand Formation) contains numerous gravel beds. The same types of sediments continue downwards in the Pliocene (Újfalu Formation, see Rónai, 1986, Figs. 4 and 5). The sediments were transported by river channels of the Palaeo-Danube from NW direction in Late Pliocene and Early Pleistocene times. Volcanogenic heavy minerals in Middle and Upper Pleistocene sands show more northern affinity similar to the deposits of the recent Tisza river (Gheith, 1982). No variegated clay occurs in this basin. Intercalated silt and clay layers were investigated by XRD. Bulk samples, the <2 μm fraction and - for experimental reasons - also the <5 μm fraction were studied (Viczián, 1979, published by Gheith, 1982, revised).

Similarly to the *Kecskemét-1* borehole, the bulk samples along the whole sequence have a very uniform composition: major clay minerals are *illite* and *chlorite*, there are less smectite and illite/smectite and occasionally kaolinite. K-feldspar and plagioclase are somewhat less abundant than at *Kecskemét*, there is less feldspar in the samples containing kaolinite. The quartz/feldspar ratio varies typically between 1 and 4 (Table 1), higher values indicate a certain degree of alteration. The sediments are rich in carbonates, both *calcite* and *dolomite* are present, microscopic observations have shown that the sediments are "enriched in detrital carbonate minerals" (Gheith, 1981b).

The <2μ m fraction contains much *smectite + illite/smectite* and discrete *illite*, while kaolinite and chlorite are invariably low throughout the whole Quaternary and Pliocene section. The 001/001 basal reflection of the expandable minerals ranges from 10 to 14 Å, the maximum is at about 12 Å indicating that the majority of the expanding phases is mixed-layer illite/smectite of high but variable smectite proportion (S %). S % values were determined on the glycolated specimens. Two broad maxima were found, one at about 0 to 20 % and another between 40 and 100 % smectite proportions. Glycolated and heated samples show that there is also

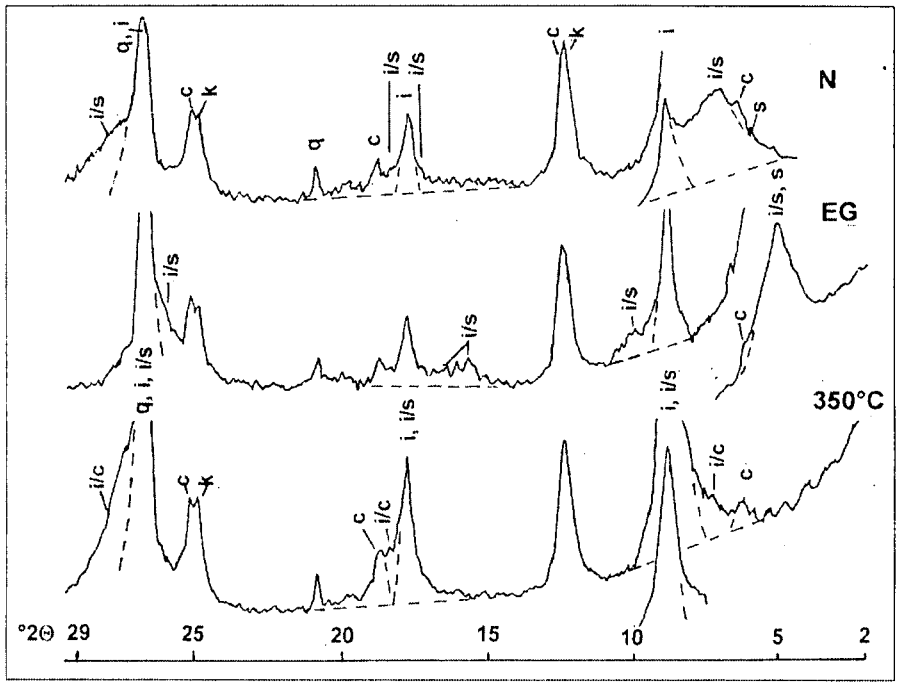

Fig. 6. X-ray diffraction patterns. Borehole Csongrád-1, core No. 10, 275.50-279.60 m, light grey calcareous siltstone, <2 μm fraction, Csongrád Sand Formation, Lower Pleistocene. Original analysis by Viczián (1979, revised). Conditions of the measurement: CuK_α radiation, N: untreated, EG: ethylene glycol treated sample, 350 °C: heated at 350 °C for 2 hours, oriented specimens by the smear-on-glass method. Abbreviations of minerals: see Fig. 2.

smectite/chlorite interstratification. Other minerals in the <2μ m fraction have normal sharp basal reflections (Fig. 6). The composition of the <5μ m fraction does not differ from the <2μ m fraction except that it contains slightly more illite and chlorite and slightly less kaolinite and smectite+illite/smectite. Chlorite is nearly equal to kaolinite in the <2μ m fraction and more than kaolinite in the <5μ m fraction, showing that kaolinite enriches in the finest grain fraction.

Usually these types of mixed-layer illite/smectite minerals are interpreted by pedogenic origin. Samples interpreted by micromineralogic analysis as being inherited from volcanic areas, do not display any systematic difference in the clay mineral composition, compared to the terrigeneous sediments of the Palaeo-Danube.

Alluvial fan of the Maros river (Vésztő and Nagyalföld Variegated Clay Formations)

The *Maros river alluvial fan* occupies the SE part of the Great Hungarian Plain. The facies of Quaternary and of underlying Upper Pliocene is variegated clay (Vésztő and Nagyalföld Formations, respectively), similarly to the *Körös Basin*, however, here the thickness of the formations is lower and the facies is more sandy. The samples taken from the fine-grained varieties of sediments were investigated in three water exploratory wells (Fig. 4).

In the well *Pusztaottlaka-1/P* the thickness of the Quaternary is 369 m, from here until the bottom of the well at 500 m, there are beds of Upper Pliocene (369-448 m) and Upper Pannonian (below 448 m) age (Franyó, 1983). 26 clayey and sandy siltstone samples were taken. The colour is partly grey, partly grey with yellowish brown spots. X-ray diffraction analyses on the bulk samples were made by Viczián (1979, unpublished data). Clay minerals are *smectite, illite/smectite, illite* and *chlorite*. Kaolinite is normally absent, however, there is an interval in the middle of Pleistocene where there is systematically about 5 % kaolinite. In this bore hole the value of the cation exchange capacity of the bulk samples was determined, 7-10 $mol.10^{-3}/100$ g (=15-20 meqv./100 g) which mostly depends on the smectite+ illite/smectite complex. Exchangeable cations are about ½ Ca, ¼ Mg, ¼ Na and little K.

Other minerals display systematic differences between Quaternary and Pliocene: quartz varies between 20-40 %, determining the quantity of the rest of phases. There is about 5 % K-feldspar in the Quaternary and missing in Pliocene, similarly, *plagioclase* contents are higher in Quaternary than in Pliocene. The reason of this distribution is perhaps stronger feldspar weathering in Pliocene. The dominant carbonate is calcite. Quaternary bulk samples are carbonate-poor (calcite 0-5 %, sometimes magnesian calcite, but the concretions consist of pure calcite). Pliocene samples are richer in *calcite* and *siderite*.

Data relating the <2 μm fraction were published by Viczián (1982). Contrary to the typical differences in the bulk composition, the proportion of clay minerals is practically the same throughout the section: the only dominant phase is *smectite+illite/smectite*, while illite, kaolinite and chlorite are present in low but nearly constant amounts. The smectite proportion of the expanding phases varies between 70 and 90 %. One systematic variation seems to be clear: Quaternary sediments contain *chloritic interlayers* in the mixed-layer structure while Pliocene mixed-layers are of the *illite/smectite* composition only. The overall character of the clay fraction resembles more the Danube river sediments of the *South Tisza Basin* than those of the *Körös* and *Jászság Basins*.

Another borehole investigated in detail in the course of the same water exploration project was *Kevermes II/P*. According to Franyó (1983), the thickness of the Quaternary is 320 m, there are beds of Upper Pliocene (320-489 m) and Upper Pannonian (below 489 m, until the bottom of the well at 500 m). A total of 31 samples were taken from the Quaternary and Pliocene interval. The rocks are alternating variegated siltstone indicating palaeo-weathering and humic clay of swamp horizons. X-ray diffraction analyses on the bulk samples were made by Rischák (1980, revised), thermal analysis by Földvári (1980). The dominant clay minerals are *smectite, illite/smectite* and *illite*, chlorite is less abundant. There is more smectite and illite in the Pliocene than in the Quaternary. A few per cent of kaolinite is present in most samples, slightly less frequently in the Quaternary. A peculiarity of the smectite is in almost every sample, that the 001 basal reflection splits into two maxima, one at about 12.5 Å and a stronger one at about 15 Å. This can be interpreted by the separation of *Na-* and *(Ca,Mg)-smectites*. Illite and chlorite are generally well crystallised, with sharp basal reflections. The highest quartz contents were found in sands of riverbed facies. Quartz and plagioclase are more abundant in the Quaternary than in the Pliocene, probably because slight differences in the grain size of the samples (more silt in the Quaternary and more clay in the Pliocene). A few percent of K-feldspar is present invariably in most Quaternary and Pliocene samples. The sediments are poor in carbonate minerals, the total carbonate contents are normally below 10 %, consisting mainly of calcite and less abundantly of dolomite. Magnesian calcite occurs throughout the whole Pleistocene but is missing in Upper Pliocene. Carbonate occurs in the sediments as nodules, spots, fill of fine network of veins and Mollusc shells. A carbonate nodule analysed consists of pure calcite.

In the <2 μm fraction the dominant clay minerals are *smectite, illite/smectite* and *illite,* kaolinite and chlorite are less abundant (originally analysed by Rischák, 1980, revised). The quantity relations are nearly the same as in the well *Pusztaottlaka-I/P*, here illite is slightly higher and chlorite somewhat lower. Kaolinite exceeds chlorite. There is practically no difference between the composition of the Quaternary and Pliocene samples. Smectite proportions in the *illite/smectites* vary in broad ranges, but normally are high, up to 100 %. The mixed-layer *illite/smectite* contains *chloritic interlayering*, as deduced from incomplete collapse of the basal reflection to 10 Å upon heating to 490 °C. This is true in the Pliocene samples, unfortunately, it was not determined in the Quaternary, because no heated specimens were made. Kaolinite is typically disordered, transitional to *mixed-layer kaolinite/smectite.* Typical weathering products are goethite in the Quaternary and anatase in the Pliocene, as minor amounts in the <2 μm fraction.

The third borehole in the *Maros alluvial fan* area was *Tótkomlós-III/P*. Geological and stratigraphic relations are nearly identical with those of the two previous wells (Quaternary: 0-248 m, Upper Pliocene: 248-480 m, Upper Pannonian below 480 m, Franyó, 1983).

X-ray analyses of the *Tótkomlós-III/P* samples were carried out by Rischák (1981, revised), thermal analysis was made by Rimanóczy (1981). Unfortunately, neither these data were published. The silicate phases of the bulk composition show basically the same quantitative relations as in *Pusztaottlaka-I/P*, however, differences between the Quaternary and Upper Pliocene are not so clear. As compared with *Pusztaottlaka-I/P,* there is somewhat more *smectite* and *illite/smectite* and less illite, chlorite and plagioclase in the *Tótkomlós-III/P* samples. Like in other occurrences of the Maros Alluvial Fan area, calcite, dolomite and siderite contents are low or zero both in Quaternary and in Upper Pliocene.

In the <2 μm fraction the type and quantity of the clay minerals is essentially the same, as in any other borehole of the Great Hungarian Plain, however, slight differences can be observed which are typical to the Maros river alluvial fan: *smectite+illite/smectite* are somewhat higher and *illite* lower than in other basins. Kaolinite is clearly higher than chlorite and there is *kaolinite/smectite mixed-layering* as indicated on broadening of the 001 basal reflection of kaolinite towards higher d-values. This kaolinite/smectite mixed-layering is more pronounced in the Pliocene than in the Quaternary. The smectite proportion in the illite/smectite varies in broad ranges, practically between 0 and 100 %, but it is most frequently in the range near 100 %. Illite/smectite seems to contain chloritic interlayers. This is typical invariably along the whole section. The general character of the clay fraction indicates even more "weathered" detrital sedimentary material, than at *Pusztaottlaka-I/P,* resembling more to *Kevermes-II/P*.

Alluvial deposits of the Körös Basin (Vésztő and Nagyalföld Variegated Clay Formations)

The *Körös Basin* represents a sub-basin in the *SE Alföld* area where especially thick Quaternary sequences were revealed. The dominant rock types are siltstone and clay interrupted by layers of sandy riverbed sediments (Vésztő Variegated Clay Formation). The formation continuously develops from similar formations deposited in the Upper

Pliocene period (Nagyalföld Variegated Clay Formation). The Upper Pliocene beds differ from the Quaternary ones only by their more lacustrine and marshy and less fluviatile character (Fig. 3).

The core material obtained from these formations from the borehole *Dévaványa-1* was object of detailed petrographic analysis by Gheith (1981a). Silt and clay samples were taken in 50-100 m intervals of the fine grained portions of the 1100 m thick sequence (Quaternary: 0-416 m). The XRD analysis of the bulk rock and of the <2 μm fraction was carried out by Szemethy (1978, revised) in the laboratory of the Geological Institute of Hungary. In the composition of the bulk samples the clay minerals *smectite*, *illite*, and *chlorite*, in lesser amounts mixed-layer illite/smectite and kaolinite occur. There are great differences between two types of mineral associations. In the *"weathered"* type samples the basal reflections are broad and uncertain, the quantity of smectite+illite/smectite is nearly equal to illite, there is a few percent of disordered kaolinite, the 001 basal reflection of kaolinite is asymmetrically broadened towards higher d values indicating *kaolinite/smectite interstratification*. There is another type which may be called *"fresh"*, in which basal reflections are sharp, well crystallised *illite* and *chlorite* are the dominant phases, the quantity of expanded phases is low and there is no kaolinite. There is a third type in the lowermost portion of the Upper Pliocene in which smectite disappears and well crystallised kaolinite becomes more abundant. Among the other minerals of detrital origin quartz and plagioclase are constantly present while K-feldspar occurs only sporadically. Contrary to the sediments of Palaeo-Danube in the *Kecskemét* and *Csongrád* area, all rock types are poor in carbonate, only little calcite may be found in some cases.

In the <2 μm fraction the same clay minerals were found as in the bulk rock, however, *smectite* becomes the dominant phase and kaolinite appears in nearly equal amounts as chlorite, similarly, as in the <2 μm fraction of *Csongrád-1*. In this borehole both minerals are relatively high, compared to other localities (Fig. 7). Slight decrease of smectite and increase of kaolinite can be observed toward the bottom of the sequence (see Gheith, 1981a, Fig. 6). The maximum of the 001 basal reflection of *smectite*+illite/smectite is in this bore hole at about 14 Å. Another type of illite/smectite, present in lesser amounts, has basal reflection in the range 10-14 Å. This is a difference e.g. from the clay fraction of the samples of other bore holes of the Great Plain where the dominant basal spacing is almost invariably near 12 Å. As determined in the ethylene glycol treated samples, there are two ranges of composition of the smectite+illite/smectite expandable complex: one near 100 % smectite proportion and another one in the range of 20-40 % smectite proportion. Pliocene samples are slightly less expandable than Quaternary ones. *Kaolinite is disordered* and indicates *mixed-layering with smectite*, especially in the samples classified as "weathered" according to the bulk rock analysis (Fig. 7). Another difference from the *Csongrád-1* samples is the absence of chlorite/smectite interstratification.

In general, one can agree with Gheith (1981b, p. 179) who characterised *Dévaványa* sediments as "more mature which were deposited during quiet, more stagnant water conditions than those in *Csongrád* and *Kecskemét*".

Very similar figures were obtained for the bulk mineral composition of the 1200 m thick Upper Pliocene to Quaternary sequence of another key borehole, *Vésztő-1* (Quaternary: 0-482 m): smectite, illite/smectite, illite, kaolinite, chlorite, quartz, plagioclase and very little K-feldspar, calcite, dolomite, goethite and pyrite (traces in some cases). Quartz varies in broad ranges, between 30-50(-70) %, depending mainly on variations of grain size. This sequence seems to contain almost exclusively only the *"weathered"* type of the clay mineral suite which is reflected in the nearly equal ratio of smectite+illite/smectite to illite. No systematic variation in the quantity of most detrital minerals with depth or stratigraphic position can be observed, except variations due to grain size in the range of clay to fine sandy siltstone. The clays are almost carbonate-free, however, calcite is somewhat higher and contains 2-6 mol % Mg(+Fe?) in some Upper Pliocene samples. The unpublished XRD analyses were made by Viczián (1979, revised). The <2 μm fraction was not analysed.

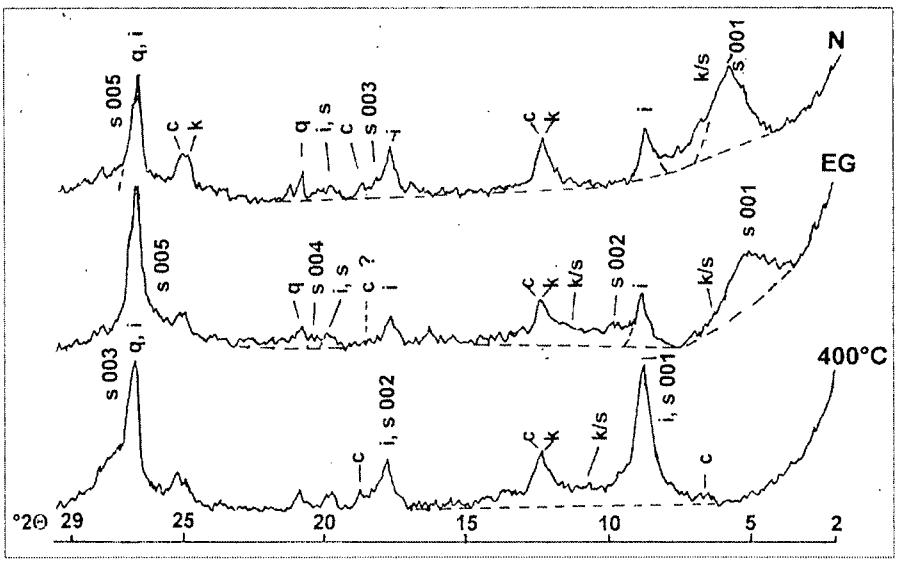

Fig. 7. X-ray diffraction patterns. Borehole Dévaványa-1, 172.9-181.0 m, variegated clayey silt, <2 μm fraction, Vésztő Variegated Clay Formation, Pleistocene. Original analysis by Szemethy (1978, revised). *"Weathered"* type bulk sample. Conditions of the measurement: see *Fig. 6*, 400 °C: heated at 400 °C for 2 hours. Abbreviations of minerals: see Fig. 2.

DISCUSSION

Considerations on relation of clay mineralogy to palaeoclimatic conditions and source areas in the Körös Basin

It was attempted to find correlation between the mineralogy and *palaeoclimatic conditions* of deposition in the *Körös Basin*. The mineralogical data were compared with the results of palynological studies (Mihált-Faragó, 1982). Mihált-Faragó divided the Quaternary sections into 11 climatic zones which she identified with the Alpine glacial and interglacial periods. Her subdivision was accepted and highly estimated in the review paper by Jámbor (1998). The samples studied for clay minerals coincide with both warm and cold climatic conditions according to the pollen studies. However, no systematic variation of the mineralogy with the climate could be demonstrated except probably that some calcite is typical only in the colder stages while the warmer stage samples are carbonate-free.

An alternative view of the palaeoclimatic conditions during the deposition of the Quaternary sequences in the two bore holes was proposed recently by Nádor et al. (2000). Based on detailed sequence stratigraphic analysis, micromineralogical and palaeontological data and measurements of magnetic susceptibility, they recognised the existence of higher periodicity (100 and 40 Ky) Milankovitch cycles in the time interval of the Quaternary in the *Körös Basin*. According to this new model, sandy beds coincide well with maxima of magnetic susceptibility and in most cases with warm climatic periods. On the other hand, fine-grained beds may have different palaeo-environmental interpretation depending on the prevailing climatic conditions. In cold periods, due to low discharge, only fine-grained dispersed sediments reached the central parts of the basin and silts may have been deposited in the river bed facies while only fine clays reached the flood plains. On the other hand, in warm periods, due to higher discharge, the rivers deposited sand in the river bed and silt on the flood plain. By the finest resolution, however, in a dm to m scale of bed thickness the development of fine grained beds depends primarily on autocyclic shift of river bed and the effect of climatic variations is shown much more in the higher, approximately ten metres scale of the smoothed curve of grain size variation.

Unfortunately, the sampling density is not sufficient to check the possible compositional variations during an autocyclic or climatic cycle, on the basis of mineralogical data available at present. The present considerations are based on a very limited number of samples of Quaternary age, 6 from the *Dévaványa-1* and 4 from the *Vésztő-1* borehole.

It can be expected that the quartz/feldspar ratio or kaolinite contents may vary also in fine-grained rocks depending on the weathering conditions on the source area. The XRD data on quartz/feldspar ratios of fine-grained samples vary in the range 1 to 11 (Table 1). The most frequent values are at *Vésztő* 5 to 6 and at *Dévaványa* 2 to 4, i. e. the *q/fp ratio* of XRD analyses varies in the same range and probably in the same sense as the quartz/(feldspar+rock fragments) ratio in sandstones of the *Vésztő-1* borehole as determined by micromineralogical observations (Nádor et al. 2000). In the same time the palaeoclimatic interpretation may be discouraged by the fact that the same magnitude and range of variation of the quartz/feldspar ratio may be observed in the Quaternary as in the Upper Pliocene parts of the sections when a more balanced and less variable climate prevailed. The conclusion is much more plausible that for a long period of time a more mature material was deposited at *Vésztő-1* than at *Dévaványa-1*, independently of eventual climatic fluctuations during deposition.

Another discouraging aspect is the high degree of homogeneity in the mineralogical record in the <2 μm fraction throughout the whole sections of the two boreholes (Fig. 3). Even kaolinite contents are remarkably constant in the *Dévaványa-1* borehole, irrespective of eventual climatic variations. The remarkable fact that detrital clay mineral patterns may be *highly independent on palaeoclimatic conditions* was observed recently e. g. in the Mesozoic of England (Jeans et al., 2001). Similarly, Alcalá-García et al. (2001) have found that clay mineralogy of detrital sediments is more dependent on geodynamic factors than on palaeo-climate or facies of deposition. What is promising, however, it is the difference found between the "weathered" and "fresh" types of clay mineral assemblages in the Körös Basin Quaternary. Systematic comparison with other palaeoclimatic indicators would be necessary to check the correlation with these types of clay assemblages.

Similarly to the climatic variations, not much of the eventual variations of *the source areas* is reflected in the clay mineral record and bulk composition of the fine-grained sediments. Minerals of the *Dévaványa-1* borehole were interpreted by Gheith (1981a,b) as detrital depending on the source area, illite being derived from weathering of metamorphic rocks and smectite from volcanic rocks. This latter might be probably true for the major part of smectites because volcanogenic smectites should be discrete smectite phases and, indeed, 100 % smectite proportions are here the most common expandable types. There is, however, no much correlation with the eventual change of the source areas.

According to micromineralogical analysis, the source area of the *Körös Basin* sediments was generally the *Apuseni Mts.* from which the sediments were transported alternatively from NE-E and SE directions. Heavy minerals indicate predominantly metamorphic and redeposited Tertiary sedimentary rocks. In addition to these sources northern volcanic areas contributed material mostly in later periods of Quaternary at *Dévaványa* (Thamó-Bozsó and Kercsmár, 2000). The composition of the pelitic rocks does not reflect these variable source areas and *remains uniform* throughout the section.

The essential uniformity of the detrital material derived from the source areas was shown also by *isotope geochemical* studies. According to the study of the $^{87}Sr/^{86}Sr$ isotope ratio of the formation waters Varsányi (2000) concluded that in the Körös Basin this ratio is systematically different from the ratio observed in the Danube-Tisza Interfluve area and South Tisza Basin, reflecting different source areas of the sediments. Sediments of the Körös Basin have lower $^{87}Sr/^{86}Sr$ isotope ratios and, consequently, are derived from younger formations than those coming from the catchment area of the Danube river. These ratios and the corresponding source areas, however, remained essentially unchanged over the long time period from Late Miocene to Pleistocene.

The reason of this uniformity lies probably in the more averaged nature and slow speed of the development of the weathering crust which is one of the main sources of the pelitic material in the areas of denudation. Judging from the composition of the basin-filling material, the mineralogy of this weathering crust in the *Apuseni Mts.* may be similar to that of the Tengelic Formation in the Transdanubian area. Another source of the basin filling may be the redeposition of various Tertiary sedimentary rocks around the *Apuseni Mts.* which themselves may have rather uniform clay mineral composition. This can be identified partly with a frequently occurring chlorite-rich heavy mineral assemblage. The provenance of this assemblage was uncertain in the interpretation of the micromineralogical data but it was pointed out that Pannonian sediments commonly have similar chlorite-rich heavy mineral composition (Thamó-Bozsó and Kercsmár, 2000).

Similar observations were made by comparing Alpine source areas with Tertiary sediments in the South German Molasse Basin (Viczián, 1984), where a more uniform clay mineral assemblage was observed than it might be expected from heavy mineral studies. It was shown, however, that probably more accurate measurements of structural parameters of micas may reveal differences in different metamorphic source rocks.

Diagenesis of iron minerals in the variegated sediments of the Great Hungarian Plain

Vary-coloured sediments of the Great Hungarian Plain with typical yellowish rusty spots give good insight into the repartition and transformation of iron minerals after deposition.

In deeper zones of the borehole *Csongrád-1* traces of siderite and pyrite show the reduced state of iron. Gheith (1982) observed that in higher levels most of the Quaternary fine-grained "samples have stained patches of *limonite*". This, however, does not appear in the X-ray record.

The typical rusty yellow and reddish spots correspond to traces of goethite in borehole *Dévaványa-1* in the *Körös Basin* area. The high ferric/ferrous iron proportions (2:1 to 5:1) in the chemical analyses show the oxidised state of the pelitic sediments (see Fig. 4 of Gheith, 1981a). It is more clearly seen in the borehole *Vésztő-1*, than in *Dévaványa*, that rusty spots may be attributed to the iron mineral *goethite*, especially in the Upper Pliocene part of the section. In the Upper Pliocene also iron-containing calcites may occur.

Variegated clays from the *Komádi-1* borehole were investigated by Rischák (1984). The samples were taken from the deeper part of the sequence (Upper Pliocene Nagyalföld Formation, see Fig. 3). The studies were focused to the genesis of the red spots. In the red parts of the samples the iron minerals *goethite, lepidocrocite* and *siderite* were identified by XRD, thermal (Rimanóczy, 1981, see Rischák, 1984, Table 2) and chemical analysis. Ferric iron is derived of *pyrite* by the oxidation of sulphide to sulphuric acid, migration of ferrous ions to the spots in a local scale, precipitation of ferrous carbonate and finally oxidation and precipitation in form of ferric hydroxides. Bulk mineral composition remains unchanged during this process and is practically identical with that of the two other boreholes studied in the *Körös Basin.*

In the water exploratory well *Pusztaottlaka-I/P* in the *Maros alluvial fan* area Upper Pliocene (Nagyalföld Fm.) samples may contain much *siderite* (0-10 %, in some cases up to 25 %, according to the quantitative determinations of Földvári by thermal method). Siderite and traces of pyrite indicate reductive marshy environment. No crystalline goethite was indicated by the XRD, however, "limonite" was identified in the deeper Quaternary and higher Pliocene samples by thermal analysis. This indicates that *poorly crystallised iron(III) hydroxide* of the higher zones is replaced by reduced iron carbonate in the deeper horizons of the Pliocene Nagyalföld Fm.

On the other hand, in the well *Kevermes-II/P* iron carbonates, such as Fe-containing dolomites and traces of siderite occur in the upper 120 m zone of Quaternary. Crystalline goethite in the bulk samples appears only in the Upper Pliocene, however, in the <2 μm fraction it can be traced also in the Quaternary.

The relation among iron minerals in the water exploratory well *Tótkomlós-III/P* is the same as in *Pusztaottlaka-I/P*: Almost no crystalline goethite was indicated by XRD but "limonite" was frequently identified by thermal analysis in the Quaternary sediments, indicating that *iron hydroxides* are *partly amorphous* or poorly crystallised. *Siderite* occurs sporadically in the Quaternary but it is a more common component in the Upper Pliocene. Siderite may be identified both by thermal analysis (0-15 %) and X-rays (in one sample: 10 %, commonly 0-5 %). In organic-rich dark sediments also *pyrite* occurs.

The reduction of iron (III) minerals and the simultaneous desorption of arsenic compounds (possibly arsenite anions) from the surface of iron (III) hydroxides is closely related to the formation of *arsenic groundwater* in the area of the *Maros alluvial fan* (Bartha et al., 1999, 2000) and other areas of the *Great Hungarian Plain* (Csalagovits, 1999).

Possible illitisation in palaeosols

Tanács and Viczián (1995) observed increase of the variability of the smectite proportions in the mixed-layer illite/smectites of fluvial and continental sediments and palaeosols in the upper part of the Upper Pannonian (Pliocene) and in the Pleistocene, as compared to underlying lacustrine or marine Pannonian deposits. As it was shown in the present review, smectite ratios may vary in the same sample within broad ranges, sometimes between 20 and 100 %.

Tanács and Viczián (1995) considered to be not probable that this high variability of the smectite ratios in the highest levels is related to burial diagenesis. Most probably it is due to *palaeo-pedological processes of illitisation* during subaerial exposure of the sediments immediately after deposition. Details of these processes are, however, not yet clear.

Diagenesis of clay minerals, water-rock interaction

Thermal data were published by Rónai (1985, Fig. 334, p. 367) in a geological cross section of the *Körös Basin*, crossing the wells *Szarvas, Dévaványa* and *Vésztő*. The 40 °C isotherm runs in the depth interval of 400-500 m and the 60 °C isotherm in the depth interval of 800-1000 m. On the other hand, data from the whole Pannonian Basin show that the burial diagenesis of illite/smectites starts at temperatures somewhat higher than 60 °C (Viczián, 1994). This means

that diagenesis of the expanded clay minerals caused by thermal effects cannot be expected in the Quaternary, even in the deepest basins.

In this zone the main controlling factor of diagenesis is the *interaction of the sediments with the flowing groundwater*. The chemical reactions between water and solid phases modify the original composition of both the waters and of the enclosing sediments. In the following it will be attempted to compare data related to groundwater and solid phases, and to find evidence in the mineralogical analyses supporting the results of hydrogeochemical calculations.

There are hydrogeochemical studies on interaction of formation waters with young sediments in various parts of the southern Great Hungarian Plain (see review papers by Varsányi and Ó.Kovács, 1994 and Varsányi, 2000, 2001). Unfortunately, there are no similar detailed studies yet available from other parts of the Pannonian Basin. Based on earlier studies of Erdélyi (1979), Varsányi et al. (1997) and Varsányi (2000) came to the important conclusion, that water *flow systems* developed *above the Lower/Upper Pannonian* lithostratigraphic boundary. *Under this boundary* there is a completely different water regime with practically *stagnant, concentrated* $NaCl\text{-}NaHCO_3$ type waters.

Above the Lower/Upper Pannonian boundary two main water flow regimes were separated. The lower one, a *regional-scale water flow regime* in the Upper Pannonian (Upper Miocene, "Pontian M_3Po" of Varsányi, 2000, 2001) is less well known from geochemical point of view. Water-rock interaction was especially well studied in the *upper intermediate-scale water flow regimes* that comprise the Upper Pliocene and Pleistocene sediments of the southern Great Hungarian Plain. As shown in Tables 1 and 2 and in Figs. 2, 3 and 4, the majority of the samples reviewed in the present paper belongs to this *upper water flow regime*.

The *Danube-Tisza Interfluve Area* and the western part of *South Tisza Basin* represent the recharge area of the groundwater flow regime where the chemistry of the water is controlled by *dissolution of calcite and dolomite* and by irreversible *solution of albite* in an open system. The other controlling factor is the Na *ion exchange* for Ca and Mg on clay minerals. The ion exchange came to equilibrium with the present composition of groundwater, the clay minerals contain Ca and Mg exchangeable cations (Varsányi, 1989a,b, 1991, Varsányi and Ó.Kovács, 1997). Two boreholes reviewed in this paper, *Kecskemét-1* and *Csongrád-1* are close to the northern boundary of this area. *Chloritic interlayers* in the expandable structure (Fig. 6) may reflect the adsorption and fixation of Mg ions in the interlayer space. High detrital calcite, dolomite and feldspar contents provide sufficient material for dissolution. Calcites and dolomites in the *Kecskemét-1* borehole proved to have nearly ideal stoichiometric composition by X-ray analysis.

The *Maros alluvial fan* is a similar flowing groundwater system, in a similar geological setting (Varsányi, 1989a,b). This is reflected in the similar character of the clay mineral assemblage. Flow direction is from SE to NW. The recharge area is mostly beyond the state borders. The wells *Kevermes-II/P* and *Tótkomlós-III/P* are situated closer to the recharge area and the well *Pusztaottlaka-I/P* closer to the discharge area. The main chemical reaction that may be expected according to the hydrogeochemical calculations, is *ion exchange*. This can be probably related to the Na-smectite contents of the *Kevermes* samples and to the dominantly divalent exchangeable cations in the *Pusztaottlaka* samples. *Chloritic interlayers* in the mixed-layer structure occur in all three wells, at *Pusztaottlaka* only in the upper few hundred metres. Low carbonate contents and carbonate concretions may indicate *dissolution and later precipitation of carbonates* from the flowing groundwater.

Contrary to the previous two flow systems the *Körös Basin* is a *discharge area*. The aquifer is filled either with stagnant, or very slowly upward flowing water. The boreholes *Dévaványa-1* and *Vésztő-1* are situated in the central part of the Quaternary basin. According to hydrogeochemical calculations dissolution of calcite and dolomite resulted in *equilibrium* between solids and water in relation of the ions Ca and Mg in lower levels while *oversaturation and precipitation* of carbonates occurs in the upper zones. The mineralogical record shows extremely little average carbonate contents and occasionally carbonate concretions of non-ideal calcite composition. This is probably partly due to dissolution and precipitation by the groundwater. On the other hand, no equlibrium composition in respect to silicate minerals was achieved according to the calculations and additional *dissolution of albite* proceeded in upper levels. In the <2 μm fraction of *Dévaványa* samples there are 14 Å smectite, kaolinite and mixed-layer kaolinite/smectite as well (Fig. 7). The product of albite dissolution may be *kaolinite* and not only *smectite* as it was supposed by Varsányi and Ó.Kovács (2001) and Varsányi (2001).

Hydrochemical data show decrease of Na contents in the upper 300 m zone of the Körös Basin. Accordingly adsorption of Na on clay minerals was supposed by Varsányi (2000). This does not appear on the smectites studied. Both in the boreholes *Dévaványa-1* and *Vésztő 1* the d values of the 001 basal reflection are at 14 Å, both in the bulk rock and in the <2 μm fraction, invariably in the whole depth interval of 0 to 1000 m.

Because of the upward flow of Lower Pannonian waters there is no strict boundary between the Lower Pannonian and Upper Pannonian water regimes in the Körös Basin. According to Varsányi (2000, 2001) the effect of the upward flowing Lower Pannonian water can be traced up to 1000 m depth. It is interesting that this boundary coincides with the change of the clay mineral composition (less smectite, more kaolinite) in the lowermost part of the *Dévaványa-1* bore hole.

A remarkable conclusion of the geochemical calculations discussed so far is that in the groundwater flow regime comprising the Pliocene and Pleistocene, *reactions involving* potassium do not play any role. On the other hand, according to investigations of Eberl (1993) in the Gulf Coast area the charge of the smectite layers may be increased by substitutions in the silicate layer and K^+ ions may be accumulated in interlayer sites of the high-charge smectite in shallow levels, at temperatures below cca. 80 °C. Potassium can be enriched in the formation water by dissolution of the K-bearing minerals K-feldspar and mica. All that leads only to slight gradual decrease of the smectite proportion in the mixed-layer structure from about 80 % to 60 %, but this is the first important step in the smectite to illite transition.

Data on the composition of *mixed-layer illite/smectites* published by Viczián (1992) and by Tanács and Viczián (1995) from 10 bore holes show that similar processes proceeded also in the Great Hungarian Plain *roughly above the Lower/Upper Pannonian boundary*. The boundary does not sharply coincide with the lithostratigraphic boundary, in the same manner as also water regimes may communicate across the boundary in the *Körös Basin*. Data of the papers cited and of the present review show, that variable composition is typical feature of the mixed-layer illite/smectites occurring above the Lower Pannonian. The composition is variable within a single sample and it varies also with the subsurface depth. The average smectite proportion of the samples drops with increasing depth from S=80-100 % to 30-50 %. In Lower Pannonian and older Neogene sediments illite/smectites are rather uniform within a single sample and generally low smectite proportions occur (S=10-50 %).

These data show that the *first main phase* of the smectite to illite diagenetic transition proceeds above the Lower/Upper Pannonian lithostratigraphic boundary, but below the Pliocene. What is left, is the *Upper Pannonian* (Upper Miocene, Újfalu and Zagyva Formations, "Pontian"). The water-rock interaction in this lithostratigraphic horizon is not yet well known, but mineralogical data show that dissolution of potassium minerals and fixation of potassium ions in the smectitic layers may proceed in this zone. Simultaneously, the same "Pontian" layers are considered by Varsányi et al. (1997) as "the main zone of kerogen diagenesis", in which the reactions resulting in kerogen formation, polymerisation and polycondensation are going on.

Conclusions

1. There is a wealth of mineralogical data on the composition of alluvial sediments of the Great Hungarian Plain (Alföld). The composition is basically the same in the whole basin: a *polymineralic detrital* clay mineral suite displaying slight systematic regional differences. There is no significant difference between the composition of various stratigraphic horizons in the time interval Upper Pannonian – Upper Pliocene – Pleistocene. Neither the clay mineral relations, nor the quartz to feldspar ratio differ significantly (Tables 1 and 2, Figs. 2, 3 and 4). This is especially interesting because it shows that the composition of sediments was practically independent from the highly varying climatic conditions. On the other hand, sub-basins differ from each other for long periods of time which is the result of the different source areas and shows the importance of the palaeo-tectonic setting.

1.1. The limited number of data from the Jászság Basin indicate higher *smectite* contents which is probably the effect of the northern volcanic areas.

1.2. The most "fresh" material, consisting of *illite* and *chlorite* and of many detrital non-clay minerals, such as *carbonates* and *feldspars* came from the ancient Danube into the Danube-Tisza Interfluve area and South Tisza Basin.

1.3. The composition of the Maros River Alluvial Fan is similar to the sediments derived from the Palaeo-Danube, but it contains *less carbonate*. Among the clay minerals there is much *smectite+illite/smectite* and a little *kaolinite*.

1.4. Sediments of the Körös Basin have the most mature composition, they are almost *carbonate-free*. Clay minerals are less well crystallised, disordered. Typical phases are *disordered kaolinite*, *mixed-layer kaolinite/smectite* and *iron hydroxides* (from *amorphous phases* to *goethite)*. The dominant expanding phase of the <2 μm fraction is here discrete *smectite* while in other basins *mixed-layer illite/smectites* are more frequent.

2. Correlation may be found between variation of chemical composition of groundwater flow regimes and mineralogy of enclosing sediments.

2.1. In the Pleistocene and Pliocene horizons of the South Tisza Basin and Maros Alluvial Fan water flow regimes may cause dissolution of carbonate minerals and albite and ion exchange on clay minerals. Secondary carbonate concretions and neoformed clay minerals may be precipitated. *Ion exchange for magnesium* and subsequent fixation in the interlayer space may produce *chloritic interlayers* in mixed-layer illite/smectites. However, decrease of smectite proportions in mixed-layers in this zone may be related to *palaeopedological illitisation* rather than to diagenetic reactions.

2.2. In the Pleistocene and Pliocene horizons of the Körös Basin interaction of albite with the very slowly upward flowing water regime causes neoformation of *pure smectite* and *kaolinite*, however no chloritic interlayers were formed in this sub-basin.

3. The first phase of diagenetic illitisation involving reactions with *potassium-bearing* minerals coincides well with the water flow regime developed in the Upper Pannonian sediments. In this zone *smectite proportions* drop to 30-50 % with increasing depth, however, wide compositional ranges are typical throughout the zone.

Acknowledgements

The paper is devoted to the memory of Prof. András Rónai, who contributed probably the most to the understanding of the basic geological structure of the Great Hungarian Plain.

The author is indebted to the members of the research team Basin Analysis of the Hungarian Institute of Geology, Annamária Nádor, Györgyi Juhász, Edit Thamó-Bozsó and Zsolt Kercsmár, for their valuable comments.

The writing of the present paper benefited much from the results of Irén Varsányi (Department of Mineralogy, Geochemistry and Petrology, University of Szeged) who discussed the same geologic formations from a hydrogeochemical point of view.

References

Alcalá-García, F. J., Martín-Martín, M., López-Galindó, A. (2001): Clay mineralogy of the Tertiary sediments in the Internal Subbetic of Málaga Province, S Spain: implications for geodynamic evolution. Clay Min. **36**, 4, 615-620.

Bartha, A., Csalagovits, I., Horváth, I., Siewers, U., Stummeyer, J. (1999): Arsenic speciation of Békés county arsenic waters) (abstract). **42**. Magyar Spektrokémiai Vándorgyűlés (Hungarian Spectrochemical Conference), Veszprém, 1999. Előadások összefoglalói (Abstracts of papers) 16-19. (in Hungarian)

Bartha, A., Csalagovits, I., Horváth, I., Siewers, U., Stummeyer, J. (2000): Simple field method for arsenic speciation of Békés county arsenic waters and their geochemical

characterisation (abstract). 4th Euroconference on Environmental Analytical Chemistry, Visegrád, 2000. Abstracts 66-67.

CSALAGOVITS, I. (1999): Arsenic-bearing artesian waters of Hungary. Annual Rept. of Geol. Inst. of Hungary (MÁFI Évi Jel.) 1992-1993/II. 85-92.

CSÁSZÁR, G. (ed.) (1997): Basic lithostratigraphic units of Hungary. MÁFI (Geol. Inst. of Hungary), Budapest.

EBERL, D. D. (1993): Three zones for illite formation during burial diagenesis and metamorphism. Clays Clay Min., **41**, 1, 26-37.

ERDÉLYI, M. (1979): Hydrodynamics of the Hungarian Basin. Proc. **18**. VITUKI (Research Inst. of Water Management), Budapest.

FRANYÓ, F. (1983): Geological and hydrogeological evaluation of the exploratory bore holes of the Maros alluvial fan (Pusztaottlaka I/P, Kevermes II/P, Tótkomlós III/P). Manuscript, Archives of the Hungarian Geological Survey, Budapest. (in Hungarian)

GHEITH, A. (1981a): On the origin of Dévaványa subsurface sediments, Great Hungarian Plain. MÁFI Évi Jel. (Annual Rept. of Hung. Geol. Inst.) 1979, 169-179. (in Hungarian)

GHEITH, A. (1981b): Sedimentological, mineralogical and geochemical studies on the subsurface sediments of Dévaványa, Csongrád and Kecskemét boreholes, Great Hungarian Plain, Hungary. C. Sc. Thesis, Budapest. 194 p.

GHEITH, A. (1982): Mineralogical and geochemical variations in relation to sedimentation rates in the Hungarian Basin. Acta Geol. Hung., **25**, 3-4, 365-393.

HORVÁTH, Z., MINDSZENTY, A., MICHELI, E., BERÉNYI UVEGES, J. (2001): Large-scale early Quaternary soil erosion and resedimentation along the uplifting northern margins of the Pannonian-basin (abstract). IAS 21st Meeting, Davos, 2001. Abstracts and Programme 153-154.

JÁMBOR, Á. (1998): Review of the stratigraphy of Hungarian Quaternary formations. In: BÉRCZI, I., JÁMBOR, Á. (eds.): Magyarország geológiai képződményeinek rétegtana (Stratigraphy of geological formations of Hungary). 495-517. MOL Co. and MÁFI (Hung. Inst. of Geol.), Budapest. (in Hungarian)

JÁMBOR, Á. (2001): Quaternary. In: HAAS, J. (ed.): Geology of Hungary 265-278. Eötvös University Press, Budapest.

JEANS, C. V., MITCHELL, J. G., FISHER, M. J., WRAY, D. S., HALL, I. R. (2001): Age, origin and climatic signal of English Mesozoic clays based on K/Ar signatures. Clay Min., **36**, 4, 515-539.

JUHÁSZ, Gy. (1992): Pannonian (s. l.) lithostratigraphic units in the Great Hungarian Plain: distribution, facies and sedimentary environment. Földt. Közl. (Bull. Hung. Geol. Soc.), **122**, 2-4, 133- 165. (in Hungarian)

KOLOSZÁR, L., LANTOS, M., CHIKÁN, G. (2001): Correlation of the Quaternary sediments in the Görgeteg G-I and the Udvari U-2A borcholes. Földt. Közl. (Bull. Hung. Geol. Soc.), **131**, 3-4, 443-460. (in Hungarian)

KONTA, J. (1993): 14 Å-sheet silicates in clay fraction of Recent river sediments in Czechoslovakia. In: KONTA, J. (ed.): 11th Conference on Clay Mineralogy and Petrology, České Budějovice, 1990, 237-250. Geologica. Univerzita Karlova, Praha.

KRALIK, M., AUGUSTIN-GYURITS, K. (1994): Stauraumsedimente als "Geochronometer" von Schad- oder Rohstoffen: Moderne Sedimentologie, Mineralogie, Geochemie und Verwertung der Donausedimente von Aschach (Oberösterreich). In: LOBITZER, H., CSÁSZÁR, G., DAURER, A. (eds.): Jubiläumsschrift 20 Jahre Geologische Zusammenarbeit Österreich-Ungarn 2, 437-464.

MIHÁLTZ-FARAGÓ, M. (1982): Palynological examination of key boreholes to the East of the Tisza River. MÁFI Évi Jel. (Annual Rept. of Hung. Geol. Inst.) 1980, 103-120. (in Hungarian)

MOLNÁR, B. (1965): Changes in area and directions of stream erosion in the eastern part of the Hungarian basin (Great Plain) during the Pliocene and Pleistocene. Acta Min. Petr. Szeged, **17**, 39-52.

NÁDOR, A., MÜLLER, P., LANTOS, M., THAMÓ-BOZSÓ, E., KERCSMÁR, ZS., TÓTH-MAKK, Á., SÜMEGI, P., FARKAS-BULLA, J., NAGY, E. (2000): Climate controlled sedimentary cycles in the Quaternary fluvial sequence of the Körös basin). Földt. Közl. (Bull. Hung. Geol. Soc.), **130**, 4, 623-645. (in Hungarian)

RISCHÁK, G. (1984): Some geochemical factors of the formation of variegated clays). MÁFI Évi Jel. (Annual Rept. of Hung. Geol. Inst.) 1982, 469-477. (in Hungarian)

RÓNAI, A. (1972): Quartärsedimentation und Klimageschichte im Becken der Ungarischen Tiefebene (Alföld). MÁFI Évk. (Annals of Hung. Geol. Inst.), **56**, 1, 1-421. (in Hungarian and German)

RÓNAI, A. (1985): The Quaternary of the Great Hungarian Plain. Geol. Hung., Ser. Geol., **21**, 446 p. (in Hungarian and abbreviated English version)

RÓNAI, A. (1986): Quaternary formations of Hungary: geological features and structural setting. Földt. Közl. (Bull. Hung. Geol. Soc.), **116**, 1, 31-43. (in Hungarian)

SZÉKELY, Á. (1965): (unpublished DTA curves). See: bore hole Jászladány-1. Archives of the Hungarian Geological Survey, Budapest.

TANÁCS, J., VICZIÁN, I. (1995): Mixed-layer illite/smectites and clay sedimentation in the Neogene of the Pannonian Basin, Hungary. Geol. Carpath., Ser. Clays, **4**, 1, 3-22.

THAMÓ-BOZSÓ, E. (1997): Geological evaluation of mineralogical composition of Hungarian Cenozoic sand and sandstone formations. C. Sc. Thesis, Budapest. 80 p. (in Hungarian)

THAMÓ-BOZSÓ, E., KERCSMÁR, Zs. (2000): Changes of transport directions into the Körös basin during the Quaternary). Földt. Közl. (Bull. Hung. Geol. Soc.), **130**, 4, 647-671. (in Hungarian)

VARSÁNYI, I. (1989a): Tracing groundwater flow using chemical data in artesian waters of the southern Great Hungarian Plain). Hidrológiai Közlöny, **69**, 5, 257-263. (in Hungarian)

VARSÁNYI, I. (1989b): Tracing groundwater flow using chemical data. Hydrological Sciences Journal, **34**, 3, 6, 265-275.

VARSÁNYI, I. (1991): Geochemical modelling of chemical alterations during the movement of artesian waters. Hidrológiai Közlöny, **71**, 5, 300-304. (in Hungarian)

VARSÁNYI, I. (2000): Separation of groundwater flow systems in the southern part of the Great Hungarian Plain – based on chemical and isotopic data. Hidrológiai Közlöny, **80**, 3, 145-156. (in Hungarian)

VARSÁNYI, I. (2001): Groundwater of the southern Great Hungarian Plain: hydrogeochemical processes and hydrogeological conclusions. D. Sc. Thesis, Szeged. 126 p. (in Hungarian)

VARSÁNYI, I., MATRAY, J.-M., Ó. KOVÁCS, L. (1997): Geochemistry of formation waters in the Pannonian Basin (southern Hungary). Chem. Geol., **140**, 89-106.

VARSÁNYI, I., Ó.KOVÁCS, L. (1994): Combination of statistical methods with modelling mineral-water interaction: a study of groundwater in the Great Hungarian Plain. Appl. Geochem., **9**, 419-430.

VARSÁNYI, I., Ó.KOVÁCS, L. (1997): Chemical evolution of groundwater in the River Danube deposits in the southern part of the Pannonian Basin (Hungary). Appl. Geochem., **12**, 625-636.

VARSÁNYI, I., Ó.KOVÁCS, L. (2001): The source of sodium in groundwater, Pannonian Basin, Hungary. Proc. Intern. Symp. on Water-Rock Interaction, Villasimius (in prep.)

VICZIÁN, I. (1982): An expanding mixed-layer clay mineral in Upper Pannonian to Pleistocene fine-grained clastic rocks of the borehole Pusztaottlaka I/P, SE Hungary. MÁFI Évi Jel. (Annual Rept. of Hung. Geol. Inst.) 1980, 449-456. (in Hungarian)

VICZIÁN, I. (1984): Clay mineralogy of pelitic sediments of the South German Molasse Basin. *in* KONTA, J. (ed.): 9th Conference on Clay Mineralogy and Petrology in Zvolen, 1982, 101-105. Univerzita Karlova, Praha.

VICZIÁN, I. (1986): X-ray analysis of the samples of the bore hole Tiszapalkonya-I. Manuscript, Archives of the Hungarian Geological Survey, Budapest. (in Hungarian)

VICZIÁN, I. (1987): Clay minerals in sedimentary rocks of Hungary. D. Sc. Thesis, Budapest. 205+139 p. (in Hungarian)

VICZIÁN, I. (1992): Clay minerals of a thick sedimentary sequence in SE part of the Pannonian Basin (Hungary). Geol. Carpath., Ser. Clays, **1**, 27-30.

VICZIÁN, I. (1994): Smectite - illite geothermometry. Földt. Közl. (Bull. Hung. Geol. Soc.), **124**, 3, 367-379. (in Hungarian)

VICZIÁN, I. (2002): Clay mineralogy of Quaternary sediments covering mountainous and hilly areas of Hungary. Acta Geol. Hung., **45**, (in prep.)

Received: November5, 2002; accepted: December13, 2002

Acta Mineralogica-Petrographica, Szeged 2002, Vol. 43, pp. 55-58

ACTA
Mineralogica
Petrographica

ELECTROSTATIC MODELLING OF THE LUNAR SOIL – HOW ELECTROSTATIC PROCESSES IN THE LUNAR DUST MAY GENERATE THE ION-CLOUD LEVITATING ABOVE THE SURFACE ON THE MOON – EXPERIMENTS IN A MODEL INSTRUMENT

TIVADAR. FÖLDI[1], SZANISZLÓ BÉRCZI[2]

[1] FOELDIX, H-1117 Budapest, Irinyi J. u. 36/B. Hungary,
[2] Department of General Physics, Cosmic Materials Space Research Group, Eötvös University
H-1117 Budapest, Pázmány Péter sétány 1/C, Hungary
e-mail: bercziszani@ludens.elte.hu

ABSTRACT

According to the measurements of Surveyor landers and Apollo 17 LEAM experiments a levitating lunar dust cloud appears above the lunar surface. We studied the united acts by UV radiation and solar wind from the Sun and the micrometeorite bombardment processes which we suggest generate through electrostatic processes an ion-cloud above any dusty (i.e. lunar) planetary surface. This levitating ion-cloud form a quasiatmosphere where charged dust particles can take part in different processes. We studied such electrostatic mechanisms of lunar (and planetary) dust in an instrumental experimental arrangement of FOELDIX-1. In these studies we concluded that dust particles can agglutinate by the alternating process of receiving and loosing charge. We found that during a longer interval in this process the electrostatically charged dust particles may produce larger and larger grains. The agglutinating grains also attract and include H_2O molecules. As a consequence of these recognitions we suggest that considering longer time intervals there is a trend on any dusty planetary surface for composite agglutinated particles to be dragged by the solar radiation pressure toward the poles. In the vicinity of poles larger agglutinated particles are discharged, fall down and accumulate on the surface. The summary of the application of our model is the suggestion of accumulation of H_2O molecules in the fine dust of the polar regions of planetary surfaces, especially on the Moon.

INTRODUCTION

Storm Electricity

In the late 1930s there were an instrument and experiments inside the clouds (In Germany). The instrument was carried up to the atmosphere by balloons. In the measurements a recording cylinder writing equipment showed that the direction of the electric field was alternately changing polarity, when the uplifting balloon crossed the cloud. This measurement sketched a picture that the shower cloud consists of layers with alternating electric field charge. (Later this experiment was carried out in a finer equipment in the United States.)

In the early 1940s Simson measured and modelled the water droplet processes (disruption, charging, coagualtion) in storm electricity ionization processes in terrestrial clouds. A water droplet collects small charges in the column where it crosses during its falling. The additive summation of the charges results in gradually greater and greater charge on the surface of the droplets. Finally sparks discharge droplets with oppositely charges. But the ion-channel between these oppositely charged droplets remains open for a short time. Finally lightning uses these earlier channels to form a larger and longer ionization channel pathway toward the ground.

Finally, in their measurements Americans found that there is a 50 V/m field strength in the atmosphere. They also made hurricane modelling, but no engineering consequences were utilized. In these experiments and in electrostatic modelling they did not mixed the gas, the dust and the vapor effects together with aerosol pollution. (It is important to mention that vapour-water droplet-ice system was investigated because of the dangerous precipitations, too).

Early atmospheric electricity experiments in Hungary

Historical retrospective: Before the First World War (1908-1909) there were atmospheric electricity experiments on the Adratic Sea, made on the St. Stephen flagship of the Austro-Hungarian Monarchy Navy. The experimental arrangement consisted of an antenna and a capacitive voltage electrometer. The antenna was electrically separated from the board by a ceramic insulator, as reported by a navy newspaper.

In 1958-1961 Simonyi (Budapest Technology University, Department of Theoretical Electricity) initiated 4 types of complex experiments on atmospheric electricity in order to find relations between atmospheric electricity and human physiological processes. The experiments, carried out by Földi, were the following: 1) electric field measurements by a field-mill type experiment (Földi et al, 2001), 2) ion-density measurements by capacitive way, 3) insulated capacitive antenna (+ electrometer) measurements by using a radioactive isotope on the top of the antenna, 4) insulated capacitive antenna (with DC amplifier) measurements by using an electrometer-tube with great resistance. When the instruments were built the measurements and registration of the data were carried out for a half year continuously on the Budapest Technology University, in the tower of the Building of Agriculture. The relations between atmospheric electricity and human physiological processes were not found at that time, but the system of measurements were reproduced and developed.

Molecular water on surface in vacuum: the role of the mixed system

In the electron tubes production of Tungsram Factory, in 1935, Bródy and Palócz discovered that on the inner surface of the electron tube, even in the case of hypervacuum, a monomolecular water molecule layer can be found. This molecular water layer considerably destroyed the efficiency of electron tubes and diminished the lifetime of the cathode and affected the electron emission of the cathode. In 1957, Isreal in the Potsdam Atmospheric Research Institute found that the water molecules, which belong to the small negative ions, have far longer lifetime (even with order of magnitudes longer) then that of the small positive ions. If in the near vicinity of a surface there exists a space charge of electron cloud, then the water molecules, (occurring in this cloud) will act as if they were negitvely charged. These water molecules preserve their charge even if the negative space charge ceases. (The average velocity of electrons is far larger then the coexisting water molecules).

Electrostatic Processes in the Lunar Dust and Formation of Levitating Ion-Cloud above the Lunar Surface

Micrometeorite bombardment is a continuous source of dust production on the Moon. The distribution of dust particles from impact may cover the size range from 200 micrometers to the molecular region. The ultraviolet radiation of the Sun, (depending on the escape energy for electrons) causes strong electron emission from the lunar surface. Most of the emitted electrons escape the lunar surface therefore the lunar surface becomes charged up positively (which retards the electron escape and which may produce a negative field charge similarly to that of virtual cathode in the electron tube).

Above the negative space charge field of the electron cloud a layer of positively charged dust cloud forms in the lunar vacuum. That dust cloud consists of ions (ion-cloud) coagulated from smaller dust particles, which have great mass and low velocity. During solar radiation (on the lunar day) these larger particles are alternately charged up and discharged. In the intervals when they are positively charged, they levitate in the near vicinity of the surface (between a few decimeters and 1 meter from the lunar surface). This cloud has been measured by the Surveyor landers and by the Apollo 17 LEAM experiments (Criswell, 1972; Berg et al., 1973; Horányi et al.; 1998) (Fig. 1).

With negatively charged water molecule-ions these coagulated particles can gradually grow larger and they oscillate in the near vicinity of the surface. We modelled this process in the FOELDIX-1. instrument. In the following cartoon we show the main characteristics of the lunar quasiatmosphere, where we can find all the various types of particles referred in the coagulation experiments of the next section (Fig. 2).

Experimental Coagulation of Dust Particles

We studied the production of cosmic dust in an electrostatic experiment (Földi et al, 1999). In this work we studied the possibility of the experimental production of extrafine dust fraction. We used a chamber with 2000 X 1000 X 250 millimeters volume. There were atmospheric pressure and laboratory temperatures. Two systems of electrodes were arranged in this space. One operated on + 15 kV and the other on - 15 kV potential. The electrodes were 800 mms long, their diameter was 10 mms. In a distance of 45 mm from each electrodes a 0.1 mm diameter special nickel wire was placed. The large electrodes with opposite potential were arranged in a comb like pattern (Földi et al, 1999).

We used a power supply which can be varied between 8 kV to 15 kV potential. If the system is opened to the free air, the air molecules begin to move through the instrument, by getting constant velocity of 1 meter/secundum along the alternating electrodes.

In the experiments the instrument was in a columnal arrangement, open up and down: on the bottom of the tube liquid stirol was placed. The wapor of stirol - together with the air - streamed into the space of the instrument. The stirol molecules polimerized to resin particles, as a result of their going through the alternating potential of electrodes. The coagulated particles have a spherulitic form. Getting through 20 electrodes, the final mass of the coagulated particles was 540.000. times that of the initial molecular mass.

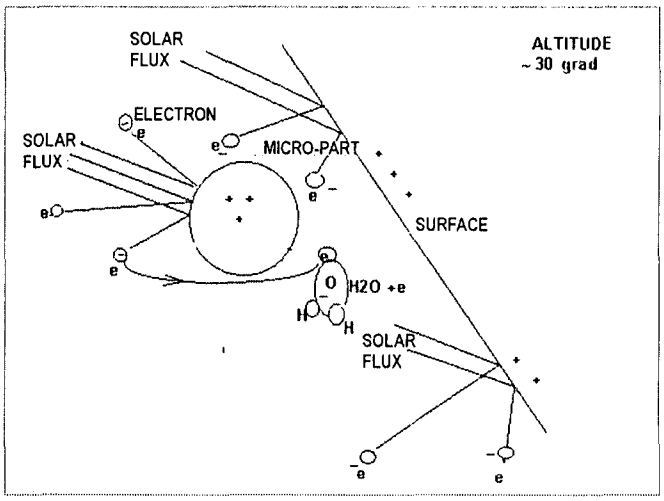

Fig. 1. The uprising of a microparticle from the lunar surface by the effect of the solar UV irradiation

Dust Coagulation with Included Water Molecules

Now we use the recognition found in electron-tube industry that water molecules may retain one negative electric charge (Tungsram Factory, Budapest, 1935; Bródy and Palócz, 1953). On the inner surface of the electron tube, in hypervacuum, a monomolecular water molecule layer was found. This molecular water layer was negatively charged while the glass surface wall was positively charged. As later found (Israel, 1957) the negatively charged water molecules have very a long lifetime and they do not recombine. This lifetime is an order of magnitudes longer, then that of the small positive ions. Such charged water molecules can survive even the cosmic travel time from the Earth's upper atmosphere to the surface of the Moon.

The Source of Lunar Water Molecules

During full Moon the tail of the Earth (magnetic and radiation belts of the Earth) sweep over the Moon. Terrestrial magnetosphere tubes retain the escape of charged particles

from this tube, because for the ionized particles the "wall" of terrestrial magnetosphere tail behaves as a reflecting wall. Together with ionized particles the water molecules, which have one negative electric charge (adhered to the water molecule) are also reflected on this tube wall. The reflecting force from the wall is: v X B (where v is velocity, B is magnetic induction) the electrostatic accelerating force is e X E (where e is the electron charge unit, E is electric field strength in V/m) the acceleration by E is F_E Electric Force per molecular mass.

Reaching the lunar surface the negatively charged water particle meets the positively charged (from UV radiation) dust particles. With charged dust particles water molecule forms a complex coagulated particle. At the same time, in the near vicinity of the lunar surface there exists a space charge of electron cloud, which recharge and so neutralize the coagulated particle. But this coagulated particle will not remain neutral for a long time, and it becomes charged again by the space charge of electron cloud. This periodic charging up and discharge 1) enlarges the coagulated particle, and 2) levitates the particle, which will be the object of a transporting mechanism moving it toward the lunar pole. The step-by-step drag by the solar radiation pressure toward the poles, where agglutinated particles become discharged, results in their fall-down, and accumulation on the surface.

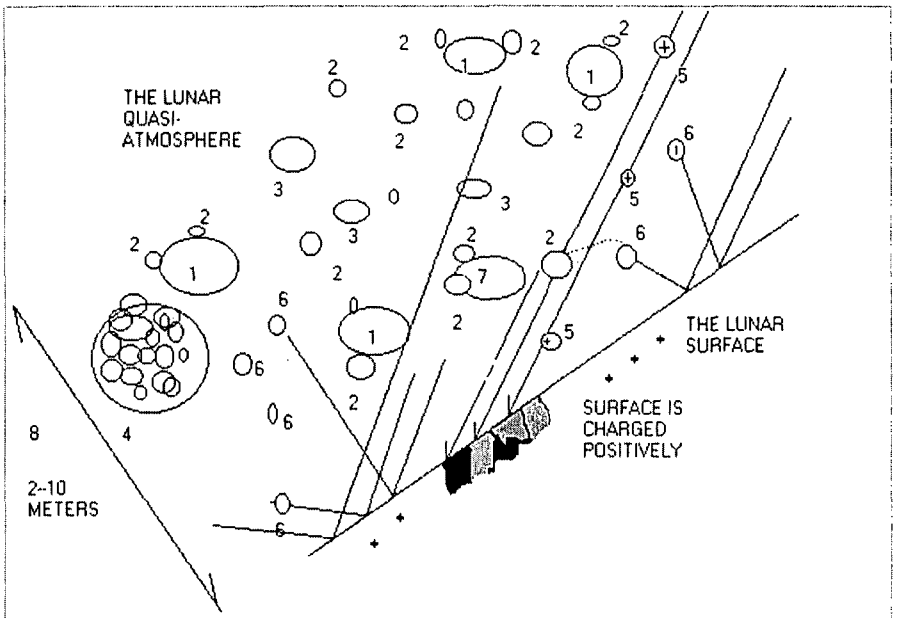

1 - OXYGEN, 2 - HYDROGEN, 3 - DUST PARTICLE, 4 - COAGULATED PARTICLE (THIS PARTICLE INCLUDES WATER MOLECULES), 5 - SOLAR WIND PROTON, 6 - ELECTRON EMITTED BY SOLAR UV RADIATION, 7 - WATER MOLECULE, 8 - THE HEIGHT OF THE LUNAR QUASIATMOSPHERE, WHERE COLLISIONS ARE FREQUENTLY OCCURRING, THERMAL PARAMETERS (ESTIMATED VALUES): 1: 600 K, 2: 5000 K, 3: 400 K, 4: 300 K, 5: 6000 K, 6: 12000 K.

Fig. 2. The lunar quasiatmosphere has many constituents which alternate between charged up and electrically neutral states

DRAG OF COAGULATED DUST PARTICLES TOWARD THE POLES

Let us follow the way of a coagulated particle. Start the observation at the 45 degrees latitude. Three main forces act on this particle: gravity, solar wind pressure and electrostatic force. The gravity force, determined by particle mass and G specific gravity, remains constant (a good approximation). The solar wind pressure force is determined by the effective cross section (surface given by the diameter of coagulated particle): solar wind force is also constant in absolute value, but its components projected to the gravitational force, changes according to the cosine function with latitude. The electrostatic force is determined by the field strength coming from the surface charge of the planetary body multiplied by the charge of the coagulated particle. This force is oscillating depending on the absorption of negative or positive ions. As a result of the combined action of the three forces the coagulated particle periodically sinks or rises to the surface. But because the components of the solar wind force gradually changes with latitude, *the tangential component of the solar wind pressure force* (changing with sinus function of the latitude) *will drift the particle toward the poles between two* (rising and sinking) *oscillations.* When the particle approaches the polar region the local vertical component of this force becomes zero (cos 90° =0) while the tangential component becomes almost one (sin 90°=1). Therefore, if the coagulated particle reached the pole, it will remain in the vicinity of the pole (there is no force to move it out from this region).

CONSEQUENCES OF THE MODEL

On the surface of the dusty planetary body the size distribution of the dust particles in the vicinity of the equator will not exhibit a gaussian because the fine fraction of the dust slowly moves toward the poles.

In the vicinity of a new great impact crater the dust produced by sublimation from the plasma originally have a gaussian size distribution. After some time elapsed the size distribution will loose the fine fraction because of the drift toward the poles. We suggest that the age of the crater can be estimated on the extent of lacking fine fraction drifted.

The coagulated particles - together with the accompanying water component, - will accumulate in the vicinity of those craters (in the planetary polar regions) which are always in shadow.

CONCLUSIONS

On the basis of Surveyor and Apollo observations and theoretical considerations we defined a mechanism how lunar (and dusty planetary) quasiatmospheres may form. This quasiatmosphere mainly consists of charged dust particles. On the basis of our experimental experiences on coagulation in an electrostatic tube, we proposed a mechanism acting in the lunar quasiatmosphere. There the coagulation of electrostatically charged dust particles may produce larger and larger grains. These grains attract H_2O molecules on dusty planetary surfaces and continue in growing during time. The coagulated particles will be dragged by the solar radiation pressure toward the poles where they are discharged, fall down and accumulate on the surface. This electrostatic mechanism accumulates H_2O molecules on polar regions of dusty planetary surfaces in craters which are always in shadow.

REFERENCES

ALLEN, C., MORRIS, K., LYNDSTROM, M. ET AL. (1998): Martian Regolith Simulant JSC MARS-1. Lunar and Planetary Science XXIX. Houston, LPI, #1690

VON ARDENNE, M. (1958): Tabellen für Angewanten Physik, Leipzig, pp. 460.

BÉRCZI, SZ., FÖLDI ,T., KUBOVICS, I., SIMONITS, A., SZABÓ, A. (1998): In: Lunar and Planetary Science XXIX, Abstract #1082. Houston (CD-ROM).

BERG, O. E., RICHARDSON, F. F., BURTON, H. (1973): Lunar Ejecta and Meteorites Experiment. (In: Apollo 17 Preliminary Science Report, Lyndon B. Johnson Space Center) NASA SP-330, Washington D. C. 16-1.

BRÓDY, I., PALÓCZ, K. (1953): Lecture on Techn. Univ. Budapest (personal communication).

CRISWELL, D. R. (1972): Horizon glow and motion of Lunar dust. Lunar Science III. p. 163. LPI, Houston.

FÖLDI, T., EZER, R. BÉRCZI, SZ., TÓTH, SZ. (1999): Creating Quasi-Spherules from Molecular Material Using Electric Fields (Inverse EGD Effect). In: Lunar and Planetary Science XXXII, Abstract #1266. LPI, Houston (CD-ROM).

FÖLDI, T., BÉRCZI, SZ., PALÁSTI, E. (2001): Water and bacteria transport via electrostatic coagulation and their accumulation at the poles on the dusty planet. In: Lunar and Planetary Science XXXII, Abstract #1059, Lunar and Planetary Institute, Houston (CD-ROM).

FÖLDI, T., BÉRCZI, SZ., (2001): The source of water molecules in the vicinity of the Moon. In: Lunar and Planetary Science XXXII, Abstract #1148, Lunar and Planetary Institute, Houston (CD-ROM).

FÖLDI, T., BÉRCZI, SZ. (2001): Indicating the deep structure (below the icy and liquid layers) of Europa and Titan by measurements with a giant solenoid system on board of an orbiting space probe. In: Forum on Innovative Approaches to Outer Planetary Exploration 2001–2020, p. 28. LPI Contribution No. 1084. Lunar and Planetary Institute, Houston.

FÖLDI T., BÉRCZI, SZ. (2001): Quasiatmospheric Electrostatic Processes on Dusty Planetary Surfaces: Electrostatic Dust and Water molecule Coagulation and Transport to the Poles. 26th NIPR Symposium Antarctic Meteorites, Tokyo, p. 21-23.

FÖLDI, T., BÉRCZI, SZ. (2001): Measurements on the ion-cloud levitating above the Lunar surface: Experiments and modelling on Hunveyor experimental lander. 64. Met. Soc. Ann. Meeting, Abst #5126, (Rome, Vatican City, 10-15. Sept, 2001).

HORÁNYI, M., WALCH, B., ROBERTSON, S. (1998): Electrostatic charging of lunar dust. LPSC XXIX. LPI, CD-ROM, #1527.

ISRAEL, H. (1957): Atmospherische Elektricitet. Leipzig, pp. 350.

MCKAY, G., CARTER, BOLES, ALLEN, C. (1995): JSC-1. A New Lunar Regolith Simulant. LPSC XXIV, 963.

REID, G. C. (1997): On the influence of electrostatic charging on coagulation of dust and ice particles in the upper mesosphere. Geophysical Res. Letters, **24,** No. 9. 1095.

SICKAFOOSE, A. A., COLWELL, J. E., HORÁNYI, M. ROBERTSON, S. (2001): Dust particle charging near surfaces in space. In Lunar and Planetary Science XXXII, Abstract #1320, Lunar and Planetary Institute, Houston (CD-ROM).

VANZANI, V., MARZARI, F., DOTTO, E., (1997): In Lunar and Planetary Science XXVIII, Abstract #1025, Lunar and Planetary Institute, Houston (CD-ROM).

Received: November 11, 2002; accepted: December 28, 2002

Acta Mineralogica-Petrographica, Szeged 2002, Vol. 43, pp. 59-63

ACTA
Mineralogica
Petrographica

RADIOACTIVE CHARACTERISTICS OF THE LIASSIC COAL OF PÉCSBÁNYA AND EFFECTS OF ITS MINING ON THE ENVIRONMENT (MECSEK MTS. – SOUTH HUNGARY)

BALÁZS KÓBOR[1], JÁNOS GEIGER[2], WALTER GÖSSLER[3], ELEMÉR PÁL-MOLNÁR[1]

[1] Department of Mineralogy, Geochemistry and Petrology, University of Szeged
H-6701 Szeged, P. O. Box 651, Hungary
[2] Department of Geology and Paleontology, University of Szeged
[3] Department of Analythical Chemistry, University of Graz
e-mail: koborb@hotmail.com

ABSTRACT

It is a widely known fact that the Liassic coal mined for more than 200 years in the environs of Pécs-Komló (Mecsek-Mts., South-Hungary) represents a higher radioactivity than that of the formation average. Hence, in order to carry out a successful recultivation it is necessary to determine precisely the radioactive state of the involved areas and measure the amount of excessive radioactivity affecting citizens. This is important especially because measurements of this kind haven't been made in the area before. By performing in situ and laboratory measurements on waste heaps, accumulated over several hundred years, and areas under different stage of mine works the values of total gamma-ray activity, the specific activity of rocks building up the area and the concentration of the three most significant natural radionuclides (U, Th, K) were determined.

Based on in situ measurements, both the winter and the summer-time (representing totally different meteorological conditions) gamma-ray dose rate distribution map of the Karolina opencast mine, and its vicinity was drawn. The background value of total gamma-ray dose rate, based on values measured in the farther environs of the mine was 85-90 nGy/h in the dry hot summer period and 75-80 nGy/h during the humid and cold wintertime. On areas still under active mine works the same measurements gave 220% higher results in average, and in terms of uncovered waste heaps these values were just slightly lower (150-160 nGy/h). On the other hand, in case of covered waste heaps the applied 40-60 cm thick soil cover almost completely absorbs excess activity, thus values received on covered heaps were only 10 % higher than the environmental background.

Gamma-ray spectroscopic measurements have shown that not only U bound to organic material is responsible for increased radioactivity, but K and Th as well. The concentration of these later elements proved to be the highest in rocks abundant in argillic minerals. Hence, the activity is the highest especially in those rock types which are characterised not only by a high organic material content but argillic mineral content too.

Key words: Liassic coal, gamma ray activity, gamma-ray spectrometry, Mecsek-Mts.

INTRODUCTION

Rocks of high organic material content (oil-shales, coals) are usually rich in radioactive elements as well. U and Th contents often exceed by several times or even by an order of magnitude the characteristic world average referred to coals. The world average is claimed to be 1-5 ppm and 1-7 ppm for U and Th, respectively (Valkovic, 1983; Hoffman, 1988; Swaine, 1990, 1997; Eisenbud and Gesell, 1997).

The radioactive element content of Hungarian coals was first examined by Szalay and Földvári parallel to fissile material explorations in the country (Szalay, 1948; Földvari, 1951; Szalay and Földvari, 1951). According to them, the following Hungarian coals proved to represent higher radioactivity than the usual value: the Cretaceous coal of Ajka; the deposits of Kisgyón, certain deposits in the Tatabánya coal basin and the Liassic coal of the Mecsek Mts. (Szalay, 1952, Szalay and Almássy, 1956; Bodrogi et al., 1959; Upor et al., 1960). In his summarising work Szalay states that only those deposits are enriched in radioactive elements – primarily uranium – that are located relatively close to the denudation zones of still traceable granitoid bodies. Based on laboratory research, he explained the increased radioactivity – significantly higher than the formation average – with the uranium accumulating character of organic material (primarily humic acids) (Szalay, 1952).

As a continuation of the above studies, the aim of the present research is to measure the total gamma-ray activity appearing in the Karolina opencast coal mine and in its surroundings, and besides, to aid an environmentally successful recultivation by determining the amount of excess exposure dose affecting not just the environment but local people as well.

Preliminary laboratory gamma-ray spectroscopic analyses had shown that the sometimes astonishingly high values of total gamma-ray activity (250-300 nGy/h) should not be caused by the average 1-6 ppm uranium concentration alone. Thus, in situ total gamma-ray activity measurements were extended to three elements: U, Th and K^{40}. Field results were always supplemented by laboratory gamma spectroscopy, and the concentration of radioactive elements was controlled by the ICP-MS method.

STUDIED AREA

Detailed in situ total gamma-ray activity analyses were performed in the Mecsek Mountains (South Hungary),

7 km ENE of the region's centre, Pécs, on samples collected in the Karolina opencast coal mine, located west of village Pécsbánya. Further samples were taken from recultivated and unrecultivated waste heaps north and south of the mine, the neighbouring settlement, and areas not involved in mining activity. The mineworking conditions of the Karolina opencast mine are presented on Fig. 1.

The mine explores a Lower Liassic sedimentary complex, which contains 18-22 exploitable coal deposits, 50-120 cm thick each. The waste material of the coal deposits is composed of aleurolites of low organic material content and arkosaic sandstone.

Methods

Factors determining the radiological conditions of an area (total gamma-ray activity, radon concentration and exhalation, falling dust or aerosol activity) are highly dependant on meteorological parameters. During the cold and windy wintertime the dust and aerosol content of the air is significantly lower, and during long lasting humid periods the radon exhalation of soils and the base rock is also lower. Meanwhile, the dry and warm summertime is adequate for high dust and aerosol content, and dry weather results increased radon exhalation, too. Hence, when examining the quality and quantity of total gamma-ray activity it is necessary to repeat the measurements in different seasons.

During total gamma dose rate analyses regardless of its actual components the intensity of gamma-ray was determined, as it is the most penetrating radiation and thus occurs everywhere. In situ total gamma-ray activity measurements were carried out both during summer- and wintertime at 375 locations in the Karolina opencast area and its environs maintaining a 50 x 50 m sampling grid. The measurements were made with a portable NC-483 nuclear analyser equipped with a NaI(Th) scintillation detector (MEV, ND-482), which enabled the required energy-independent determination. Measurements were made following the recommendations of the International Atomic Energy Agency, 1 m above ground level with a 10 s sampling time. The method provides a precise result even in terms of close to background values, still, the measurements were repeated three times in each sampling points and the final result was the average of these. Nevertheless, on the area of the actual mine the very intensive relief inhibited the use of a grid when sampling, thus average values detected above boundaries of different rock types were applied in order to characterise the area of the mine works.

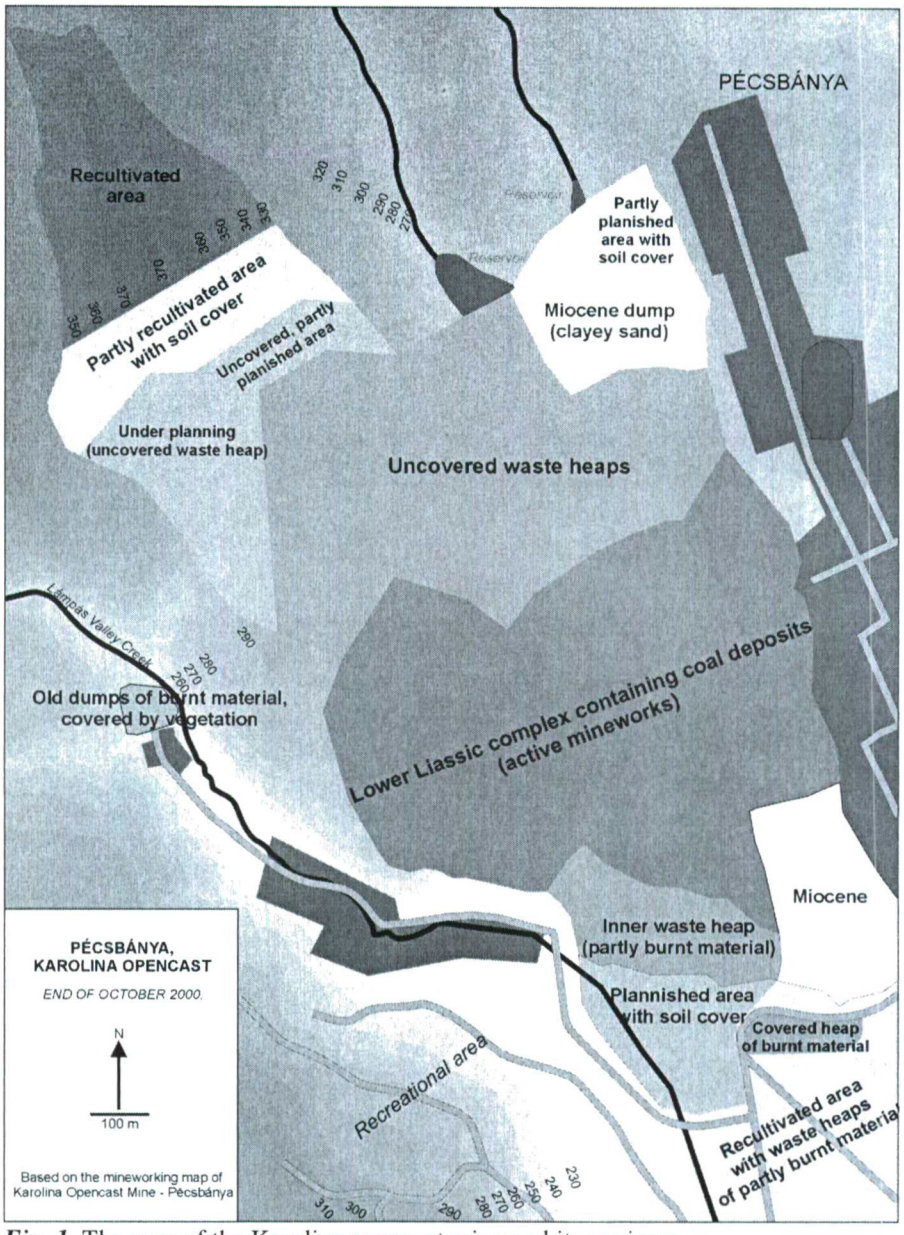

Fig. 1. The map of the Karolina opencast mine and its environs

In situ gamma-ray spectroscopic analyses aimed at the measurement of the main radioactive elements – Th, U(Ra), K – occurring in the soil and the base rock. Actually, in case of uranium the radium content of the samples was determined, and the uranium content was calculated assuming a radioactive equilibrium. It is possible during gamma-ray spectrometric measurements to determine the concentration of radioelements and radiaoactive families, too, by selectively detecting the photons of different energy level that make up the total gamma-ray radiation. Measurements were carried out with a ND-482 scintillation detector attached to a MEV NC-483 analyser following IAEA recommendations, i.e. with a probe placed on the ground and due to low concentrations with a long measuring time (10 min). For increasing the preciseness of the results two measurements were made in each point.

The collected samples' laboratory analyses was carried out with a four banded nuclear analyser (NP484-P), while the control samples were processed following the ICP-MS (HP 7500) method after partial nitric acid extraction (using microwave, 40 minutes, 250 °C)

Discussion and conclusions

In situ total gamma-ray activity and gamma-spectroscopy

The measurement of total gamma-ray dose rate and gamma-ray spectroscopy performed on samples originating from the Karolina opencast mine, surrounding waste heaps and village Pécsbánya enabled the detection of excess radioactive exposure and the determination of the environmental background or zero radioactivity both of which is crucial for launching successful recultivation works in the area. Applying the data of summer and winter measurements two maps were drawn representing the distribution of total gamma-ray dose rate in the two different meteorological periods (Fig. 2, 3).

The average values of environmental background were determined on the basis of 30 measuring points, that were located farther of the mine and represented areas that have never been involved in mining activity and have a different rock base but always with a soil cover. Thus values during the dry, hot summer period were 85-90 nGy/h, while at wintertime, when the weather is cold and humid the measurements gave 75-80 nGy/h. Concerning the settlement of Pécsbánya, due to traffic, coal transportation and heating the average value of total gamma-ray dose rate was 95-103 Gy/h. Values measured on the territory of the mine works and on uncovered waste heaps

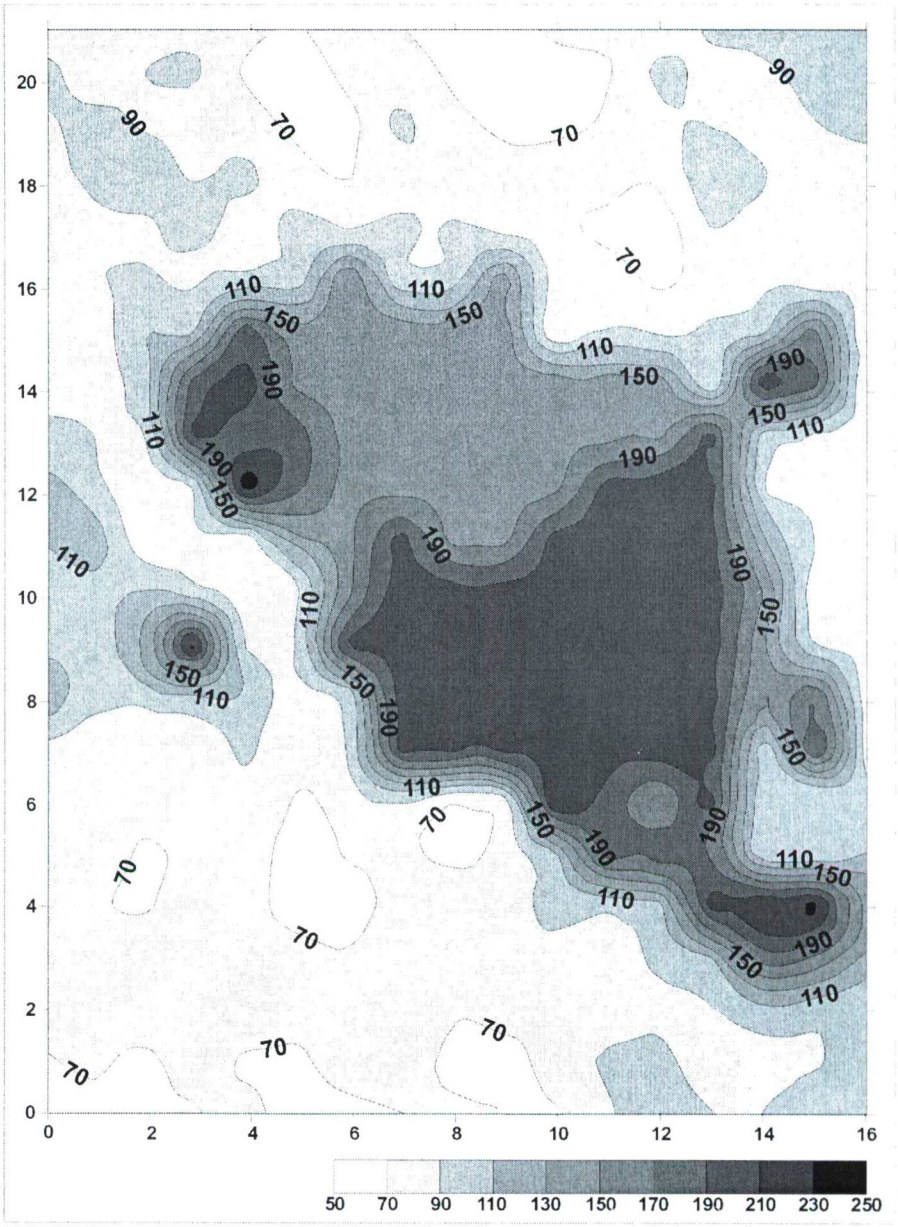

Fig. 2. The summertime distribution of total gamma-ray activity in the area of the Karolina opencast mine

are 220% higher in average than the zero dose rate measured in the undisturbed environs of the mine (Table 1). However, it is notable that high total gamma activity concluded in terms of the opencast mine is partly resulted by the fact that more samples were taken from above productive coal layers, thus measuring points of higher radioactivity are slightly over-represented in the measurement series. The mean total gamma-ray activity of

Table 1. Values of total gamma ray activity in the summer- and winter period at locations of different mining activity

Types of mining activity	Total gamma-ray activity (nGy/h)							
	Summer period:				Winter period:			
	mean	max.	min.	sampled	mean	max.	min.	sampled
Opencast	219	320	121	57	207	334	120	38
Uncovered, „active" waste heaps	169	247	85	31	154	223	81	31
Uncovered, planished waste heaps	176	154	205	6	177	205	141	6
Covered, planished waste heaps	90	112	67	13	85	110	65	13
Recultivated waste heaps	97	181	76	31	89	131	71	31
Partly covered waste heaps of burnt	212	247	161	12	171	201	101	12
Settlement (Pécsbánya)	103	231	56	33	95	185	61	33
The vicinity of the opencast mine (max.	82	141	52	194	76	131	50	194

the opencast therefore is closer to that of the uncovered waste heaps but it is still higher due to vast coal deposits of high radionuclide concentrations and aerial dust deposition. Data on gamma-ray dose rates determined on the territory of the open cast, and the calculable concentrations of elements are presented in Table 2.

In case of uncovered and/or planished waste heaps the value of total gamma-ray activity is twice as high as the environmental background, i.e. 154-177 nGy/h. Nevertheless, on permanently recultivated waste heaps the 40-60 cm soil cover almost completely absorbs the excess radiation, and values measured here are higher than the environmental zero only by 10% (Table 1).

The precise determination of excess exposure affecting nearby living people would require the measurement of falling dust and aerosol activity, too. Total gamma-ray activity measurements however suggest that the rate of excess exposure on the dwellers of Pécsbánya is approximately 15-25%. Based on international data, the ratio of the time spent inside the dwelling and outside is 20/80 %. Thus, counting with an annual 1800-2200 hours of exposure, the dose equivalent of the excess load on citizens of Pécsbánya, resulted by the additional gamma activity due to coal mining, is 20-30 μSv/year. However, the calculated dosimetric quantities even in case of unreal length of exposure are well below medical thresholds, still they draw the attention to old waste heaps of burnt material and the accumulated clinker of the power station of Pécs, the recultivation of which has not been solved yet. Total gamma-ray activity values were far the highest (170-210 nGy/h) at these locations.

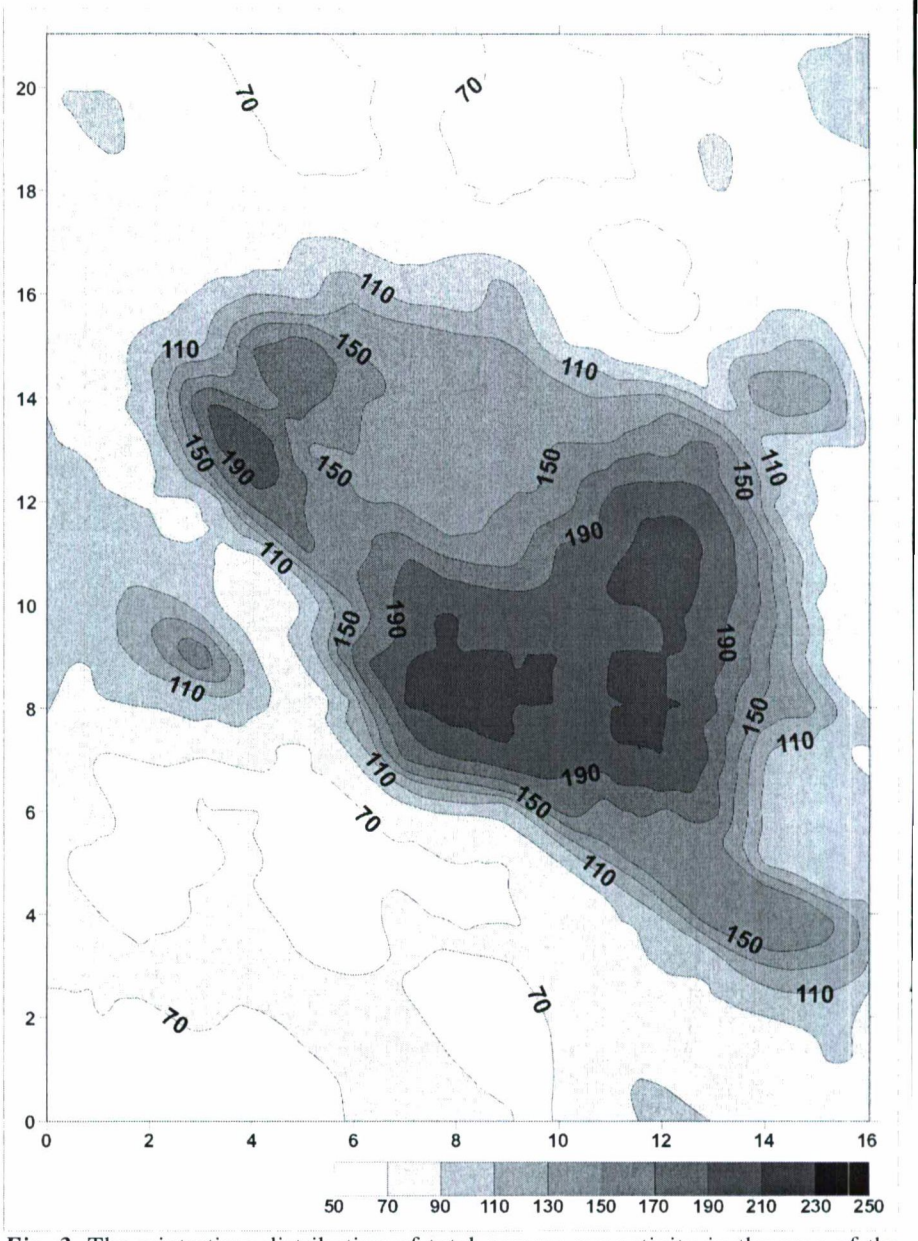

Fig. 3. The wintertime distribution of total gamma-ray activity in the area of the Karolina opencast mine

Gamma-ray spectroscopy

Productive layers occurring on the area of the opencast mine and adjacent waste sandstones and aleurites were all sampled for gamma-ray spectroscopy.

The measurements have proved that not exclusively the concentration of U, which shows an average value, is responsible for increased total gamma-ray activity but also the unusually high

Table 2. Calculated concentrations of radioactive elements in different rock types of the Karolina open cast

Rock type	No. of samples	Mean TOC (%)	Specific activity (Bq/kg)			Average radioactive element concentrations (gamma-spectroscopy)			Average radioactive element concentrations (ICP-MS)			
			mean	min.	max.	U (ppm)	Th (ppm)	K %	No. of sampl.	U (ppm)	Th (ppm)	K %
Coal	12	77	276	141	396	6	13	1,7	6	4,0	13	1,9
Argillaceous coal	14	61	298	198	387	5	21	2,2	5	4,9	15	2,3
Carbonaceous claystone	12	46	312	205	497	6	22	2,3	5	5,3	16	2,2
Aleurolite	6	17	216	149	326	3	15	2,0	4	3,8	12	2,1
Sandy aleurolite	7	16	178	123	213	4,5	14	2,2	5	4,2	9	2,2
Sandstone	8	6	148	111	245	3,5	12	2,0	5	2,7	10	2,1

Table 2. continued

Measuring points	Gamma-ray dose rate (nGy/h)	Calculated concentrations of elements		
		K (%)	Th(pp	U(pp
Soil cover	69	1,8	3	1,5
Sandstone (deposit 7)	101	2,2	8	4
Sandstone (deposit 21)	123	2,3	10	2,5
Aleurolite (deposit	201	2,4	18	7
Aleurolite (deposit 7)	156	2,2	16	5,5
Coal (deposit 11)	181	1,8	29	8
Coal (deposit 23)	169	2	18	7
Coal (deposit 25)	212	2,1	27	12

– compared to the world average – Th concentration of coals and K-content of argillites, aleurites and sandstones (Table 2.). Uranium and thorium content can mainly be related to organic material rich coals and carboniferous claystones. However, higher Th concentrations can also be detected in rocks of relatively low organic material content, but these samples proved always to be rich in clayey minerals and their grain-size was also small. Thus, the concentration of radionuclides (U, Th) is highly determined by clayey minerals, i.e. those samples were representing the highest specific activity that contained both organic material and clayey minerals in a significant quantity (carboniferous claystones, clayey coals). In case of certain samples the Th/U ratio can even be 7-9 (Table 2).

Further analyses would be necessary to determine the radiological characteristics of the clinker produced in the power station of Pécs, which is fuelled with the coal of Pécsbánya. Here, even higher values can be expected, since radioelements may further concentrate in the ashes of the burnt coal.

REFERENCES

BODROGI, F., VADOS, I. (1959): Az ajkai szénmedence felsőcsingeri bányamezőjében előforduló lencsés településű urán felhalmozódások. MEV Adattár, Kővágószőlős J-1882.

EISENBUD, B., GESELL, T. (1997): Environmental radioactivity from natural indsutrial and military sources. Academic Press. San Diego.

FÖLDVÁRI, A. (1951): A magyarországi radioaktív anyagkutatás földtani és kőzettani vonatkozásai. Magyar Állami Földtani Intézet évi jelentése. Budapest. Vol. 10, 35-54.

HOFFMAN (1988): Concretations of uranium and thorium in the different varieties of U.S. coal. AAAS Publication. Vol. 87. 30.

SWAINE, D. J. (1990): Trace Elements in coal. Butterworths. London. 278 p.

SWAINE, D. J., GOODARZI, F. (1997): Environmental aspects of trace elements in coal. Kluwer Academic Publishers. Dordrecht. 312 p.

SZALAY, S. (1948): Kutatások urán és tórium magyarországi előfordulásai után korszerű atomfizikai módszerekkel. Magyar Állami Földtani Intézet évi jelentése. Budapest. Vol. 10. pp. 5-24.

SZALAY, S., FÖLDVARI, A. (1951): Kőzetek radiológiai vizsgálata. Magyar Tudományos Akadémia Matematikai és Természettudományi Osztályának Közleményei Budapest. I. kötet pp. 60-72.

SZALAY, S. (1952): Hazai kőszenek radiológiai vizsgálata. Magyar Tudományos Akadémia Műszaki Tudományok Osztályának Közleményei. Budapest. 168-185.

SZALAY, S., ALMÁSSY, GY. (1956): Analitikai vizsgálatok hazai kőszenek urántartalmára vonatkozólag. MTA Kémia Tudományok Osztályanak Közlemenyei, 8, 39.

UPOR, E., ZETHNER, GY. (1960): Zárójelentés a tatabányai barnakőszén-medencében végzett 1956-57. Években végzett hasadóanyagkutatásról. MEV Adattár, Kővágószőlős J-0313.

VALKOVIC, V. (1983): Trace elements in coal. CRC Press, Boca Raton

Received: October 1, 2002; accepted:November25, 2002

Acta Mineralogica-Petrographica, Szeged 2002, Vol. 43, pp. 65-69

ACTA
Mineralogica
Petrographica

GEOCHEMISTRY AND ORIGIN OF THE BATTONYA UNIT GRANITOIDS, SE HUNGARY

ELEMÉR PÁL-MOLNÁR[1], GÁBOR KOVÁCS[2]

[1] Department of Mineralogy, Geochemistry and Petrology, University of Szeged
H-6701 Szeged, P. O. Box 651, Hungary
[2] Environmental Protection Inspectorate of Lower Tisza Region
H-6721 Szeged, Felső-Tisza part 17, Hungary
e-mail: palm@geo.u-szeged.hu

ABSTRACT
Boreholes deepened in the axis zone of the uplifted Pusztaföldvár-Battonya High (Battonya Unit, Békésia Terrane, Tisia Composite Terrane, Pannonian Basin) reached granitoid rocks in the Variscan crystalline basement at a depth of 1000-2000 m. On the basis of trace and rare earth elements geochemistry and zircon morphology investigations, the granitoids of the Pusztaföldvár-Battonya High have a peraluminous, subalkaline, calc-alkaline character. The studied rocks are S-type, and were formed in a syn-collisional (continent-continent collision zone) environment.
Key words: granite, geochemistry, crystalline basement, Battonya Unit, Tisia Composite Terrane, Hungary

INTRODUCTION

The Tisia Composite Terrane Alpine megatectonic unit forms the pre-Neogene crystalline basement of South, Southeast Hungary. As an independent unit the Tisia Composite Terrane existed from the Late Cretaceous, when its rotation began, till the Early Miocene. Concerning the territory of Hungary it involves three large Variscan Terranes (Slavonia-Dravia Terrane, Kunságia Terrane and Békésia Terrane), all of which are covered by an Alpine overstep sequence (Kovács et al., 2000). The Békésia Terrane can be divided into four units: Kelebia Unit, Csongrád Unit, Battonya Unit and the Sarkadkeresztúr Unit (Szederkényi, 1984, 1996). The crystalline mass of the Tisia Composite Terrane is characterised by granitoid ranges and anticline wings of middle and high grade metamorphites.

In this paper, we concentrate on the granitoid rocks located in the characteristic uplift of the basement (Pusztaföldvár-Battonya - [PB] High) of the Békésia Terrane (Battonya Unit) – Tisia Composite Terrane (Pál-Molnár et al., 2001) by presenting trace and rare earth elements geochemistry and zircon morphology investigations.

According to Buda (1996), the granitoid rocks have a compound crustal-mantle origin, and formed in a degrading plate boundary environment, therefore, the S-type origin is mixed with a certain degree of I-type granitoid origin. At Battonya-Mezőhegyes the magma of the abyssical plutonic body was slightly compressed upwards due to an "in situ" melting in the late kinematic phase of the Variscan Orogenesis. As a result of this, a slight contact zone developed (Szepesházi, 1969; Szederkényi, 1984; Kovách et al., 1985).

Petrological and main element geochemistry investigations (Pál-Molnár et al., 2001) have shown that the granitoid rocks of the available Battonya Unit boreholes can be considered of similar character on the basis of their composition. The main rock forming minerals of the studied samples are: quartz ± orthoclase + microcline + plagioclase feldspar (albite-oligoclase) ± biotite + muscovite. Accessory components are apatite, zircon, monacite and less frequently titanite. Their modal composition refers to that of syenogranites, monzogranites and granodiorites. On the basis of their major element geochemical composition the studied rocks are subalkaline and calc-alkaline syenogranites, monzogranites and granodiorites with a peraluminous character. From a tectonical aspect the studied rocks are of orogenous, syn-collisional, continental collisional origin (CCG). Most of the characteristics of the Battonya Unit samples indicate that they are S-type granitoids.

SAMPLING AND ANALYTICAL METHODS

The research was based on samples stored in the rock collection of the Department of Mineralogy, Geochemistry and Petrology, University of Szeged. The following boreholes were examined: Battonya-48, 63, 72, Battonya-K-9, 11, 13, 14, 17, 18; Dombegyháza-DNY-2; Kunágota-1, 2; Mezőhegyes-13, 15, 18, 19, 20; Mezőhegyes-K-1. The samples are drill-cores, and both their number and quantity are very limited.

The trace and rare earth element compositions of samples representing the main rock types were determined with an atomic emission spectrometer (ICP-AES) at the University of Stockholm.

Three samples of the examined granitoid rocks [ÁGK-1610-es (Mezőhegyes-19), ÁGK-1318 (Kunágota-1), ÁGK-1816-os (Battonya-48)] were chosen for the separation of zircon crystals on the basis of previous petrological analyses. After the separation process the zircon crystals were examined by SEM.

Table 1. Trace and REE compositions of the examined samples of Battonya Unit.

	ÁGK-1816 Battonya -48 1174-1176 m	ÁGK-1835 Battonya -63 1029-1034 m	ÁGK-1837 Battonya -72 1136-1137 m	ÁGK-1846 Battonya K-9 1058-1060 m	ÁGK-1848 Battonya K-11 1046-1050 m	ÁGK-1849 Battonya K-13 1069-1071 m	ÁGK-1850 Battonya K-14 1075-1077 m	ÁGK-1853 Battonya K-17 1052-1075 m	ÁGK-1854 Battonya K-18 1079-1082 m	ÁGK-1315 Dombegyhá z DNY-2 1350-1352 m	ÁGK-1317 Kunágot a-2 1908-1911 m	ÁGK-1318 Kunágot a-1 1797-1804 m	ÁGK-1603 Mezőh. -13 1184,5-1190 m	ÁGK-1605 Mezőh.- 15 1194-1198 m	ÁGK-1609 Mezőh.- 18 1220-1220,8 m	ÁGK-1610 Mezőh.- 19 1180-1182,5 m	ÁGK-1612 Mezőh. -20 1184-1186 m	ÁGK-1613 Mezőh K-1 1328-1330 m
Ba	619,3	450,7	290,3	685,2	405	418,8	613,1	344,9	769,3	301	859,1	279,6	622,6	382,8	568,2	241,7	741,1	404,2
Be	1,63	4,73	5,28	2,42	2,83	3	1,91	2,59	3,22	4,41	3,27	3,94	2,01	2,15	1,07	2,27	0,82	4,02
Co	4,49	2,14	4,12	3,35	4,89	5,15	3,45	2,91	4,13	6,5	8,99	2,61	4,2	8,6	5,24	6,55	4,23	4,52
Cr	5,2	9,6	4,5	7,1	11,8	12,9	7,6	11,1	6,7	118,7	18,6	3,7	7	17,9	4,3	26,2	4,2	4,6
Cu	9,85	18,83	15,03	31,85	33,72	35,64	36,59	18,29	41,03	25,12	23,53	28,51	22,42	23,44	36,39	34,09	14,96	42,19
Ga	18,85	15,21	19,23	18,09	19,73	18,61	18,81	18,16	16,83	19,71	29,13	17,4	14,59	22,37	22,08	20,42	16,32	16,75
Hf	n/a	2,29	n/a	3,39	3,69	3,89	3,21	3,23	2,98	0,51	n/a	2,39	n/a	0,44	4,77	1,28	0,48	3,75
Mo	n/a	2,5	n/a	3,17	2,4	1,64	0,65	0,79	2,21	n/a	n/a	3,69	n/a	n/a	2,74	n/a	n/a	1,27
Nb	5	6	9,8	8,6	12,1	8,9	8,6	8,5	9,2	8,5	8,3	5,4	6,1	8,9	8,2	9,8	3	5,8
Ni	5,09	6	3,16	4,6	7,4	7,1	4,3	5,7	5,2	15,06	13,75	4,3	5,97	9,67	3,9	19,48	4,58	6,1
Pb	23,8	16,7	15,77	17,6	11,3	9,5	195	11,7	20,4	11,54	19,88	39	22,64	10,85	5	19,81	17,02	11,9
Rb	294,5	280,2	417,7	256	219,6	241,4	203,2	211,3	284,6	257,7	402	333	231,8	239	238,5	227,7	318,8	189,5
S	13,71	253,22	33,53	179,69	352,07	348,77	129,69	76,29	194,93	84,78	62,22	62,79	32,21	75,57	327,62	34,44	56,69	88,29
Sc	4,1	2,3	4,39	3,6	4,5	4,5	4,1	3,9	2,9	7,74	7,58	3,4	4,82	8,29	3,5	9,84	4,38	3,1
Sr	132,3	192,2	121,2	277,3	188	204,9	318,4	168,8	269,8	255,1	113,2	109,4	205,6	170,5	266,6	222,6	138,2	218,2
Ta	n/a	1,493	1,869	n/a	0,809	n/a	n/a	n/a	n/a	1,284	n/a	0,416	n/a	n/a	n/a	n/a	n/a	n/a
Tb	n/a	n/a	0,176	n/a	n/a	n/a	n/a	n/a	n/a	0,313	0,443	n/a	n/a	0,616	n/a	0,816	n/a	n/a
V	17,38	12,1	17,1	27,8	34,3	35,3	32,9	29,8	23,7	34,86	49,1	10,9	21,75	62,84	49,9	50,09	16,72	27,8
Y	7,4	8,3	11,1	8,5	11,2	8,9	9,8	8,6	7,7	13,9	6,4	10,3	10,8	9,1	7,1	29,9	9,3	6,8
Zn	42,24	36,58	40,63	48,7	51,88	49,89	51,94	46,34	54,21	56,92	103,72	225,49	41,69	101,3	60	73,49	51,82	44,24
Zr	107,5	69	60,5	115,2	121,4	135	123,8	113,4	110,2	166,7	114,9	53,5	112,2	201,4	182	200,7	164,2	139,1
Ce	42,82	33,44	25,55	57,19	65,61	64,79	66,39	51,27	59,85	59,39	68,61	31,21	35,2	88,75	90,75	69,95	65,92	47,42
Dy	1,42	1,97	1,64	2	2,53	2,21	2,39	2,05	2,15	2,46	1,64	2,37	2,02	1,78	2,04	4,52	2,29	1,78
Er	1,94	2,12	2,34	2,24	2,75	2,4	2,42	2,53	2,21	3,2	2,64	2,19	2,17	2,95	2,69	5,05	2,09	2,35
Eu	0,51	0,581	0,354	0,813	1,019	1,015	1	0,788	0,916	0,792	0,798	0,474	0,545	0,73	1,273	0,846	0,675	0,881
Gd	4,1	2,3	2,87	4,66	5,61	5,66	5,13	4,63	4,82	6,09	7,83	3,51	3,8	7,58	6,59	8,39	5,17	4,5
La	19,16	13,69	n/a	26,26	29,98	30,53	30,45	23,36	29,8	28,52	34,95	13,8	17,73	43,1	42,37	34,83	28,15	20,61
Lu	0,429	0,338	0,416	0,515	0,589	0,595	0,579	0,546	0,463	0,651	0,738	0,469	0,489	0,812	0,594	0,974	0,385	0,537
Nd	12,18	7,64	4,54	16,84	20,15	21,39	21,58	14,67	19,76	19,69	24,76	8,09	9,76	29,39	33,04	25,28	21,31	13,64
Sm	4,94	3,71	3,4	5,52	6,64	6,59	6,58	4,97	6,05	6,49	7,19	3,39	4,1	7,43	8,45	7,87	6,75	4,97
Yb	0,43	0,46	1,03	0,424	0,633	0,477	0,477	0,415	0,302	1,08	0,23	0,683	0,86	0,57	0,115	2,87	0,39	0,246

TRACE AND RARE EARTH ELEMENT GEOCHEMISTRY

Eighteen samples of the Battonya Unit were analysed with respect to their major element (Pál-Molnár et al., 2001), trace element and rare earth element (REE) compositions (Table 1).

On the Harker's variation diagrams for trace elements (not shown) the patterns of the plotted samples are not as regular as it is in the case of major elements. Ni, Cr, V, Zn, Zr and Ga decrease with increasing SiO_2. Y and Nb contents are more or less constant. Sr shows a slight increase, while Ba and Rb are scattered. However, Ba decreases with increasing CaO, and the Sr vs. CaO diagram shows an inverse relation too.

We found some differences in the pattern of samples originating from different areas of the Battonya Unit. Nb/Ta ratio indicates heterogeneity in the studied samples, as it ranges between 4.02 and 14.96. Ce/Yb (24.4-789.1) and Ce/Nb (2.6-22.0) ratios represent a wide range, while the Ba/La ratio varies from 1.96 to 2.44. The fractionation trend is quite clear on the basis of trace elements as well. It seems that samples from the Mezőhegyes area are less fractionated.

Zircon saturation temperatures were calculated (after Watson and Harrison, 1983) in order to determine accurate temperatures at which zircons formed. Values of T_s range between 708-828 °C. However, these results seem to be slightly high. A reason for this can be that the inherited cores of zircons might have crystallised under different conditions than the examined samples, and this way increased Ts values can be received. Ts values can also be characterised with a differentiation trend shown by the Ts vs. SiO_2 and TiO_2 diagrams (Fig 1). The most fractionated samples have the lowest Ts value and the least fractionated ones represent the highest.

On the basis of discrimination diagrams for trace elements, the studied samples plotted in the field of orogenic granite type (OGT) (unfractionated I and S-type granites) and syn-collision granites (Fig. 2), which correspond to the results of tectonic discrimination given by major elements (Pál-Molnár et al., 2001).

In multi-element diagrams the examined samples show a similar pattern, with Ba, Nb, Hf, Ti and Yb depletion and enrichment in other LILE and LREE (Fig. 3).

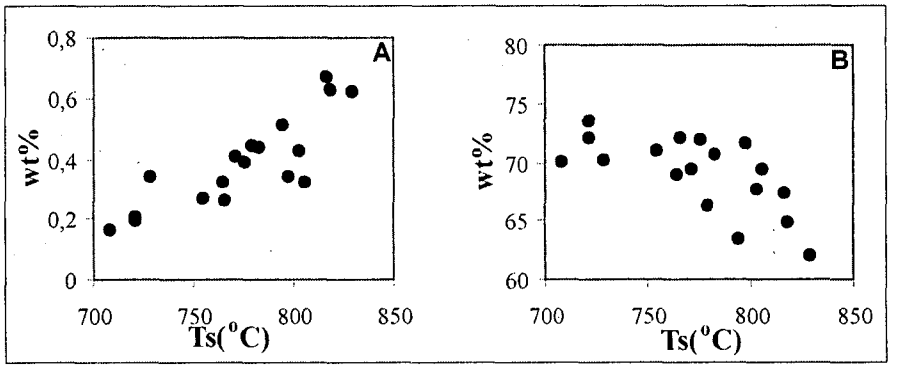

Fig. 1. Zircon saturation temperatures vs. TiO_2 *(A)* and SiO_2 *(B)* according to the calculation from Watson and Harrison (1983)

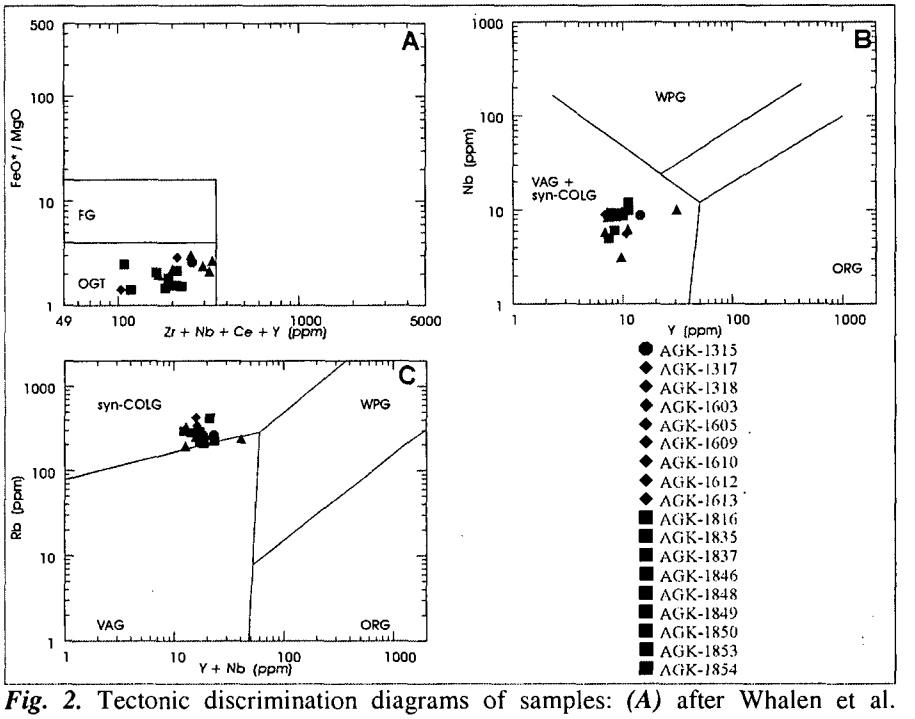

Fig. 2. Tectonic discrimination diagrams of samples: *(A)* after Whalen et al. (1987), and *(B)*, *(C)* after Pearce et al.

The total REE contents are moderate or low, varying between 0.12 and 90.75 ppm. The REE contents of the studied samples and their ratios normalised on chondrite (Masuda et al. 1973) are summarised in Table 1. On the basis of these ratios the examined granites are enriched in the LREEs, since the $(La/Lu)_{ch}$ ratio ranges between 3.05 and 7.57. The REE spider diagrams (Fig. 3) represent similar features: the LREEs slightly decrease and reflect the $(La/Sm)_{ch}$ ratio (2.31-3.64). Furthermore, the HREEs display a more or less flat pattern which is marked by the low values of the $(Gd/Lu)_{ch}$ ratio (0.84-1.65). Nevertheless, these diagrams can be characterised by negative Nd, Eu, Dy and Yb anomalies.

The value of $(Eu/Eu^*)_{ch}$ represents the degree of fractionation: the highest value is 0.56 and belongs to the least fractionated sample (ÁGK-1835), while the most fractionated sample has the lowest value (0.29) (ÁGK-1605). Thus, the average $(Eu/Eu^*)_{ch}$ value of the Battonya area is slightly smaller than in the samples of the Mezőhegyes area. The Eu anomalies are indicative for plagioclase feldspar fractionation, however, plotted samples in the diagrams of $(Eu/Eu^*)_{ch}$ vs. SiO_2 and CaO are rather scattered (Fig. 4). There is not any clear trend among the samples. However, Ba increases with $(Eu/Eu^*)_{ch}$, which can be caused by potassium feldspar fractionation.

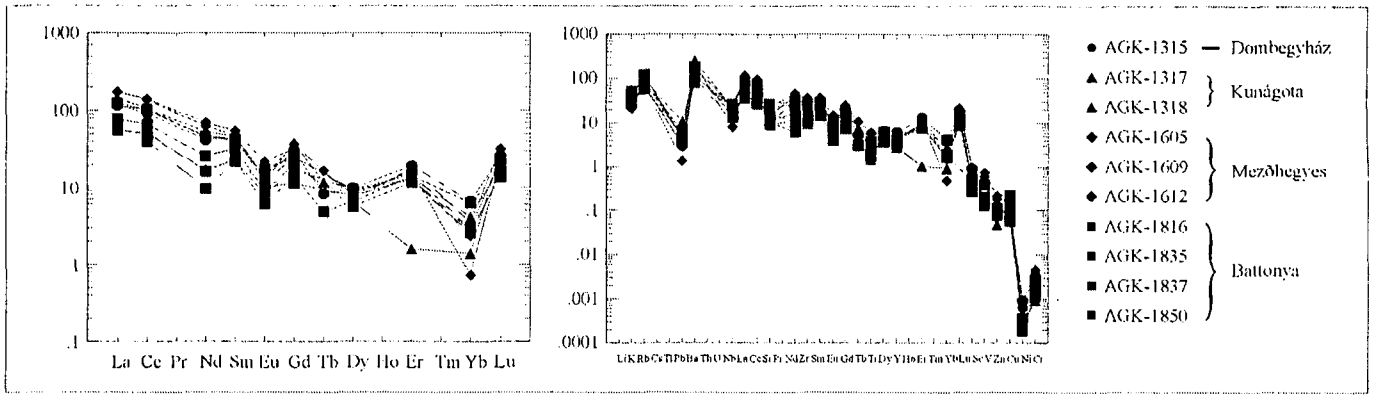

Fig. 3. Chondrite normalized (Masuda et al., 1973) REE-patterns and multielement plots for the Battonya Unit granite

ZIRCON MORPHOLOGY INVESTIGATIONS

Zircon crystals are transparent, colourless or slightly pink, brownish red. Zoning and opaque inclusions are also characteristic. Almost 250 granules were analysed for identifying different morphological types. The identified classes correspond well to the expected character of zircon population, which was predicted on the basis of main rock forming and accessory minerals. Therefore, the morphological classification of zircon crystals provides the location of zircon population in the typology diagram (Pupin, 1980). The most frequent types of zircon in the examined population are S17, S12, S22, S21, S10, S18, S7, S6, S4, S2 (Fig 5). Based on the present investigation, it can be claimed that the studied granites plot neither to the field of alkali nor to that of thoeliitic granites. It is highly probable then that they are closest to the subalkaline, calc-alkaline series.

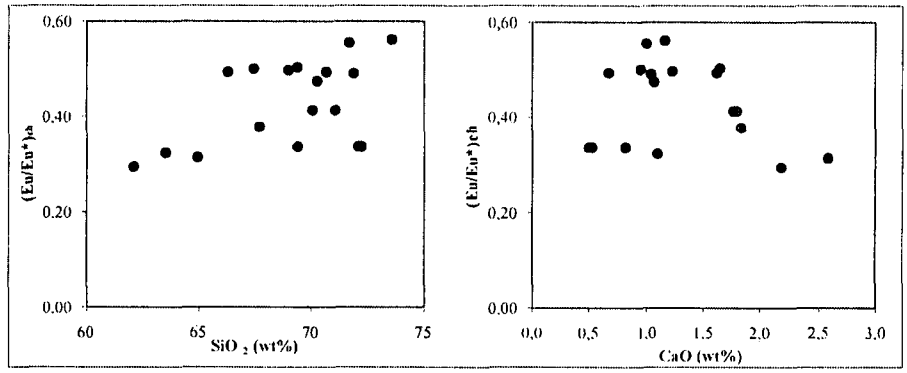

Fig. 4. Variation diagrams on $(Eu/Eu^*)_{ch}$ vs. SiO_2 and CaO

CONCLUSIONS

Based on trace and rare earth elements geochemistry, petrographical characteristics and main element geochemistry (Pál-Molnár et al., 2001), and considering also the results of the zircon morphological investigations, the granites of the PB High are of uniform character. They are peraluminuous, subalkaline, calc-alkaline granitoids of high K-content. On the basis of trace element distributions, a fractionation difference can be detected in terms of PB High

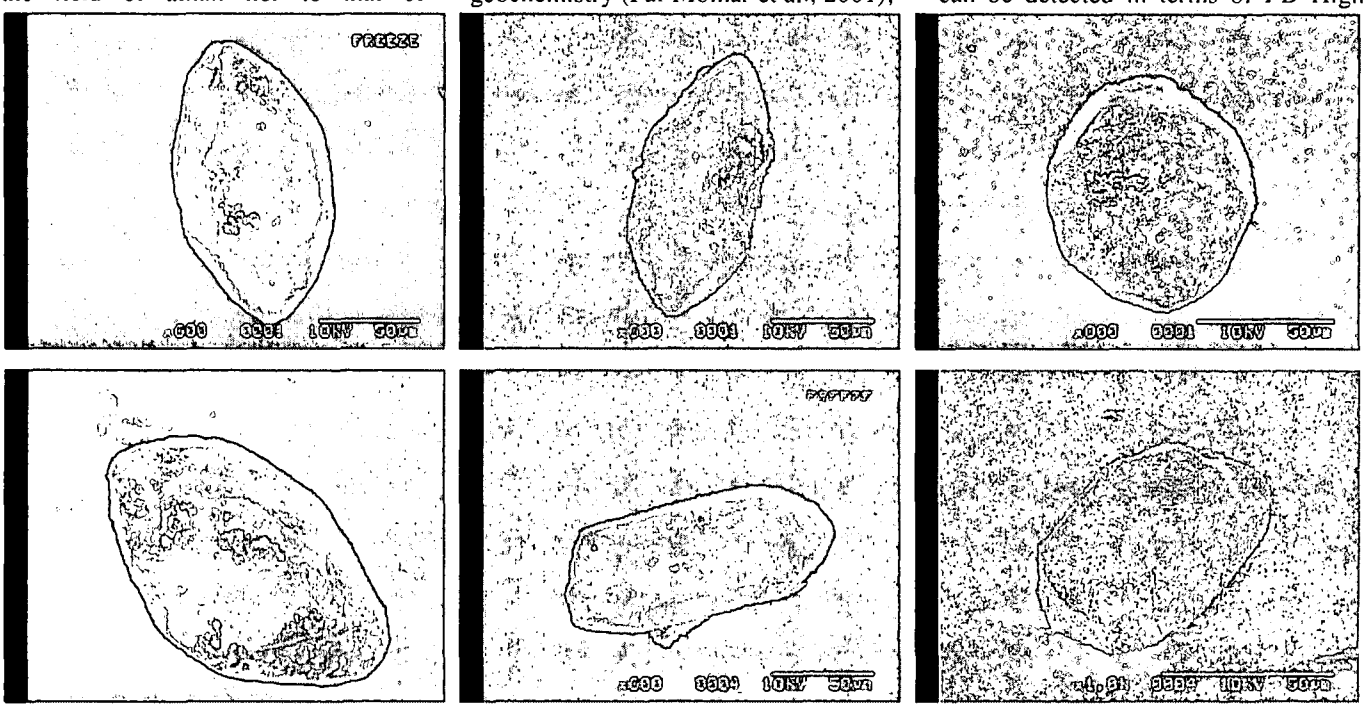

Fig. 5. Morphological types of the zircon population in the examined rocks (SEM images)

samples. In this sense the samples of the Mezőhegyes area are less fractioned.

The studied rocks are S-type, and were formed in a sycollisional (continent-continent collision zone) tectonical environment.

ACKNOWLEDGEMENTS

The financial background of this work was ensured by the Hungarian National Science Found (OTKA) (Grant No. F/029061) and János Bolyai Research Grant.

REFERENCES

BUDA, GY. (1996): Correlation of Variscan granitoids occuring in Central Europe. Acta Mineralogica-Petrographica, Szeged, **37**, Suppl., 24.

OVÁCH, Á., SVINGOR, É., SZEDERKÉNYI, T. (1985): Rb-Sr dating of basement rocks from the southern foreland of the Mecsek Mountains, Southeastern Transdanubia, Hungary. Acta Mineralogica-Petrographica, Szeged, **27**, 51-56, Szeged.

OVÁCS, S., HASS, J., BUDA, GY., NAGYMAROSY, A., SZEDERKÉNYI, T., ÁRKAI, P., CSÁSZÁR, G. (2000): Tectonostratigraphic terranes in the pre-Neogene basement of the Hungarian part of the Pannonian area. Acta Geologica Hungarica, **43**/3, 225-328.

PÁL-MOLNÁR, E., KOVÁCS, G., BATKI, A. (2001): Petrological characteristics of Variscan granitoids of Battonya Unit boreholes (SE Hungary), Acta Mineralogica-Petrographica Szeged, **42**, 21-31.

PEARCE, J. A., HARRIS, N. B. W., TINDLE ,A. G. (1984): Trace element discrimination diagrams for the tectonic interpretation of granitic rocks. Journal of Petrology, **25**, 956-983.

SZEDERKÉNYI, T. (1984): Az alföld kristályos aljzata és földtani kapcsolati (Crystalline basement and geological relations of the Great Plain). D.Sc. Thesis. MTA Library, Budapest, (in Hungarian).

SZEDERKÉNYI, T. (1996): Metamorphic formations and their correlation in the Hungarian part of the Tisza Megaunit (Tisa Composite Terrane). Acta Mineralogica-Petrographica Szeged, **37**, 143-160.

SZEPESHÁZY K. (1969): Petrographische Angaben zur Kentniss des Battonyaer Granits. M. Áll. Földt. Int. Évi Jel. 1967, 227-266, Budapest, (in Hung., with German summ.).

WATSON, E. B.,HARRISON, T. M. (1983): Zircon saturation revisited: temperature and composition effects in a variety of crustal magma types. Earth and Planetary Science Letters, **64**, 295-304.

WHALEN, J.B., CURRIE, K.L., CHAPPELL, B.W. (1987): A-type granites: geochemical characteristics, discrimination and petrogenesis, Contrib. Mineral. Petrol., **95**. 407-419.

Received: February 4, 2002; accepted: May 17, 2002

Acta Mineralogica-Petrographica, Szeged 2002, Vol. 43, pp. 71-77

ACTA
Mineralogica
Petrographica

MINERAL COMPOSITION OF THE GYÓD SERPENTINITE BODY, SOUTHERN TRANSDANUBIA, HUNGARY

GÁBOR KOVÁCS[1], BÉLA RAUCSIK[2], PÉTER HORVÁTH[3]

[1] Environmental Protection Authority of Lower Tisza District
H-6721 Szeged, Felső-Tiszapart 17.
[2] University of Veszprém Department of Earth and Environmental Sciences
H-8200 Veszprém, Egyetem u. 10.
[3] Laboratory for Geochemical Research, Hungarian Academy of Sciences
H-1112 Budapest, Budaörsi út 45.
e-mail: kovacsg@sol.cc.u-szeged.hu

ABSTRACT
Re-examination of mineral composition of Gyód Serpentinite Body is accounted for by the different results in literature. On the base of qualitative and semiquantitative XRD determinations, the main phases of the examined rocks are mostly serpentine minerals (30-60 %), talc (10-30 %) and chlorite (10-20 %). Chrysotile ($2Or_{cl}$ symmetry orthochrysotile) and 1T-lizardite could have been analysed surely in several samples. The amount of dolomite, quartz, olivine and spinel reaches 10-20 % in several samples; however, these are generally minor phases together with calcite and orthopyroxene. Olivine (Fo_{90-91}) and orthopryroxene (En_{88-93}) composition and also Cr# of spinels suggest that the examined rocks are the partial melting residua of a mantle source material. On the base of spinel composition, we assumed that the Gyód Serpentinite Body was probably formed in an island-arc environment.
Key words: harzburgite, serpentinization, mineral chemistry, Tisia Unit.

INTRODUCTION

In Southern Transdanubia field magnetic, aerogamma and aeromagnetic investigations indicated strong magnetic anomalies in the crystalline basement and, subsequently, some of these anomalies were penetrated by boreholes (boreholes of G–2 and He–1,–2). These resulted in the discovery of a serpentinized body in the region of Gyód (Fig. 1) and Helesfa. In the 1970s and 1980s more detailed research was carried out on the Gyód Serpentinite to identify its mineralogy and geochemistry. In these studies different mineral compositions of Gyód Serpentinite Body were determined from which different conclusions were drawn in the point of view of ultramafic protolith and its alteration processes. On the basis of X-ray diffraction analysis Erdélyi (1970) determined numerous minerals (Table 1) of the serpentinized peridotite. Szederkényi (1974) and Ghoneim (1978) claimed that the protolith of the serpentinite must have been pyroxenite or lherzolite or dunite. According to Papp (1989) the most frequent serpentine minerals are lizardite, chrysotile and polygonal serpentine. Balla (1980, 1985) established that the chemical composition of Gyód body is harzburgitic, and stated a multi-step metamorphic evolution path of it.

The aim of this paper to re-examine the mineral composition of the Gyód Serpentinite Body in order to determine the type of protholith and know more accurate the evolution of this body.

METHODS

The X-ray powder measurements were made at the Department of Earth and Environmental Sciences at the University of Veszprém using a Philips PW 1710 type diffractometer with a PW 1730/10 generator, a PW1050/70 type goniometer, a graphite single crystal monochromator and a proportional counter detector. The instrumental parameters of the measurements were CuK_α X-ray source, 40 mA tube current, 50 kV tube voltage, 1°-1° slit system, 0.035°/s velocity of goniometer. Bulk samples were measured on disoriented specimens. <2 μm fraction was separated by sedimentation after dissolution of $CaCO_3$ by 10% acetic acid and ultrasonic deflocculation. X-ray diffraction analysis of clay minerals was performed on oriented specimens made by smear on glass method. Two X-ray diagrams were taken on each samples of <2 μm fraction: one under natural, air-dried conditions, one after saturation with ethylene glycol.

EMP analyses were performed in the Laboratory for Geochemical Research, Hungarian Academy of Sciences using a JEOL JCXA-733 electron microprobe equipped with an Oxford INCA 200 EDS. Operating conditions were 15 keV accelerating voltage, 4 nA sample current, and 100 s counting time. The PAP correction procedure was applied for data preparation.

Mineral chemistry data was calculated by MINPROG computer program written by Sz. Harangi (Eötvös University, Budapest). For spinel Fe^{2+}–Fe^{3+} calculation Droop's equation (1987) was used.

X-RAY POWDER DIFFRACTION INVESTIGATIONS

From the whole drilling sequence of Gyód-2 borehole twelve samples were chosen for X-ray powder diffraction (Table 2). Qualitative and semiquantitative determinations were carried out on whole samples and fraction of <2 μm.

The main phases of the examined rocks are mostly serpentine minerals (30-60 %), talc (10-30% in the samples of No. ÁGK-7004, 7033, 7083/b and 7084) and chlorite (10-20% in the samples of No. 7004, 7033, 7083/b and 7084) (Fig 2A-D). The amount of dolomite can be estimated 10-20% (in the samples of No. ÁGK-7004, 7022, 7024, 7028, 7029 and 7039). Quartz (7022), olivine (7083/b) and spinel (7033, 7035) reaches 10-20% in several samples, however, these are generally minor phases together with dolomite, calcite and orthopyroxene. The sample No. 400389 contains unique components which were not detected elsewhere in this well log. It consists of mostly chlorite (clinochlore), talc and anthophyllite. As a minor phases actinolite and serpentinite were analysed.

The determination of multiphase serpentine minerals is rather uncertain, however, in several samples we can analyse surely chrysotile (probably $2Or_{cl}$ symmetry orthochrysotile) and (probably 1T) lizardite. Most samples consist of more than one serpentine mineral, but antigorite was not detected in anyone.

Regarding some uncertainties in the determination of phyllosilicates, the separated, oriented samples of <2 μm fractions were examined again, which represent Mg-chlorite, and swelling phase was not detected. On the base of peak maxima between 7.06-7.10 Å and 3.48-3.53 Å, presence of kaolinite can be precluded.

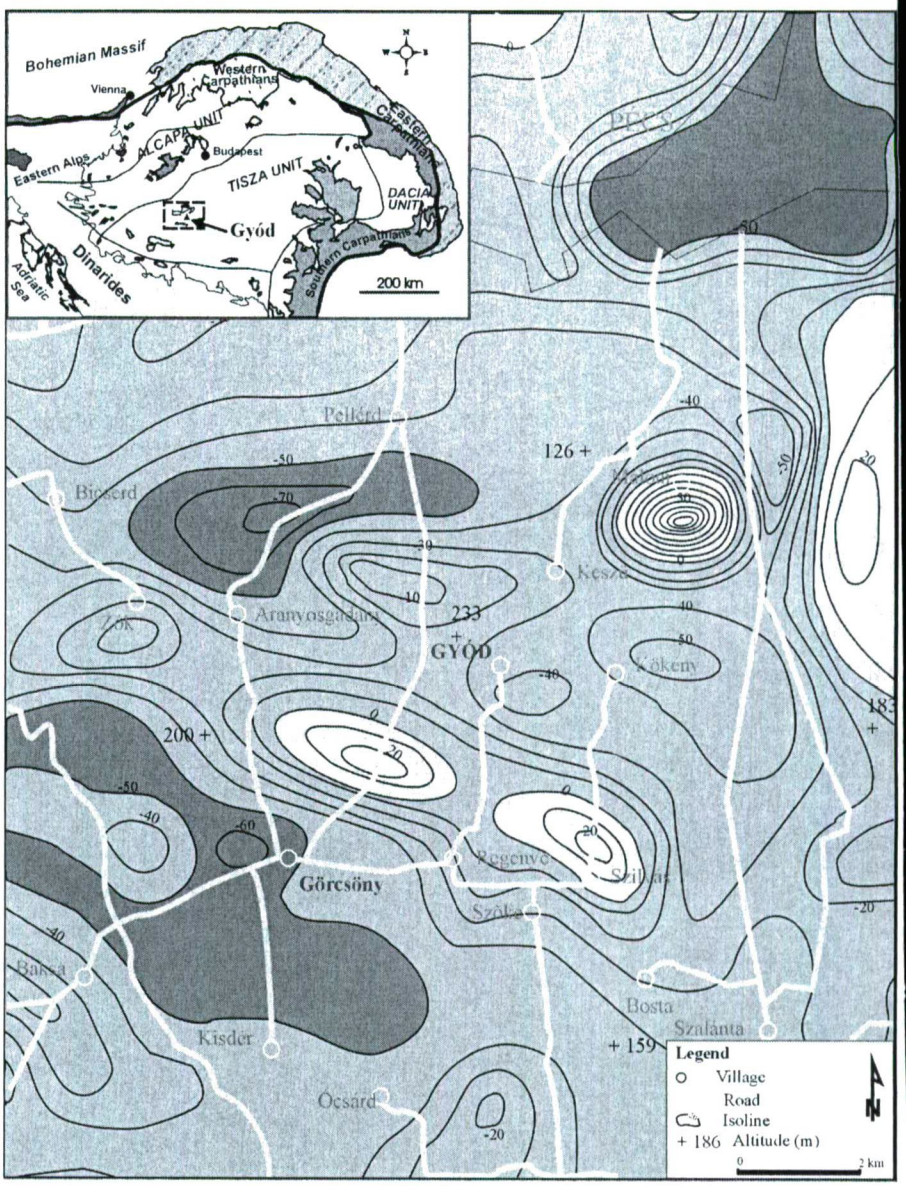

Fig. 1. Schematic geomagnetic map of the location of Gyód Serpentinite Body (after Barabás et al., 1969)

Table 1. Mineral composition of Gyód Serpentinite body in the earlier studies

Authors	minerals
Erdélyi, 1970	lizardite, hydrochrysotile, clinochrysotile, chlorite, talc, montmorillonite, biotite, muscovite, albite, bytownite, clinoenstatite, tourmaline, magnetite, boehmite, diaspore, lepidocrocite, brucite, wilkeite, calcite, dolomite, ankerite
Ghoneim, 1978	enstatite+olivine, lizardite+chrysotile, chlorite+dolomite, chromite, magnetite, pentlandite, pyrrhotine
Balla, 1985	$enstatite_1$, olivine, $enstatite_2$, anthophyllite, $talc_1$, $magnetite_1$, antigorite, $talc_2$, carbonates, $magnetite_2$, chlorite, Cr-magnetite, chrysotile, lizardite

Mineral chemistry

During microprobe analysis we tend to determine the chemical compositions of the relic minerals in three samples. Mostly olivine and orthopyroxene composed the unaltered ultramafic rock. According to the pervasive serpentinization, only these two primary minerals can be found in certain sheared, strongly foliated, mylonitized lenses, zones (Fig. 2C, D). Other parts of the well log are completely serpentinized where olivine altered to mesh structure unites, pyroxenes and/or amphiboles to bastites.

There are textural and chemical differences between Opx of No. ÁGK-7084 and ÁGK-7083 sample. In the No. ÁGK-7084 sample the Opx are more elongated and larger (up to several cm) than in the No. ÁGK-7083. The NiO content (mean value: 0.15 wt%), CaO content (0.11 wt%) is higher, and MnO content (not determined) is smaller in ÁGK-7084 than in the ÁGK-7083 (Table 3) where NiO and CaO are not determined, MnO is 0.3-6.3 wt%. The FeO content is the same in the samples, ca. 6-7 wt%. The Mg# is higher in the ÁGK-7083 (0.96-1.0) while 0.91 in the ÁGK-7084. Orthopyroxenes are enstatite 88-92%. Olivine compositions are rather similar; there are not any significant differences between the studied samples (Fo_{91-92}).

Table 2. Results of XRD analysis - abbreviations used after Kretz (1983)

sample	sample description	major components	minor components or uncertain analyses
ÁGK-7004	whole rock: white-greenish matrix	chl, tlc, liz, dol	cal (?), qtz, kln (?)
ÁGK-7022	white lamellar cast	dol, qtz, chry	mgs (?)
ÁGK-7024	greenish-brownish vein	dol, chry	liz (?), qtz
ÁGK-7028	complex vein: green srp and white fibrous cast	chry, dol	qtz
ÁGK-7029	white fibrous vein	chry, dol	-
ÁGK-7031	light green, yellowish vein	chry	liz (?)
ÁGK-7033	whole rock	chry, liz, tlc, chl, spl	cal, dol (?), kln (?)
ÁGK-7035	whole rock	chry, liz, spl	chl, dol, qtz
ÁGK-7037	elongated, columnar bastites	chry, liz	spl, dol
ÁGK-7039	whites grey massive crystalline cast	dol, liz	spl
ÁGK-7083/b	relic ultramafite	chl, tlc, ol	opx, spl (?), chry (?), liz (?), kln (?)
ÁGK-7084	whole rock	liz, chl, tlc	opx, dol (?), mgs (?), spl (?), kln (?)
400389	whole rock	chl, tlc, ath	act, srp

abbreviations: cal: calcite, chl: chlorite, chry: chrysotile, dol: dolomite, spl: spinel, kln: kaolinite, liz: lizardite, mgs: magnezite, ol: olivine, opx: orthopyroxene, qtz: quartz, tlc: talc, srp: serpentine minerals, ath: anthophyllite, act: actinolite.

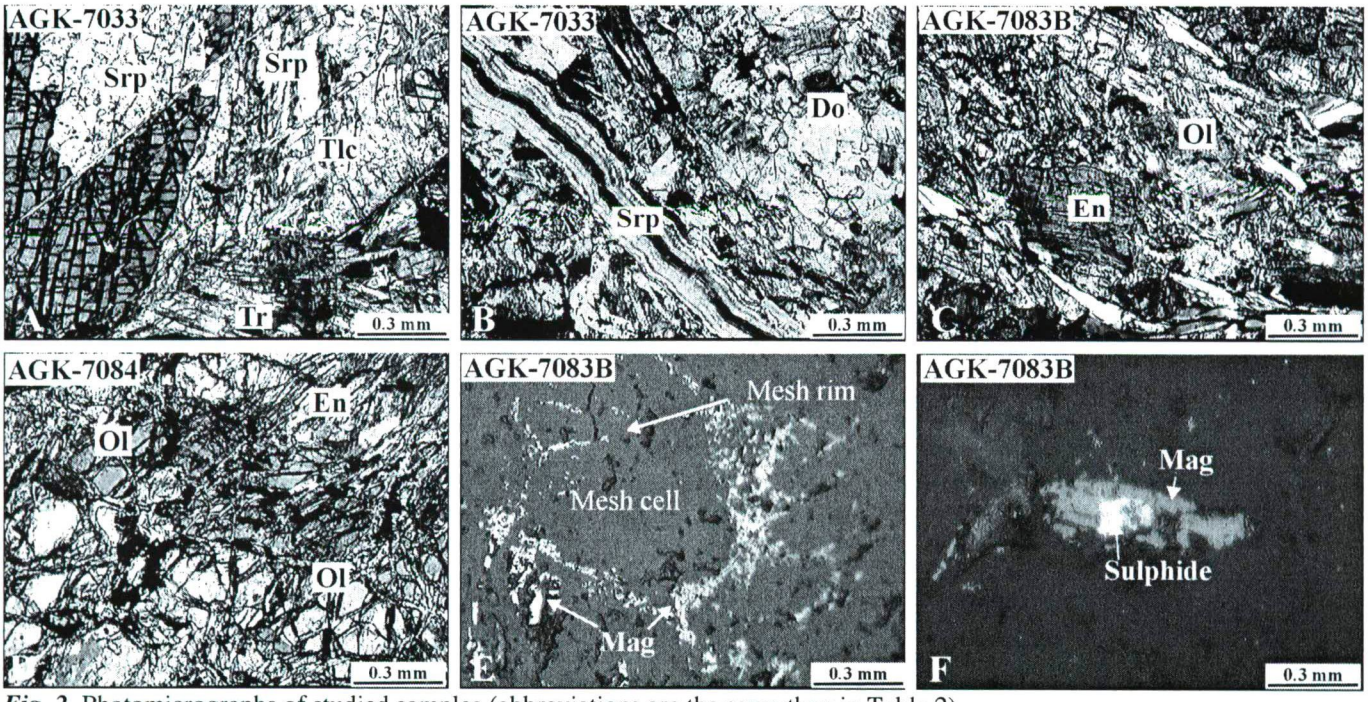

Fig. 2. Photomicrographs of studied samples (abbreviations are the same than in Table 2)

Table 3. Chemical composition of examined pyroxenes

sample	7083B			7084			7083		
	Opx1	Opx2	Opx3	Opx1	Opx2	Opx3	Opx1	Opx2	Opx3
MgO	36.95	36.67	36.36	37.41	37.03	36.79	36.32	36.98	36.47
Al_2O_3	0.00	0.10	0.38	0.24	0.25	0.00	0.00	0.09	1.06
SiO_2	56.06	55.78	55.56	55.93	55.99	56.46	56.34	55.78	55.52
CaO	0.12	0.05	0.15	0.11	0.17	0.13	0.00	0.00	0.14
TiO_2	0.00	0.05	0.10	0.00	0.07	0.00	0.19	0.00	0.19
V_2O_3	0.00	0.00	0.00	0.00	0.00	0.00	0.00	0.00	0.00
Cr_2O_3	0.00	0.00	0.00	0.00	0.00	0.00	0.00	0.00	0.35
MnO	0.00	0.00	0.32	0.00	0.00	0.00	0.27	0.25	6.28
FeO	6.87	7.35	7.13	6.31	6.37	6.62	6.88	6.91	0.00
NiO	0.00	0.00	0.00	0.00	0.12	0.00	0.00	0.00	0.00
Sum	100.00	100.00	100.00	100.00	100.00	100.00	100.00	100.01	100.01

Table 3. continued

sample	7083B			7084			7083		
	Opx1	Opx2	Opx3	Opx1	Opx2	Opx3	Opx1	Opx2	Opx3
cation numbers on the basis of 6 oxygens									
T site									
Si^{4+}	1.9165	1.9105	1.9049	1.9063	1.9120	1.9308	1.9328	1.9071	1.8980
AlIV	0.0000	0.0039	0.0153	0.0096	0.0100	0.0000	0.0000	0.0035	0.0427
total:	1.9165	1.9144	1.9202	1.9159	1.9220	1.9308	1.9328	1.9106	1.9407
M1 site									
Ti^{4+}	-	0.0013	0.0026	-	0.0018	-	0.0048	-	0.0048
Ni^{2+}	-	-	-	-	0.0033	-	-	-	0.0094
Mg^{2+}	1.0000	0.9987	0.9974	1.0000	0.9949	1.0000	0.9952	1.0000	0.9858
total:	1.0000	1.0000	1.0000	1.0000	1.0000	1.0000	1.0000	1.0000	1.0000
M2 site									
Mg^{2+}	0.8828	0.8734	0.8608	0.9004	0.8900	0.8752	0.8620	0.8846	0.8724
Fe^{2+}	0.1963	0.2104	0.2044	0.1798	0.1819	0.1893	0.1973	0.1976	-
Mn^{2+}	-	-	0.0093	-	-	-	0.0078	0.0072	0.1818
Ca^{2+}	0.0043	0.0018	0.0054	0.0039	0.0062	0.0047	-	-	0.0050
total:	1.0834	1.0856	1.0799	1.0841	1.0781	1.0692	1.0671	1.0894	1.0592
iCAT#:	4.0563	4.0580	4.0571	4.0599	4.0546	4.0465	4.0418	4.0614	4.0477
OXNUM:	5.9164	5.9138	5.9152	5.9111	5.9189	5.9308	5.9375	5.9088	5.9288
mg#:	0.91	0.90	0.90	0.91	0.91	0.91	0.90	0.91	1.00
end-members for pyroxenes									
Ka	-	-	0.9300	-	-	-	0.7838	0.7200	18.3952
CaTi	-	0.1801	0.5200	-	0.3600	-	-	-	0.5059
Di	0.4300	-	0.0200	0.3900	0.2600	0.4700	-	-	-
En	88.2800	87.3749	86.0800	90.0400	89.0000	87.5200	86.6158	88.4600	81.0989
Fs-En	11.2900	12.4450	12.4500	9.5700	10.3800	12.0100	12.6005	10.8200	-
inSUM:	1.0000	0.9996	1.0000	1.0000	1.0000	1.0000	0.9952	1.0000	0.9883
IMA names	Enstatite	Ferroan Enstatite	Ferroan Enstatite	Enstatite	Enstatite	Enstatite	Enstatite	Enstatite	Manganoan Enstatite

The Mg# number of olivines is 0.91 (Table 4). General occurrence of plagioclase, clinopyroxene and amphiboles were not pointed out. Although completely serpentinized amphiboles can be seen as bastites, so these cannot be identified. However, fresh amphiboles can be found only in two samples. First, tremolite (Fig. 2A) occurs together with talc in the alteration rim of enstatite. Second, unaltered anthophyllite and actinolite was found only in a special location, near an aplite dyke.

Spinels can be characterised with high Cr_2O_3 (about 39.7-40.2 wt%) and high Fe content (Table 5.), relatively low TiO_2 (0.9-1.3 wt%) and MgO component (2.6-3.8 wt%). On the base of Fe^{3+}, Al^{3+}, Cr^{3+} triangular diagram, these spinels fall into the field of ferrichromite (Fig. 3). According to the nomenclature of Stevens (1944), these spinels can be called ferrian chromite. The average spinel compisition of the examined samples can be given by the following order of the end-members: $Chr_{58.12}$, $Mag_{25.56}$, $Mfe_{6.21}$, $Spi_{4.46}$, $Qua_{2.98}$, $Cou_{0.91}$, $Jac_{1.75}$, respectively. Cr# [Cr#=(Cr/(Cr+Al)] and Mg#

Table 4. Mineral chemistry of olivines in studied samples

sample	ÁGK-7083B				ÁGK-7084			
	ol1	ol2	ol3	ol4	ol1	ol2	ol3	ol4
MgO	51.68	52.32	51.61	51.64	51.75	51.07	50.85	51.31
Al2O3	0.00	0.00	0.00	0.00	0.04	0.00	0.00	0.00
SiO2	39.04	38.81	38.11	38.48	38.84	38.76	38.60	38.75
CaO	0.00	0.00	0.00	0.00	0.00	0.00	0.00	0.00
TiO2	0.00	0.00	0.00	0.00	0.00	0.00	0.00	0.00
V2O3	0.04	0.07	0.05	0.18	0.06	0.16	0.21	0.00
Cr2O3	0.00	0.00	0.00	0.00	0.00	0.00	0.00	0.00
MnO	0.00	0.00	0.00	0.00	0.00	0.00	0.00	0.00
FeO	8.97	8.50	9.30	9.25	9.16	8.89	9.49	9.37
NiO	0.27	0.30	0.93	0.45	0.14	0.88	0.66	0.12
Sum:	100.00	100.00	100.00	100.00	99.99	99.76	99.81	99.55
olivine cation numbers on the basis of 4 oxygens								
Mg	1.8920	1.9130	1.9030	1.8980	1.8960	1.8800	1.8750	1.8890
Al	-	-	-	-	0.0010	-	-	-
Si	0.9590	0.9520	0.9420	0.9490	0.9550	0.9570	0.9550	0.9570
Ca	-	-	-	-	-	-	-	-
Ti	-	-	-	-	-	-	-	-
V	0.0010	0.0010	0.0010	0.0040	0.0010	0.0030	0.0040	-
Cr	-	-	-	-	-	-	-	-
Mn	-	-	-	-	-	-	-	-
Fe2	0.1840	0.1740	0.1920	0.1910	0.1880	0.1840	0.1960	0.1930
Ni	0.0050	0.0060	0.0180	0.0090	0.0030	0.0170	0.0130	0.0020
inCAT	3.0410	3.0470	3.0570	3.0490	3.0440	3.0410	3.0430	3.0420
End-members for olivines								
Fa:	8.87	8.35	9.18	9.13	9.03	8.90	9.47	9.29
Fo:	91.13	91.65	90.82	90.87	90.97	91.10	90.53	90.71
Mg#	0.91	0.92	0.91	0.91	0.91	0.91	0.91	0.91

[Mg#=Mg/(Mg+Fe)] of spinels show a small compositional variety, ranging from 0.91 to 0.94 and from 0.14 to 0.20.

During examination of opaque minerals pentlandite ($(Fe_{18.73}Ni_{33.82}Co_{0.63}S_{46.82})$) was analysed in which other iron sulphide (pyrrhotite, or pyrite) component phase was pointed out (Fig. 2E). Magnetite grains compose the boundary (central parting) of mesh cell and rim the sulphide phases (Fig. 2F).

Discussion and Conclusion

Pervasive serpentinization caused alteration of primary minerals and formation of chrysotile, lizardite, talc, Mg-chlorite, quartz, magnetite and carbonates. Anthophyllite was formed probably by thermal effect of an aplite dyke because it occurs exclusively close to it. Consequently, serpentinization was a general process which affected the whole serpentinite body, while formation of anthophillyte should have meant local event. We assume that anthophyllite formation followed the serpentinization, because of they have much more fresh texture than primary olivine and enstatite. Probably the intruded aplite dyke metamorphosed the ultramafic rocks which had already been serpentinized.

Mineral compositions of Gyód Serpentinite were determined by X-ray powder diffraction and electron microprobe. On the basis of the composition of relict minerals (Fo_{90-91}, En_{90-92}) the unaltered rock should have been harzburgite corresponding with earlier results (Balla, 1983; Kovács, 2000). The high ratio of forsterite component in olivine can suggest that the partial melting of a lherzolitic protolith resulted this depleted residuum. The spinel composition also confirms depleted character of the studied rocks since Cr# is 0.92-0.94. Cr# of spinel in lherzolites and harzburgites depends mainly on the degree of partial melting and the initial composition of the melting rocks. On the base of literature (e.g. Stevens, 1944; Pober and Faupl, 1988) one can distinguish the less depleted lherzolites from harzburgites in the sense of Cr# of spinels (Fig. 4). The upper limit of Cr# in lherzolites are 0.5, and 0.3 is the lower in harzburgites. The high Cr# value of the examined spinels reinforces the harzburgitic composition of unaltered rock of Gyód Serpentinite.

Table 5. Chemical composition of studied spinels

sample	ÁGK-7083B		ÁGK-7084			
	spl1	spl2	spl1	spl2	spl3	spl4
MgO	2.66	3.08	3.82	3.06	3.04	2.72
Al2O3	2.00	2.25	2.67	1.80	1.71	2.04
SiO2	0.00	0.00	0.00	0.00	0.00	0.00
CaO	0.00	0.00	0.00	0.00	0.00	0.00
TiO2	0.90	0.95	1.07	1.16	1.13	1.32
V2O3	1.07	0.58	0.56	0.28	0.72	0.54
Cr2O3	40.20	40.17	41.17	40.47	39.70	40.14
MnO	0.08	0.70	0.29	0.70	0.58	1.06
Fe2O3	24.07	24.73	23.42	24.85	25.33	24.14
FeO	28.59	27.53	26.99	27.68	27.79	28.03
Sum.:	99.57	99.99	99.99	100.00	100.00	99.99
Cation numbers based on 32 (spinel phases) or 3 (rhombohedral phases) oxygens						
Mg	1.1640	1.3368	1.6440	1.3312	1.3232	1.1848
Al	0.6912	0.7720	0.9088	0.6192	0.5888	0.7024
Si	-	-	-	-	-	-
Ca	-	-	-	-	-	-
Ti	0.1984	0.2080	0.2320	0.2544	0.2480	0.2896
V	0.2512	0.1344	0.1296	0.0648	0.1680	0.1264
Cr	9.3336	9.2496	9.4024	9.3408	9.1704	9.2752
Mn	0.0192	0.1720	0.0704	0.1728	0.1432	0.2624
Fe3	5.3192	5.4200	5.0904	5.4592	5.5688	5.3088
Fe2	7.0216	6.7056	6.5200	6.7576	6.7896	6.8512
CAT#:	23.9992	24.0000	23.9976	24.0000	24.0000	24.0008
mg#:	0.14	0.17	0.20	0.16	0.16	0.15
cr#:	0.93	0.92	0.91	0.94	0.94	0.93
End-members for spinels						
Spi	4.33	4.83	5.68	3.87	3.68	4.39
Her	-	-	-	-	-	-
Gah	-	-	-	-	-	-
Gal	-	-	-	-	-	-
Qua	2.48	2.60	2.90	3.18	3.10	3.62
Mfe	5.27	6.69	9.07	6.41	6.66	3.18
Cou	1.57	0.85	0.81	0.41	1.05	0.79
Tre	-	-	-	-	-	-
Fra	-	-	-	-	-	-
Jac	0.24	2.15	0.88	2.16	1.79	3.28
Usp	-	-	-	-	-	-
Nic	-	-	-	-	-	-
Mnc	-	-	-	-	-	-
Pic	-	-	-	-	-	-
Chr	58.36	57.84	58.78	58.41	57.34	58.00
Mag	27.75	25.05	21.87	25.56	26.37	26.73
SUM:	99.95	99.96	99.97	99.96	99.95	99.95

The plots of examined samples fall into the metamorhpic spinel field.

On the base of spinel composition the different alpine type peridotites can be divided into three groups (Dick and Bullen, 1984). The Cr# of the examined spinels is greater than 0.6, consequently these belong to Type III which are refractory and pyroxene-poor, consisting largely harzburgite and enstatite-rich dunite. Previous petrographic and geochemical studies resulted similar mineral composition (Balla, 1983, 1985; Kovács and M. Tóth 2000; Kovács, 2000). Type III. peridotites are related to the earliest stages of arc-formation on oceanic crust environments which may be preserved in the tectonized material found in the forearc regions of many modern island-arcs. Most of the Alpine-type peridotites are the residues of partial melting and the generation of magmas in island-arc.

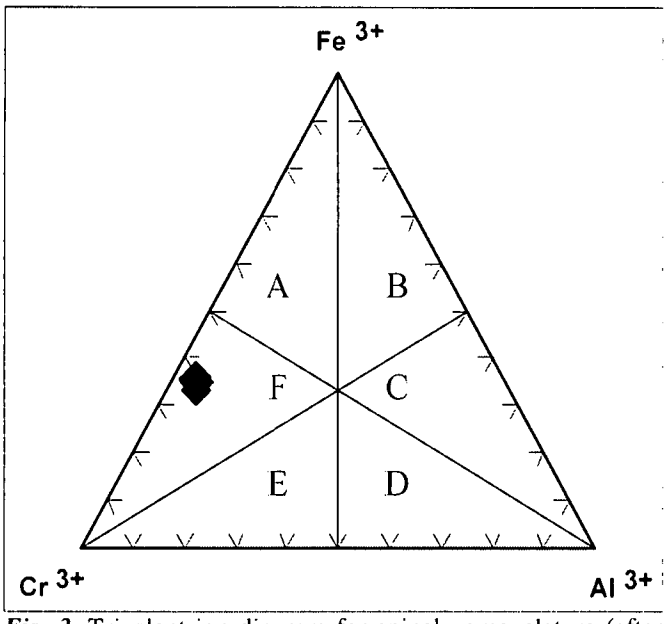

Fig. 3. Trivalent ion diagram for spinel nomenclature (after Stevens. 1944): A, chromian magnetite; B, aluminian magnetite; C, ferrian spinel; D, chromian spinel; E, aluminian chromite; F, ferrian chromite

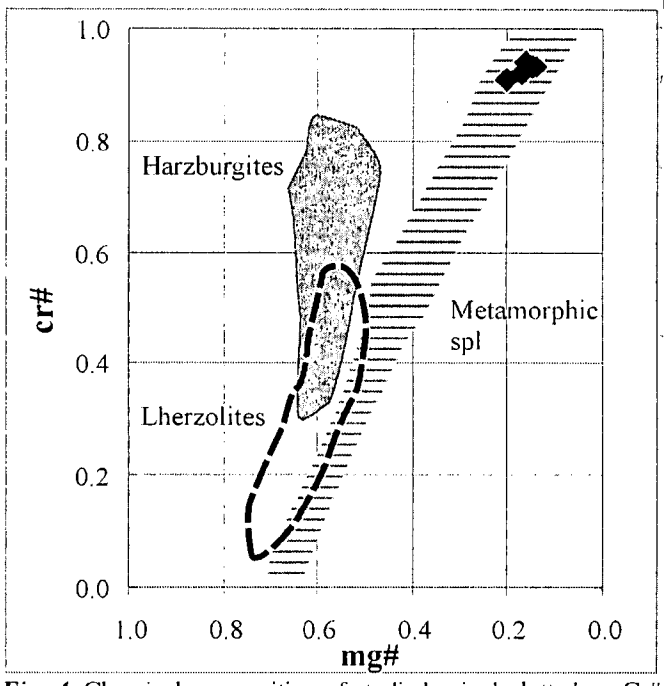

Fig. 4. Chemical composition of studied spinel plotted on Cr# vs. Mg# diagram using compositional field after Stevens (1944)

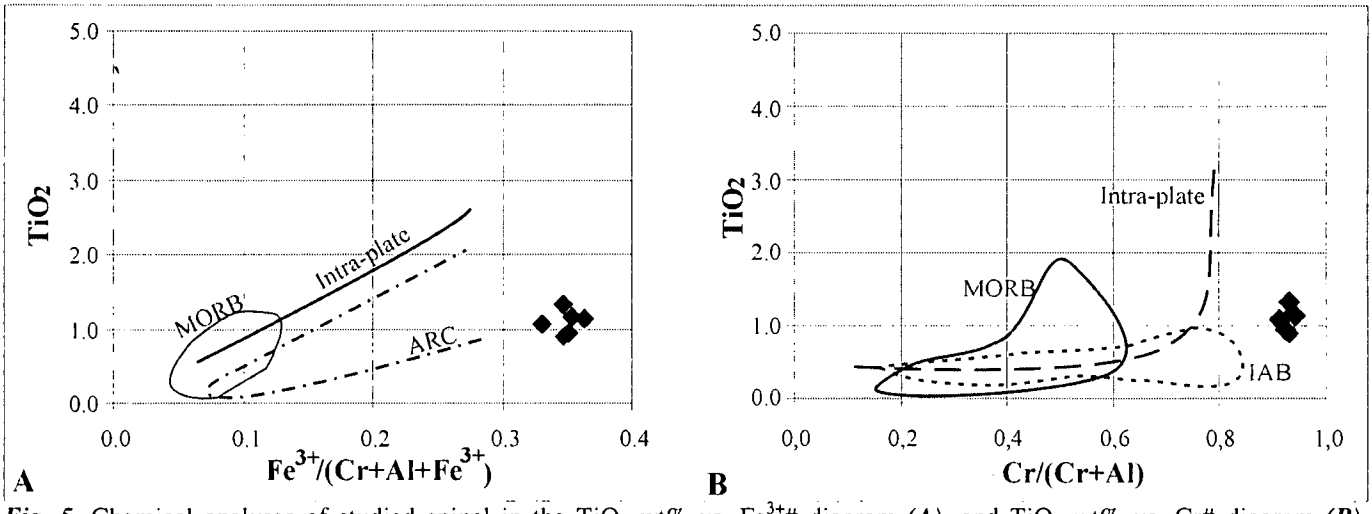

Fig. 5. Chemical analyses of studied spinel in the TiO_2 wt% vs. Fe^{3+}# diagram *(A)*, and TiO_2 wt% vs. Cr# diagram *(B)*. Discrimination lines after Arai (1992)

The TiO_2 content of chromian spinels is useful for separating mid-ocean ridge, island-arc and intra-plate basalts (Arai, 1992). TiO_2 content increases from island-arc magmas through MORB to intra-plate tholeiitic basalts. Spinels derived from upper mantle peridotites usually have TiO_2 content lower than 1.0-1.2 wt%. On the diagrams of TiO_2 vs. Fe^{3+}# and TiO_2 vs. Cr#, (Aria, 1992) (Fig. 5A, B), we suggest that the samples related more to island-arc region than to intra-plate or ocean ridge environment. This is supported by the Type III peridotites character of the examined rocks, but further geochemical investigations are necessary to verify this statement.

ACKNOWLEDGEMENTS

The authors wish to thank László Merényi for his technical assistance, Zoltán Máthé for his help in sampling as well as Csaba Szabó and Enikő Bali for their constructive comments.

REFERENCES

ARAI, S. (1992): Chemistry of chrome spinel in volcanic rocks as a potential guide to magma chemistry. Mineralogical Magazine, 56, 173-184.

BALLA, Z. (1983). A dél-dunántúli ultrabázitok lemeztektonikai értelmezése. Földt. Közl., **113**: 39-56.

BALLA, Z. (1985): Doverhnekamennougolnüje bazitü i ultrabazitü Vengrii. In Dobrecov, N. L. ed.: Rifejszko-Nizsnepaleozojszkije ofiolitü. Szevernoj Evrazii, 136-148.

BARABÁS, A., BARANYAI, I., JÁMBOR, Á., SZABÓ, J., SZÉNÁS, GY. (1969): A Mecsek- és a Villányi-hegység geofizikai kutatásának eredményei. MAELGI Évkönyv, 1.

DICK, H.J.B., BULLEN, T. (1984): Chromian spinel as a petrogenetic indicator in abyssal and alpine-type peridotites and spatially associated lavas. Contrib. Mineral. Petrol., **86**, 54-76

DROOP, G.T.R. (1987): A general equation estimating Fe3+ concentrations in ferromagnesian silicates and oxides from microprobe analyses, using stoichiometric criteria. Mineralogical Magazine, **51**, 431-435.

ERDÉLYI, J. (1970). Jelentés a "Magyarországi szerpentinitek vizsgálata" témában, 1970. II. félév. Kézirat, T. 2574.

GHONEIM, M. F. (1978): Petrogenesis of the eugeosynclinal metamorphites and related rocks. Mecsek Mountains, Hungary. Kandidátusi értekezés, MTAK Kézirat

KOVÁCS, G. & M. TÓTH, T. (2000): Serpantinization of Gyód ultramafic body - a low temperature partial hydratation story. Acta Miner. Petr. Supplementum, Szeged, **XLI**: 64.

KOVÁCS, G. (2000): Petrographical characteristics of the Gyód Serpentinite Body, South-eastern Transdanubia, Acta Miner. Petr., Szeged, **XLI**, 79-91.

KRETZ, R. (1983): Symbols of rocks–forming minerals. American Mineralogist, **68**, 277-279.

PAPP, G. (1989): Szerpentinásványok minerológiai vizsgálata, különös tekintettel a honi előfordulásokra. Egy. Dokt. Ért., ELTE Kőzettani-Geokémiai Tanszék, Budapest.

STEVENS, R.E. (1944): Compodition of some chromites of the western hemisphere. Am. Mineral. **29**. 1-34.

SZEDERKÉNYI, T. (1974): Paleozoic magmatism and tectogenesis in South-East Transdanubia. Acta Geol. Sci. Hung., **18**: 305-313.

Received: September 25, 2002; accepted: December 3, 2002

Acta Mineralogica-Petrographica, Szeged 2002, Vol. 43, pp. 79-83

ACTA Mineralogica Petrographica

PHYSICAL AND CHEMICAL CHARACTERISTICS OF SILICA SAND DEPOSITS (WHITE SAND) OF WADI WATIR REGION, SINAI

IBTEHAL FATHI ABDEL-RAHMAN

Department of Geology, Faculty of Science, Suez Canal University
Ismailia 41522, Egypt

ABSTRACT

Preliminary investigation on the silica sand deposits (white sands) of Wadi Watir region shows that they are of well-sorted grain size, considerable purity and high grade. They might be suitable for art and domestic glass manufactories. The present paper shows that only simple screening must be for upgrading of silica sands. Neither acid treatment of the silica sands nor removal of their content of heavy minerals improves the silica sand grade to any extent.

Key words: glass sand deposits, physical and chemical properties, Wadi Watir, Sinai, Egypt

INTRODUCTION

At the request of the new Egyptian factories for white sands, a comprehensive investigation to look for these deposits in Sinai took place in last few years. Silica sand deposits are widely used in glass and ceramic industries. Preliminary estimation shows that the Egyptian glass industries need more than 1500 tons per year of silica sands (Kamel et al., 1997). Computation of silica sand reserves has not been completed.

The present study is the preliminary investigation for about twenty representative samples as an introductory step to do more detailed studies in the near future. To determine the suitability of the silica sand deposits of Wadi Watir region for glass industry, physical and chemical studies are being carried out. Preliminary results indicate that most of these sands may be suitable for the manufacture of art, domestic and optical glass as well.

The main goal is to provide a brief description of the chemical composition, grain size and heavy mineral content of the silica sands. In addition, its chemical composition is compared with some samples collected from the present day beach sands of Gulf of Aqaba coast. The upgrading processes of silica sands through laboratory experiments are presented and evaluated.

Khalid (1993) studied the economic mineral deposits including; gold and

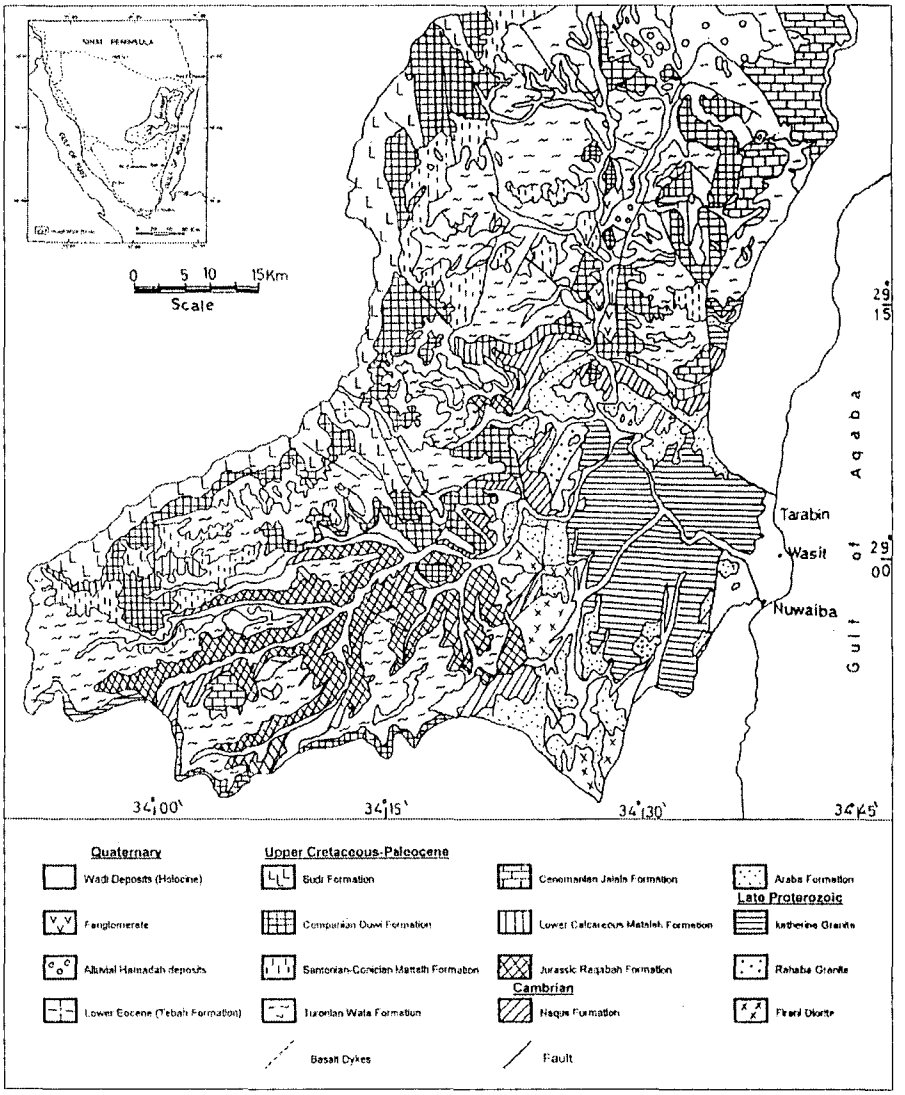

Fig. 1. Geological map of Wadi Watir, South Sinai, Egypt. (After Geological Survey of Egypt, 1994)

white sands of the Nuweibe area, south Sinai. El Fawal (1994) and Kamel et al (1997) shed some light on the economic accumulations of these sands within the Carboniferous Abu Tora Formation, west-central Sinai. Abu Shabana (1998) estimated the reserve of the glass sands at Abu-Rodeiyim and Abu-Heish localities, west-central Sinai to about 8 million tons.

The area under investigation is located to the west of Nuweiba city, west of the Gulf of Aqaba. It lies between latitudes 29° 10' and 28° 55' N, and longitudes 34° 17' and 34° 35' E (Fig. 1). The silica sand deposits occur within the Naqus Formation of Early Paleozoic age. The stratigraphic definition of Naqus Formation was introduced by Said (1971) after Hassan (1967) describing a thick siliciclastic sequence, attaining 250 m thick. It unconformably overlies the Araba Formation and is overlained by the Malha Formation. Twenty representative samples were collected from the Naqus Formation that cropping out across Wadi Ghazalla, from the south outlet of the wadi at the north side of Katherina-Nuweiba asphaltic road to the north direction (Figs. 1 and 2). In the studied section the Naqus Formation measures 70-100 m of white sandstones. They are devoid of any organic remains, indicate fluvial deposition as reported by Issawi and Jux (1982). The lower and middle parts of the section are fine to medium white, massive and thick bedded sandstone with occasional thin bands of coarse grained sandstone. The upper part of the studied section is mainly white to light grey, friable to slightly hard, fine grained sandstones. The most striking feature distinguishing the sequence is Mashrabia structure of fenester structure (Fig. 3) and ripple marks as well as quartz pebbles which distributed randomly or parallel to the bedding planes. Ferruginous bands are also common.

Watir area is characterized by some big, wide and flat domal structures dissected by long faults (Fig. 1) which have dominantly strike-slip movements. The main faults are meridionally directed, commonly hidden by smaller faults. Near Aqaba, most of these faults have NE and NS trends. NW faults (Suez trend) are of less extension. The intersection of these set of faults with equatorial faults resulted in forming the very rugged topography in the sedimentary blanket of Watir area as along the course of wadi Ghazalla (South Sinai water resources project, 1995).

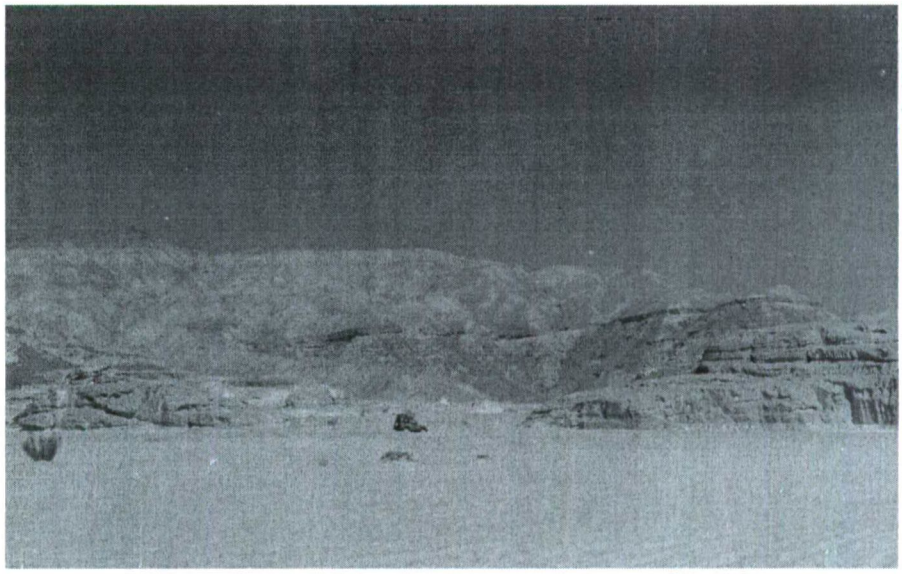

Fig. 2. Naqus Formation underlying Cretaceous rocks, across Wadi Ghazalla

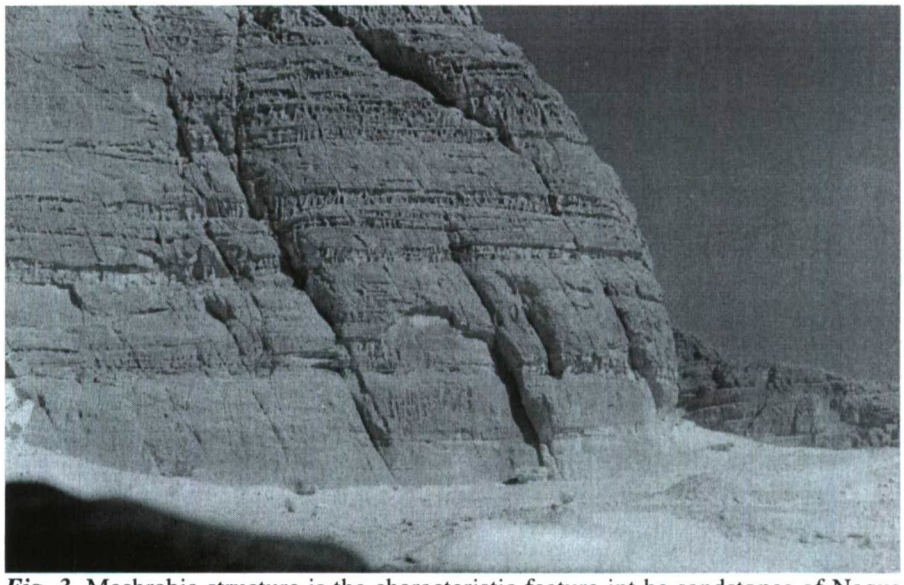

Fig. 3. Mashrabia structure is the characteristic feature int he sandstones of Naqus Formation, Wadi Ghazalla, Southeastern Sinai

LABORATORY METHODS AND FINDINGS

Screen Analysis

The samples are quartered. A representative dry sample of about 100 gms is taken out of each original sample. Weighted amount is sieved 30 min through a set of sieves with opening diameters of 2.0, 1.0, 0.5, 0.250, 0.125, and 0.063 mm; using sieve shaker. The average result of twenty samples is plotted on a histogram as shown in Figure 4. It shows that the silica sands are very well-sorted; more than 90% of the grains are with grain size of 0.125 to 1.00 mm; coarse to fine sand range. More than 50% of the grain size is within 0.25 to 1.00 mm which is within the medium to coarse sand range (Table 1A).

Mineralogical Composition

The sieved fractions are examined under the binocular microscope to study their physical and mineralogical properties (Table 2). It is observed the bulk fractions composed essentially of single quartz grains, with few polycrystalline quartz grains and small amounts of heavy minerals. The coarser grains (0.5 mm) are usually sub-rounded whereas the finer-grains (0.125 mm) are angular. The impurities are: heavy minerals, dark-grey polycrystalline quartz; in contrast to clean white quartz grains.

Table 1. Result of screen and chemical analyses of bulk samples and 1.00-0.125 mm fractions of silica sand from Wadi Watir region

(A) Screen Analyses										
sample no./mm sieve	(1)	(2)	(3)	(4)	(5)	(6)	(7)	(8)	(9)	(10)
over 2.00 mm	nil	0.3	nil	0.1	nil	1.2	0.1	nil	nil	0.1
2-1 mm	3.2	15.4	0.7	4.3	3.8	36.0	1.00	3.72	0.8	4.2
1-0.5 mm	20.3	21.2	5.4	18.0	16.0	19.4	14.3	23.8	1.2	13.5
0.5-0.25 mm	69.2	55.3	70.7	71.0	66.2	26.9	62.4	61.0	50.8	70.4
0.25-0.125 mm	6.8	7.0	21.5	5.3	12.7	11.8	19.8	9.2	39.7	9.1
0.125-.063 mm	0.1	0.3	1.0	0.3	0.8	0.4	1.4	1.08	5.26	1.3
<0.063 mm	0.1	0.2	0.7	0.5	0.5	0.1	0.8	0.7	2.18	0.6
(B) Chemical analyses of bulk samples (%)										
sample no./oxides	(1)	(2)	(3)	(4)	(5)	(6)	(7)	(8)	(9)	(10)
L.O.I.%	0.22	0.25	0.19	0.34	0.13	0.48	0.28	0.29	0.12	0.20
SiO_2	98.62	97.93	98.01	97.53	99.38	97.96	98.19	98.39	99.34	98.59
Fe_2O_3	0.04	0.07	0.03	0.08	0.03	0.08	0.08	0.09	0.04	0.06
TiO_2	0.16	0.10	0.07	0.17	0.06	0.21	0.20	0.17	0.09	0.04
Al_2O_3	1.02	1.84	1.79	1.92	0.41	1.29	1.28	1.09	0.50	1.26
CaO+MgO	Tr	Tr	Tr	Tr	Tr	Tr	Tr	Tr	Tr	Tr
Total	100.06	100.19	100.09	100.04	100.01	100.02	100.03	100.03	100.09	100.15
Grade**	5	7	3	7	2	7	7	7	2	5
(C) Chemical analyses of chosen 1.00-0.125 mm fractions										
L.O.I.%	0.14	0.18	0.13	0.22	0.12	0.32	0.20	0.19	0.10	0.12
SiO_2	99.04	98.81	98.87	98.63	99.45	98.08	99.27	99.02	99.43	99.61
Fe_2O_3	0.01	0.03	0.02	0.03	0.02	0.02	0.01	0.05	0.02	0.02
TiO_2	0.10	0.16	0.11	0.24	0.08	0.27	0.21	0.19	0.11	0.10
Al_2O_3	0.12	0.20	0.27	0.25	0.05	0.17	0.30	0.35	0.18	0.14
CaO+MgO	Tr	Tr	Tr	Tr	Tr	Tr	Tr	Tr	Tr	Tr
Grade**	2	3	2	3	2	2	2	4	2	2

Grade**: Based on U.S. specifications, chemical composition only. Tr: < 0.1% L.O.I. % Loss of Ignition

Heavy Mineral Analysis

Bulk samples are subjected to heavy mineral separation using Bromoform solution. The heavy fractions are washed and dried. Percentage of heavy fractions from selected samples calculated. It ranges from trace to about 0.5%. The dominant minerals are opaque minerals, zircon, rutile and tourmaline. Zircon ranges in abundance from 2 to 10.5%, tourmaline from 2.5 to 5.5% and rutile from 1.5 to 3.5% by weight of the heavy fractions. Biotite, staurolite, epidot and apatite found in trace amounts.

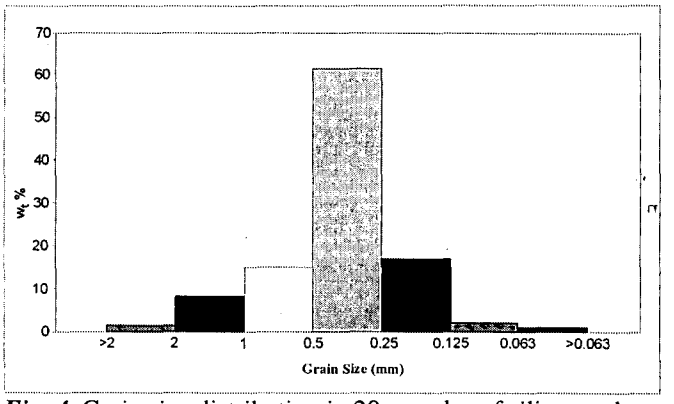

Fig. 4. Grain size distribution in 20 samples of silica sands

CHEMICAL UPGRADING PROCESS

Chemical composition of bulk sample and chosen fraction:

Initially chemical analysis was done on the bulk samples by XRF technique. The results of the chemical composition of ten bulk samples are given in Table 1B. It shows that SiO_2 ranges from 97.53 to 99.38% representing the most abundant oxide in the studied samples. From visual examination of the various fractions under the binocular microscope, it was observed that the main impurities distributed throughout coarser and finer fractions. Therefore, the analysis of chosen fractions might upgrade the silica sands for glass manufacture. The chosen fractions are with grain size of 0.125 to 1.00 mm. Chemical compositions on the chosen fractions for the same samples show a slight improvement of SiO_2 content (from 98.87 to 99.61%) and lower content of the undesirable impurities compared with the bulk samples. The results are shown in Table 1C.

Chosen fraction free from heavy minerals:

Although heavy minerals occur in trace amount in the silica sand (Less than 0.5%), their Fe_2O_3 content may affect the overall grade of the silica sand. Therefore the chemical

Table 2. Physical and mineralogical properties of the fractions

+2.00 mm	Sub-rounded white quartz grains, a few polycrystalline grains and dark-grey rock fragments. More than one quartz grains with fine ilmenite embedded.
+1.00 mm	Sub-rounded to sub-angular white quartz grains. A trace of grey to light-brown polycrystalline quartz. Few embedded ilmenite grains in quartz.
+0.50 mm	Similar to above.
+0.250 mm	Angular to sub-angular quartz grains, white, very clean. Few grains of dark-grey polycrystalline quartz.
+0.125 mm	Angular white quartz grains. Trace amounts of heavy minerals: iron oxides, ilmenite and zircon.
+0.063 mm	Angular, white and pink quartz grains. Minor percent of heavy minerals 2%.
-0.063	About 5% heavy minerals. Angular quartz grains.

analyses were done on eight samples of 0.125 mm-1.00 mm fraction after the removing of the heavy minerals. It was carried out to show whether removal of the heavy minerals would improve the grade of sands or not, in terms of glass manufactory. The obtained results indicate that the removal of the heavy minerals from 0.125-1.00 mm fraction does not improve the grade and composition to any extent. The results are shown in Table 3A.

Acid treatment of sands:

Because some of sand grains have iron oxides coatings, the treatment with acid may be able to dissolve the surface films or stains. Six samples of 1.00-0.125 mm fraction free from heavy minerals were immersed in 10% hydrochloric acid for 24 hours. The results are shown in Table 3B. The obtained result shows that acid treatment of white sands does not intensively reduce the Fe_2O_3 content.

General specifications and standards for Glass Sands

Generally, the glass sand is graded according to its silica and alumina contents. The percentage content of lime, magnesia may also taken in consideration. Specifications vary within certain limits from one glass manufacturer to another and also from country to another one as shown in Tables 4 and 5. For example sands containing more than 99.5% SiO_2 and 0.1% Al_2O_3 are considered of high grade and may be suitable for optical purposes.

CONCLUSIONS

The results of the grain size, heavy mineral content and chemical composition of the Wadi Watir silica sand deposits (white sands) indicate that:

1. The silica sand deposits are very well-sorted, more than 90% of gains lie between coarse to fine sand size range. They consists essentially of white and clean single, sub-rounded to angular, quartz grains. The impurities are represented by heavy minerals, coloured polycrystalline quartz grains and iron oxides occurring in the micro-coatings.

2. Heavy mineral assemblage includes opaque minerals, zircon, rutile, andalusite and tourmaline.

3. The acid treatment of glass sand by dilute hydrochloric acid the removal of the heavy minerals not improve the grade of silica sands to any extent. Simple process of screening may be the most effective method of upgrading the silica sand and can be applied to larger extent on other accumulation of these sands.

4. Most of the silica sand deposits of Wadi Watir region are of second and third grade according to the U.S. specifications (Norton, 1957). They can be suitable for the making art domestic glass. According to the report of the ceramic industry magazine (1966), silica sand deposits used for making containers must have 0.03-0.04% Fe_2O_3. In addition the present study refers that beach sands from Gulf of Aqaba coastal plain are generally not suitable for glass manufactures.

Table 3. Chemical analyses of 0.125-1.00 mm fraction of silica sands without heavy minerals and acid-treated samples

(A) Chemical analyses of 8 selected samples after heavy minerals removed								
Sample No. Oxides	*(11)*	*(12)*	*(13)*	*(14)*	*(15)*	*(16)*	*(17)*	*(18)*
L.O.I.%	0.16	0.16	0.17	0.20	0.19	0.21	0.19	0.17
SiO_2	99.02	98.75	98.68	99.60	99.47	98.42	99.31	99.01
Fe_2O_3	0.02	0.02	0.02	0.03	0.03	0.03	0.03	0.03
TiO_2	0.01	0.02	0.03	0.04	0.02	0.14	0.04	0.04
Al_2O_3	0.14	0.12	0.11	0.12	0.13	0.14	0.19	0.21
CaO+MgO	t	t	t	t	t	t	t	t
Grade**	2	2	2	2	2	3	2	2
(B) Chemical analyses of acid treated of above 6 samples								
L.O.I.%	0.14	0.15	0.11	0.16	0.16	0.18		
SiO_2	98.91	98.71	98.60	99.57	99.45	98.36		
Fe_2O_3	0.02	0.02	0.01	0.02	0.02	0.01		
TiO_2	0.01	0.01	0.02	0.01	0.01	0.01		
Al_2O_3	0.25	0.19	0.16	0.25	0.25	0.16		
CaO+MgO	t	t	t	0.1	t	t		
Grade**	2	2	2	2	2	3		

Grade** U.S. specifications, based on chemical compositions, t < 0.01% L.O.I. % Loss of Ignition

Table 4. Specifications for chemical composition for glass sand**

	SiO_2 % (Min.)	Al_2O_3 % (Max.)	Fe_2O_3 % (Max.)	CaO+MgO % (Max.)
1st quality (optical glass)	99.8	0.1	0.02	0.1
2nd quality (flint containers and table ware)	98.5	0.5	0.035	0.2
3rd quality (flint glass)	95.0	4.0	0.035	0.5
4th quality (sheet and plate glass)	98.5	0.5	0.06	0.5
5th quality (same)	95.0	4.0	0.06	0.5
6th quality (green glass, containers and windows glass)	98.0	0.5	0.3	0.5
7th quality (green glass)	95.0	4.0	0.3	0.5
8th quality (amber glass containers)	98.0	0.5	1.0	0.5
9th quality (amber glass)	95.0	4.0	1.0	0.5

**Recommended by the American Ceramic Society and the National Bureau of Standards (Norton, 1957)

Table 5. Iron oxide standards set by glass manufactures*

Product	Maximum Fe_2O_3 %
Optical glass	0.015-0.016
Containers (colourless)	0.03-0.04
Containers (amber)	0.05-0.08
Plate glass (general)	0.15
Plate glass (windows)	0.08

*Reported by Ceramic Industry Magazine (1966)

ACKNOWLEDGEMENTS

The author would like to thank Dr. Juhas E. and Dr. Imbarak S. Hassen, for the chemical analyses, to Dr. Hassen El-Sherif for help in carrying out the field work. Special thanks to Prof. Dr. M. El-Ghawaby for his critical comments and suggestions.

REFERENCES

ABU-SHABANA, M. (1998): Glass sands of Abu-Thora formation west-central Sinai: lithostratigraphy, geochemistry, suitability, and reserve estimation (abstract). 5th Conference on geology of Sinai for development. Oct. 27-30, Saint Catherine, South Sinai.

CERAMIC INDUSTRY MAGAZINE (1966): Materials for ceramic processing, **87**, 137-140.

DEVELOPMENT PROJECT OF SOUTH SINAI WATER RESOURCES (1995): Geological studies at Wadi Watir and its tributaries, report no. 1.

EL-FAWAL, F. M. (1994): Abu Thora Formation, west-central Sinai, facies analysis and depositional environment. Egyptian Journal of Egypt, **38**.

FATHI, I., HERTELENDI, E., HAAS, J. (1997): Geochemistry and dolomitization of Pleistocene coral reefs, in the Gulf of Aqaba region, South Sinai, Egypt. Acta Mineralogica-Petrographica, **38**, 73-94.

HASSAN, A. A. (1967): A new Carboniferous occurrence in the Abu Durba, Sinai, Egypt. 6th Arab. Petroleum Conference, Baghdad, 2, 8p.

ISSAWI, B., U. JUX (1982): Contribution on the stratigraphy of the Paleozoic rocks in Egypt. Geological Survey of Egypt, **64**, 28.

KAMEL, O. A., ABDOU-SOLIMAN, F. H., ABD EL-MAABOUD, M. H. M. (1997): Sinai Carboniferowhite sands: their heavy mineral assemblages, fabric, geochemistry, and suitability for glass industry. 3rd conference on geochemistry. Alexandria, Egypt.

KHALID, A. M. (1993): Geology and geochemistry of Nuweiba area, South Sinai, Egypt. Ph.D. Thesis. Suez Canal University, Ismailia, Egypt.

NORTON, F. H. (1957): Elements of Ceramics. Addision-Wesley Publishing Co. Inc. Reading, Massachusetts.

SAID, R. (1971): Explanatory notes to accompany the Geological Map of Egypt. Geological Survey of Egypt, **56**, 123.

Received: May20, 2002; accepted: September 26, 2002

INSTRUCTIONS FOR AUTHORS

General

Acta Mineralogica-Petrographica (AMP) publishes articles (papers longer than 4 printed pages but shorter than 16 pages, including figures and tables), notes (not longer than 4 pages, including figures and tables), and short communications (book reviews, short scientific notices, current research projects, comments on formerly published papers, and necrologies of 1 printed page) dealing with crystallography, mineralogy, ore deposits, petrology, volcanology, geochemistry and other applied topics related to the environment and archaeometry. Articles longer than the given extent can be published only with the prior agreement of the editorial board. Occasionally, in the form of supplement issues AMP publishes materials of conferences, or other events of scientific interest.

The journal accepts papers that represent new and original scientific results, which have not appeared elsewhere before, and are not in press either.

All articles and notes submitted to AMP are reviewed by two referees (short communications will be reviewed only by one referee) and are normally published in the order of acceptance, however, higher priority may be given to Hungarian researches and results coming from the Alpine-Carpathian-Dinaric region. Of course, the editorial board does accept papers dealing with other regions as well, let they be compiled either by Hungarian or foreign authors.

The manuscripts (prepared in harmony of the instructions below) must be submitted to the Editorial office in triplicate. All pages must carry the author's name, and must be numbered. At this stage (revision), original illustrations and photographs are not required, though, quality copies are needed. It is favourable, if printable manuscripts are sent on disk, as well. In these cases the use of Microsoft Word or any other IBM compatible editing programmes is suggested.

Language

The language of AMP is English.

Preparation of the Manuscript

The different parts of the manuscript need to meet the instructions below:

Title

The title has to be short and informative. No subtitles if possible. If the main title is too long, an additional shortened title is needed for the running head.

Author

The front page has to carry (under the main title) the full name(s) (forename, surname), affiliation(s), current address(es), e-mail address(es) of the author(s).

Abstract and keywords

The abstract is required to be brief (max. 250 words), and has to highlight the aims and the results of the article. The abstracts of notes are alike (but max. 120 words). As far as possible, citations have to be avoided. In the near future the abstracts are going to be distributed in digital form, as well.

The abstract has to be followed by 4 to 10 keywords.

Text and citations

The format of the manuscripts is required to be: double-spacing (same for the abstract), text only on one side of the page, size 12 Times New Roman fonts. Margin width is 2.5 cm, except the left margin, which has to be 3.5 cm wide. Underlines and highlights ought not be used. Accents of Romanian, Slovakian, Czech, Croatian etc. characters must be marked on the manuscript clearly.

When compiling the paper an Introduction – Geological setting – Materials and Methods – Results – Conlclusions structure is suggested.

The form of citations is: the author's surname followed by the date of publication e.g. (Szederkényi, 1996). In case of two authors: (Rosso and Bodnar, 1995) If there are more than two authors, after the first name the co-authors must be denoted as "et al.", e.g. (Roser et al., 1980).

References

The reference list can only consist of published papers, M.Sc., Ph.D. and D.Sc. theses, and papers in press.

Only works cited previously in the text can be put in the reference list.

Examples:

LE MAITRE, R. W. (ed.) (1989): A Classification of Igneous Rocks and Glossary of Terms. Blackwell, Oxford.

PÁL-MOLNÁR, E. (1998): Geology and petrology of the Ditró Syenite Massif with special respect to formation of hornblendites and diorites. PhD. thesis, University of Szeged, Szeged, Hungary.

ROSSO, K. M., BODNAR, R. J. (1995): Microthermometric and Raman spectroscopic detection limits of CO_2 in fluid inclusions and the Raman spectroscopic characterization of CO_2. Geochimica et Cosmochimica Acta, **59**, 3961-3975.

SZEDERKÉNYI, T. (1996): Metamorphic formations and their correlation in the Hungarian part of Tisia Megaunit (Tisia Megaunit Terrane). Acta Mineralogica-Petrographica, **37**, 143-160.

ZIEGLER, A. M., SCOTESE, C. R., BARETT, S. F. (1983): Mesosoic and Cenozoic paleogeographic maps. In P. Borsche, J. Sundermann (eds.): Tidal Friction and the Earth's Rotation, II. Springer Verlag, New York, 240-252.

The full titles of journals ought to be given. In case more works of the same author are published in the same year, then these has to be differentiated by using a, b, etc. after the date.

Illustrations

Finally, each figure, map, photograph, drawing, table has to be attached in three copies, they must be numbered and carry the name of the author on their reverse. All the illustrations ought to be printed on separate sheets, captions as well if possible. Foldout tables and maps are not accepted. In case an illustration is not presented in digital form then one of the copies has to be submitted as glossy photographic print suitable for direct reproduction. Photographs must be clear and sharp. The other two copies of the illustrations can be quality reproductions. Coloured figure, map or photograph can only be published at the expense of the author(s).

The width of the illustrations can be 56, 87, 118, or 180 mm. The maximum height is 240 mm (with caption).

All figures, maps, photographs and tables are placed in the text, hence, it is favourable if in case of whole page illustrations enough space is left on the bottom for inserting captions. In the final form the size of the fonts on the illustrations must be at least 1,5 mm, their outline must be 0,1 mm wide. Digital documents should be submitted in JPG-format. The resolution of line-drawings must be 400 dpi, while that of photographs must be 600 dpi. The use of Corel Draw for preparing figures is highly appreciated, and in this case please submit the .CDR file, as well.

Proofs and Offprints

After revision the author(s) receive only the page-proof. The accepted and revised manuscripts need to be returned to the Editors either on disc, CD or as an e-mail attachment. Proofreading must be limited to the correction of typographical errors. If an illustration cannot be presented in digital form, it must be submitted as a high quality camera-ready print.

The author(s) will receive 25 free offprints. On payment of the full price, further offprints can be ordered when the corrected proofs are sent back.

Manuscripts for publication in the AMP should be submitted to:

Dr. Pál-Molnár Elemér
e-mail: palm@geo.u-szeged.hu
Phone: 00-36-62-544-683, Fax: 00-36-62-426-479
Department of Mineralogy, Geochemistry and Petrology
University of Szeged
P. O. Box 651
H-6701 Szeged, Hungary

Published in 450 copies/issue (300 in Hungary, 150 abroad).
Distributed by the Department of Mineralogy, Geochemistry and Petrology, University of Szeged, Szeged, Hungary.
Price of subscription to volume 43, 2002 (including Postage): HUF 3500 in Hungary, USD 20 in all other countries.

established in 1922

ACTA MINERALOGICA-PETROGRAPHIC

VOLUME 43 2002

HU ISSN 0365-8066

CONTENTS:

Printed in Hungary by Páskum Nyomda, H-7103 Szekszárd, P.O. Box 627